

Modulators of Spinocerebellar Ataxia Type 3-associated Ataxin-3 Aggregation

Su-Ling Leck
Bachelor of Science (Honours)

A thesis submitted for the degree of Doctor of Philosophy at
Monash University

Department of Biochemistry and Molecular Biology,
Monash University, Melbourne, Australia

July 2016

© The author 2016. Except as provided in the Copyright Act 1968, this thesis may not be reproduced in any form without the written permission of the author.

Abstract

Spinocerebellar ataxia type-3 (SCA3), also known as Machado-Joseph disease, is proposed to be the most common dominant autosomal ataxia. It is a progressive, fatal neurodegenerative disease with no known cure. Ataxin-3 protein, which is expressed ubiquitously in the brain, initiates the early onset of SCA3 with a polyglutamine (poly-Q) expansion within the protein. Non-expanded ataxin-3 (non-pathogenic) has a poly-Q repeat threshold between 12–46 residues, while disease expansion coincides with 51 residues and above. The pathological hallmark of SCA3 is the presence of nuclear inclusions of aggregated ataxin-3, co-localised with ataxin-3 fragments, ubiquitin and other interacting proteins. The aggregation of ataxin-3 is more complex than many other misfolded proteins that are associated with neurodegenerative diseases (ND). It has been shown to undergo a two-stage aggregation pathway, which relates to the Josephin domain and the length of the poly-Q tract. In addition, it has also been well documented that ataxin-3 aggregation can be modulated by a number of interacting partners or factors.

This thesis therefore sought to investigate the interrelationship between the length of the poly-Q tract and the effects of a range of factors and modulators on ataxin-3 aggregation, including ataxin-3 fragments generated by proteolytic cleavage and also chemical chaperones. Proteolytic cleavage has been implicated in the development of toxic fragments that initiate the aggregation in ND-associated proteins. Since ataxin-3 has been shown to be a substrate for the protease, calpain-2, the possible role of toxic fragments of ataxin-3, (*i.e.* toxic fragment hypothesis), was investigated in this study, together with an investigation into whether expanded poly-Q ataxin-3 leads to a faster rate of proteolysis. Also, osmolytes or ‘chemical chaperones’ have been increasingly used in the study of protein folding and aggregation. The osmolyte, trimethyl-N-oxide (TMAO) has been shown to reduce misfolding of proteins, stabilising native conformations and in particular, reduce the aggregation of ataxin-3 fragments expressed in cultured cells. Thus, the modulation of ataxin-3 aggregation using a range of ataxin-3 variants in the presence of TMAO was also further explored.

Overall, the results demonstrated that calpain-2 cleaved all ataxin-3 variants (poly-Q length of 15, 28, 50, 64 residues), as the cleavage sites of ataxin-3 were mostly located after the Josephin domain. Proteolysis of ataxin-3 variants by calpain-2 were analysed kinetically and it was found that the rate of proteolysis was independent of the length of the poly-Q tract. Subsequently, a C-terminal poly-Q containing fragment of ataxin-3 namely (242Q15) and (242Q64) were expressed as a recombinant fusion protein and purified. The aggregation of both fusion and fragment proteins were analysed *in vitro*. It was determined that the fragments (242Q15) and (242Q64) have a high propensity to aggregate. Importantly, the result that both fragments can accelerate the aggregation of full-length ataxin-3 (Q64) to form SDS-insoluble aggregates, confirms the toxic fragment hypothesis as an overarching mechanism for ataxin-3 induced disease. Lastly, non-pathological and pathological lengths of ataxin-3 rapidly aggregated in the presence of TMAO. Intriguingly, the de-ubiquitinating activity of ataxin-3 was also enhanced with TMAO. Taken together, the data in this thesis provides a deeper insight into the influence of modulators on ataxin-3 aggregation, which may benefit the development of potential therapeutics in targeting protein aggregation in SCA3 pathogenesis.

General Declaration

In accordance with Monash University Doctorate Regulation 17.2 Doctor of Philosophy and Research Master's regulations the following declarations are made:

I hereby declare that this thesis contains no material which has been accepted for the award of any other degree or diploma at any university or equivalent institution and that, to the best of my knowledge and belief, this thesis contains no material previously published or written by another person, except where due reference is made in the text of the thesis.

Su-Ling Leck

Acknowledgements

A wise friend, Vita once said that the undertaking of a PhD is an arduous journey that would test your dedication to science. I would add that persevering to complete that journey brings home a really sweet sense of achievement. My endeavour to start and complete this PhD after a hiatus would not be possible without the help of the people who had gone down this path or shared the path with me.

First, I would like to thank Monash University for the award of the Monash International Postgraduate Scholarship, as well as the Monash Graduate Scholarship, that enabled me to start off my PhD.

I would like to express my utmost gratitude towards my supervisors Marie-Isabel Aguilar and Stephen Bottomley. To Mibel, for her mentorship, scientific enthusiasm, invaluable expertise, encouragement and patience in the careful review of my drafts even while on holidays. To Steve, providing an opportunity to pursue a PhD in his laboratory and then navigating me through the world of protein aggregation.

I am sincerely grateful towards the following people for their valuable input and had collectively reviewed my work over the years - Steve, Robert Pike, Ong Poh Chee, Andrew Ellisdon, Amy Robertson, Vita Levina, Victoria Hughes and Chris Lupton.

I would also like to thank all the people of the Bottomley group, past and present, for a supportive work environment and the invigoration of my scientific passion when failed experiments brought on darker days. To Mary Pearce, Weiwen Dai, Noelene Quinsey for sharing their depth of knowledge and experience in protein expression and refolding. To good friends that made lab life so much better -Vita, Anja, Amy, Victoria, Evelyn and Chris who believe as much as I do that great insight into life and science is definitely over meals, coffee breaks and Russian dumplings.

I am deeply grateful to Evelyn Yip, Gary Mak, Summy Fung and Leslie Young for hosting my stay here in Melbourne, in order for me to present my seminar and write up my thesis. To Evelyn and Vita, your own successes and perseverance towards your PhD journeys inspired me not to give up on mine.

To friends and family both Melbourne and in Singapore from all walks of life, thank you for your unflappable support and encouragement. To Westin, thank you for putting things into perspective when things felt difficult.

Last but not least, I would like to express my deepest gratitude to my family; Dad, Mum and Edmund for their unwavering support and love throughout the years. I could not have done it without their encouragement to pursue and complete this challenging but fulfilling journey.

Table of Contents

Abstract.....	i
General Declaration.....	iii
Acknowledgements.....	iv
Table of contents.....	v
List of Figures.....	x
List of Tables.....	xii
List of Abbreviations.....	xiii
Chapter 1 General Introduction.....	2
1.1 Neurodegenerative diseases.....	3
1.2 Spinocerebellar ataxia Type-3.....	3
1.3 Polyglutamine repeats human disease.....	4
1.4 MJD-1 gene product, Ataxin-3 product.....	7
1.4.1 Structure of ataxin-3.....	7
1.4.2 Biological roles of ataxin-3.....	10
1.4.2.1 Protein degradation.....	10
1.4.2.2 Transcriptional regulator.....	11
1.5 Protein misfolding is a main feature of ataxin-3 pathogenesis.....	11
1.5.1 Protein folding and quality control.....	11
1.5.2 Protein aggregation and fibril formation.....	14
1.5.3 Ataxin-3: Protein context and its two-stage aggregation pathway.....	16
1.5.4 Ataxin-3 proteolysis and aggregation.....	17
1.5.5 Influence of osmolyte on ataxin-3 aggregation.....	20
1.6 Aims of this study.....	22
Chapter 2 Material and Methods.....	24
2.1 Chemicals and Reagents.....	25
2.1.1 Determining the concentration of TMAO in Tris buffer.....	26
2.2 Microbial Techniques.....	26
2.2.1 Growth Media.....	26
2.2.2 Bacterial Strains.....	26

2.3 Molecular Biology Techniques.....	27
2.3.1 Expression vectors.....	27
2.3.2 Primers.....	27
2.3.3 Polymerase Chain Reaction.....	28
2.3.4 Quikchange™ mutagenesis.....	29
2.3.5 Agarose gel electrophoresis.....	30
2.3.6 Restriction Enzyme digestion.....	30
2.3.7 Gel purification.....	31
2.3.8 Ligations.....	31
2.3.9 Plasmid purification.....	31
2.3.10 Preparation of competent cells.....	31
2.3.11 Bacterial transformations.....	32
2.3.12 Colony screening.....	32
2.4 Preparation of Proteins.....	33
2.4.1 Protein sequence of ataxin-3 variants.....	33
2.4.2 Constructs engineered and used for protein expression.....	34
2.4.3 Buffers or solutions.....	35
2.4.3.1 Ataxin-3 proteins purification.....	35
2.4.3.2 (SpA242Qn) proteins purification.....	35
2.4.4 Expression of ataxin-3 variants.....	35
2.4.5 Expression of (SpA242Qn) fusion ataxin-3 variants.....	36
2.4.6 Expression of TEV protease.....	36
2.4.7 Purification of ataxin-3 variants and the Josephin domain.....	36
2.4.8 Unfolding of SpA242Ataxin-3 variants inclusion bodies.....	37
2.4.9 Refolding and purification of (SpA242Qn) ataxin-3 variants.....	38
2.4.10 Purification of TEV protease.....	38
2.4.11 Determination of protein concentration.....	38
2.5 Analytical Techniques.....	39
2.5.1 SDS-PAGE.....	39
2.5.2 Size exclusion chromatography.....	40
2.5.3 Transmission Electron Microscopy.....	41
2.5.4 Circular Dichroism.....	41

2.5.5 Western Blotting.....	42
2.5.6 N-terminal peptide sequencing.....	42
2.5.7 Membrane filter trap assay.....	43
2.5.8 Mass Spectrometry sample preparation.....	44
2.6 Assays involving protein aggregation and cleavage.....	44
2.6.1 Ataxin-3 variants.....	44
2.6.2 (SpA242Qn) Ataxin-3 fusion proteins.....	44
2.6.3 QBP1 peptide assays.....	45
2.6.4 Calpain-2 cleavage on ataxin-3 variants.....	45
2.6.5 TEV cleavage on (SpA-242Qn) fusion ataxin-3 variants.....	45
2.6.6 GST-Ub52 proteolytic assay in TMAO.....	46
2.7 Assays involving intrinsic fluorescence and peptide fluorescence.....	46
2.7.1 Kinetic analysis of Suc-LY-AMC peptide by calpain-2.....	46
2.7.2 Kinetic analysis of ataxin-3 cleavage by calpain-2.....	46
2.7.3 Thioflavin-T (ThT) fluorescence.....	47
2.7.3.1 Discontinuous ThT measurements.....	47
2.7.3.2 Continuous ThT measurements.....	47
2.7.4 Ubiquitin-AMC protease activity assay.....	47
2.7.5 Intrinsic fluorescence protein assays.....	48
Chapter 3 Proteolysis of Ataxin-3 is independent of polyglutamine tract length.....	50
3.1 Introduction.....	51
3.2 Results.....	52
3.2.1 Calpain-2 cleaves non-pathological and pathological length ataxin-3 similarly in vitro.....	52
3.2.2 Identification of ataxin-3 cleavage sites via mass spectrometry and N-terminal sequencing.....	54
3.2.3 Ataxin-3 variants have similar rate of proteolysis.....	56
3.3 Discussion.....	60
3.3.1 Calpain-2 cleaves all ataxin-3 variants at identical sites.....	60
3.3.2 Ataxin-3 protein cleavage is independent of poly-Q length.....	61
3.4 Summary and conclusions.....	62

Chapter 4 Characterisation of Ataxin-3 fragments initiating and accelerating aggregation of ataxin-3 full-length proteins.....	64
4.1 Introduction.....	65
4.2 Results.....	66
4.2.1 Design and selection of fusion partners for the ataxin-3 fragment.....	66
4.2.2 Purification and refolding of fusion ataxin-3 proteins, (SpA242Qn)	70
4.2.3 Refolded ataxin-3 fusion proteins are monomeric and retained α -helical conformations.....	72
4.2.4 Release of ataxin-3 fragments (242Q15), (242Q64) from SpA fusion partner by TEV proteolysis.....	78
4.2.5 Detection of fragment (242Q15), (242Q64) proteins by immunoblotting with S-tag antibody.....	79
4.2.6 Morphology of ataxin-3 fusion and fragment protein aggregates.....	81
4.2.7 Fusion and fragment ataxin-3 aggregates displays low sensitivity to ThT fluorescence.....	83
4.2.8 Fusion and fragment Q64 forms SDS-insoluble aggregates through their polyQ tract.....	87
4.2.9 Monitoring aggregation kinetics of (SpA242Q64) and (242Q64) via SDS-insolubility.....	90
4.2.10 Acceleration of SDS-insoluble full-length ataxin-3 (Q64) aggregation initiated by poly-Q length fragments.....	93
4.2.11 Fragments (242Q15) and (242Q64) do not bypass first stage of ataxin-3 aggregation pathway.....	96
4.3 Discussion.....	97
4.3.1 Fusion ataxin-3 proteins can be successfully purified from inclusion bodies and be refolded into structured monomers.....	97
4.3.2 Fusion and fragment proteins emit weak ThioT fluorescence but form aggregates with distinct morphology.....	99
4.3.3 Aggregation of fusion (SpA242Q64) and fragment (242Q64) can be monitored through SDS-stability.....	100
4.3.4 Ataxin-3 Poly-Q fragments accelerated the formation of second stage SDS-stable aggregates of ataxin-3 (Q64).....	100
4.4 Summary and conclusions.....	104
Chapter 5 Effects of Trimethylamine-N-oxide, TMAO on Ataxin-3 aggregation and activity.....	106
5.1 Introduction.....	107
5.2 Results.....	108

5.2.1	Ataxin-3 aggregation is enhanced by TMAO.....	108
5.2.1.1	TMAO accelerates ataxin-3 first stage (Stage 1) aggregation.....	108
5.2.1.2	TMAO also accelerates ataxin-3 Stage 2 aggregation.....	112
5.2.2	TMAO does not alter the morphology of ataxin-3 aggregates.....	112
5.2.3	TMAO accelerates Josephin aggregation without altering its aggregate morphology.....	113
5.2.4	TMAO does not significantly alter the native structure of both ataxin-3 and Josephin proteins.....	114
5.2.5	Deubiquitinating (DUB) activity of ataxin-3 is enhanced in the presence of TMAO.....	121
5.2.6	Enhancement of DUB activity of ataxin-3 is independent of the UIMs located in the C-terminal region.....	125
5.3	Discussion.....	127
5.4	Summary and conclusions.....	135
	Chapter 6 Perspectives.....	137
6.1	Discussion.....	138
6.2	Overview.....	146
	References.....	150
Appendix A	Determination of kinetic parameters of ataxin-3 (Q28) and (Q50).....	169
Appendix B	TANGO prediction of S-tag aggregation propensity.....	170
Appendix C	TANGO prediction of Ataxin-3 hydrophobic tail aggregation propensity.....	171

List of Figures

- Figure 1.1 The relationship between the age of disease onset and the poly-Q repeat length in patients
- Figure 1.2 Schematic representation of the ataxin-3 protein
- Figure 1.3 The solution structure of Josephin domain
- Figure 1.4 The protein folding energy landscape
- Figure 1.5 Negative stained electron micrograph of typical ataxin-3 (64) fibrils
- Figure 1.6 The ataxin-3 two-stage model aggregation pathway
- Figure 1.7 Structure of TMAO
- Figure 3.1 A Schematic diagram showing the domain organisation of the ataxin-3 protein
- Figure 3.2 Identification of cleavage sites for calpain-2 in ataxin-3 variants
- Figure 3.3 Determination of K_S and V_S of Suc-LY-MC
- Figure 3.4 Ataxin-3 proteins compete for calpain-2 hydrolysis in the presence of fluorogenic substrate, Suc-LY-AMC
- Figure 3.5 Comparison of the apparent K_M values of corresponding ataxin-3 variants
- Figure 4.1 Summary of constructs designed for the expression of the ataxin-3 fragment
- Figure 4.2 Illustration of the final expression construct of ataxin-3, (SpA242Qn)
- Figure 4.3 Chromatogram of the refolding process of ataxin-3 fusion proteins, (SpA242Q15) and (SpA242Q64)
- Figure 4.4 Purified and refolded fusion ataxin-3 proteins analysed on SDS-PAGE.
- Figure 4.5 SEC analyses of ataxin-3 fragment fusion proteins
- Figure 4.6 Predicted secondary structure of SpA242Qn fusion proteins
- Figure 4.7 MALDI and CD analysis of ataxin-3 fusion proteins (SpA242Q15) and (SpA242Q64)
- Figure 4.8 Sensitivity of ataxin-3 fusion proteins to TEV proteolysis and S.tag immunoblotting
- Figure 4.9 TEM images of fusion and fragment ataxin-3
- Figure 4.10 Discontinuous measurement of ThT fluorescence of fusion and fragment ataxin-3 proteins after aggregation assay
- Figure 4.11 Continuous Thioflavin-T fluorescence measurement of (SpA242Q15) and (SpA242Q64) aggregation
- Figure 4.12 Formation of SDS-insoluble aggregates of ataxin-3 fusion proteins, (SpA242Q15) and (SpA242Q64), following S-tag antibody in Western blotting
- Figure 4.13 Effect of QBP1 peptide on fusion and fragment ataxin-3 (Q64) proteins monitored via filter trap membrane assay

- Figure 4.14 Fusion and fragment ataxin-3 proteins (SpA242Q64) and (242Q64) aggregation monitored by SDS-insolubility
- Figure 4.15 Acceleration of full-length ataxin-3 (Q64) SDS-insoluble aggregation initiated by fragment ataxin-3 proteins, (242Q15) and (242Q64)
- Figure 4.16 Illustration of a proposed model of ataxin-3 fragments initiating SDS-insoluble aggregation of expanded ataxin-3 (Q64)
- Figure 5.1 Aggregation of ataxin-3 in the presence of increasing amounts of TMAO
- Figure 5.2 Aggregation monitored by size exclusion chromatography
- Figure 5.3 Morphology of ataxin-3 aggregates in the presence of TMAO
- Figure 5.4 The effect of TMAO on the aggregation of Josephin
- Figure 5.5 The secondary structure of all proteins in the presence of TMAO by CD
- Figure 5.6 The native structure of the variants in the presence of TMAO by fluorescence spectroscopy
- Figure 5.7 DUB activities of the variants in the presence of TMAO
- Figure 5.8 Quantitative analysis of de-ubiquinating activity of the variants in the presence of TMAO
- Figure 5.9 Determination of the specificity of ataxin-3 DUB activity
- Figure 5.10 Solution structure of Josephin domain with binding sites for mono-ubiquitin
- Figure 5.11 Proposed model for the compaction of Josephin molecule by TMAO resulting in the enhancement of DUB activity

List of Tables

Table 1.1	Summary of different human poly-Q diseases
Table 3.1	Apparent kinetic parameters for proteolysis of ataxin-3 variants by calpain-2
Table 4.1	The various designs of fusion ataxin-3 fragment constructs
Table 4.2	Molecular weights predicted of the fusion and fragment proteins of ataxin-3 based on the bioinformatics resources portal, ExPASy and online tool, ProtParam
Table 4.3	ThT midpoints of the aggregation of fusion, fragment and full length proteins
Table 4.4	SDS-insolubility midpoints of SpA-242Q64 and -242Q64 aggregation
Table 4.5	SDS-insolubility midpoints of the aggregation reaction of ataxin-3 fragments on full-length ataxin-3.
Table 5.1	Summary of aggregation kinetics of ataxin-3
Table 5.2	Summary of aggregation kinetics of Josephin
Table 5.3	De-convolution of CD spectras of ataxin-3 variants and Josephin
Table 5.4	Deubiquitination rates of all proteins in the presence of TMAO by fluorogenic assay
Table 5.4	Deubiquitination rates of ataxin-3 and UIM mutants in the presence of TMAO

List of Abbreviations

A β	Amyloid- β
Ab _{s280}	Absorbance at 280 nm
Amp	Ampicillin
AMC	7-amino-4-methylcoumarin
APP	Amyloid precursor protein
APS	Ammonium Persulfate
AR	Androgen receptor
BCA	Bicinchoninic Acid
BME	β -mercaptoethanol
BSA	Bovine Serum Albumin
Ca	Calcium
CACNA1A	alpha1 voltage-dependent calcium channel
CBP	CREB binding protein
CD	Circular dichroism
CFTR	Cystic fibrosis transmembrane conductance receptor protein
CHIP	C-terminal HsP70 interacting protein
CREB	cAMP response element-binding protein
DMSO	Dimethyl Sulfoxide
DRPLA	Dentatorubral-pallidoluysian atrophy
DTT	Dithiothreitol
DUB	Deubiquitinating enzyme
ECL	Enzymatic chemiluminescence
EDTA	Ethylenediaminetetraacetic Acid
ER	Endoplasmic Reticulum
E1	Ubiquitin-activating enzyme
E2	Ubiquitin-conjugating enzyme
E3	Ubiquitin ligases
FPLC	Fast Protein Liquid Chromatography
GST	Glutathione S-transferase
GuHCl	Guanidium Hydrochloride
GuSCN	Guanidium Thiocyanate
HD	Huntington's disease
HsP	Heat shock protein
Htt	Huntingtin

Ig	Immunoglobulin
IPTG	Isopropyl- β -D-thiogalactopyranoside
K	Lysine
kDa	KiloDalton
λ_{em}	Emission Wavelength
λ_{ex}	Excitation Wavelength
MJD	Machado Joseph disease
NES	Nuclear export signal
NLS	Nuclear localisation sequence
nm	Nanometre
NMR	Nuclear Magnetic Resonance
NOESY	Nuclear Overhauser Effect Spectroscopy
OD ₆₀₀	Optical Density at 600 nm
OPMD	Oculopharyngeal muscular dystrophy
QBP1	PolyQ-binding peptide 1
PABPN1	Polyadenine binding protein 1
PAGE	Polyacrylamide Gel Electrophoresis
PCR	Polymerase Chain Reaction
PCAF	p300/CBP associated factor
PMSF	Phenylmethyl sulphonyl fluoride
Poly-Q	Polyglutamine
Poly-Ub	Poly-ubiquitin
p300	E1A-binding protein p300
SBMA	Spinal bulbar muscular atrophy
SCA	Spinocerebellar ataxia
SDS	Sodium dodecyl sulphate
SEC	Size Exclusion Chromatography
sHsp	small heat shock protein
Suc	Succinyl
SpA	<i>Staphylococcus aureus</i> Protein A B domain
θ	Molar Ellipticity
TBP	TATA-binding protein
TBS	Tris-buffered saline
TEM	Transmission Electron Microscopy
TEMED	Tetramethylethylenediamine

ThT	Thioflavin-T
TMAO	Trimethyl-N-oxide
TRiC	TCP-1 ring complex
UIM	Ubiquitin interacting motif
Ub	Ubiquitin
UPP	Ubiquitin proteasome pathway
UV	Ultraviolet
W	Tryptophan
2UIM	First splice isoform of ataxin-3 without 3 rd UIM
3UIM	Second splice isoform of ataxin-3 with 3 rd UIM

CHAPTER 1

INTRODUCTION

1.1 Neurodegenerative diseases

In recent years, a range of debilitating, amyloid deposition medical disorders has emerged, such as Alzheimer's and Parkinson's diseases. There is recognition that these disorders are associated with ageing, especially with neurodegenerative diseases (1). Neurodegeneration is usually progressive and sporadic and their pathology is characterized by neuronal and synaptic loss or abnormalities (2). Genetic background and familial mutations may contribute towards early onset of the disease (3, 4). A number of neurodegenerative diseases (ND) that are associated with protein misfolding fall under a broad category termed as 'protein misfolding diseases'. They are, but not exclusive to Alzheimer's (5), Parkinson's (6), prion encephalopathies (7) and polyglutamine (poly-Q) diseases (8). Protein misfolding is generally referred to as the conversion of a protein into a structure that differs from its native conformation and functional state (3). Correct protein folding, through distinct processes is essential for its full functional activity (9). Hence, when protein misfolding occurs, it often leads to an induction of pathogenic behaviour. A characteristic feature of these diseases is the formation of amyloid plaques or inclusions within the brain cells (4). These proteinaceous deposits or inclusions have also been shown to contain various components. "Lewy bodies", observed in Parkinson's disease are comprised of aggregated alpha-synuclein (α -syn) and ubiquitin (10). In spinocerebellar ataxia type-3, the poly-Q-containing protein, ataxin-3 aggregates and forms nuclear inclusions (NI) comprised of ataxin-3 fibrils, ubiquitin and other proteasome constituents (11). The presence of these interacting components within the NI also suggests the importance and role of the cell quality control system, which will be explored later in this chapter.

1.2 Spinocerebellar ataxia Type 3

Spinocerebellar ataxia type 3 (SCA3), also known as Machado-Joseph disease (MJD), is an autosomal dominant neurodegenerative disorder. It was first described among individuals of Azorean descent and it is now known to exist as the most common dominantly inherited ataxia (12). SCA3 is clinically characterized by progressive ataxia, ophthalmoplegia and abnormalities of posture and movement (12). Degeneration of the substantia nigra, deep nuclei of the cerebellum and of the

spinocerebellar nuclei are also observed (13). SCA3 belongs to a group of nine poly-Q diseases, such as Huntington's disease (HD), spinal and bulbar muscular atrophy, dentatorubral pallidoluysian atrophy and seven other SCA types (1, 2, 6, 7, 8 and 12). SCA3 is caused by the expansion of a poly-Q encoding CAG repeat in the *MJD-1* gene that codes for the protein, ataxin-3 (14), where MJD patients are found to have more than 55 consecutive CAG repeats while healthy populations have a CAG repeat range between 10 and 51 (15). The causative agent, ataxin-3 is a protein that is both localised in the cytoplasm and in the nucleus (16-19). The ataxin-3 protein comprises of an N-terminal Josephin domain that has similar catalytic properties to cysteine proteases; two ubiquitin interaction motifs (UIMs) and an expandable poly-Q tract in the C-terminus. The structure and function of ataxin-3 will be further discussed in Section 1.4 of this chapter. Table 1 below summarises the different types of human diseases that are associated to polyglutamine (CAG) diseases.

1.3 Polyglutamine repeats and human disease

Trinucleotide repeats expansion has been associated with neurological disorders for the past two decades (20) and some of these disorders are summarised in Table 1. Each disease has a distinctive pattern of degeneration within the central nervous system, with considerable overlap between disorders (21, 22). In all of these diseases, there is a poly-Q threshold length generally in the range of 35 - 45 repeats, which differentiates normal and pathogenic length proteins (15, 23, 24). The age of onset of disease also shows a strong negative correlation with poly-Q length (23, 25), with longer repeats being correlated with earlier age onset and increased disease severity (Figure 1.1).

Table 1.1 Summary of the different human polyQ diseases The differences in the pathological lengths of poly-Q repeat expansion, the location of repeats and its respective unique functions are compared (adapted from (13)).

Disease	Gene	Repeat location	Normal repeat length	Disease repeat length	Protein	Function of Protein
Spinal and bulbar muscular atrophy (SBMA)	<i>AR</i>	N-term	9-36	38-62	Androgen Receptor	Transcription, transcription regulation
Huntington's Disease (HD)	<i>HTT</i>	N-term	6-34	36-121	Huntingtin	Apoptosis
Dentatorubral-pallidouysian atrophy (DRLPA)	<i>ATN1</i>	C-term	7-34	49-88	Atrophin	Transcription, transcription regulation
Spinocerebellar ataxia Type 1 (SCA 1)	<i>ATXN1</i>	N-term	6-39	40-82	Ataxin-1	Transcription, transcription regulation
Spinocerebellar ataxia Type 2 (SCA 2)	<i>ATXN2</i>	N-term	15-24	32-200	Ataxin-2	Function currently unknown
Spinocerebellar ataxia Type 3 (SCA 3)	<i>ATXN3/</i> <i>MJD</i>	C-term	10-50	55-87	Ataxin-3	Transcription, transcription regulation, UBL conjugation pathway
Spinocerebellar ataxia Type 6 (SCA 6)	<i>CACNA1 A</i>	C-term	4-20	20-29	CACNA1 _A	Calcium and ion transport
Spinocerebellar ataxia Type 7 (SCA 7)	<i>ATXN7</i>	N-term	4-35	37-306	Ataxin-7	Transcription, transcription regulation
Spinocerebellar ataxia Type 8 (SCA 8)	<i>ATXN8</i>	3' UTR	2-130	>110	Ataxin-8	Cell death
Spinocerebellar ataxia Type 12 (SCA 12)	<i>PPP2R2B</i>	5' UTR	7-45	55-78	Serine/ threonine-protein phosphatase 2A 55 kDa subunit B β isoform	Apoptosis
Spinocerebellar ataxia Type 17 (SCA 17)	<i>ATXN17</i>	N-term	25-42	47-63	TATA box binding protein	Transcription, transcription regulation, host-virus interaction

In 1997, Paulson and his group identified intracellular inclusions containing the expanded ataxin-3 protein. This led to the suggestion that poly-Q expansion could induce aggregation, resulting in the search for the mechanisms of poly-Q disease pathogenesis (26). It was subsequently established that inclusions containing poly-Q proteins, whether localised in the cytoplasm or in the nucleus are hallmarks of these diseases irrespective of their pathogenesis pathways (16, 27-32). These inclusions are also enriched with ubiquitin, chaperones and even proteasome subunits (13). This observation indicated that most of the poly-Q expanded proteins are likely to be associated with DNA-dependent transcription regulation, as well as neurogenesis (33).

The X-linked motor neuron disease, spinal bulbar muscular atrophy (SBMA) as listed in Table 1.1, is caused by an expansion of the poly-Q tract of the androgen receptor protein (AR) (20). AR is a member of the nuclear receptor superfamily, regulating gene expression by the levels of androgen (34). It was suggested that the pathogenesis may be induced by androgen activation of a mutant AR via the ligand-binding region although its exact mechanisms are still unknown (35-37). The Huntingtin protein (Htt), associated with HD is involved in certain important transcriptional pathways, namely CBP/p300. cAMP response element-binding protein (CREB) binding protein (CBP) was first detected with Htt aggregates (38). It was later shown that Htt and CBP interact via their poly-Q stretches and that an expanded poly-Q region of Htt interferes with CBP-activated gene expression, while over-expressed CBP rescued poly-Q-induced toxicity in cultured cells (39, 40).

Other evidence appears to contradict the central idea, *i.e.*: poly-Q aggregates being the main toxic species. Some studies observed that certain poly-Q diseases showed the absence of visible cellular inclusions despite cell specific vulnerability to the disease (41). This suggests the possibility that the major toxic species may not be the large aggregates, rather the soluble intermediates such as misfolded beta-rich poly-Q monomers or polymers (41-45). This view is aligned with the concept that amyloids can also play a protective role in sequestering toxic misfolded protein conformers (13). It is also accepted that the expansion of the poly-Q region can also induce the self-assembly of its carrier protein or the surrounding protein domains (46, 47). This leads to possible pathogenic interactions and formation of toxic protein

species. As a result, insoluble amyloid-like oligomers may be formed while also sequestering both the wildtype and expanded proteins along with it (48). It is also very possible that pathogenesis can occur through an imbalance of the association of the mutant protein with its cellular partners (13). As such, this may result in self-assembly and functional alterations, leading to toxicity and neuronal death (13).

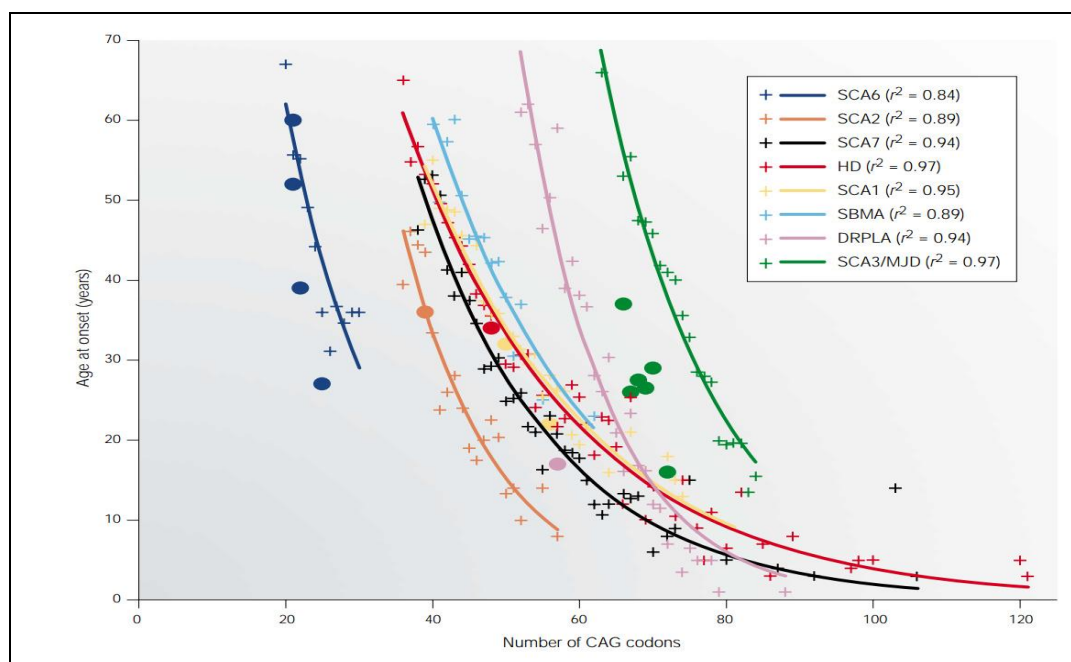


Figure 1.1 The relationship between the poly-Q repeat length and the age of disease onset in patients with poly-Q disorders. An inverse exponential correlation between repeat length and age at onset is evident in these poly-Q disorders (49). Huntington's disease (HD) is shown as red, while SCA3 is shown as green.

1.4 MJD1 gene product, Ataxin-3 protein

1.4.1 Structure of Ataxin-3

It is established that the protein context of a poly-Q protein does play a major role in poly-Q disease pathogenesis (15). The aim of this thesis is to understand the protein of interest, ataxin-3, in order to elucidate the mechanisms leading to the debilitating neurodegenerative disease, SCA3. Figure 1.2 shows a schematic representation of the different domains of ataxin-3. Ataxin-3 is a 42-kDa modular protein that is ubiquitously expressed throughout the body (50). It contains an N-terminal globular Josephin domain, followed by two ubiquitin-interacting motifs

(UIM). A nuclear localisation sequence (NLS) is situated before the expandable poly-Q domain, followed by a hydrophobic stretch of amino acids in the C-terminal tail region (11, 51-53). The Josephin domain is a de-ubiquitinating enzyme (DUB) (54-58), with a predominantly α -helical fold, typical of a cysteine protease (51, 52, 57, 59).

The active site of Josephin (Cys14, His119 and Asn134) catalyzes ubiquitin chain cleavage (55, 60-62). The poly-Q domain tract is unstructured in solution (63, 64). Ataxin-3 has two alternatively spliced isoforms with differences at its C-terminus. The ataxin-3 transcript used in this thesis belongs to the first isoform described by Kawaguchi *et. al.* (14) and is termed as 2UIM. Another splice variant was subsequently isolated and found to encode a third UIM (3UIM) in the C-terminal region instead of the hydrophobic tail (65, 66). Both isoforms are expressed in human SCA3 diseased brains (53, 66) but the extent and level of expression of each isoform has yet to be fully determined.

There are also several motifs found within the protein that suggests ataxin-3 cell localisation. The NLS has been suggested to attribute nuclear import activity (18, 19). However, deleting the sequence resulted in no significant change in the localisation of the ataxin-3, hence questioning its role in the function of the protein (67, 68). The two nuclear exporting signal (NES) motifs in Josephin have been shown to have active nuclear export activity (18, 69). In 2005, Nicastro *et. al.* (57) solved the solution structure of the Josephin domain, shown in Figure 1.3. The Josephin domain is reported to be highly conserved from humans to *Caenorhabditis elegans* (62). The catalytic triad is highlighted in red (51, 60), similar to cysteine proteases (57) and the domain has been implicated in the binding of Rad23 and histones (70). The three tryptophan residues (W87, W120, W130) are highlighted in orange in both Figures 1.2 and 1.3.

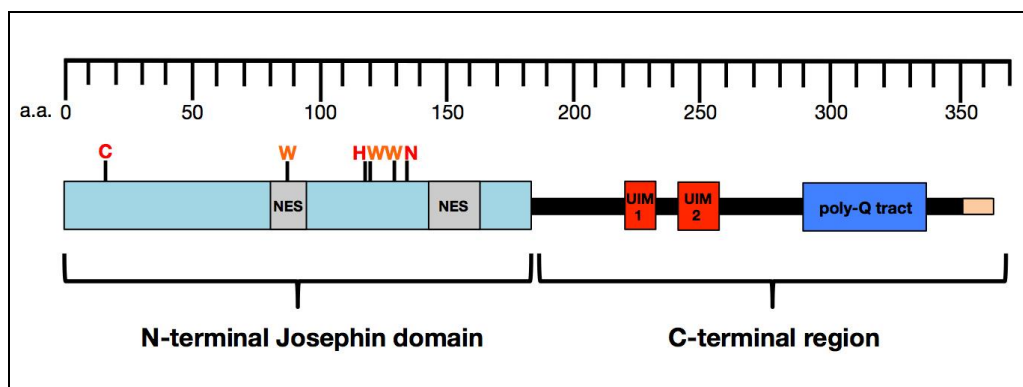


Figure 1.2: Schematic representation of the ataxin-3 protein. The wild type ataxin-3 (isoform 2UIM) protein is adapted from (50) and illustrated here with 362 amino acids, with a poly-Q tract length (blue) of 15Qs. The active site at C14, H119 and N134 (red) of the Josephin domain (light blue) catalyses the cleavage of poly-Ub chains. The domain consists of two NES motifs and three tryptophan residues are at W87, W120 and W130 (orange). The C-terminal region consists of two UIM motifs and the variable length poly-Q tract. The location of the hydrophobic tail is highlighted in beige.

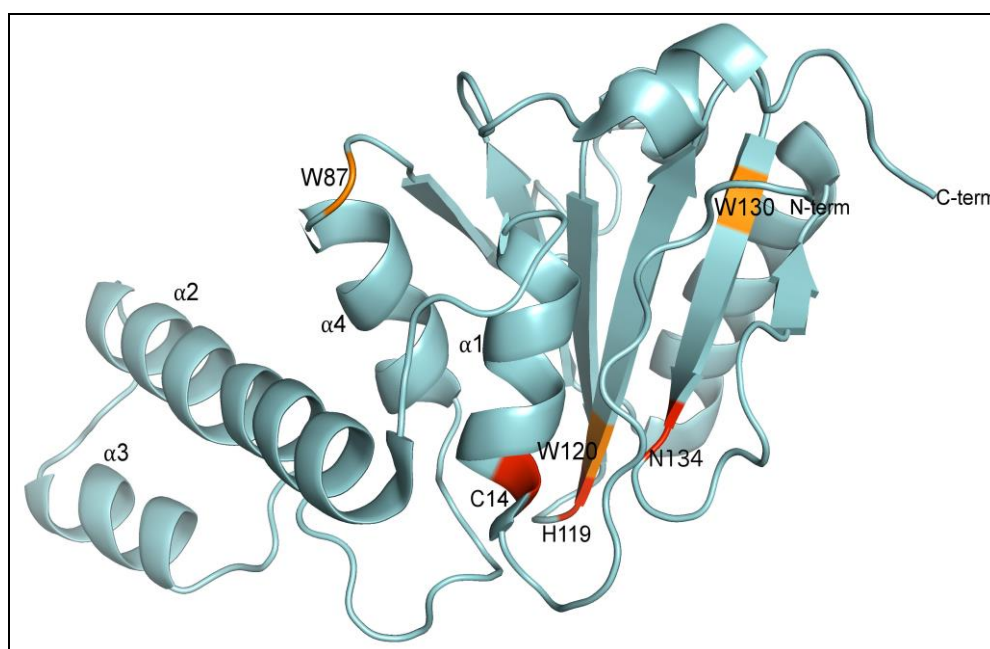


Figure 1.3: The solution structure of Josephin domain Structural determination of nuclear magnetic resonance (PDB code: 1yzb)(57) shows a predominant α -helical fold that is typical of cysteine proteases. The catalytic triad is highlighted in red while the three tryptophan residues are in orange. The flexible hairpin consists of both α 2- α 3 helices.

1.4.2 Biological roles of ataxin-3

1.4.2.1 Protein degradation

One of the many functional roles suggested for ataxin-3 is in the regulation of protein degradation through de-ubiquitination. Ubiquitination is a cascade that essentially involves the activating enzyme (E1) in transferring proteins to ubiquitination conjugating enzymes (E2). Ubiquitin ligase (E3) proceed to ligate ubiquitin from the lysines of the protein via isopeptide linkages (71). The editing of polyubiquitin (poly-Ub) chains and recycling of ubiquitin is necessary for cellular homeostasis (72).

Ataxin-3 has been known to cleave poly-Ub chains *in vitro* (70). It was shown that it preferentially cleaves linear, lysine 63 (K63) linked ubiquitin (Ub) chains (73). K63-linked Ub chains are thought to be involved in autophagy and possibly results in the biogenesis of protein inclusions (72). Poly-Ub chains have been shown to bind to the UIMs of ataxin-3 with near similar affinities, with UIM1 having a slightly stronger affinity (60, 73, 74). Interestingly, the Josephin domain was shown to contain two mono-ubiquitin binding sites using nuclear magnetic resonance (NMR) spectroscopy (69). These two binding sites are hydrophobic and their binding affinities are found to be both weaker, compared to the either of UIMs (69).

The deubiquitinating (DUB) activity of ataxin-3 in the ubiquitin proteasome pathway (UPP) correlates to its association to the ubiquitin-like domains, hHR23A and hHR23B (69, 70, 75). These proteins are involved both in DNA repair pathways and the directing of ubiquitinated proteins to the proteasome for degradation (75). Ataxin-3 has also been found to bind to valosin-containing protein (VCP)/p97 protein (70, 75, 76). The protein complex was mapped to bind to a potential arginine/lysine rich motif that lies before the poly-Q tract of ataxin-3 (77). VCP/p97 is known to regulate misfolded protein from the endoplasmic reticulum (ER). Indeed, the ataxin-3-VCP/p97 complex is thought to assist targeted proteins to the proteasome (78). The ability of ataxin-3 to edit poly- and monoubiquitin chains, as well as interact with proteins associated with protein degradation, implicates ataxin-3 playing an important role in the UPP.

1.4.2.2 Transcriptional regulator

Apart from its putative role and function in the UPP, ataxin-3 has been proposed to be involved in transcriptional regulation. Ataxin-3 interacts with several transcription factors such as TATA box-binding protein-associated factor (TBP) (79), CBP, p300, p300/CBP-associated factor (PCAF) (80-82). This interaction is proposed to result in the inhibition of transcription in specific promoters by either blocking access to histone acetylation sites or through the recruitment of histone deacetylases (82, 83). Through co-immunoprecipitation experiments, p300, CBP and KAT2B/PCAF was shown to bind to a leucine zipper motif that was proposed to be located in the poly-Q containing C-terminal region of ataxin-3 (83). Ataxin-3 is also postulated to regulate transcription complexes, such as the C-terminal HsP70 interacting protein (CHIP) through ubiquitination (84). Ubiquitination of transcription factors by E2 ligases allows ataxin-3 to be recruited to the CHIP complex, stimulating the transcription of the targeted DNA. Hence the de-ubiquitination of mono-ubiquitinated transcription factors by ataxin-3 will repress transcription completely (27, 84).

1.5 Protein misfolding is a main feature of ataxin-3 pathogenesis

As mentioned previously, the characteristic hallmark of SCA3 is the presence of neuronal inclusions that contains the mutant ataxin-3 protein (8, 15). This evidence supports the hypothesis that ataxin-3 protein aggregation is a central feature to its pathogenesis.

1.5.1 Protein folding and quality control

Only about two decades ago, it was shown that a simple protein develops its most stable native structure under suitable physiological conditions (85). It was established that a polypeptide is more likely to undergo a stochastic search of possible conformations than mandatory steps between partially folded states (86, 87). Dobson

and his team suggested that the native-like interactions between different residues within the polypeptide take on a lower energy state. This state is more favourable compared to one involving non-native like interactions (86-88). The rapid and efficient protein folding is proposed to depend on the amino acid sequence of the protein to enable this process (86, 87). A simplified protein folding landscape is illustrated in Figure 1.4

Transition states in this folding landscape have been shown to be important (87). They are critical regions of energy surfaces through which all molecules must pass to reach the native fold. Studies show that these transition states facilitate and allow the formation of partially folded intermediates as a result of the intermediate structure's inability to overcome significant kinetic barriers as it travels down the landscape (Figure 1.4). The consequences would render a protein to be misfolded and possibly exposing residues that enhance aggregation (86, 87).

Another folding mechanism that has been proposed especially for larger proteins (> 100 residues) is folding in 'modules'. It has been suggested that certain protein sequences adopt a specific structural fold, which different domains fold independently of each other, resulting in the formation of one or more intermediates (24, 89). Along with these factors, preferential hydrophobic and polar residues are often favoured and play a role in determining essential elements of folding. These interactions altogether stabilise the protein structure, acting as a quality control process to avoid protein misfolding (86).

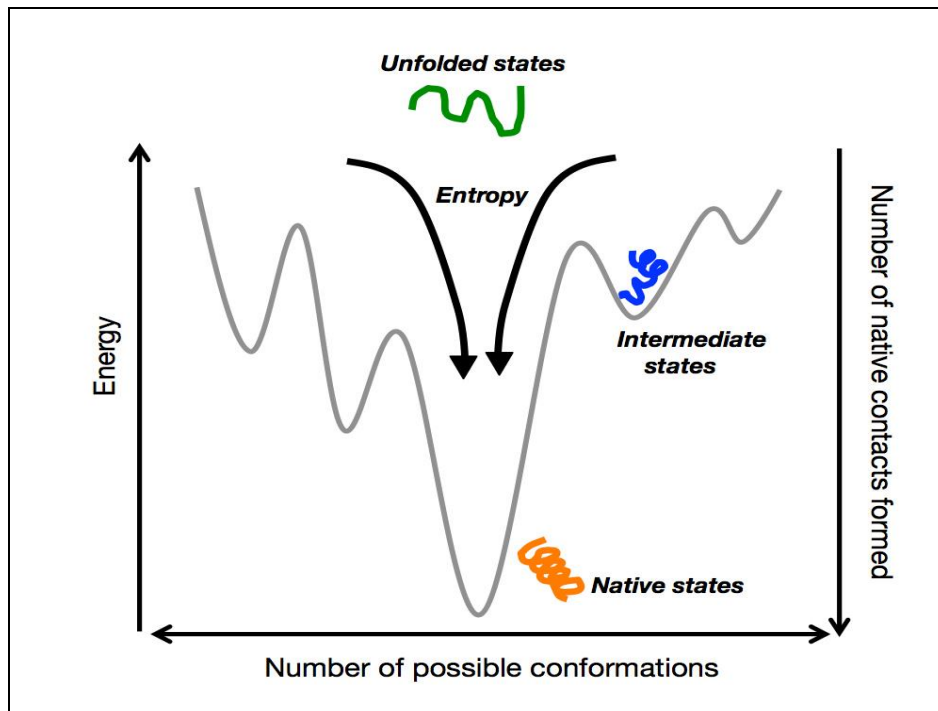


Figure 1.4 The protein folding energy landscape Unfolded proteins transit towards the native folded states, indicated by the ‘funnel’ effect and pass through critical ‘saddle points’. The saddle point corresponds to the transition state where all proteins will have to pass in order to fold to its native state (86, 87). Partially folded intermediates become trapped in these saddle points when they are unable to overcome barriers kinetically (87).

In a cellular environment, the interactions between molecules in different conditions increase the complexity of the energy landscape. There are several quality control processes that further ensure the efficiency of protein folding within the cell. The majority of the proteins synthesized from the ribosome are subject to folding within the cytoplasm, or at the mitochondrial or endoplasmic reticulum (ER) compartments. The ER contains a significant number of molecular chaperones and protein folding is assisted by molecular chaperones (90, 91) they work in tandem to ensure efficient protein folding. Unlike certain classes of peptidylprolyl isomerases, where they act as folding catalysts (92), most molecular chaperones (*e.g.* heat shock proteins) do not increase the rate of protein folding but assist in the folding process (93). The chaperonic effect is evident especially during cellular cell stress, reducing competing reactions such as aggregation and even ‘rescuing’ misfolded proteins by helping them to refold again (90, 91, 93). Proteins recognised as misfolded are designated for degradation through the ubiquitin-proteasome system (94). This

regulation mechanism ensures that only properly folded proteins are sent for glycosylation at the Golgi apparatus (95, 96). Overall, these processes all depend on folding and unfolding of protein events (87, 97, 98). A malfunctioning of these systems will lead to disease and even accumulation of protein deposits within the cell or extracellular space (86, 98). In the next half of the chapter, the formation of these protein deposits will be examined.

1.5.2 Protein aggregation and fibril formation

In spite of a variety of proteins that are involved in aggregation diseases, the structure of fibrils is found to be remarkably similar (99). Amyloid fibrils share the same dye-binding properties, such as Congo Red or Thioflavin-T (ThT) dyes, optical properties and appear very similar in size and structure under the electron microscope (100). Temussi *et. al.* (101) discussed the possibility of a shared mechanism between the proteins that cause neurological protein disorders. They described some structural differences between amyloid- β ($A\beta$) and poly-Q fibrils. For AD, the amyloid precursor protein, APP is cleaved by different secretases to form $A\beta$ peptides. These peptides, especially $A\beta$ (1-42) peptide then readily aggregate and seed the formation of fibrils and neurotoxic plaque formation (102). On the other hand, expanded poly-Q tract proteins are prone to aggregate, regardless of the location of the poly-Q domain within the respective protein and neurotoxicity is also observed when nuclear inclusions are formed (Table 1). Thus, a common trait between these two neurodegenerative disorders is the structural transition of polypeptide chains from the native fold to a misfolded conformation (101).

Current literature on poly-Q peptide structures reports that they adopt random coil or unstructured conformations, irrespective of their poly-Q tract length. When the length of glutamine residues extends beyond a threshold, the native conformation of the poly-Q tract is destabilised and fibril formation is promoted (103-105). Under X-ray diffraction, amyloid fibrils structures consist mainly of β -sheet conformations (101, 106). Studies have shown that poly-Q chains can form anti-parallel β -strands through hydrogen bonds with side and main chain amides, forming polar zippers, despite the technical difficulties in studying poly-Q peptide structure (107, 108).

When these polar zippers interact intermolecularly, aggregates form. Another possible model for poly-Q fibre was subsequently proposed, whereby the fibre is formed by a single cylindrical β -sheet, stabilized by backbone and side-chain hydrogen bonds (109, 110). End stage fibrils of mutant poly-Q proteins, such as Htt and ataxin-3 observed under transmission electron microscopy (TEM), are found to be large and long in length (101, 111). The width of each poly-Q fibril strand can measure up to 100 nm or more (58, 111). Figure 1.5 shows the fibril morphology of ataxin-3 (Q64) after a 100 h incubation period at 37 °C (58).

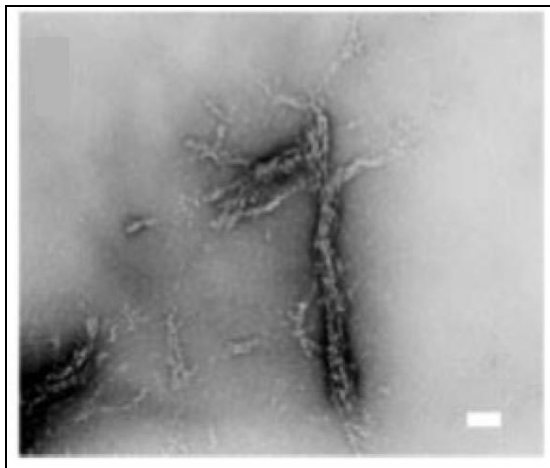


Figure 1.5 Negative stained electron micrograph of typical ataxin-3 fibrils (64). Large and filamentous fibrils were formed after a 100 h incubation at 37 °C. Scale bar = 100 nm (58).

Poly-Q disorders are the most common of the dynamic repeat expansion diseases. As a class, poly-Q diseases share common toxic features that is triggered by the expansion of the poly-Q tract (112) (Table 1.1) . The propensity for poly-Q proteins to misfold, oligomerise and form intracellular aggregates is one classical hallmark shared among all ten poly-Q disorders, making class wide therapeutics quite targetable. Yet, each poly-Q disorder has its own characteristic pathology and clinical symptoms. Each poly-Q protein has different protein domains, giving rise to unique biological functions, suggesting the specific protein context plays a significant role in the pathogenesis of each disease (101).

1.5.3 Ataxin-3: Protein context and its two-stage aggregation pathway

In early *in vitro* studies, expanded poly-Q tract ataxin-3 was found to form insoluble β -rich fibrils (16, 17, 113) and was sensitive to amyloid-specific dyes (114). It was shown that upon destabilization of ataxin-3 by temperature, denaturing agents or pressure, non-pathological polyQ tract length of ataxin-3 could also form aggregates (115, 116). In another study, under partially destabilizing conditions, the Josephin domain itself was found to form amyloid-like aggregates (117). Josephin fibrils were also observed to be rather large, adopting a more curvilinear fibrillar structure (117). They also observed by circular dichroism (CD) and NMR spectroscopy that the Josephin domain did not interact with the C-terminus of ataxin3 (117). A subsequent finding further corroborated this result that the expansion of the poly-Q tract does not destabilise the native conformation of ataxin-3 (115). This indicated that while the expanded poly-Q tract can play a toxic role, the protein context, such as the presence other domains within the structure of ataxin-3 also play important roles in ataxin-3 pathogenesis (58, 117, 118).

A two-step mechanism has been proposed for ataxin-3 aggregation and is illustrated in Figure 1.6 (58). The first stage is thought to involve the self-association or dimerisation of the Josephin domain (44, 58, 119). The Josephin domain was found to retain most of its secondary structure when a subtle change in its conformation pushes it to fibril assembly (119-121) and forming SDS-soluble, ThT fluorescence reactive protofibrils (58, 122). The first stage of the ataxin-3 aggregation pathway does not involve the poly-Q tract, hence all non-expanded ataxin-3 also forms SDS-soluble fibrils and are ThT reactive. Stage 1 aggregates have been shown to have aggregation kinetics that is characteristic of a nucleation-dependent process (103, 122). Expanded ataxin-3 undergoes the first stage of the pathway as well and at a faster aggregation kinetics compared to non-expanded ataxin-3 (58). The expanded poly-Q tract drives the formation of the Stage 2 SDS-insoluble fibrils as the poly-Q regions interact in a concentration-dependent manner (122).

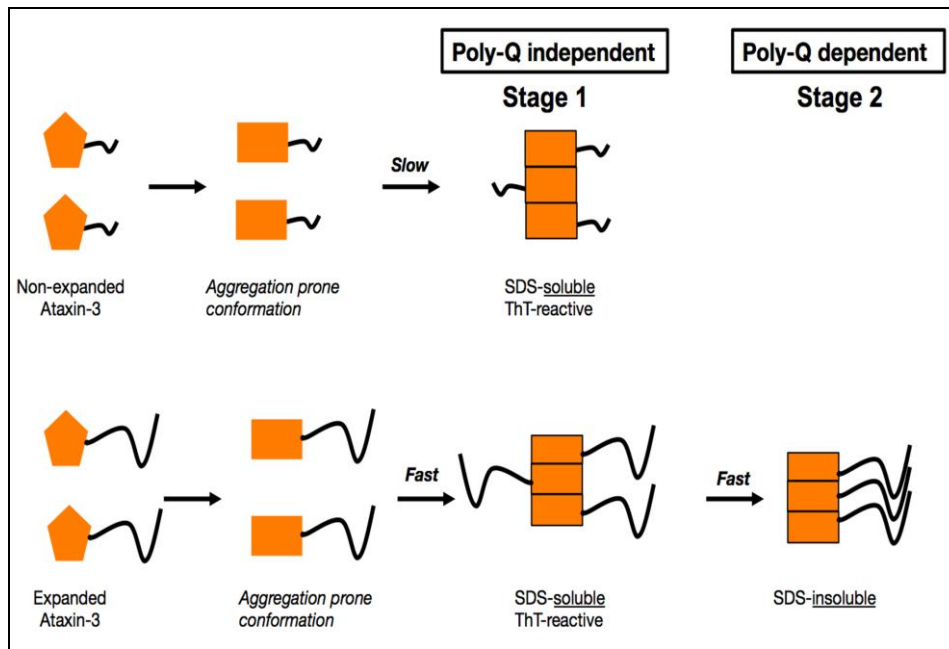


Figure 1.6 The ataxin-3 two-stage model aggregation pathway The native Josephin domain is represented by the hexagon (orange) and its subtle changes results in an aggregate prone conformation (orange rectangles). The tail in black represents the C-terminus region. The figure was adapted from (58).

Studies show that while the Josephin domain plays a role in initiating the aggregation process of ataxin-3, its C-terminal region (the UIMs and the poly-Q tract) contribute significantly to the aggregation of the full-length ataxin-3 protein (64, 123, 124). An expanded poly-Q tract appears to additionally lead ataxin-3 to subsequent rapid, highly stable fibril formation, even though the neighbouring, non poly-Q domains predispose ataxin-3 for aggregation (13). It would be interesting to observe if fragments of ataxin-3, minus the Josephin domain, could also drive the formation of fibrils with other ataxin-3 molecules, resulting in SDS-insoluble fibrils.

1.5.4 Ataxin-3 proteolysis and aggregation

Proteolytic cleavage of poly-Q proteins has been proposed as one of the pathogenic mechanisms towards disease progression (11, 15, 125). Poly-Q containing fragments derived from proteolysis were observed in several poly-Q related diseases, such as SCA1, 2, 3, 6, 7, 17 and HD (125). Expanded poly-Q Htt exon-1 fragments induced toxicity when aggregated in cell models (126). Mice models also displayed disease phenotypes when expanded poly-Q Htt exon-1 fragments were expressed

(127). The evidence suggests that the N-terminal poly-Q containing fragment of the Htt protein was sufficient to induce pathogenesis *in vivo* (127). A hypothesis proposed for the initiation of aggregation of poly-Q disease related proteins by its proteolytically derived fragments is commonly known as the 'toxic fragment hypothesis' (11, 125, 128, 129). This aggregation process is often related to inclusion formation and cellular dysfunction, as poly-Q fragments are often detected within these inclusions (56, 130-133). Likewise, mice model expressing poly-Q containing ataxin-3 fragments resulted in the development of more severe ataxic phenotypes, compared to mice expressing full-length ataxin-3 protein that displayed mild phenotypes (134). Transgenic SCA3 mice showed accumulation of a truncated C-terminal ataxin-3 fragment and the authors suggested proteolysis by an unknown protease was involved (135). Subsequent studies showed ataxin-3 fragments having a high propensity to aggregate in cell culture, forming inclusions with its full-length counterparts and resulting in cytotoxicity (67, 129).

The cysteine protease, caspase, was first proposed to play a role in poly-Q protein proteolysis (136). Caspases are known to cleave proteins at specific aspartate residues (137) and are part of the apoptotic signaling pathway (138). Its activation has been associated with proteolysis of Htt (125). Indeed, it has been shown that Htt is susceptible to proteolysis by a few caspases, from caspase-1, caspase-3, caspase-6 and caspase-8 (125). More specifically, caspase-3 was found to induce Htt fragmentation (136) while caspase-6 was suggested to mediate neurodegeneration *in vivo* (133). Correlating the studies of caspase proteolysis on Htt, Berke and colleagues showed using cell culture that SDS-insoluble aggregates were formed upon ataxin-3 cleavage with caspase-1 and caspase-3 (132). The aggregate formation appears to be diminished when respective caspase inhibitors were introduced (132). However, when the experiments were conducted in our laboratory *in vitro* (data not shown), we found that both caspases had little or no proteolytic effect on non-expanded and expanded ataxin-3 proteins. This result from our laboratory was corroborated by other studies that showed caspase cleavage of ataxin-3 was much less efficient compared to other poly-Q proteins, such as Htt and atrophin-1 (136, 139). Subsequently, caspase-1 and -3 inhibitors were unable to inhibit aggregate formation in a SCA3 patient derived induced pluripotent stem cell (iPSC) cell line (140).

It has been reported that another cysteine protease that is activated by intracellular Ca^{2+} is involved in poly-Q diseases, especially in SCA3 (125). Human calpain-1 and -2 are ubiquitously distributed throughout in cells (141). Both proteases are heterodimeric and each has a 78 kDa catalytic subunit and a common 29 kDa regulatory subunit. Both proteases are activated by Ca^{2+} and they differ by their sensitivities to micromolar free Ca^{2+} and calpain-2 is activated by a higher Ca^{2+} concentration (141). Using sequence homology comparison, calpain-2 was identified to be a cysteine protease (142) with part of its catalytic triad residue Cys105 found in the subdomain IIa, while other residues His262 and Asn 286 are found in the subdomain IIb (143, 144). It is suggested that a calcium-induced conformational change draws the two subdomains closer, allowing the catalytic triad residue Cys and His to be functional (141). Recently, Haacke *et. al.* observed that ataxin-3 was susceptible to calpain-2 cleavage, and that inhibition of calpain-2 activity suppresses the proteolytic cleavage of ataxin-3 and the generation of expanded poly-Q fragments (56). In another study, it was shown that temporary increases of intracellular Ca^{2+} levels in pluripotent stems cells resulted in the activation of calpain-2 proteases that initiated ataxin-3 proteolysis, giving rise to the formation of the ‘early aggregates’ or fragments that precede SDS-insoluble aggregate formation (140). Hübener and colleagues demonstrated in mice brain homogenates and cell culture that over-expressed ataxin-3 is specifically cleaved by calpain-2 (145). In line with these studies, calpain-2 is suggested to be one of the main modulators of ataxin-3.

Increasing studies have suggested that proteases preferentially cleave pathological length of poly-Q proteins (127, 134, 146). As a result, there is a high probability of an increased population of expanded poly-Q containing fragments leading to inclusion body formation within the cell (15). Pathological Htt was shown to be more susceptible to proteolysis by calpain-2 than non-pathological Htt (146). Similarly, only mutant atrophin-1 fragments were released to aggregate in the nucleus (147) and expanded AR protein was shown to be sensitive to caspase-3 in a poly-Q repeat-length dependent manner (148). Hübener and colleagues also suggested that over-expressed expanded poly-Q length ataxin-3 in cells could be more susceptible to calpain-2 cleavage (145). However, no study has yet to accurately establish if expanded poly-Q proteins are more prone to proteolysis. As the above-mentioned

studies suggest, understanding the mechanisms of proteolysis of ataxin-3 would enable further development of potential therapeutics for SCA3 disease.

1.5.5 Influence of osmolyte on ataxin-3 aggregation

Osmolytes, also known as “chemical chaperones”, are small organic molecules found in all kingdoms of life and increase the ability of cells to adapt to osmotic stresses (149-151). Osmolytes do not negatively interfere with the structure or the function of biological molecules (149, 151, 152). There are two classes of osmolytes, either protecting or denaturing. An example of a denaturing osmolyte is urea, which thermodynamically destabilise proteins but can reduce aggregation at the same time (153, 154). It is suggested that urea molecules bind to the peptide intra-backbone by hydrogen bonds, resulting in destabilising and unfolding of the protein (155). Within the protecting class of osmolytes, there are the (i) polyols such as glycerol, sucrose, trehalose and other sugars; (ii) amino acids including proline, glycines and (iii) methylamines, such as betaine, sarcosine and tri-methylamine N-oxide (TMAO). In our study, we are interested in the naturally occurring, protecting osmolyte, TMAO (151) and its effects on protein aggregation.

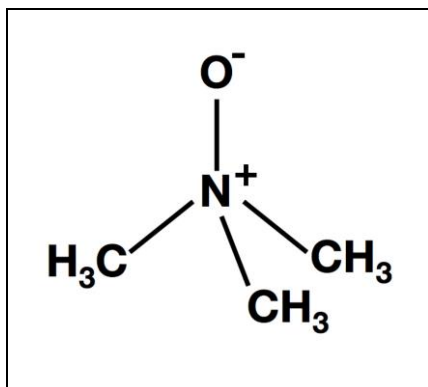


Figure 1.7 Structure of TMAO The ‘chemical chaperone’, TMAO is a naturally occurring osmolyte, used often to counter the effect of urea in protein folding experiments.

TMAO is known to be a strong protein ‘stabiliser’, commonly used in biotechnology (156). Its chemical structure is illustrated in Figure 1.7. Protein stabilisers generally act by ‘preferential exclusion’. The feature of preferential exclusion is described simply as exhibiting a tendency to be excluded from the protein hydration shell (a layer of water molecules bound to the protein surface) (151, 157). This effect tends to stabilise the protein’s structure as the protein folds more

compactly, especially α -helical secondary structures, to reduce exposed surface areas (150, 151, 158). However, the exact forces associated with preferential exclusion of TMAO are not fully understood. There is a current understanding that TMAO possibly binds water molecules strongly at its oxygen moiety and its methyl groups forms a lattice of water molecules (158, 159). It is suggested that this enhanced water structure of TMAO does not allow exposed peptide backbone to dissolve in solution, displaying an effect called ‘osmophobicity’ and favouring protein folding (160, 161). One study used environmental stresses to explain the accumulation of specific osmolytes in an organism and its ability to oppose particular stress conditions (162). Certain polyols, such as glycerol and sucrose are said to oppose desiccation and high salt concentrations respectively. Methylamines, like TMAO appear to oppose the deleterious effects of urea in cells in a 2:1 TMAO: urea ratio (150, 162). Interestingly, it was suggested that TMAO also neutralise structures such as glutamine amino acids as they were proposed to adopt a urea-like denaturing activity in solvents (163, 164). In cells that is undergoing protein misfolding or neurodegeneration, TMAO can be used to stabilise aberrant misfolding.

TMAO has been used in a number of protein misfolding studies (150, 165) and the results have yielded variable results. Interestingly, the α -helical prion protein, PrP was converted to a soluble β sheet structure molecule in the presence of TMAO at high temperatures (166). TMAO was observed to induce secondary structure of an intrinsically disordered C-terminal tau fragment, resulting in aggregation and enhanced microtubule activity (167). For α -synuclein protein, TMAO induced mixed folding at different concentrations, whereby a partial intermediate was formed at low concentrations while high concentrations of TMAO resulted in compact folding of the protein to form oligomers (168). On the other hand, TMAO prevented the misfolding of mutant cystic fibrosis transmembrane conductance receptor protein (CFTR) (169). Mutant CFTR is associated with cystic fibrosis which causes a dysfunction in ion channels and fluid retention (170). Most importantly, it was previously demonstrated in another study, that TMAO reduced aggregation of ataxin-3 poly-Q containing fragments expressed in cell culture (171). At present, there is little evidence on the modulation of TMAO on full-length ataxin-3. It would be fundamental to establish if TMAO can stabilise the ataxin-3 and result in the inhibition of aberrant misfolding and aggregation.

1.6 Aims of this study

The poly-Q protein, ataxin-3 and its aggregation have been of interest in a number of studies over the years. More recently, the subject and interest in the ‘toxic fragment hypothesis’ was raised when ataxin-3 was found to be cleaved by calpain-2. The toxic effect of the ataxin-3 derived fragments, in particular the C-terminal region containing the poly-Q domain, was demonstrated in cell culture and mice models (67, 129, 134). At present, it is unclear if the poly-Q tract length modulates calpain-2 proteolysis of ataxin-3, possibly resulting in the formation of expanded poly-Q fragments being released into the cell environment. The aim of this thesis was to conduct a detailed analysis of the ability of these ataxin-3 derived, C-terminal region fragments to initiate and accelerate the aggregation of full-length ataxin-3 proteins. In addition, the osmolyte, TMAO has been previously shown to reduce aggregation of ataxin-3 fragments but no study has yet been conducted to analyse its effects on the full-length protein. We hypothesise that ataxin-3 protein and its misfolding is controlled by a variety of factors and/or modulators. This thesis aims to investigate the effect of specific modulators on ataxin-3 protein aggregation by:

- (a) Examining if poly-Q tract expansion leads to increased calpain-2 proteolysis by determining the kinetic parameters of proteolytic cleavage *in vitro* (Chapter 3).
- (b) Expressing and characterising the ataxin-3 ‘toxic fragment’ and using it to test whether it can accelerate full-length ataxin-3 aggregation (Chapter 4).
- (c) Characterising ataxin-3 aggregation and DUB function in the presence of TMAO (Chapter 5).

CHAPTER 2

MATERIAL AND METHODS

2.1 Chemicals and Reagents

All chemicals and reagents were purchased from companies located in Australia, in the state of Victoria unless otherwise stated.

Enzymes used for molecular biology were obtained from Promega and New England Biolabs.

Phenylmethyl sulphonyl fluoride (PMSF), lysozyme, Thioflavin T (ThT), β -mercaptoethanol (BME), ethylenediamine tetraacetic acid (EDTA), guanidium hydrochloride (GuHCl), guanidinium thiocyanate (GuSCN), trimethylamine-N-oxide (TMAO), Tris(hydroxymethyl)aminomethane (Tris), benzamidine hydrochloride and ampicillin (Amp) were all purchased from Sigma Aldrich Co, New South Wales (NSW), Australia.

The ThT and GuHCl were prepared analytically by weight and passed through a 0.22 μm filter. The concentration of TMAO in Tris buffer was determined from the refractive index of the prepared solution (Section 2.1.1).

Benzenesulfonyl fluoride hydrochloride (AEBSF) under the trade name *Pefabloc*, complete protease cocktail EDTA-free tablets (CPC) and deoxyribonuclease I (DNase I) were purchased from Roche.

The isopropyl- β -D-thiogalactopyranoside (IPTG) was prepared analytically by weight and purchased from Astral Scientific (NSW, Australia).

The N,N,N',N'-Tetramethylethylenediamine (TEMED) and ammonium persulfate (APS) were obtained from ICN (now known as MP Biomedicals, NSW Australia).

Enzymatic chemiluminescence reagents (ECL) were obtained from GE Lifesciences (NSW, Australia).

2.1.1 Determining the concentration of TMAO in Tris buffer

An amount for TMAO was measured accordingly to make up 3.5 M TMAO. TMAO salts were dissolved in 10 mL 1x Tris Buffered Saline (TBS). The pH of solution was adjusted to 7.4 at 37 °C. Once the salts are dissolved completely, the concentration of TMAO was determined using a hand refractometer and its corresponding refractive index. The index is indicated as Δn and is applied to the equation that is provided by the refractometer manufacturer's instructions:

Where $\Delta n = B$ (value from TMAO) – A (value from 1x TBS alone)

$$\text{Concentration of TMAO (in M)} = -0.0038 + 103.3151 (\Delta n) - 259.43 (\Delta n)^2 \quad (\text{Eq.2.1})$$

2.2 Microbial Techniques

2.2.1 Growth Media

The media used for bacterial growth was 2YT [16 g/L tryptone, 10 g/L yeast, 5 g/L NaCl], and also on occasions, SOC media [20 g/L tryptone, 5 g/L yeast, 0.5 g/L NaCl, 2.5 mM KCl, 20 mM glucose (added after autoclaving)] was used.

Agar plates were prepared by the addition of 1.5 % (w/v) agar to 2YT medium prior to autoclaving. Ampicillin was added to the media at a concentration of 0.1 mg/mL once the solution had cooled to below 50 °C post-sterilization.

2.2.2 Bacterial Strains

The bacterial strain JM107 was used for general cloning and plasmid maintenance. DH5 α bacterial strain was used for Gateway® (Life Technologies) BP and LR combination reactions. NovaBlue Competent Cells (Novagen) were used for transformation of products of Quikchange site-directed mutagenesis. For protein expression, BL21 (DE3) was used for the pET21a (SpA-242Ataxin-3 variants) and pLIC vectors (ataxin-3 variants).

2.3 Molecular Biological Techniques

2.3.1 Expression vectors

Gateway® Technology (Life Technologies) utilized a recombination system where genes of interest can be transferred from an entry vector to a variety of destination or expression vectors, termed as ‘clones’. All Gateway® cloning methods were used according to the manufacturer’s instructions. The ataxin-3 fragment, with TEV cleavage site at its N-terminal was first amplified and cloned into the entry vector, pENT21. It was recombined with pre-engineered destination vectors, pDEST-His-ZZ, pDEST-His-Z_Z. The entire construct was finally recombined to a protein expression vector, pExp. The pET vector 21a (Novagen) was used for the incorporation of a native B domain of Protein A as a fusion partner to the ataxin-3 fragment.

2.3.2 Primers

All oligonucleotides were purchased from Geneworks (Australia). 40 nmol of freeze-dried PCR/Sequencing grade oligonucleotides were obtained and reconstituted in sterile ddH₂O to a final concentration of 100 µM and stored at -20 °C. The letter ‘n’ denotes the polyQ length of 15 or 64 residues. The primers are listed below.

Primers	Function	Sense/Antisense	Sequence (5’-3’)
5'At3242SpeI	Amplifies fragment from residue 242 of ataxin-3 from existing pLIC ataxin-3 full-length vector	Sense	gactagtgaaaatctgtatttt cagggcatggaagatgagg aagcagatctc
Braudattbat33'	Amplifies the 3' end of ataxin-3 from existing pLIC ataxin-3 full-length vector	Antisense	gggggggggaccactttgt acaagaaagctgggtcttat gtcagataaagtgtgaaggt
242 Fragment BamHI	Amplifies the 242Ataxin-3 fragment with BamHI restriction site at the 5' end from Z-TEV-242At2-Z construct	Sense	gcaggttcggaatccgaga atctttat

242 Fragment XhoI	Amplifies the 242Ataxin-3 fragment with XhoI restriction site at the 3' end from Z-TEV-242At2-Z construct	Antisense	caagaaagcctcgagttatg tcagata
SpA242At3Qn KETTA	QuikChange mutagenesis of first 5 a.a. of S-peptide to C'terminal end of 242 fragment	Sense	cttcacactttatctgacaaaa gaaaccgctgcttaactcga gcaccaccac
SpA242At3Qn KETTA	QuikChange mutagenesis of first 5 a.a. of S-peptide to C'terminal end of 242 fragment	Antisense	gtggtggtgctcgagttaag cagcggtttcttttgcagata aagtgtgaag
SpA242At3Qn AKFER	QuikChange mutagenesis of next 5 a.a. of S-peptide to C'terminal end of 242 fragment	Sense	gacaaaagaaaccgctgct gctaaattcgaacgtaactc gagcaccaccac
SpA242At3Qn AKFER	QuikChange mutagenesis of next 5 a.a. of S-peptide to C'terminal end of 242 fragment	Antisense	gtggtggtgctcgagttagc gttcgaatttagcagcagcg gtttctttgtc
SpA242At3Qn QHMSD	QuikChange mutagenesis of final 5 a.a. of S-peptide to C'terminal end of 242 fragment	Sense	ctgctgctaaattcgaacgcc agcacatggacagctaactc gagcaccaccac
SpA242At3Qn QHMSD	QuikChange mutagenesis of final 5 a.a. of S-peptide to C'terminal end of 242 fragment	Antisense	gtggtggtgctcgagttagct gtccatgtgctggcgttcgaa tttagcagcag

2.3.3 Polymerase Chain Reaction

Amplification of DNA was performed by the polymerase chain reaction (PCR) in a Corbin Research Thermal Cycler using the oligonucleotides in Section 2.3.2. *Pfu* DNA polymerase (Promega) was used for all PCR reactions.

General PCR conditions

Reagents	Stock	Final Concentration	Volume (μL)
Pfu DNA polymerase buffer	10x	1x	2.5
Primers (Sense, antisense)	10 μM	500 nM	1.25
dNTP's	2 mM	200 μM	2.5
DNA template	400 ng/μL	10-500 ng	0.5
<i>Pfu</i>	3 u/μL	3 u	0.5
ddH ₂ O	-	-	to 25

Temperature cycling, where $X=5^{\circ}\text{C}$ below the melting temperature of the primer

Step	Temperature	Time	Cycles
Initial Denaturation	85°C	1 min	1
Denaturation	95°C	1 min	
Annealing	X°C	1 min	30
Extension	72°C	2 min/kb	
Final Extension	72°C	2 min/kb	1
Hold	25°C	-	-

2.3.4 QuikChange™ mutagenesis

The QuikChange™ (Stratagene) method was used to introduce restriction sites and short segments of the S-tag within the template DNA of the ataxin-3 fragment (242Qn). Complementary primers containing the mutation of interest were used to amplify the whole plasmid (Section 2.3.2). The enzyme, *DpnI*, digests the methylated parental DNA and leaves the unmethylated mutated PCR product. The mutated DNA is subsequently transformed and the *E. coli* machinery repairs the nick.

QuikChange™ PCR conditions

Reagents	Stock	Final Concentration	Volume (μL)
Pfu DNA polymerase buffer	10x	1x	2.5
Primers (Sense, antisense)	10 μM	320 nM	1.25
dNTPs	2 mM	200 μM	2.5
DNA template	50 ng/μL	50 ng	0.5
<i>Pfu</i>	3 u/μL	3 u	0.5
ddH ₂ O	-	-	to 25

Temperature Cycling:

Step	Temperature	Time	Cycles
Initial Denaturation	95°C	1 min	1
Denaturation	95°C	1 min	
Annealing	X°C	1min	Y
Extension	72°C	2 min/kb	
Final Extension	72°C	2 min/kb	1
Hold	25°C	-	-

$X = 5^{\circ}\text{C}$ below the melting temperature of the primers

$Y =$ The number of cycles were dependent on the nature of the insertion. 18 cycles were used for the introduction of single mutations and restriction sites and 20 cycles were used for insertion of short segments of S peptide DNA sequence.

Dpn1 digest

PCR product	20 μ L
Buffer (10x)	2.5 μ L
<i>Dpn</i> 1	1 μ L
ddH ₂ O	1.25 μ L

Reactions were incubated at 37 °C for 2 h. 5 μ L of the reaction mixture was then used to transform 50 μ L of NovaBlue™ (Novagen) competent cells. Resulting colonies were screened to confirm the presence of the insertion.

2.3.5 Agarose gel Electrophoresis

A 50x TAE stock solution was prepared [242 g Tris, 57.1 mL glacial acetic acid, 100 ml 0.5 M EDTA, pH 8.0]. To 1x TAE, a final concentration of 1 % (w/v) or 2 % (w/v) of agarose (Promega) was added and dissolved by heating. The solution was cooled before pouring into a DNA gel frame with comb and allowed to set. The gel frame was then placed into the tank containing 1x TAE. The samples were mixed with 1 μ L EZ-Vision™ One (Amresco) and loaded into the wells. Electrophoresis was performed at a constant voltage of 100 V until the dye front had reached the bottom. DNA was then visualized using UV light and bands measured against a 1K base pair DNA ladder (NEB).

2.3.6 Restriction Enzyme digestion

Restriction enzyme digests of PCR products and plasmids were performed using enzymes and their respective buffers from Promega and New England Biolabs (NEB).

Double digest reaction setup:

DNA (PCR product/plasmid)	30 μ L
Buffer (10x)	5 μ L
Enzyme 1	5 μ L
Enzyme 2	5 μ L
BSA (100x)	0.5 μ L
ddH ₂ O	To 50 μ L

Double digest reactions with BamH1 and Xho1 were performed with compatible buffering systems. Digests were typically incubated for 3 hours at 37 °C.

2.3.7 Gel purification

To obtain purified DNA fragments prior to ligation, the fragment of interest was excised from an agarose gel and gel purification performed using the Wizard PCR and Gel purification kit (Promega) according to the manufacturer's instructions.

2.3.8 Ligations

T4 DNA ligase and the 10x ligation buffer (Promega) were used for the ligation reactions. For cohesive end ligations, 1:3 or 3:1 molar ratios of vector to insert were used. The ligation reactions were incubated at room temperature for 3 hours. The amount of insert required for each molar ratio was determined using the equation below:

$$\frac{\text{ng vector} \times \text{size of insert (kb)}}{\text{size vector (kb)}} \times \text{molar ratio} = \text{ng insert} \quad (\text{Eq.2.2})$$

2.3.9 Plasmid purification

All expression plasmids contained genes conferring ampicillin resistance to host cells. 5 mL of 2YT media was inoculated with *E. coli* cells containing the plasmid of interest. The cells were grown overnight in a shaking incubator at 37 °C. Plasmid DNA was purified using a Wizard Plus SV Miniprep DNA purification system (Promega) according to the manufacturer's guidelines.

2.3.10 Preparation of competent cells

Competent cells were prepared using rubidium chloride method of Hanahan (1972).

Transformation Buffer	Components
1	100 mM Rubidium Chloride, 50 mM Manganese Chloride, 10 mM Calcium Chloride, 30 mM Potassium acetate, 15 % (w/v) Glycerol, pH 5.8.
2	10 mM Rubidium Chloride, 75 mM Calcium Chloride, 10 mM MOPS, 15 % (w/v) Glycerol, pH 6.8

Solutions were filter sterilized (0.2 μm) and stored at 4 °C. A scraping of cells from a glycerol stock was added to 5 mL 2YT media and allowed to grow overnight at 37 °C. 500 μL of the starter culture was used to inoculate 50 mL of 2YT in a 250 mL flask and incubated at 37 °C under shaking conditions until the optical density at 600 nm (OD_{600}) was approximately 0.5. The culture was then chilled on ice for 10 min. The cells were pelleted at 3000 rpm for 10 min. The supernatant was discarded and the cells re-suspended in 15 mL of Transformation buffer 1. The cells were allowed to incubate on ice for 15 - 30 min and then pelleted again. The cell pellet was then re-suspended in 4 mL of Transformation buffer 2 and allowed to incubate on ice for 15 min. Cells were aliquoted into 100 μL volumes, snap frozen in a dry ice/ethanol bath and immediately transferred to - 80 °C for storage.

2.3.11 Bacterial transformations

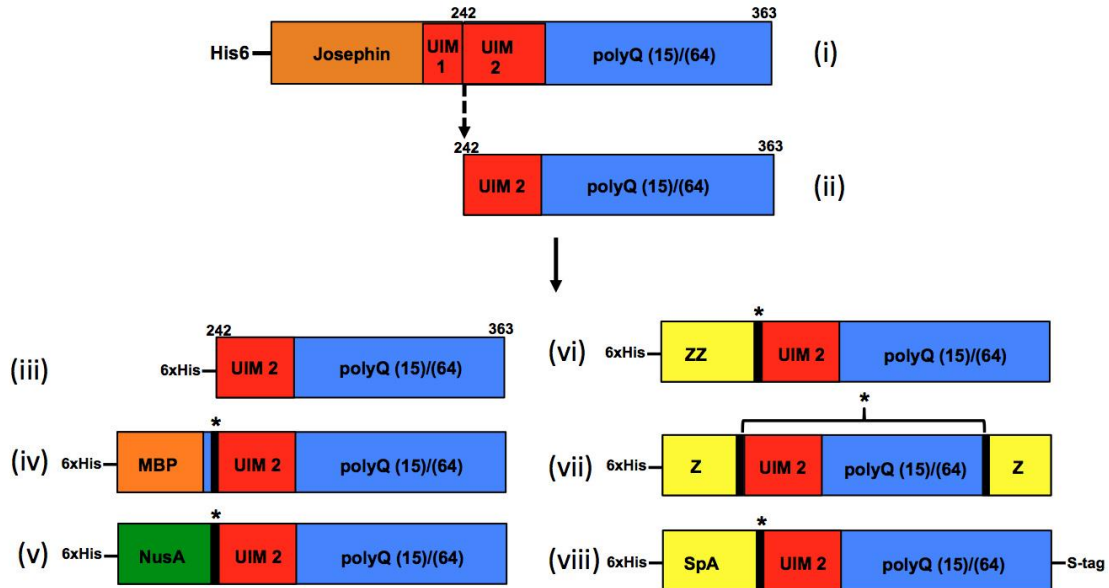
One μL of purified plasmid or 5 μL of PCR product/ligation product was added to 100 μL of competent *E. coli* cells and incubated on ice for 30 min. The cells were heat-shocked at 42 °C for 90 sec and then incubated on ice for 2 min to recover. When PCR products were transformed, cells were allowed to recover for 1 h in 150 μL of SOC media at 37 °C, 200 rpm. Cells were then plated onto 2YT agar plates containing 0.1 mg/mL Amp and incubated at 37 °C for 12 - 16 h.

2.3.12 Colony screening

Transformants were screened by restriction enzyme digestion in reactions where a novel restriction site was introduced. For confirmation of restriction site or point mutation insertion, positive transformants of the reactions were submitted to Micromon DNA sequencing centre (Microbiology department, Monash University). Samples were set up as follows:

DNA	500 ng
Primer	0.5 pmol
Big Dye Terminator v3.1	1 μL
10x Taq Buffer	2 μL
ddH ₂ O	To 20 μL

2.4.2 Constructs engineered and used for protein expression



The ataxin-3 fragment (242) DNA sequence (ii) was amplified from (i) and cloned into expression vectors as described in Section 2.3 and/or according to manufacturer's instructions. The fragment was cloned into Gateway™ vectors (Life Technologies) for (iii), (iv), (v), (vi) and (vii). The fragment was cloned into pET21a vector (Novagen) for (viii). DNA sequencing was conducted to check for the correct sequence and poly-Q length of the fragments. Different fusion partners were used to test for solubility, expression and the extent of proteolysis during and after the purification process. Maltose-binding protein (light orange box) and N-utilisation substance protein A (green box) were first tested but solubility of the fusion protein was low. The engineered B domain of Protein A (*Staphylococcus aureus*) was incorporated as a double (ZZ) (yellow box, vi) and single (Z) (yellow box, vii) domain to the construct (ii), before incorporating into a Gateway™ expression vector. However, the proteolysis was still evident. The final fusion partner chosen is the single B-domain, SpA that is fused to construct (ii) and cloned into the expression vector pET21a, forming the final construct (viii). This construct will be referred to as (SpA242Qn) fusion protein.

2.4.3 Buffers or solutions

2.4.3.1 Ataxin-3 proteins purification

Buffer	Components
Lysis	50 mM NaH ₂ PO ₄ , 300 mM NaCl, 1 mM BME, 0.1 % (v/v) Triton X-100, pH 8.0.
Wash	50 mM NaH ₂ PO ₄ , 300 mM NaCl, 1 mM BME, 0.1 % (v/v) Triton X-100, 20 mM imidazole, pH 8.0.
Elution	50 mM NaH ₂ PO ₄ , 300 mM NaCl, 1 mM BME, 0.1 % (v/v) Triton X-100, 250 mM imidazole, pH 8.0.
Final Storage	Tris buffered saline with glycerol (TBSG): 100 mM Tris-HCl, 80 mM NaCl, pH 7.4 (at 37 °C) with 10 % (v/v) glycerol 100 mM Tris-HCl, 80 mM NaCl, pH 7.4 (at 37 °C) without 10 % (v/v) glycerol (TBS)

2.4.3.2 (SpA242Qn) proteins purification

Buffers	Components
Dilution	50 mM Tris, 90 mM NaCl, pH 8.0
Unfolding	6.18 M Guanidine hydrochloride, 50 mM Tris, 90 mM NaCl, 20 mM BME, pH 8.0
Equilibration	6.18 M Guanidine hydrochloride, 50 mM Tris, 90 mM NaCl, 20 mM BME, 20 mM imidazole, pH 8.0
Wash	6.18 M Guanidine hydrochloride, 50 mM Tris, 90 mM NaCl, 20 mM BME, 20 mM imidazole, pH 8.0
Elution	6.18 M Guanidine hydrochloride, 50 mM Tris, 90 mM NaCl, 20 mM BME, 250 mM imidazole, pH 8.0
Refolding	100 mM TrisHCl, 80 mM NaCl, pH 7.4 (at 37 °C) with 10 % (v/v) glycerol (TBSG)

2.4.4 Expression of ataxin-3 variants

Ataxin-3 (Q64) and Josephin variants in pExpLicHis vector were expressed in BL21 (DE3) *E. coli* cells. 2YT supplemented with 0.1 mg/mL ampicillin was inoculated with these cells and grown for 12 - 16 h at 37 °C, 180 rpm. This culture was added to 2YT media at 1 % (v/v) and grown at 37 °C, 180 rpm until OD₆₀₀ ~ 0.6. Protein expression was induced by the addition of IPTG to a final concentration of 0.5

mM and the bacterial cultures incubated for a further 4 h at 28 °C, 180 rpm. Cells were harvested by centrifugation at $2,429 \times g$ and pellets re-suspended in lysis buffer (Table 2.4.2.1) and stored at - 80 °C.

2.4.5 Expression of (SpA242Qn) fusion ataxin-3 variants

(SpA242Qn) fusion ataxin-3 variants in pET21 vector were expressed in BL21 (DE3) *E. coli* cells. 2YT supplemented with 0.1 mg/mL ampicillin was inoculated with these cells and grown for 12 - 16 h at 30 °C, 180 rpm. This culture was added to 2YT media at 1 % (v/v) and grown at 37 °C, 180 rpm until $OD_{600} \sim 0.6$. Protein expression was induced by the addition of IPTG to a final concentration of 0.5 mM and the bacterial cultures incubated for a further 4 h at 28 °C, 180 rpm. Cells were harvested by centrifugation at $2,429 \times g$ and pellets re-suspended in lysis buffer (Table 2.4.2.1) and stored at - 80 °C.

2.4.6 Expression of TEV protease

The double mutant TEV protease (L56V/S135G) established by our group was selected and the expression of His₆-tagged TEV protease is described by Cabrita *et.al.* (173). This highly soluble mutant protease was favoured, as it has been shown that its activity is maintained and not compromised.

2.4.7 Purification of ataxin-3 variants and the Josephin protein

The cell lysate was thawed and incubated with lysozyme (1.4 mM), DNase 1 (0.1 mg/mL) and Pefabloc (0.5 mg/mL) for 20 min at 4 °C. Cells were sonicated and additional Pefabloc (0.5 mg/mL) was added. Lysed cells were centrifuged at $47,808 \times g$ rpm for 30 min at 4 °C. The pellet was discarded and the supernatant collected and filtered through a 0.45 µm filter. 10 % (v/v) p-aminobenzamidine agarose was then added to the lysate and incubated on a rotary orbitor for 1 h at 4 °C. The flow through was collected and Pefabloc (0.5 mg/mL) and imidazole (10 mM) were added. This solution was loaded onto a 5 mL HisTrap HP column (Amersham) that was pre-

equilibrated with wash buffer. The column was washed with 10 column volumes of wash buffer using an ÄKTA FPLC system (Amersham), and then eluted with an imidazole gradient from 20 mM (wash buffer) to 250 mM (elution buffer). 1 mL fractions were collected and analysed by SDS-PAGE. Appropriate fractions were pooled and Pefabloc (0.5 mg/mL) was added. The protein was then loaded onto a Hiload Superdex™ 200 prep grade column that was pre-equilibrated with TBSG or TBS. Fractions were collected as they eluted and the presence of purified protein verified by SDS-PAGE. Protein was obtained at >95 % purity. The protein was concentrated using an Amicon Ultra (Millipore) centrifuge concentrator with a 10 kDa molecular weight cut off. The protein was filtered through a 0.45 µm filter, aliquoted and stored at - 80 °C.

2.4.8 Unfolding of SpA242Ataxin-3 variants inclusion bodies

The cell lysate was thawed and incubated with lysozyme (1.4 mM), DNase 1 (0.1 mg/mL), Pefabloc (0.5 mg/mL), benzamidine-HCl (0.5mg/ml) and one CPC tablet, for 20 min at 4 °C. Cells were sonicated and further Pefabloc (0.5 mg/mL) added. Lysed cells were centrifuged at 47,808 $\times g$ for 30 min at 4 °C. The pellet was retained and re-suspended into 0.5% (v/v) Triton-X in dilution buffer using a glass rod. Pefabloc (0.5mg/ml), benzamidine-HCl (0.5mg/ml), one CPC tablet and lysozyme (1.4mM) was added to the solution and incubated in ice for 10 min. The suspension was sonicated again until the solution appears homogenous in texture and was centrifuged at 7,649 $\times g$ for 20 min at 4 °C. The pellet was centrifuged three times, at 4,303 $\times g$ for 20 min at 4 °C by washing twice with 0.5% (v/v) Triton-X in dilution buffer and a final rinse with dilution buffer alone. The pellet was weighed and dissolved at 2.5 g per 40 ml unfolding buffer. The inclusion bodies were incubated to unfold on a rotary orbitor for 16 h at 4 °C. The solution was finally centrifuged at 38,724 $\times g$ for 45 min at 4 °C. The supernatant was collected and filtered through a 0.45 µm filter before use.

2.4.9 Refolding and purification of (SpA242Qn) ataxin-3 variants

A 5 mL HisTrap HP column (Amersham) was pre-equilibrated with equilibration buffer. The unfolded inclusion bodies solution was injected onto the column at 1.0 mL/min. The column was washed with 10 column volumes of wash buffer using an ÄKTA FPLC system (Amersham) at 2.0 mL/min. The column was eluted with an imidazole gradient from 20 - 250 mM. Proteins were eluted at 50 mM imidazole and 0.5 mL fractions were collected and analysed by SDS-PAGE. Fractions were pooled and the protein solution and loaded onto a Hiloal Superdex™ 16/60 column of either 75 or 200 prep grade (pre-equilibrated with TBSG) at 1.0 mL/min. As the unfolded protein material passes through the column, the protein refolds according to its free energy state and the controlled process of diluting out the denaturant. Fractions were collected as refolded proteins eluted and the presence of purified protein verified by SDS-PAGE under non-denaturing conditions. The fractions were tested with ThT fluorescence to pool only the non-aggregating proteins. Protein was obtained at >95 % purity and non-ThT reactive fractions were pooled. The protein was concentrated using an Amicon Ultra (Millipore) centrifuge concentrator with a 10 kDa molecular weight cut-off.

2.4.10 Purification of TEV protease

The double mutant TEV protease (L56V/S135G) was purified accordingly as described by Cabrita *et.al.* (2007). The enzyme activity was determined using its specific substrate UBL-GST under the conditions also described by Cabrita *et.al.* (173).

2.4.11 Determination of protein concentration

The concentration of ataxin-3 variants and Josephin was determined by measurement of Abs₂₈₀ and a bicinchoninic acid (BCA) assay (Pierce). The BCA assays were performed according to the manufacturer's instructions using bovine serum albumin (BSA) as a protein standard. Extinction coefficients (ϵ) for all ataxin-3

variants and Josephin were obtained by using their amino acid sequences to determine it on an online tool, ProtParam on ExPASy (<http://web.expasy.org/protparam/>).

The concentration of (SpA242Qn) ataxin-3 proteins was determined by measurement of the intrinsic fluorescence of Protein A fusion unfolded in 5M guanidine thiocyanate (GnSCN). Control protein A (SpA) and SpA-fusion ataxin-3 proteins were unfolded in 1/50 dilution of 5M GnSCN for 30 min at room temperature. Triplicate samples of each were performed at excitation wavelengths of 295 nm and a scan of emission wavelengths from 320 - 450 nm on a Horiba Jobin-Yvon fluorimeter at 25 °C. Fluorescence intensities were recorded and measured the relative concentrations of (SpA242Qn) ataxin-3 variants based on the molarity of SpA.

2.5 Analytical Techniques

2.5.1 SDS-PAGE

15 % Tris-glycine SDS-PAGE were used for the analysis of (SpA242Qn) ataxin-3 variants and 12.5 % Tris-glycine SDS-PAGE was used for the analysis of ataxin-3 variants.

Solutions required for preparation of Tris-glycine gels

Buffer	Components
4x Resolving gel	1.5 M TrisHCl, pH 8.8.
4x Stacking gel	0.5 M TrisHCl, pH 6.8.
SDS Running tank	0.025 M TrisHCl, 0.192 M glycine, 0.1 % (w/v) SDS, pH 8.3.

General SDS-PAGE solutions

Buffer	Components
2x Loading buffer	0.125 M TrisHCl, 20 % (v/v) glycerol, 4 % (w/v) SDS, 0.2 M DTT, 0.02 % (w/v) Bromophenol Blue, pH 6.8.
0.2 M stain solution (w/v)	40 % (v/v) methanol, 7 % (v/v) acetic acid, 0.025% (w/v) Coomassie brilliant blue (R250).
De-stain solution	40 % (v/v) methanol, 7 % (v/v) acetic acid.

Components of two Tris-glycine SDS-PAGE gels

	<i>Resolving Gel (v/v)</i>		<i>Stacking Gel (v/v)</i>
	<i>12.5 %</i>	<i>15 %</i>	<i>4 %</i>
Bis-acrylamide (monomer) (mL)	4.12	4.94	0.44
4x Resolving buffer (mL)	2.50	2.50	-
4x Stacking buffer (mL)	-	-	0.83
10 % w/v SDS (μL)	100.0	100.0	33.0
ddH ₂ O (mL)	3.18	2.36	2.03
25 % (w/v) APS (μL)	60.0	60.0	20.0
TEMED (μL)	4.0	4.0	3.0

2.5.2 Size exclusion chromatography

Size exclusion chromatography (SEC) was carried out on an ÄKTA FPLC (Amersham). The elution profiles of Josephin, ataxin-3 variants and fusion (SpA242Qn) ataxin-3 proteins were analysed using a Superdex™ 75 and 200 10/300 gel filtration column (Amersham), pre-equilibrated with TBSG buffer and elution monitored by Abs₂₈₀ detection. In experiments monitoring the effects of TMAO on the aggregation of ataxin-3 variants and Josephin, samples were taken at indicated times and insoluble aggregates removed by centrifugation at 13,000 rpm. The supernatant was injected onto a Superose™ 12 HR 10/30 column (Amersham) that had been pre-equilibrated with TBSG.

In Chapter 5, SEC was carried out in a similar fashion as described above. Aggregate formation was monitored by the loss both the monomer and void peaks on a Superose™ 12 column. SEC was carried out on ÄKTA FPLC (Amersham). At indicated time points, protein was removed from the assay, centrifuged for 10 min at 13,000 rpm at 4 °C and then the supernatant was injected onto the column. The elution profile was monitored by absorbance at 214 nm and the peak areas were calculated utilizing Origin® 7 to fit Gaussian curves. Both prior and post centrifugation samples were removed for transmission electron microscope (TEM) analysis.

2.5.3 Transmission Electron Microscopy (TEM)

All samples designated for TEM analysis was prepared by staining with 1% (w/v) uranyl acetate solution. The image processing was carried out at the Monash Centre for Electron Microscopy.

2.5.4 Circular Dichroism

All far-UV circular dichroism (CD) studies were performed on a spectropolarimeter (model: Jasco 810) that was kept thermostatted by a Jasco peltier. For secondary structure analysis, measurements were performed using a 0.01 cm path length quartz cuvette. The spectra were measured from 190 - 260 nm using a scan speed of 50 nm/min and three scans accumulated for each sample. Far-UV CD measurements were converted to molar ellipticity (θ) using the equation:

$$[\theta]_{MW} = \frac{\theta_{obs}}{10 \cdot l \cdot c} \quad (Eq.2.3)$$

Where l is the pathlength (cm), C is the protein concentration (M) and θ_{obs} is the CD signal in millidegrees. The units for molar ellipticity are mdeg.cm².dmol⁻¹. To estimate the secondary structural contributions, the SpA-polyQ far-UV CD spectra were de-convoluted using the K2D algorithm available at the online DICHROWEB facility

Far-UV CD analysis was carried out by adding ataxin-3 proteins to the appropriate TMAO concentrations in TBS in Chapter 5. This solution was briefly vortexed and left to equilibrate for 5 min. All spectra were measured on a Jasco-810 spectropolarimeter with a path length of 0.1 mm. Spectra were recorded from 190 - 260 nm, using a 5-s/point signal averaging, and a scan speed of 50 nm/ min.

2.5.5 Western blotting

Solutions and buffers for Western blotting

Buffer	Components
1X Transfer	50mM Tris, 20 mM glycine, 0.01% SDS
Blocking	5 % skim milk powder in blotting buffer
Blotting	20 mM TrisHCl, 0.2 M NaCl, pH 7.4.
Tween-Wash	20 mM TrisHCl, 0.2 M NaCl, 0.5 % (v/v) Tween, pH 7.4.

Primary antibody solutions used:

- 1) Mouse anti-His₆ tag (Serotec), 1:5000 dilution in blotting buffer containing 0.5 % (w/v) BSA.
- 2) Mouse anti-S-tag (Millipore), 1:40,000 dilution in blotting buffer containing 0.5 % (w/v) BSA.

Western blotting was carried using the mini Trans-Blot® electrophoretic transfer system (Bio-Rad). The content of the SDS-PAGE gel is transferred across to a nitrocellulose membrane for duration of 1 h at 250 mA or 30mA if overnight at cool temperatures. The membrane is incubated with blocking buffer for 2 h and then washed. Primary antibody is utilized to probe for the protein of interest for duration from 2 h at room temperature to overnight at 4 °C, depending on the specificity of the antibody. The membrane is first washed before being probed by the HRP-linked secondary antibody and followed by enhanced chemiluminescence (ECL) developing detection system (Pierce).

2.5.6 N-terminal peptide sequencing

Solutions for N-terminal peptide sequencing

Buffer	Components
1X Transfer	10mM CAPS, 15% methanol, pH 11.0, ultrapure water
Membrane stain	0.025% Coomassie © Blue R-250 dissolved in 40% methanol and ultrapure water
Membrane de-stain	50% methanol and ultrapure water

The SDS-PAGE was performed in similar conditions as mentioned in section 2.5.1. For N-terminal peptide sequencing, the Western blotting protocol was followed except the buffers were all prepared with ultrapure water. The SDS-PAGE gel was “pre-run” for 10 min before the samples were loaded. Sequi-Blot™ PVDF (Bio-Rad) membrane was pre-equilibrated with 100 % methanol before use. After the transfer was completed, the membrane was rinsed with distilled water. The membrane was stained for 5 minutes before de-staining it until the background became light blue. Samples were sent for analysis at the Peptide Biology Laboratory, Monash University.

2.5.7 Membrane filter trap assay

Solutions for filter trap assay

Buffer	Components
Stability	4 % (w/v) SDS, 100 mM DTT
Blocking	5 % skim milk powder in blotting buffer
Blotting	20 mM TrisHCl, 0.2 M NaCl, pH 7.4
Tween-Blotting	20 mM TrisHCl, 0.2 M NaCl, 0.5 % (v/v) Tween, pH 7.4.

Primary antibody solutions used:

- 1) Mouse anti-His₆ tag (Serotec), 1:5000 dilution in blotting buffer containing 0.5 % (w/v) BSA.
- 2) Mouse anti-S-tag (Millipore), 1:40,000 dilution in blotting buffer containing 0.5 % (w/v) BSA.

Protein aliquots were diluted into stability buffer at a 1:1 (v/v) ratio. The samples were heated for 5 min at 100 °C and then diluted to 200 µL with 2 % (w/v) SDS. 100 µL of each sample was filtered through a pre-equilibrated cellulose acetate membrane (Schleicher and Schuell, 0.2 µm) using a Bio-Dot SF microfiltration unit (Bio-Rad). The membrane was washed twice by filtering through 150 µL of 0.1 % (w/v) SDS. The membrane was incubated in blocking buffer for 1.5 h and then rinsed with Tween-blotting buffer. The membrane was soaked for 1.5 h in a solution of the primary antibody with blocking buffer containing 0.5 % (w/v) BSA. The membrane was washed thrice in Tween-blotting buffer at 10 min each. The membrane was further incubated for 1.5 h in the secondary antibody with blotting buffer containing

0.5 % (w/v) BSA. The membrane was then washed again with Tween-blotting buffer (3 x 10 min). The blot was treated with ECL (Amersham) reagents for 1 min and then exposed onto film for the appropriate time durations in a Hypercassette™ (Amersham), which was then developed in a Fuji Processor FPM-100A.

2.5.8 Mass Spectrometry sample preparation

Ataxin-3 variant proteins were incubated with 50 nM calpain-2 in 100 mM Tris, 50 mM NaCl, 10 mM CaCl₂, pH 7.8 and 1 mM dithiothreitol (DTT). The reactions were incubated at 22°C for 30 min and were stopped with 10 mM EDTA. Samples were desalted to remove impurities using C8 or C18 extraction discs. Fusion ataxin-3 proteins (SpA242Q15) and (SpA242Q64) were also sent for analysis after its purification. All samples were sent for mass spectrometry (MALDI) at the Peptide Biology Laboratory, Monash University.

2.6 Assays involving protein aggregation and cleavage

2.6.1 Ataxin-3 variants

Ataxin-3 variants were incubated at a concentration of 20 µM in TBSG or TBS (pH 7.4) and also in TMAO buffer containing 2 mM PMSF, 5 mM EDTA and 15 mM BME, depending on the assay. Samples were incubated at 37 °C under non-shaking conditions in airtight containers to eliminate evaporation. At various time points, samples were removed and assayed as described in the relevant results sections.

2.6.2 (SpA242Qn) Ataxin-3 fusion proteins

(SpA242Qn) ataxin-3 fusion proteins were incubated at varying concentrations from 0 - 20 µM in TBSG (pH 7.4) buffer containing 2 mM PMSF, 5 mM EDTA and 15 mM BME. Samples were incubated at 37 °C under non-shaking conditions in microcentrifuge tubes to eliminate evaporation. At various time points, samples were removed and assayed as described for SDS-PAGE, Western blotting, membrane filter trap assay and TEM.

2.6.3 QBP1 peptide assays

The QBP1 peptide has an amino acid sequence of SNWKWWPGIFD (Nagai YT 2000) as purchased from AusPep. The peptide was obtained in a lyophilized form that was solubilised in a solution of 50 % dimethyl sulfoxide (DMSO)/50 % sodium acetate buffer to a concentration of 8 mM. QBP1 was incubated at a final concentration of 120 μ M or at a 6:1 peptide:protein molar ratio for the aggregation assays. As controls, final DMSO concentrations found to solubilise QBP1 were added to protein solutions (*i.e.*: without QBP-1 peptide). Proteins did not show any significant effect of the DMSO addition.

2.6.4 Calpain-2 cleavage on ataxin-3 variants

Ataxin-3 variants at 20 μ M were incubated with 50 nM recombinant rat calpain-2 (Calbiochem) in 100 mM Tris, 50 mM NaCl, 10 mM CaCl₂, 0.2% PEG-8000, pH 7.8 and 1 mM dithiothreitol (DTT). The reactions were started at 22 °C for 30 min and were stopped with 10 mM EDTA. The samples were analysed further by SDS-PAGE, Western blotting and MALDI.

2.6.5 TEV cleavage on (SpA-242Qn) fusion ataxin-3 variants

(SpA242Qn) fusion ataxin-3 variants at varying concentrations were incubated with TEV protease at 1:1 ratios in 1x TBSG pH 7.4 at 37 °C. The reactions were sampled at desired time points and reactions were stopped with SDS-PAGE 2x loading sample buffer with 1 mM DTT. Samples were boiled for another 5 min to completely inhibit the protease activity. The samples were analysed further by SDS-PAGE, Western blotting and membrane filter trap assay.

2.6.6 GST-Ub52 proteolytic assay in TMAO

The de-ubiquitinating (DUB) activity of ataxin-3 and Josephin was carried out as previously described (Chow et al 2004) with minor changes. The molar ratio of enzyme to substrate was 1:5 and the reaction buffer was 50 mM HEPES at pH 7.4, 50 mM EDTA, 1 mM DTT, with specified concentrations of TMAO. After incubation, the samples were analysed by SDS-PAGE and Coomassie Blue Staining.

2.7 Assays involving intrinsic fluorescence and peptide fluorescence

2.7.1 Kinetic analysis of Suc-LY-AMC peptide by calpain-2

The peptide Suc-LY-AMC (Calbiochem) was titrated in increasing concentrations from 0.02 to 1.0 mM in 100 mM Tris, 50 mM NaCl, 10 mM CaCl₂, 0.2% PEG-8000, pH 7.8 and 1 mM DTT with 50 nM calpain-2. The reaction was incubated at room temperature. Initial velocities obtained from the progress curves (time in seconds versus relative fluorescence intensities) are plotted against peptide concentrations to derive substrate K_S and V_S .

2.7.2 Kinetic analysis of ataxin-3 cleavage by calpain-2

Kinetic analysis was performed essentially as described by Blake *et. al.* (174). In this assay, complete hydrolysis of the substrate Suc-LY-AMC by calpain-2 was measured in the absence and presence of varying concentration of ataxin-3. Substrate cleavage was monitored using a Gemini EM MAX (Molecular Devices) using an excitation wavelength of 370 nm and monitoring the fluorescence emission at 435 nm. Progress curves would be obtained. The area under each the progress curve were analyzed by integration using GraphPad Prism 5.0. The difference in areas determined in the presence and absence of competitor ataxin-3 was plotted as a function of ataxin-3 concentration. The slope of the proportional dependence determined by linear regression. The kinetic parameters were then determined using the equations:

$$K_{Mapp} = \frac{K_s \cdot \ln(1/0.95)}{V_s \cdot [\text{Slope } \Delta t(5\%)]} \quad (\text{Eq. 2.4})$$

$$V_{maxapp} = \frac{K_s \cdot S_o - V_s K_{Mapp} (\text{Slope } \Delta \text{Area})}{K_s \cdot \text{Slope } \Delta \text{Area}} \quad (\text{Eq.2.5})$$

2.7.3 Thioflavin-T (ThT) fluorescence

2.7.3.1 Discontinuous ThT measurements

Samples were taken from the aggregation assays as described above and diluted in buffer containing 20 μM ThT. Samples were placed in quartz fluorescence cuvettes (Starna). The excitation wavelength was at 445 nm and the emission intensity was monitored at 480 nm. The spectrofluorimeters, Horiba Jobin-Yvon Fluoromax-4 and Perkin Elmer LS45, were alternated for use.

2.7.3.2 Continuous ThT measurements

ThT fluorescence was monitored using a BMG laboratories Fluostar Optima fluorescence plate reader. Continuous ThT fluorescence assays were set up for the aggregation reactions. 20 μM ThT was present for the reaction time course. Excitation and emission filters of 450 and 490 nm were used, respectively. The reactions were performed in black 384 clear-bottom well plates (Corning). Excitation emitted and emissions were read from the bottom of the plate. All reactions were incubated at 37 °C, without shaking, and the top of the plate was sealed to eliminate evaporation. The aggregation kinetics obtained from continuous plate reader assays performed in the presence of ThT were comparable to kinetic data obtained from discontinuous ThT measurements.

2.7.4 Ubiquitin-AMC protease activity assay

The DUB protease activity of ataxin-3 was measured against the fluorogenic substrate ubiquitin-AMC termed as Ub-AMC (Sigma-Aldrich). 0.5 μM of each ataxin-3 variant was pre-incubated in assay buffer (100 mM Tris, 50 mM NaCl, 10 mM CaCl_2 , 0.2 % PEG-8000 pH 7.8 and 2 mM DTT) containing either 0 M, 0.5 M or 1M TMAO at 37 °C for 20 min. The reaction was initiated by adding Ub-AMC to a

final concentration of 0.5 μM . The emission fluorescence was measured ($\lambda_{\text{ex}}=380$ nm) at 437 nm using slit widths of 2.5 nm and a 1 cm path length quartz cuvette (Starna). Fluorescence was read on the Horiba Jobin-Yvon Fluoromax-4 spectrofluorimeter.

2.7.5 Intrinsic fluorescence protein assays

All intrinsic fluorescence measurements were performed by preparing aliquots of protein samples at 20 μM with different concentrations of TMAO in TBS (pH 7.4). TBS and TMAO were mixed together and pre-equilibrated to 37 °C for 5 min before the addition of protein. Fluorescence spectra were immediately recorded on a Horiba Jobin-Yvon Fluoromax-4 spectrofluorometer within a thermostatted cuvette holder at 37 °C. A quartz cuvette with a 1 cm path length was used. The integration time was 0.2 s and the slit widths were 2 nm. The spectra were measured ($\lambda_{\text{ex}}=280$ nm) from 300 - 450 nm and were averaged over three accumulative scans.

CHAPTER 3

PROTEOLYSIS OF ATAXIN-3 IS INDEPENDENT OF POLYGLUTAMINE TRACT LENGTH

3.1 Introduction

SCA3 belongs to a group of nine poly-Q diseases, which also includes Huntington's disease. It is well established that these diseases share a common mode of pathogenesis, whereby expansion of the poly-Q tract above a specific repeat length threshold, culminates in protein misfolding and the formation of insoluble intracellular deposits containing the aggregated protein (29). The pathological hallmark of SCA3 involves the formation of nuclear inclusions (NIs), which contain misfolded and aggregated ataxin-3 (16, 29-32). Ataxin-3 is a 42-kDa multi-domain protein that appears to play an important role in its self-association as it aggregates via a two-stage mechanism (58). These inclusions have been shown to contain not only expanded ataxin-3 protein but ubiquitin and several other co-factors and interacting partners of the proteasome, as well as ataxin-3 fragments (70, 75).

Several studies have provided experimental evidence to suggest that proteolysis of ataxin-3 and other poly-Q-containing proteins also contributes to disease pathogenesis. Using cell models, expanded poly-Q fragments of Htt were shown to aggregate and were cytotoxic (126, 175), while transgenic mice expressing full-length poly-Q proteins, such as ataxin-3, develop milder phenotypes compared to transgenic mice expressing poly-Q-containing fragments of the respective disease proteins (134, 135). These data have led to the "toxic fragment hypothesis", which suggests that proteolytic production of poly-Q-containing fragments initiates the aggregation process associated with inclusion formation and cellular dysfunction (130-133, 136, 176). Haacke and colleagues observed that ataxin-3 was susceptible to calpain-2 cleavage, and that inhibition of calpain-2 activity suppresses the proteolytic cleavage of ataxin-3 and the generation of expanded poly-Q fragments (56). In addition, it was observed that calpain-2 preferentially cleaves pathological length Htt compared to non-pathological Htt, indicating that the poly-Q tract length could influence the susceptibility of the protein for cleavage by the enzyme (146). Similarly, only mutant atrophin-1 fragments were released to aggregate in the nucleus (147) and expanded androgen receptor (AR) protein was shown to be sensitive to caspase-3 in a poly-Q repeat-length dependent manner (148). It is currently unclear whether cleavage of ataxin-3 is dependent on the length of its poly-Q tract.

Despite extensive evidence linking poly-Q protein proteolysis and the production of toxic fragments, no study has examined the kinetics of cleavage *in vitro*. In this study, we examined the proteolysis of ataxin-3, in both its pathological and non-pathological forms, to determine the kinetic parameters of cleavage in order to investigate if its poly-Q tract expansion leads to increased proteolysis and toxic fragment production.

3.2 Results

3.2.1 Calpain-2 cleaves non-pathological and pathological ataxin-3 variants similarly *in vitro*

The aim of this study was to determine whether poly-Q tract expansion results in enhanced proteolytic cleavage and the production of toxic fragments and the first step was to compare the proteolytic profiles of each of the ataxin-3 protein by SDS-PAGE. In this chapter, ataxin-3 proteins with different lengths of the poly-Q tract are referred to as 'variants'. 20 μ M of each ataxin-3 variant with both non-pathological [ataxin-3 (Q15) and ataxin-3 (Q28)] and pathological length poly-Q tracts [ataxin-3 (Q50) and ataxin-3 (Q64)] were expressed and purified from *E. coli* as previously described in Chapter 2. All ataxin-3 variants were expressed as the second isoform type that lacks the third UIM (14) (Figure 3.1A). The ataxin-3 variants were incubated in the absence and presence of 50 nM calpain-2 for 30 min at 22 °C. The reactions were stopped with 10 mM EDTA and the samples were analysed by SDS-PAGE with Coomassie Blue staining. The degradation patterns of all four ataxin-3 variants after incubation with calpain-2 were very similar and showed no specific enhancement for each of the variant (Figure 3.1B). For each protein, three major bands with molecular weights between 19 to 26 kDa were observed, as well as several other smaller molecular weight products.

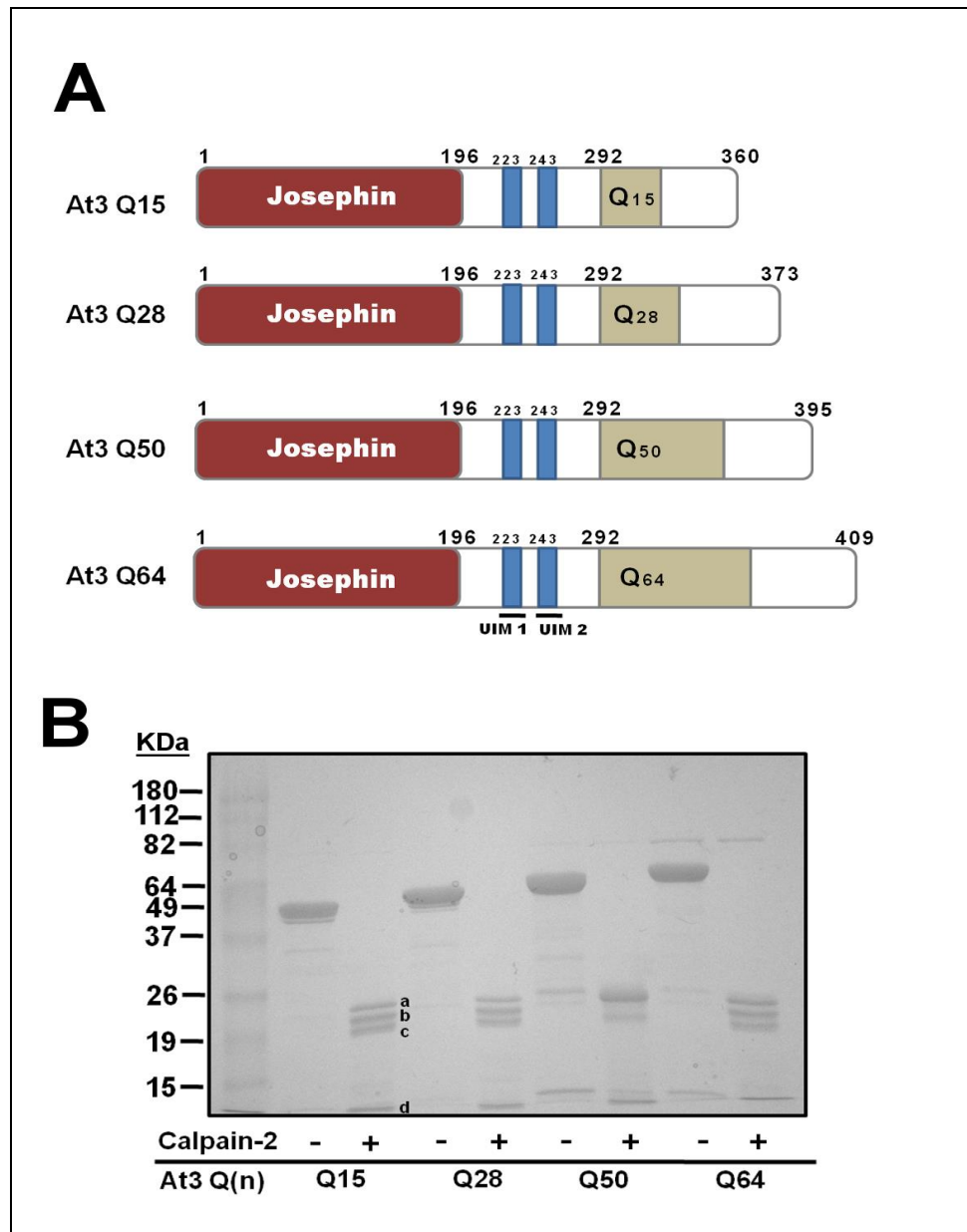


Figure 3.1 Schematic diagram showing the domain organisation of the ataxin-3 protein (A) The N-terminus contains the Josephin domain (red), followed by two other smaller domains referred to as ubiquitin-interacting motifs (UIM) (blue). The C-terminal region of the ataxin-3 molecule contains the variable length poly-Q repeat tract (green) depicting the different variant forms of ataxin-3 that were used. **(B)** Representative SDS-PAGE of the proteolysis of ataxin-3 with calpain-2. Different variant lengths of ataxin-3 (Q15), (Q28), (Q50) and (Q64) at 20 μ M were incubated with 50nM of calpain-2 for 30 min at 22°C and the entire sample volume is analysed via SDS-PAGE. The fragments (a – d) from all ataxin-3 variants were isolated for N-terminal sequencing.

3.2.2 Identification of ataxin-3 cleavage sites via mass spectrometry and N-terminal sequencing

We next determined the specific masses and protein sequences of the four most stable and major protein bands indicated in Figure 1B. Fragments (a) to (c) were observed to have molecular weights between 19 to 26 kDa, while fragment (d) had a molecular weight lower than 15 kDa. The proteins were incubated with calpain-2 as described in section 3.2.1 and were analysed by mass spectrometry using matrix-assisted laser desorption/ionization (MALDI). To determine the N-terminal sequences of the fragments, proteolysed ataxin-3 variants were first analysed by SDS-PAGE, followed by Western blotting on a sequencing specific PVDF membrane. The membrane was stained with Coomassie Blue and the fragments (a) to (d) were cut from the membrane and sent for N-terminal peptide sequencing. The MALDI and N-terminal peptide sequencing were both analysed by the Peptide Biology Laboratory, Monash University.

Figure 3.2A shows the representative N-terminal sequences obtained for ataxin-3 (Q15) and its corresponding theoretical mass from these sequences. They were then matched against the peak mass obtained from the MALDI results. The cleavage sites are mapped out and illustrated with ataxin-3 (Q15) in Figure 3.2B. The arrows indicate the C-terminal end of each fragment, which lay outside the Josephin domain, except for fragment (d). The N-terminus for fragment (d) starts outside the Josephin domain, just before 2UIM. Ataxin-3 (Q28), (Q50) and (Q64) were all treated and gave similar results with cleavage primarily occurring within and outside the N-terminal Josephin domain. These data provide evidence that despite the different poly-Q tract lengths of ataxin-3 proteins, calpain-2 did not appear to cleave discriminately.

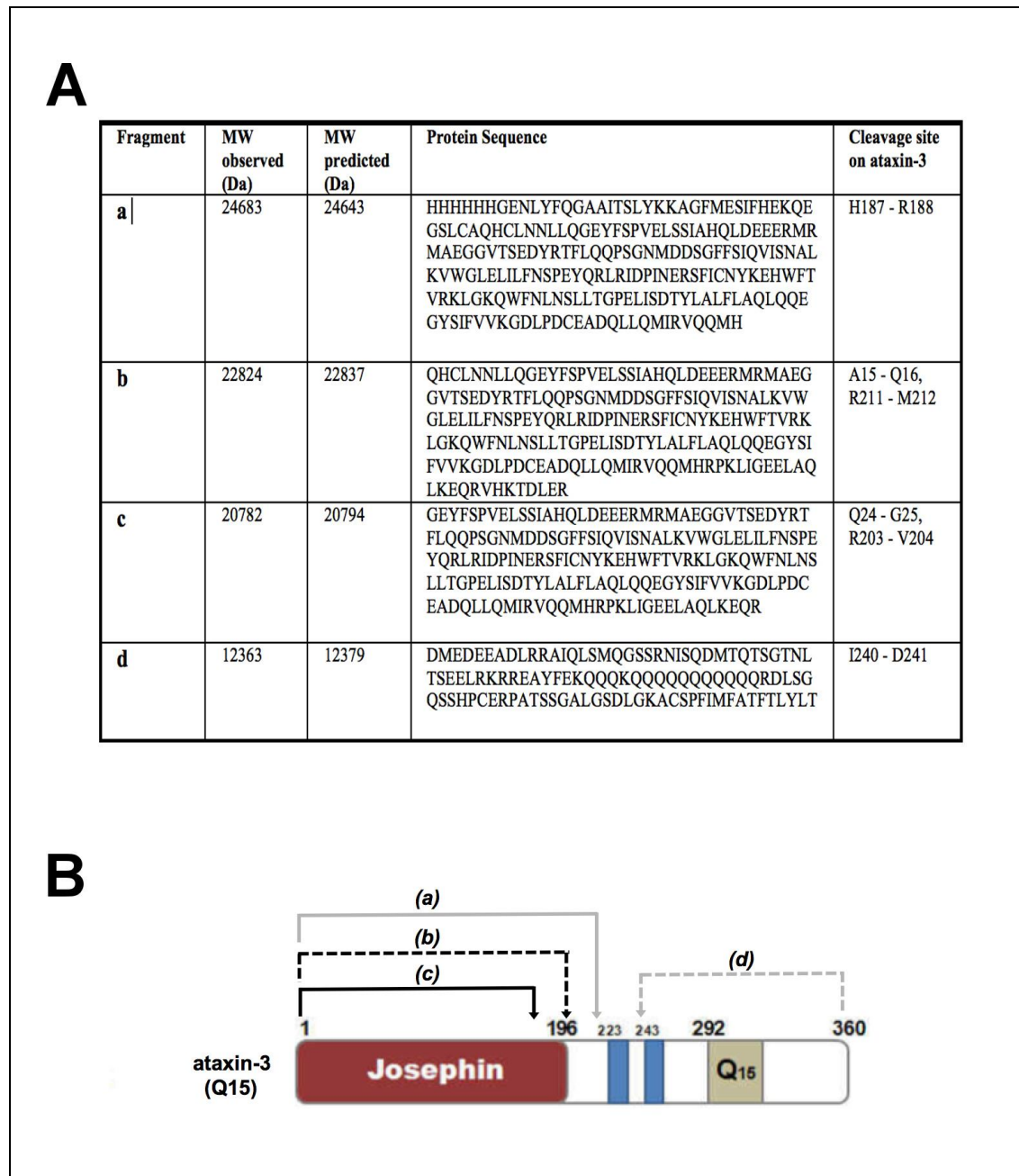


Figure 3.2 Identification of cleavage sites for calpain-2 in ataxin-3 variants (A) The Q15, Q28, Q50 and Q64 variants of ataxin-3 (20 μ M) were incubated with calpain-2 (50 nM) for 30 min at 22°C and the reaction mixtures were analysed via SDS-PAGE. The protein bands (a - d) identified in Figure 3.1B were N-terminally sequenced and cleavage sites were identified. The proteolytic mixture was analysed using MALDI-MS. (B) Cleavage sites are indicated in the representative schematic diagram of ataxin-3 (Q15). Fragment (a) is indicated by a grey solid bracket, fragment (b) is black dashed bracket, fragment (c) is black solid bracket and fragment (d) by grey dashed bracket. Arrowheads indicate the cleavage sites.

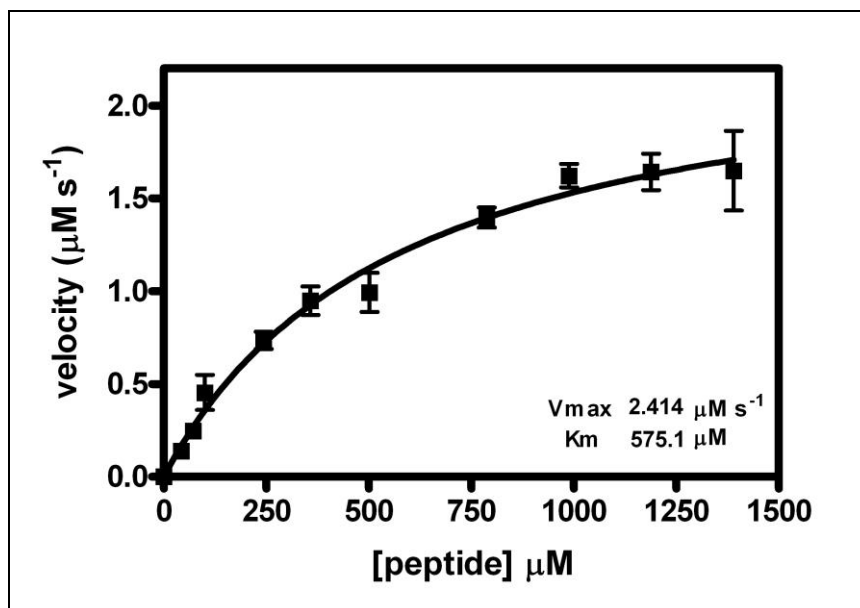


Figure 3.3 Determination of K_S and V_S of Suc-LY-MC Initial velocities ($\mu\text{M s}^{-1}$) are plotted as a function of substrate concentrations (μM) and the Michaelis-Menten equation was used to obtain the best-fit curve and parameters using the analytical software, Prism (GraphPad). The data points represent the mean of three independent experiments with each error bar representing the standard error of each mean.

3.2.3 Ataxin-3 variants have similar rates of proteolysis

Several studies have shown that certain proteases can modulate and cleave poly-Q-containing proteins with different sized poly-Q repeats (146-148). In order to further ascertain the specificity of calpain-2 proteolysis and determine if poly-Q length affects the cleavage kinetics of ataxin-3, a competitive substrate assay was employed in the analysis. The assay was first described by Blake *et. al.* (174) and adapted by various groups for their studies (177, 178). Blake and colleagues showed that apparent Michaelis-Menten constants, K_{Mapp} and V_{maxapp} can be obtained through kinetic analysis of a non-chromogenic substrate and its effects on the time course of an enzymatic interaction with a chromogenic substrate (174). In this assay, we analysed the competitive effect of ataxin-3 on calpain-2 hydrolysis of the fluorescent substrate, Suc-Leu-Tyr-AMC (AMC=7-amino-4-methylcoumarin) (Suc-LY-AMC). The derivations and calculations are previously described in (174).

The equations for the apparent (i) K_{Mapp} and (ii) V_{maxapp} are:

$$(i) \quad K_{Mapp} = \frac{K_s \cdot \ln(1/0.95)}{V_s \cdot [\text{Slope } \Delta t(5\%)]}$$

$$(ii) \quad V_{maxapp} = \frac{K_s \cdot S_0 - V_s K_{Mapp} (\text{Slope } \Delta \text{Area})}{K_s \cdot \text{Slope } \Delta \text{Area}}$$

K_S and V_S refer to the constants K_M and V_{max} of Suc-LY-AMC respectively while S_0 refers to the initial concentration of the Suc-LY-AMC. The values of K_S and V_S were determined by analysing initial velocities against a range of Suc-LY-AMC concentrations. K_S and V_S values obtained were 575.1 μM and 2.4 $\mu\text{M s}^{-1}$ respectively (Figure 3.3). The ataxin-3 variants compete against Suc-LY-AMC for calpain-2 hydrolysis. The entire enzymatic progress curve of Suc-LY-AMC and calpain-2 are monitored with each increase in ataxin-3 concentration in the reaction. This method utilizes the entire progress curve of the hydrolysis of Suc-LY-AMC to extract two values, the change in area (ΔArea) under the curve and the time required to cleave 5% of Suc-Ly-AMC [Δt (5%)].

All the ataxin-3 proteins (Q15), (Q28), (Q50) and (Q64) from 0 to 20 μM concentrations were titrated with a constant concentration of 50 nM calpain-2 and an S_0 of 145 μM at 22 °C for 2 h. Fluorescence readings were monitored every 5 s with an emission wavelength at 435 nm. The progress curves of the ataxin-3 (Q15) and ataxin-3 (Q64) in increasing concentration is shown in Figure 3.4. The progress curves obtained were first normalized and subsequently transformed using the Area Under Curve function in Prism (GraphPad) (Figure 3.4A). The calculated area under each curve is plotted against ataxin-3 (Q15) concentration in Figure 3.4C. As the curves are normalized to 100%, the time taken to convert 5% of the substrate was also plotted against each concentration of ataxin-3 (Q15) (Figure 3.4E). The ataxin-3 variants (Q64), incubated at the same conditions without calpain-2 were tested with 20 μM ThT to determine if the proteins remained monomeric throughout the assay. There was no increase in ThT fluorescence which indicated that the ataxin-3 did not aggregate at 22 °C for 2 h (data not shown).

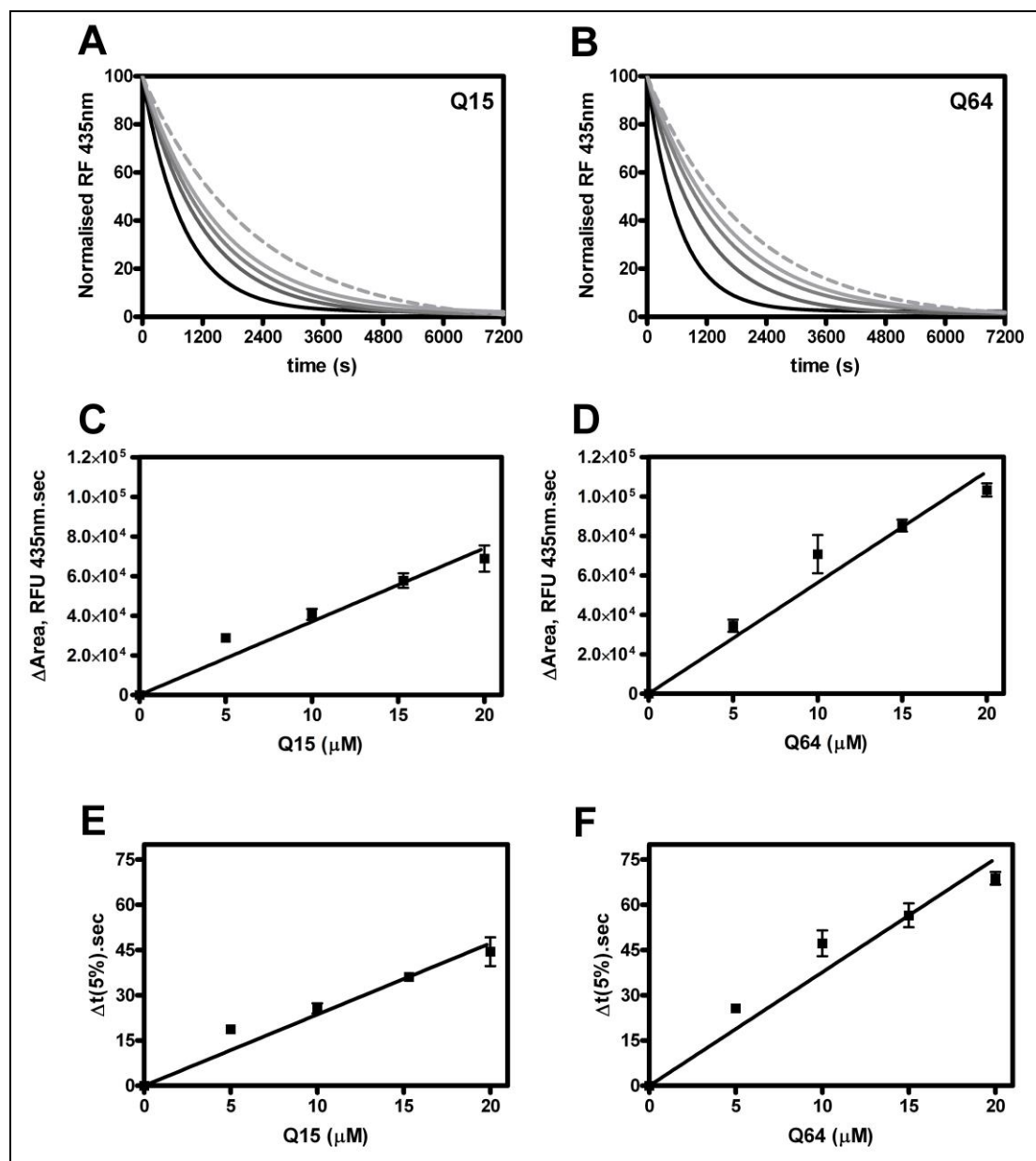


Figure 3.4 Ataxin-3 proteins compete for calpain-2 hydrolysis in the presence of fluorogenic substrate, Suc-LY-AMC. Progress curves were monitored at 435 nm when increasing concentrations of non-chromogenic substrate, ataxin-3 (Q15) (**A**) and (Q64) (**B**) compete with Suc-LY-AMC fluorogenic substrate at a constant concentration of calpain-2. In each assay, the black line represents 0 μM, dark grey 5 μM, medium grey 10 μM, light grey 15 μM and dotted grey is 20 μM protein. These kinetic experiments were carried out on a 96 well plate, in a monochromatic bench top spectrometric plate reader. Dependence of Δ Area under the curves and time taken to transform 5% of substrate upon increasing concentrations of ataxin-3 (Q15) (**C**, **E**) and ataxin-3 (Q64) (**D**, **F**) are shown. Each error bar represents the standard deviation of at least four determinations and the lines drawn through the points are determined by linear regression analysis.

Table 3.1 Apparent kinetic parameters for proteolysis of ataxin-3 variants by calpain-2.

Ataxin-3 variants				
	K_m^{app} (μ M)	V_{max}^{app} (μ M/s)	k_{cat} (sec^{-1})	k_{cat}/K_m ($\text{M}^{-1}\text{sec}^{-1}$)
Q15	5.11 ± 0.59	0.017 ± 0.002	0.34	6.65×10^4
Q28	5.34 ± 0.48	0.019 ± 0.004	0.38	7.12×10^4
Q50	3.29 ± 0.39	0.012 ± 0.002	0.24	7.29×10^4
Q64	3.25 ± 0.07	0.012 ± 0.002	0.24	7.38×10^4

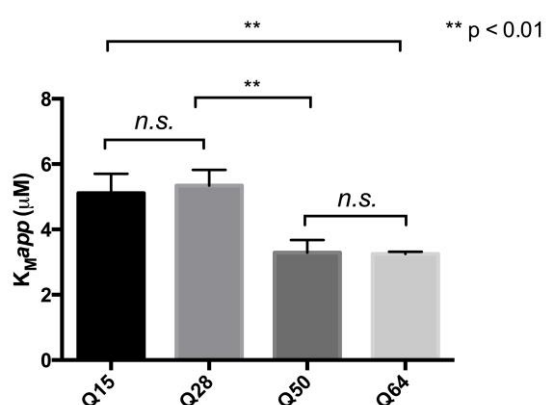


Figure 3.5 Comparison of the apparent K_M values of corresponding ataxin-3 variants. The K_M values of ataxin-3 Q15 (black), Q28 (medium grey), Q50 (dark grey) and Q64 (light grey) are tabulated in independently. The data were obtained from the average of three independent assays with the analysis of duplicates and two-tailed t-test was employed. *n.s.* denotes ‘not significant’.

Linear regression analysis was used to obtain the values for [slope $\Delta Area$] and [slope Δt (5%)]. Ataxin-3 (Q28), (Q50) and (Q64) were all analysed in the same manner. The results for the pathological length ataxin-3 (Q64) is shown in Figure 3.4B, D and F as a comparison to ataxin-3 (Q15). The results for ataxin-3 (Q28) and (Q50) are shown in Figure A1 in Appendix A. Using the equations (i) and (ii), the V_{max}^{app} for calpain-2 cleavage of the ataxin-3 variants was calculated by using the gradient value for [slope $\Delta Area$] that correlate with increasing ataxin-3 concentrations. Likewise, the K_m^{app} values were calculated by the gradient value of [slope Δt (5%)] that also correlate with increasing ataxin-3 concentrations.

The data in Table 3.1 summarizes the kinetic parameters obtained for ataxin-3 (Q15), (Q28), (Q50) and (Q64). Apparent K_M values for calpain-2 on the non-pathological variants [(Q15) and (Q28)] were 5.11 ± 0.59 and 5.34 ± 0.48 μM respectively, while both pathological ataxin-3 [(Q50) and (Q64)] had very similar values of 3.29 ± 0.39 and 3.25 ± 0.073 μM respectively. While there were no significant difference between the two short poly-Q length variants or between the two longer poly-Q length variants, the apparent K_M values for the longer variants were significantly smaller than the K_M values for the shorter variants (Q64 vs. Q15, Q50 vs. Q28, $p < 0.01$). This result suggests that calpain-2 cleaves the longer poly-Q tract length ataxin-3 at a lower concentration, compared to the shorter poly-Q length ataxin-3. Therefore, the k_{cat}/K_M value, which is a measure of calpain-2 proteolytic specificity on all four ataxin-3 variants were further calculated. The rate on ataxin-3 (Q15) cleavage by calpain-2 was $6.65 \times 10^4 \text{ M}^{-1} \text{ sec}^{-1}$, (Q28) = $7.12 \times 10^4 \text{ M}^{-1} \text{ sec}^{-1}$, (Q50) = $7.29 \times 10^4 \text{ M}^{-1} \text{ sec}^{-1}$ while ataxin-3 (Q64) was cleaved at a rate of $7.38 \times 10^4 \text{ M}^{-1} \text{ sec}^{-1}$. From these results, it is evident that the values were all well within range of one another, suggesting that the specificity of calpain-2 for each ataxin-3 variant is not influenced by the poly-Q repeat length.

3.3 Discussion

It has been shown that the poly-Q tract length of several proteins, including Htt and ataxin-3 can influence susceptibility to proteolytic cleavage (146-148). In addition, experimental evidence suggests that pathological variants of Htt are preferred substrates for calpain-2 and caspases, compared to non-pathological variants (56, 130-133, 148, 176). Although it has been shown that ataxin-3 can be cleaved by calpain-2 (56, 145), it is currently unknown whether the poly-Q tract length affects its rate of proteolysis.

3.3.1 Calpain-2 cleaves all ataxin-3 variants at identical sites

In this study, both SDS-PAGE and a competitive substrate assay were utilized to determine the apparent K_M , V_{max} and k_{cat}/K_M values for calpain-2 cleavage of ataxin-3. When both ataxin-3 (Q15) through to ataxin-3 (Q64) were incubated in the presence of calpain-2 and samples were analysed by SDS-PAGE, the results suggest that the proteins were processed in a similar manner, showing 3 major bands corresponding to molecular

weight sizes similar to the Josephin domain. These 3 major bands were confirmed to be fragments of ataxin-3 consisting of the Josephin domain via protein sequencing and MALDI. Other fragments observed by SDS-PAGE were also sequenced, and are similar to the fragments reported by other groups (56, 132), in particular, fragment (d). Fragment (d) contains an intact 2UIM and the polyQ domain, which confirms that poly-Q-containing fragments are produced upon proteolysis. The sequence for fragment (d), starting with amino acid 241 has been reported by Berke *et. al.* (132) following treatment by caspases while Haacke *et. al.* reported a cleavage site at amino acid 260 by calpains (56). In that study, Haacke *et. al.* used purified ataxin-3 protein, expressed in cells (56). This suggests that the presence of post-translational modifications to ataxin-3 protein may affect or determine specific cleavage sites, compared to recombinant ataxin-3 expressed in prokaryotic cells (179).

3.3.2 Ataxin-3 protein cleavage is independent of poly-Q length

Following the SDS-PAGE and MALDI results, the rate of proteolysis was investigated with higher sensitivity using a competitive substrate assay. From the experimental results of the kinetic assay, apparent kinetic constants K_M and V_{max} of calpain-2 for the cleavage of ataxin-3 with different poly-Q lengths, from (Q15) through to (Q64) were obtained, then followed by k_{cat}/K_M values. While there were slight differences in the cleavage rates across all the poly-Q length variants, the apparent V_{max} values and the turnover number of molecules between non-pathological ataxin-3 proteins [(Q15), (Q28)] and pathological lengths of ataxin-3 [(Q50),(Q64)] suggests the differences in K_M were not significant. Likewise, calpain-2 had similar specificity (K_{cat}/K_M) towards each ataxin-3 variant. This result suggests that the length of the poly-Q tract of ataxin-3 neither enhances nor inhibits the rate of proteolysis. Concurrently, some studies in the field have shown that the poly-Q tract behaves independently of its other domains (105, 115, 121). This may explain why the poly-Q tract does not modulate the rate of calpain-2 proteolysis. Proteolytic cleavage of ataxin-3 has been implicated as one of the key steps that contribute towards SCA3 pathogenesis (125, 129). This data supports the role of proteolysis in the generation of ataxin-3 fragments, especially fragments that contain the poly-Q expansion that gives rise to the toxic fragment hypothesis.

3.4 Summary and conclusions

The data demonstrates *in vitro* that calpain-2 cleaves ataxin-3 at specific sites and that the length of the poly-Q tract does not influence the sensitivity of calpain-2 proteolysis. This work is also the first to demonstrate proteolytic cleavage of ataxin-3 by calpain-2 and kinetic analysis of this proteolysis. In a cellular environment, ataxin-3 fragments with varying poly-Q tract lengths may be released into the cytoplasm after proteolysis, possibly accumulating in abundance prior to initiating aggregation of free ataxin-3 (11). An investigation into the toxic fragment hypothesis by comparing the influence of putative toxic fragments of ataxin-3 on ataxin-3 aggregation of is therefore described in Chapter 4. It will be interesting to determine whether aggregated ataxin-3 proteins display comparable sensitivity to calpain-2 proteolysis.

CHAPTER 4

CHARACTERISATION OF ATAXIN-3 FRAGMENTS

**INITIATING AND ACCELERATING AGGREGATION OF
ATAXIN-3 FULL-LENGTH PROTEINS.**

4.1 Introduction

Spinocerebellar ataxia type-3 (SCA3) is known to be the most common of the autosomal dominantly inherited ataxias (26). Like the other neurodegenerative diseases, such as Parkinson's, Huntington's and Alzheimer's disease, SCA3 belongs to a group of diseases whereby aggregation of its respective mutant protein is considered to be the main cause of disease. Protein expression results in the formation of inclusion bodies, degeneration and death of specific types of neuronal cells (15). In our lab, ataxin-3 has previously been shown to undergo a two-stage model aggregation mechanism that takes into account both protein context and the Poly-Q expansion (58) (refer to Figure 1.6). Ataxin-3 aggregation is thought to involve conformational changes of the protein, or self-association of the other regions of ataxin-3 other than the poly-Q tract, known as the first stage of ataxin-3 aggregation. The short poly-Q length variants, such as ataxin-3 (Q15) go through a nucleation-dependent aggregation process, resulting in changes in ThT fluorescence, intrinsic tryptophan fluorescence and SEC. The morphology of the aggregates are found to be pre-fibrillar, spherical and oligomeric, about 10-12 nm in size and are SDS-soluble (58). For the pathogenic poly-Q length ataxin-3 variants, such as ataxin-3 (Q64), the first stage of aggregation is identical to the shorter poly-Q variants although occurs at a faster rate. However, pathogenic poly-Q length ataxin-3 variants also undergo a second stage whereby SDS-insoluble aggregates are formed. These SDS-insoluble aggregates were found to be highly stable and the morphology of the aggregates were fibrillar and large, up to 50-100 nm in length (58, 180).

At the same time, the toxic fragment hypothesis predicts that proteolytic cleavage of full-length poly-Q proteins results in the generation of short poly-Q-containing fragments that act as seeds to nucleate the aggregation of full-length poly-Q proteins, leading to nuclear inclusions and cellular dysfunction (46, 129, 181, 182). In 2006, Haacke *et. al.* designed a range of ataxin-3 C-terminal fragments that were based on their limited proteolysis results (129). They showed the release of an ataxin-3 C-terminal fragment (starting from position 257 with 71Q residues) from its GST fusion partner, by TEV protease, was a prerequisite for aggregation of full-length pathogenic length ataxin-3 proteins (129). As mentioned previously in Chapter 3 (section 3.1), various studies have shown and supported the role of proteolysis in ataxin-3 pathogenesis. Calpain-2 has been found to be a novel modulator of ataxin-3 proteolysis (56, 145) and inhibition of calpain-2

protease results in the prevention of ataxin-3 proteolysis, circumventing the progression of disease in mice models (145, 182).

Toxic soluble fragments play an important role in SCA3 pathogenesis but its aggregation mechanisms are not fully understood. Furthermore, the rate of aggregation of the pathological ataxin-3 upon seeding by ataxin-3 fragments has not yet been determined. It is therefore of significant interest to investigate whether the poly-Q tract length within the ataxin-3 fragment derived from calpain-2 proteolysis, modulates the aggregation kinetics of the full-length ataxin-3 protein. This study thus aims to use an *in vitro* method to characterize and determine whether ataxin-3 fragments of different poly-Q lengths induce and accelerate the aggregation rates of full-length ataxin-3 proteins.

4.2 Results

4.2.1 Design and selection of fusion partners for the ataxin-3 fragment

Based on the N-terminal sequencing results from Chapter 3, the fragment length of ataxin-3, starting from amino acid 242 to the end of the protein (242-FTLYLTstop) was selected. This length fragment was found to contain the second UIM and also the variable length poly-Q tract. In this study, 242-Q15 and 242Q64 was first amplified out of existing gene constructs of full-length ataxin-3 (Q15) and ataxin-3 (Q64) respectively. The gene products were subsequently engineered into Gateway™ expression vectors (Chapter 2), so as to enhance protein solubility and to efficiently express the 242Q15/Q64 ataxin-3 fragments in *E.coli*. After protein expression and cell lysis, less than 20% of the soluble expression of the protein was obtained, with the majority of the expressed protein detected in the cell pellet.

As poly-Q stretches are notorious for their insolubility (38, 103, 183), fusion tags were considered to increase its solubility (63, 184). The maltose-binding protein (MBP) and the N-utilisation substance protein A (NusA) protein were first considered as they are commonly used to enhance solubility of their fusion partners with proper folding and their origin stems from *E.coli* (185). MBP plays a role in the catabolism of maltodextrins in *E.coli* and its apparent molecular weight is about 40-42 kDa, while NusA is a

transcription termination anti-termination factor, which is also a hydrophilic tag (184). The fragment was cloned from the pDEST vector into both the MBP- and NusA-Gateway vectors. After repeated attempts, the results showed that although the expressions of both fusion proteins were higher than the non-fusion fragment lengths of Q15 and Q64, the solubility of these fusion proteins was surprisingly low. The percentage solubility was estimated to be only around 20% of the total expression (Figure 4.1).

As a result, another soluble fusion partner was considered for the engineering of the expression plasmid in *E.coli*. At this point of the study, an engineered B-domain of *Staphylococcus aureus* Protein A was considered as suitable fusion partner. The Domain-Z is similar to its native B-domain except for a glycine to alanine single amino acid substitution (186). Domain Z is a small molecular weight protein of approximately 9 - 10 kDa, with three α -helices, and is readily soluble. Two domain-Z molecules were used as the fusion partner and were placed at the N-terminus of the ataxin-3 fragments and the construct was inserted into Gateway™ expression vector. Although the fusion protein was found to be soluble and expressed well, spontaneous proteolysis was observed despite the quantity or the type of protease inhibitors used, such as protease inhibitor cocktail tablets (Roche), phenylmethane sulfonyl fluoride (PMSF) and benzamidine HCl. A single domain-Z was subsequently placed at each terminus of the fragment (Z-fragment-Z) to circumvent undesired proteolysis. This was done in the hope that a structured domain would protect the C-terminus end of the fragment from exposure to proteases (Table 4.1). Despite this effort, spontaneous fragmentation of the protein was continually observed. A check on the DNA sequence of the construct was performed which confirmed that there was no stop codon in the middle of the construct that would result in the truncation of the fusion protein.

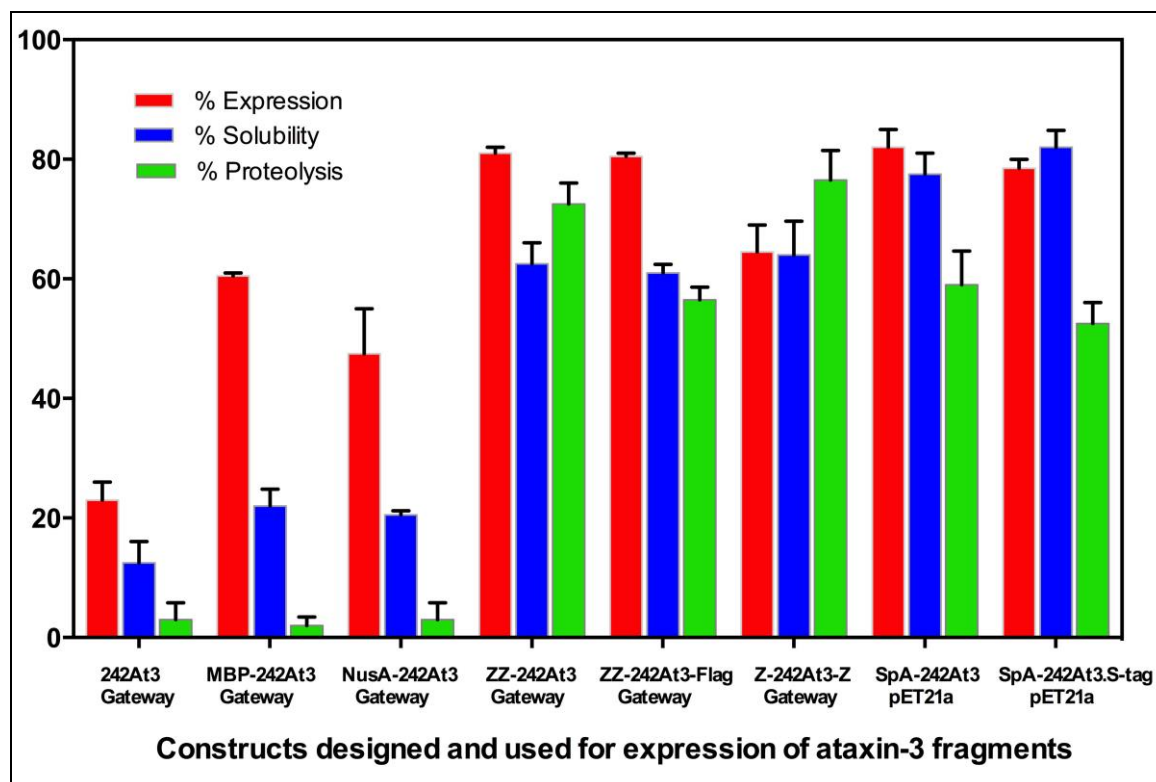

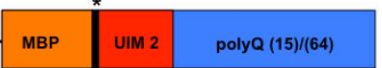
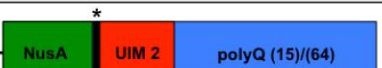

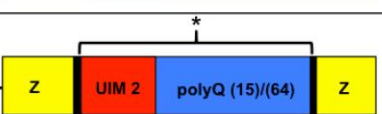



Figure 4.1: Summary of constructs designed for the expression of the ataxin-3 fragment. Red bars represent the % expression of protein versus non-transformed BL21 (DE3) E. coli cells. Blue bars represent the % solubility of protein in the soluble fraction compared to the insoluble fraction based on densitometry. Green bars represent the % spontaneous proteolysis of soluble protein after purification. “Gateway” refers to the Gateway Destination vectors by Life Technologies while pET21a refers to the pET T7 promoter expression vectors by Novagen. SpA denotes the 2 molecules of Protein A (B-domain), while ‘Z’ refers to the engineered B-domain of Protein A, Z-domain. Quantification represented here in this graph is of the non-pathological variant, ataxin-3 (Q15).

Table 4.1. The various designs of fusion ataxin-3 fragment constructs. The fragment length starting from position 242, consisting of the second UIM (2UIM), the variable poly-Q tract length domain to the tail end of ataxin-3 (blue) is placed in the C terminal end of most fusion protein partners. The fusion protein choices were MBP (orange), NusA (green), either one or two molecules of Z- and B- domain of the Protein A (SpA, yellow). The location of the SpA molecule was at either end of the construct as denoted. The asterisk (*) denotes the location of the TEV cleavage site.

Constructs of fusion proteins (in the N' to C' direction)	Expression Vector
	Gateway, pExpLIC-His
	Gateway, pExpLIC-His
	Gateway, pExpLIC-His
	Gateway, pExpLIC-His
	Gateway, pExpLIC-His
	Novagen, pET21a

A different expression vector, pET21a (Novagen) was sought out and utilised. The vector had the native B-domain incorporated into it and was readily available in the laboratory (105). The final fusion protein construct contained the hexa-histidine tagged (His₆) B-domain at the N-terminus, followed by a specific TEV protease cleavage site (ENLYFQG) (173) and then the ataxin-3 fragment. At the C-terminus, an S-tag peptide sequence (KETAAAKFERQHMDs) was cloned in using QuikChange™ mutagenesis. The peptide sequence was analysed using TANGO (187) and it was confirmed the sequence does not contribute to aggregation (Appendix B). The S-tag facilitates detection of the fragment upon release from its fusion partner in the downstream assays. Throughout this study, the fusion proteins with ataxin-3 (Q15) and ataxin-3 (Q64) fragments are termed (SpA242Q15) and (SpA242Q64) respectively. The ataxin-3 fragments, after their release from fusion proteins by TEV digestion, are referred to as (242Q15) and (242Q64) respectively. In summary, Table 4.1 provides an overview of the

total number of constructs designed and engineered, while Figure 4.2 shows a schematic diagram of the final construct employed.

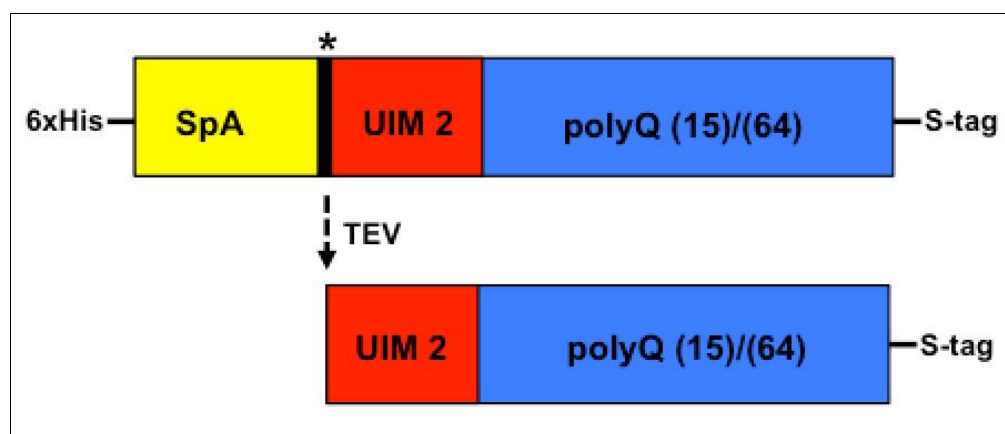


Figure 4.2: Illustration of the final expression construct of ataxin-3, (SpA242Qn). The C-terminal fragment ataxin-3 which starts from position 242 of ataxin-3 protein was amplified out of the full length ataxin-3 plasmid, with two distinct lengths of poly-Q, which are Q15 (non-pathological) and Q64 (pathological) and cloned into pET21a expression vector containing a molecule of B-domain of Protein A at its N-terminal, in which it has a His₆ tag. A S-tag was cloned to the C-terminal end of the fragment sequence. The ataxin-3 fragments (242Q15), (242Q64) would be released from SpA via TEV protease cleavage. The asterisk (*) denotes the location of the TEV cleavage site.

4.2.2 Purification and refolding of fusion ataxin-3 proteins, (SpA242Qn)

The expression and solubility of (SpA242Qn) proteins were found to be well-expressed and had high solubility. A mixture of protease inhibitors was utilised, such as protease inhibitor cocktail tablets, CFC (Roche), PMSF and benzamidine HCl. Cell lysis and centrifugation occurred at temperatures of 4 °C or below. Every step of the purification process was kept cold as much as possible. However, undesired fragmentation continued to be observed during the purification process, despite the extra precautions taken. The purification of proteins from inclusion bodies (IB) was then considered. It is known that IB contain over-expressed recombinant proteins that are protected against proteolysis (188-190). A good percentage of IB was observed in the cell pellet after cell lysis via SDS-PAGE. In order to proceed in this circumstance, inclusion bodies of (SpA242Qn) proteins were utilised for protein refolding.

The expression and cell lysis of (SpA242Q15) and (SpA242Q64) proteins, as well as the unfolding and refolding processes are all described in Section 2.4 in Chapter 2. Briefly, cell pellets were washed, weighed and solubilized in 6.18 M Tris-buffered guanidine hydrochloride (GnHCl-Tris) overnight at 4 °C. The solution of unfolded proteins was centrifuged to pellet insoluble cell debris and the supernatant was filtered through a 0.45 µm filter. The cleared filtrate was passed over a Ni²⁺ affinity column that was pre-equilibrated with 6.18 M GnHCl-Tris. This was done to allow only His₆-tagged fusion proteins to be captured, thus facilitating the purity of the refolding process downstream. The fusion proteins were eluted from the column with an isocratic gradient using imidazole, with both ataxin-3 fusion proteins observed to elute at 50 mM imidazole. A method previously described by Cabrita and Bottomley (191) for serpins was adapted for refolding ataxin-3 proteins on a gel filtration chromatography column. Eluted samples from the affinity Ni²⁺ column were pooled and filtered through a 0.45 µm membrane prior loading onto a Superdex resin gel filtration column (GE Lifesciences). The gel filtration columns were pre-equilibrated with Tris.HCl buffer with 10 % glycerol and the reducing agent β-mercaptoethanol, to aid in the refolding process as the protein gravitates down the column. The proteins that refolded well should elute in the fractions after the column's void volume. Proteins eluted in the void volume are considered mis- or unfolded (191).

Fractions of fusion (SpA242Q15) and (SpA242Q64) proteins were collected at around 60 ml and 75 ml respectively, well beyond the void volume of the column at 40 ml (Figure 4.3A and B). These fractions were analysed via SDS-PAGE for purity (Figure 4.3C and D) and simultaneously tested for its ThT reactivity before the fractions were pooled. Figure 4.3E and F shows fractions of (SpA242Q15) and (SpA242Q64) respectively, with fractions found to be ThT reactive corresponding to those in the void volume. Non-ThT fractions were pooled and concentrated using a spin column that had a cut off at MW 10,000 Da. The concentration of protein obtained for (SpA242Q15) was in the range of 0.8 - 1.0 mg/mL, while protein concentration for (SpA242Q64) was slightly lower at 0.5 mg/mL. In Figure 4.4, samples of (SpA242Q15) and (SpA242Q64) were both analyzed via SDS-PAGE. (SpA242Q15) corresponded to a molecular weight of approximately 25 kDa while (SpA242Q64) was around 30 - 32 kDa. This result correlates with the predicted molecular weights in Table 4.2. Importantly, there was an absence of smaller molecular weight fragments that was previously observed from previous protein purification protocols of the ataxin-3 fragments. These data demonstrate for the first time

that a C-terminal fragment of the poly-Q protein, ataxin-3, can be successfully refolded via the on-column technique.

4.2.3 Refolded ataxin-3 fusion proteins are monomeric and retains α -helical conformations

After obtaining soluble, refolded proteins that were not subjected to proteolysis, it was crucial to ascertain the biochemical characteristics of the proteins before using them for assay purposes. In our laboratory, proteins are often purified and stored at -80 °C for use in downstream assays. It is well established that some proteins become unstable during storage at -80 °C over time or through several cycles of freeze-thaw. In order to determine if protein stability is maintained after a freeze thaw cycle at -80 °C, size exclusion chromatography (SEC) was used to assess the monomeric nature of the two fusion proteins. Superdex™ 10/300 GL columns (GE Healthcare) are often used to do rapid checks on the monomeric state of a protein. The separation range for Superdex™ 75 is from 3,000 - 75,000 kDa sized proteins, while Superdex™ 200 is used for proteins sized 10,000 - 600, 000 kDa. After a cycle of frozen storage and thaw, a sample volume of 50 μ L of each protein was used for analysis. (SpA242Q15) was passed through the Superdex™ 75 column and a single peak was eluted off at approximately 10 mL (Figure 4.5A). (SpA242Q64) was also analysed and eluted in a single peak around 13 mL on a Superdex™ 200 (Figure 4.5B). Both proteins eluted at volumes well beyond the void volume (V_0) of their respective columns at around 8 - 9 mL, indicating that the proteins did not destabilize under freezing conditions and are monomeric in nature. Thus, these fusion proteins are suitable for use to monitor the protein fragments aggregation characteristics.

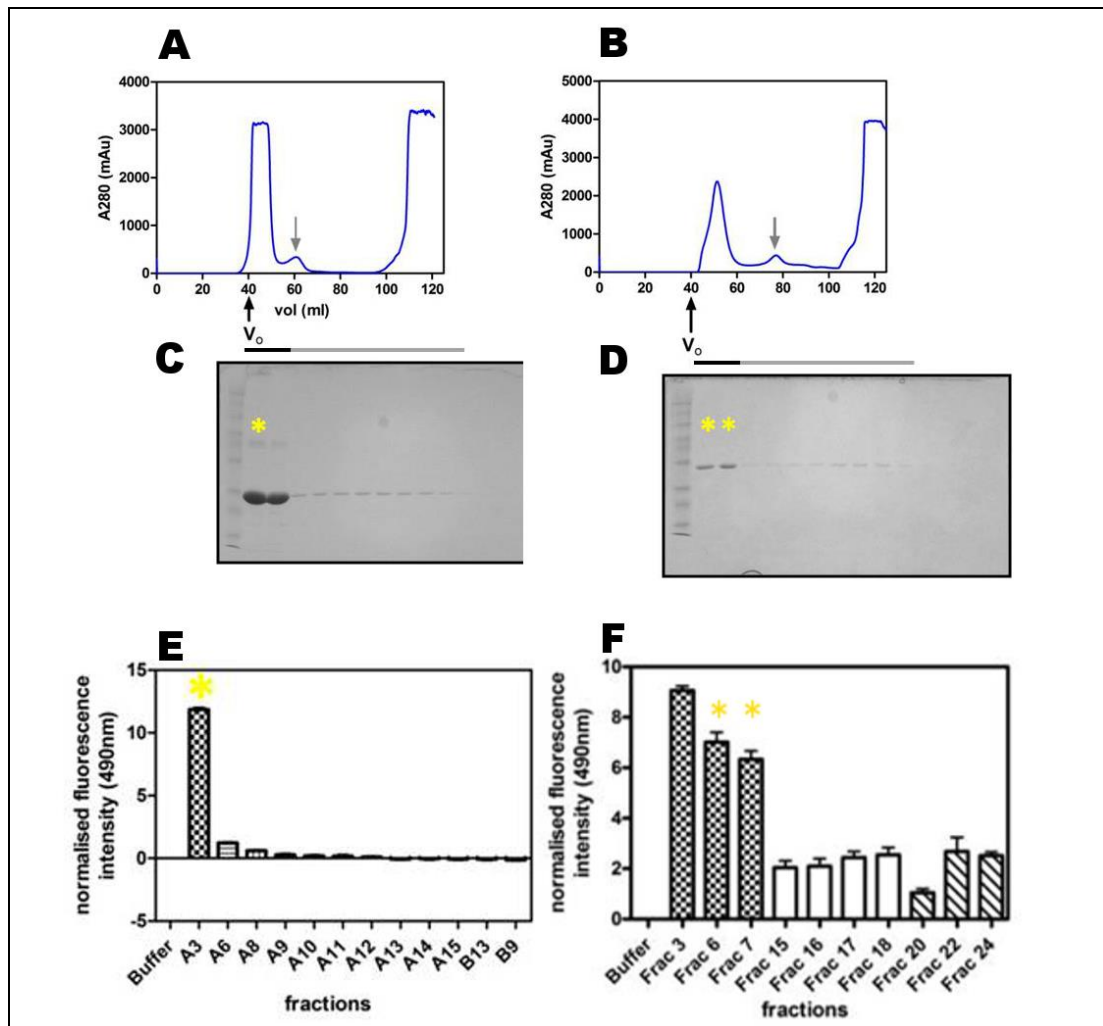


Figure 4.3 Chromatogram of the refolding process of ataxin-3 fusion proteins, (SpA242Q15) and (SpA242Q64) (A) Unfolded (SpA242Q15) protein is refolded as it passes through the HiLoad 16/60 Superdex 75 gel filtration column. Fractions that contained the refolded fusionQ15 were eluted and collected around the 60 mL volume. (B) Unfolded (SpA242Q64) protein is refolded on the HiLoad 16/60 Superdex 200 gel filtration column and eluted around 75 mL onwards. (C-D) Eluted fractions from the refolding process are analysed by SDS-PAGE analysis. The first two lanes of the SDS-PAGE, denoted by yellow asterisks, are fractions from the respective void volumes (underscored in black). Fractions that are non-ThT reactive are underscored in grey. (E-F) Eluted fractions from both refolding processes were tested with 20 μ M ThT dye solution and analyzed on a fluorimeter. The excitation wavelength is at 445 nm, emission wavelength recorded at 490 nm. Fluorescence intensities of samples were normalised to buffer alone. Yellow asterisks denote the fractions from the void volumes indicated in (C) and (D).

Superdex™ 10/300 GL columns (GE Healthcare) are often used to do rapid checks on the monomeric state of a protein. The separation range for Superdex™ 75 is from 3,000 - 75,000 kDa sized proteins, while Superdex™ 200 is used for proteins sized 10,000 - 600,000 kDa. After a cycle of frozen storage and thaw, a sample volume of 50 μ L of each protein was used for analysis. (SpA242Q15) was passed through the Superdex™ 75 column and a single peak was eluted off at approximately 10 mL (Figure 4.5A). (SpA242Q64) was also analysed and eluted in a single peak around 13 mL on a Superdex™ 200 (Figure 4.5B). Both proteins eluted at volumes well beyond the void volume (V_0) of their respective columns at around 8 - 9 mL, indicating that the proteins did not destabilize under freezing conditions and are monomeric in nature. Thus, these fusion proteins are suitable for use to monitor the protein fragments aggregation characteristics.

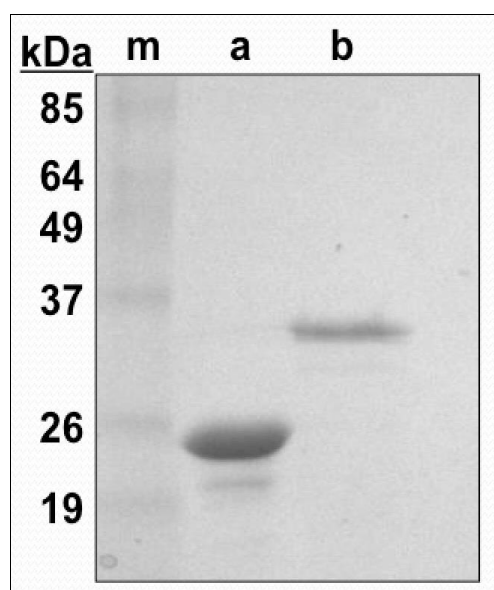


Figure 4.4 Purified and refolded fusion ataxin-3 proteins analysed on SDS-PAGE. Fractions of eluted proteins were pooled and concentrated. An aliquot of each protein was taken and analyzed on a 12 % SDS-PAGE gel. Lane (a) shows (SpA242Q15) protein at approximately 25 – 26 kDa while lane (b) shows (SpA242Q64) protein at approximately 30 – 32 kDa. BenchMark™ pre-stained protein ladder was used in lane (m).

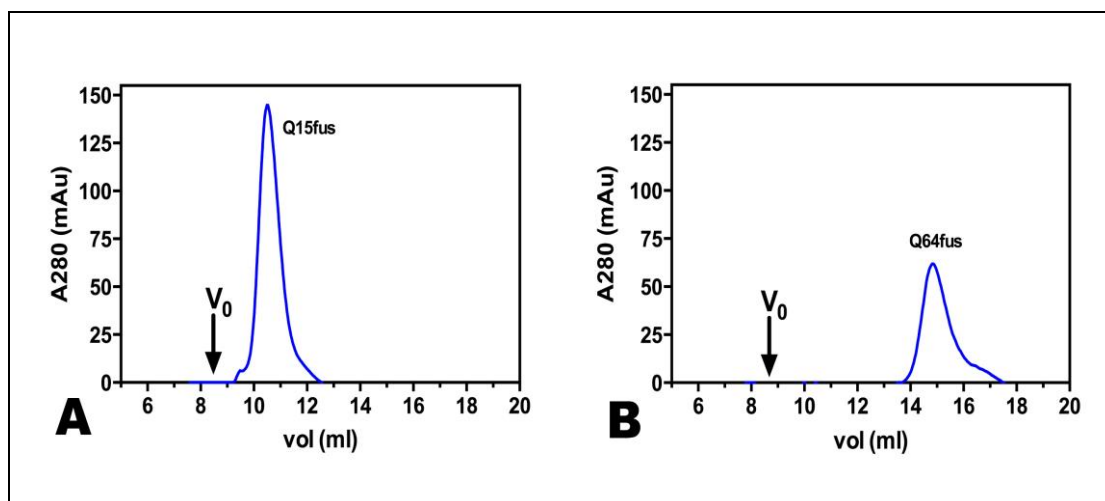


Figure 4.5 SEC analyses of ataxin-3 fragment fusion proteins. (A) (SpA242Q15) yielded a single peak on Superdex™ 75 (10/300) GL from 10 mL after the indicated void volume (V_0), suggesting that the protein remained monomeric. Similarly, (B) (SpA242Q64) yielded a single peak on the Superdex™ 200 (10/300) GL, eluting at around 14 mL, suggesting that (SpA242Q64) remained monomeric and did not form aggregates after freezing.

After determining that the proteins remained monomeric after freezing, mass spectrometry was carried out to further characterise the fragments. A sample for both proteins was first desalted using C8 or C18 extraction discs before being submitted for mass spectrometry analysis at the Peptide Biology Laboratory, Monash University. Several peaks were observed with MALDI together with a major peak for a mass of 24168 Da for (SpA242Q15) (Figure 4.7A). For (SpA242Q64), a major peak corresponding to a mass of 30493 Da was also obtained (Figure 4.7B). Despite the noisy baseline of the spectra, the results correlate with the predicted molecular weight of each protein (Table 4.2), and also support the SDS-PAGE results obtained in Figure 4.4.

Circular dichroism (CD) spectroscopy is extensively used to study chiral molecules, using polarised light and measured over a range of wavelengths in the far UV spectrum (below 260nm). Various secondary structures, such as α -helices or β -sheets can be characterized, when the chromophores of the protein polypeptide backbone are aligned, causing the optical transitions to shift into multiple transitions due to ‘exciton’ interactions (192). Hence, characteristic spectra for different structural elements will result. α -helical proteins exhibit negative bands at 222 and 208 nm and a positive band at 193 nm, whereas β -sheet proteins exhibit a negative band at 218 nm and a positive band at 195 nm (192).

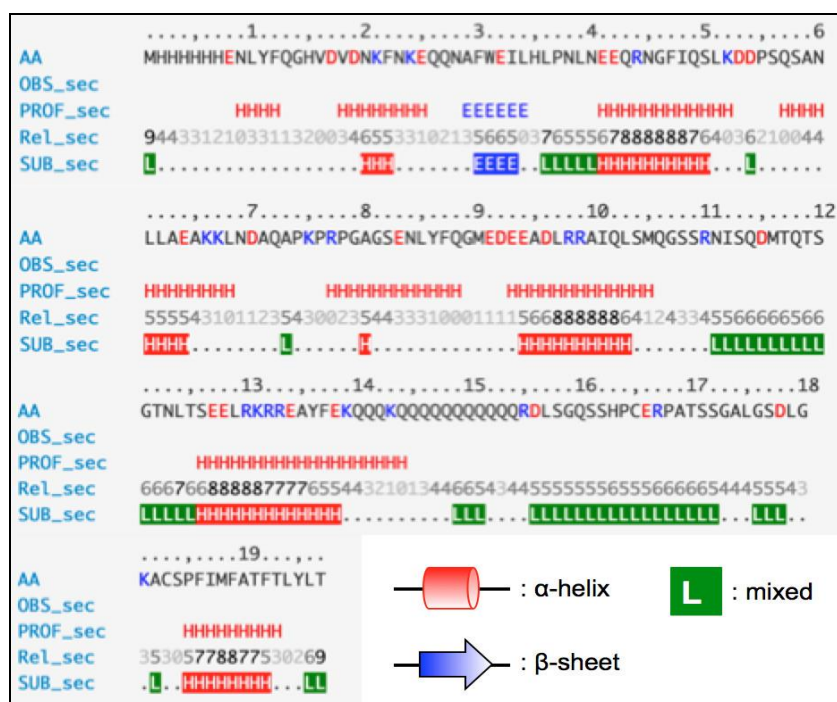


Figure 4.6: Predicted secondary structure of SpA242Qn fusion proteins Using an online web tool (193), the prediction for secondary structures is indicated by the line referenced as “SUB_sec”. The key is provided by the website and the red H denotes α -helix and illustrated within the figure itself. Blue E denotes β -sheet while Green L indicates a mixture of other types of secondary structures. The prediction tool also attributed approximately 45 % α -helix, 3 % β -sheet and 52 %, random/others secondary structures.

A quick check of SpA242Qn protein on an online web tool (<http://www.predictprotein.org>) to predict its secondary structure is illustrated in Figure 4.6. The prediction tool provided an estimate of the composition of secondary structure elements, *i.e.*: 45 % α -helix, 3 % β -sheet and 52 % random or other types structures. Subsequently, the secondary structure of both fusion proteins (SpA242Q15) and (SpA242Q64) was determined by far-UV CD analysis at 34 μ M. The results indicated that both proteins had adopted α -helical secondary structure after the refolding process. Both (SpA242Q15) and (SpA242Q64) spectra showed two minima at 222nm and at near 208 nm (Figure 4.7C). They are both followed by a positive band each, at around 193nm. The CD spectra were de-convoluted by using the online software, K2D (<http://dichroweb.cryst.bbk.ac.uk/html/links.shtml>), which provided an analysis of the composition of secondary structures of the fusion proteins. A constraint was applied on the spectral values to reflect as a sum total of one and a summary of the values is reflected in Figure 4.7D. Both fusion proteins, (SpA242Q15) and (SpA242Q64) show similar

values for α -helices and random coil structure, indicating no apparent structural differences between them. It also suggests that an increase in poly-Q tract length does not appear to result in any unfavourable structural changes within each monomeric fusion protein.

Overall, the results demonstrate clearly that (SpA242Q15) and (SpA242Q64) had refolded with a distinct conformation and remained monomeric. As such, the following section will demonstrate whether ataxin-3 fragments that are derived from calpain-2 proteolysis, (242Q15) and (242Q64) can initiate and accelerate full-length expanded poly-Q ataxin-3 aggregation. At the same time, it will be investigated whether the poly-Q tract length within the ataxin-3 fragment modulates the aggregation kinetics of the full-length ataxin-3 protein.

Table 4.2: A comparison of molecular weights predicted of the fusion and fragment proteins of ataxin-3 using ProtParam on the bioinformatics resources portal, ExPASy (194) and that obtained from MALDI. ‘n.a.’ refers to not available

Variant	Predicted molecular weight (kDa)	Experimental mass obtained (MS)
(SpA242Q15)	24.3	24168.2
(SpA242Q64)	30.5	30493.9
(242Q15)	14.0	n.a.
(242Q64)	20.3	n.a.

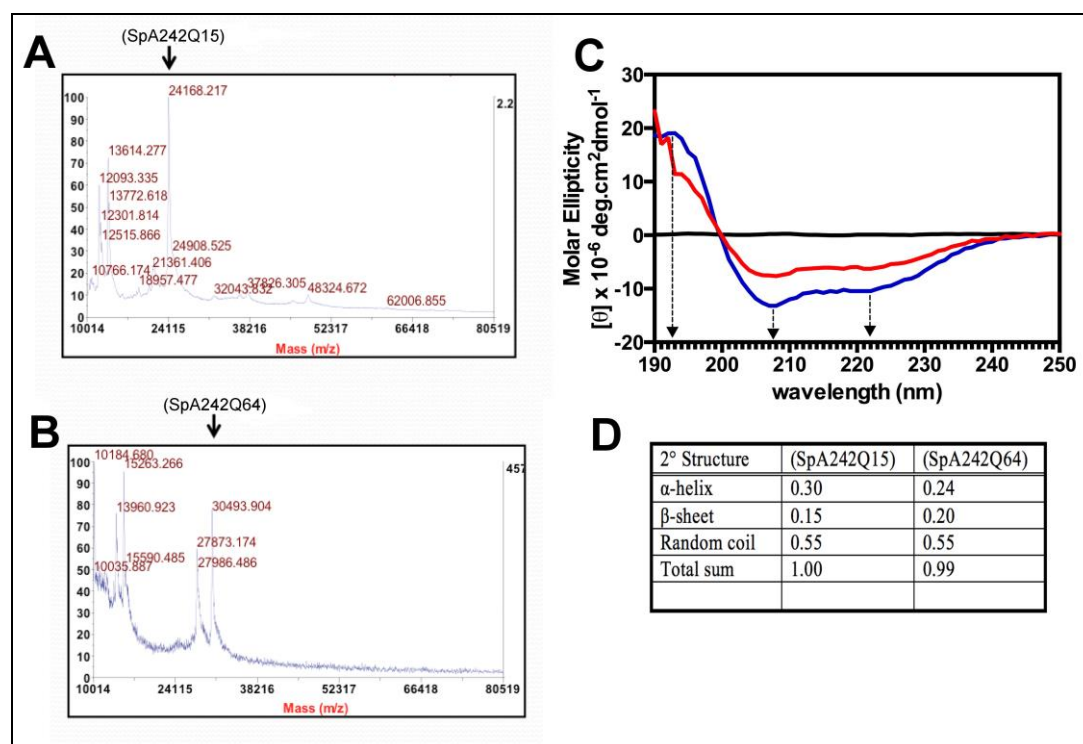


Figure 4.7 MALDI and CD analysis of ataxin-3 fusion proteins (SpA242Q15) and (SpA242Q64) Protein masses of (A) 24168 Da for SpA242Q15, while (B) 30493 Da for SpA242Q64 was detected as the major peak in its respective graphs. (C) CD analysis of both fusion proteins, with (SpA242Q15) is in blue, while (SpA242Q64) is in red. Buffer (Tris buffered saline with 10% glycerol) is in black. Both proteins show α -helical dominated structures (D) Estimated proportion of different structures after de-convoluting CD spectra of fusion proteins, (SpA242Q15) and (SpA242Q64).

4.2.4 Release of ataxin-3 fragments, (242Q15) and (242Q64) from SpA fusion partner by TEV protease proteolysis

For downstream protein aggregation assays, fusion proteins (SpA242Q15) and (SpA242Q64) were incubated with TEV protease, in order to release the fragments from its fusion partner to instigate any subsequent aggregation. This protocol would lead to TEV protease being present for the duration of the assay. It was vital that the protease does not interfere or compete in the assay, hence it was crucial to examine the degree of sensitivity of ataxin-3 fusion proteins to TEV digestion. The optimal concentration of protease necessary to release the fragment in the shortest possible time was therefore determined.

20 μ M (SpA242Q15) and (SpA242Q64) were incubated at different molar ratios of TEV protease:protein, at 10:1 and 1:1. Both fusion proteins were incubated with the His₆-tagged TEV protease for 20 min at 25 °C. Samples were obtained at 5 min time intervals and proteolytic activity was stopped with the addition of SDS-loading buffer with DTT and boiling for another 5 min. In Figure 4.8A, a representative SDS-PAGE after Coomassie Blue staining shows (SpA242Q64) protein samples cleaved by TEV protease. The protease was able to cleave (SpA242Q64) at 10:1 protease:protein ratio very quickly while (SpA242Q64) was cleaved by 5 min at 1:1 protease:protein ratio. The rate of cleavage of fusion protein (SpA242Q64) is fastest with a higher concentration of TEV protease used in the reaction. However, as TEV protease will not be removed from the assay reactions, the preferred ratio for the downstream assays adopted was 1:1 TEV protease:protein ratio. This was done to reduce possibilities of the TEV protease interfering in the following aggregation assays.

4.2.5 Detection of fragment (242Q15) and (242Q64) proteins by immunoblotting with S-tag antibody

The S-peptide is formed when RNase A is cleaved by subtilisin, giving rise to RNase S which consists of two tightly associated fragments, the S-peptide and the S-protein (195). The S-peptide, which is a 15-residue tag, (KETAAAKFERQHMS) has been used to purify tagged proteins from mammalian cell culture and in Western blots (184). The SDS-PAGE gel results from Figure 4.7A show a poor resolution of the resultant fragment proteins. Having inserted the S-peptide sequence at the C-terminal end of the fusion proteins through mutagenesis, the strategy was to monitor subsequent aggregation of fragment proteins (242Q15) and fragment (242Q64) via immunoblotting.

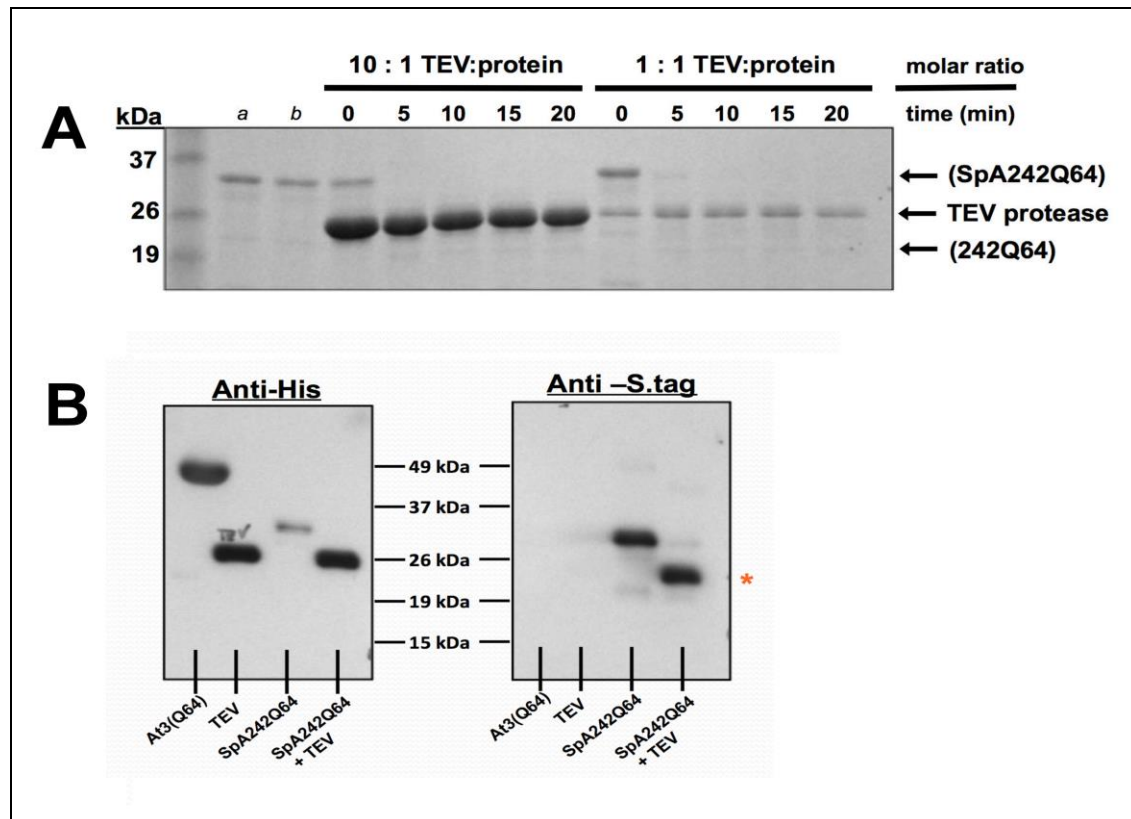


Figure 4.8 Sensitivity of ataxin-3 fusion proteins to TEV proteolysis and S-tag immunoblotting. (A) In this representation gel, fusion Q64 was used to demonstrate the molar ratios of TEV protease:protein necessary for efficient cleavage. As indicated in the gel, the ratios of 10:1, 1:1 were tested over duration of 20 min and samples were obtained every 5 min. The fragment (242Q64) protein was released from its fusion partner, SpA molecule. (B) Fusion protein (SpA242Q64) cleaved by TEV and probed with anti-His₆ and anti-S-tag antibodies via immunoblotting. The S-tag tagged fragment (242Q64) protein is released and detected at around 19 - 20 kDa, as indicated by the orange asterisk. The TEV protease is His-tagged and is only detected in the anti-His immunoblot and not in the anti-S-tag immunoblot.

In Figure 4.8B, 10 μ M of (SpA242Q64) was incubated with TEV protease at a 1:1 protease:protein ratio for 10 min at 25 °C and analysed via Western blotting. The anti-S-tag and anti-His₆ antibodies were used to visualise the fragment proteins. The results show that (SpA242Q64) showed immunoreactivity to both antibodies. As expected, fragment (242Q64) showed only immunoreactivity towards the S-tag antibody and indicated a fragment size of approximately 20 kDa. 10 μ M ataxin-3 (Q64) alone and 10 μ M TEV protease alone was used as controls for both western blots. This data demonstrates the potential of using the S-tag to follow fusion and fragment (Q15) and (Q64) proteins for SDS-insolubility assays.

4.2.6 Morphology of ataxin-3 fusion and fragment protein aggregates

Nuclear inclusions are classical trademarks of SCA3 and are known to consist of a heterogeneous mixture of pre-fibrillar aggregates, oligomers and mature fibrils (15, 113, 114). Transmission electron microscopy (TEM) is a high-resolution tool that is commonly applied to observe morphological changes in proteins such as the A β 1-42 peptide and α -synuclein (196, 197). Following the data obtained from SEC and CD, it has been demonstrated that refolded fusion (SpA242Q15) and (SpA242Q64) are monomeric. It is of interest therefore to monitor changes in morphology of the fusion and the fragment proteins of ataxin-3 before and after incubation using TEM.

Fusion (SpA242Q15) and (SpA242Q64) proteins were first incubated at 37 °C, with and without TEV protease at 1:1 TEV protease:protein ratio with no shaking. The samples were incubated for \geq 81 hours. Samples obtained at the time 0 h and at the respective endpoints were subsequently negatively stained with 1% (w/v) uranyl acetate. At time 0 h, both (SpA242Q15) and (242Q15) showed small spherical structures that are well dispersed upon the grid (Figure 4.9A and C). After 81 h, end point aggregates of (SpA242Q15) appeared to be oligomeric (Figure 4.8B). For (242Q15), the endpoint aggregates appeared small and curvilinear, resembling protofibrillar-like aggregates observed in previous studies (44, 58, 119) (Figure 4.9D). In contrast, long and large fibrils, of 50 – 100 nm in length were observed for (242Q64) after 86 h (Figure 4.9H). Large mature fibrils of expanded poly-Q tract proteins are often observed in studies that compared the morphology of expanded ataxin-3 proteins (44, 119) and the current results for fragment (242Q64) correlates with these studies. It is interesting that fusion (SpA242Q64) protein also produced curvilinear structures, instead of mature fibrils after 86 h (Figure 4.9F). In a study by Robertson *et.al.*, distinct amyloid-like fibrils were observed for SpA-cQ52 but only after 500 h incubation (105). Given the timeline of the observed endpoint aggregate of (SpA242Q64) at 86 h, it is interesting to note that the morphology observed could be an intermediate structure before it results in the formation of an amyloid fibril. Nonetheless, the observed structures of both fusion and fragment ataxin-3 proteins correlate well with previously reported studies of non-expanded and expanded poly-Q peptide aggregates (99, 198).

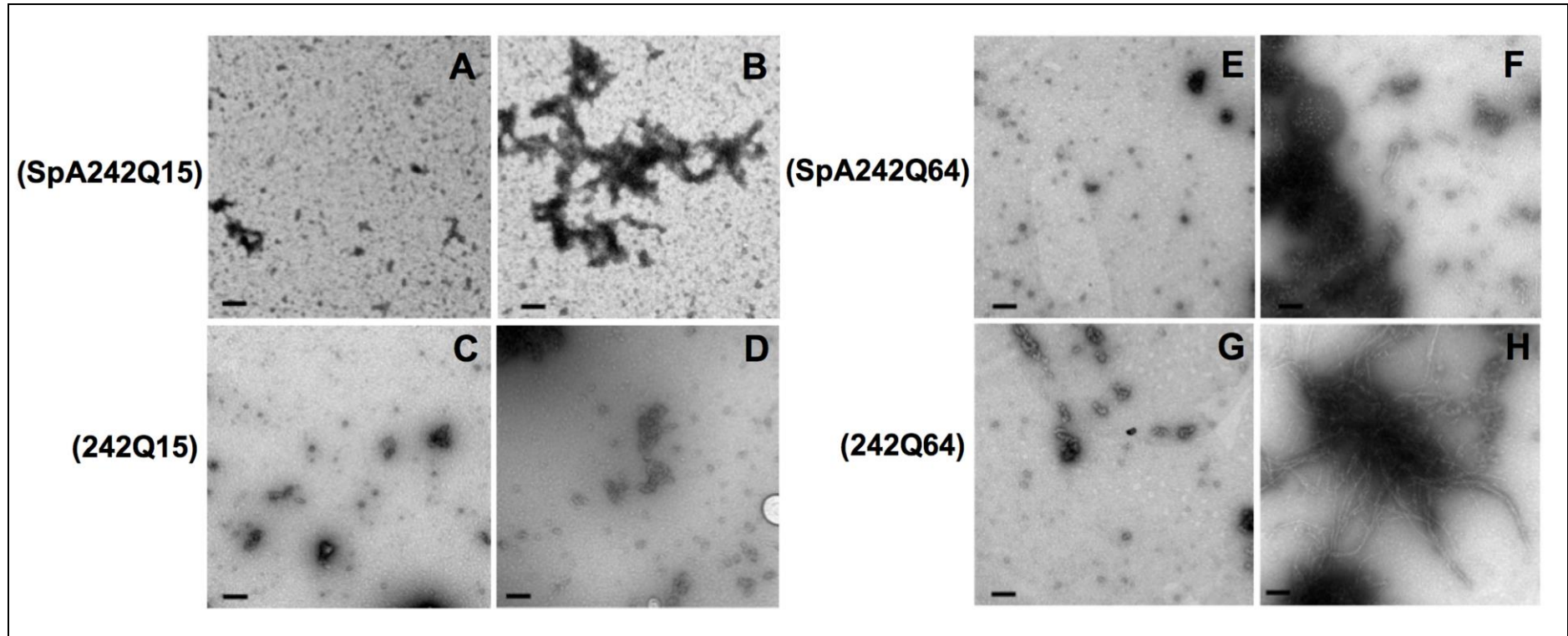


Figure 4.9: TEM images of fusion and fragment ataxin-3 Negatively stained samples images with 1% (w/v) uranyl acetate obtained after 20 μ M (SpA242Q15) was incubated at 37 $^{\circ}$ C for (A) 0 h and (B) 81 h. 20 μ M (242Q15) at 0 h (C) and (D) at 81 h, forming small curvilinear structures after incubation. (E) Structures of 20 μ M (SpA242Q64) is imaged at 0 h while (F) end point aggregates of 20 μ M (SpA242Q64) displayed prominent curvilinear structures at 86 h. In contrast, (H) (242Q64) showed distinctive large and long fibrils at 86 h while its structures at 0 h is imaged in (G). The scale bars represent 100 nm.

4.2.7 Fusion and fragment ataxin-3 aggregates displays low sensitivity to ThT fluorescence

Following the observation of fibril formation by TEM, the next step was to monitor aggregation kinetics of both fusion and fragment Q15 and Q64 proteins by ThT binding (3, 199). ThT is a fluorescent dye that is known to bind to β -sheets in fibrils, and dye-bound aggregates will emit fluorescence at a wavelength of around 485-490 nm when excited at 440 nm (198). Aliquots of end point aggregates of both fusion and fragment proteins were obtained. 20 μ M ThT dye solution was added to the protein sample and discontinuous ThT fluorescence was recorded with a fluorimeter. The fluorescence intensity of end point aggregates of fusion and fragment proteins were compared to ataxin-3 (Q64) fibrils (Figure 4.10A). It was interesting to observe that aggregates of (SpA242Q15) and (SpA242Q64) both recorded a minor increase in ThT fluorescence, but not as intensely as ataxin-3 full length Q64. Moreover, when fragment (242Q15) and fragment (242Q64) were analysed, their fluorescence intensity readings were not significantly higher than the fusion proteins themselves (Figure 4.10B and 4.10C respectively).

To further investigate if this observation was an anomaly, continuous ThT fluorescence was carried out to determine the aggregation kinetics of the fusion and fragment proteins. (SpA242Q15) and (SpA242Q64) proteins were incubated at 5 μ M and 20 μ M each with TEV protease at 1:1 molar ratio and incubated for a duration of up to 50 h. 20 μ M of ThT was added to the reaction mixture and samples were incubated on a 96-well flat bottom plate at 37°C. Readings were taken at 30 min intervals with a monochromatic plate reader. In Figure 4.11A, it can be seen that (SpA242Q15) emits approximately 4-fold less ThT fluorescence intensity compared to full-length ataxin-3 (Q15). 5 μ M and 20 μ M (242Q15) proteins recorded a low ThT fluorescence intensity compared to (SpA242Q15). In a similar fashion, the ThT intensity emitted for (SpA242Q64) was also 3.75-fold less than that of full-length ataxin-3 (Q64) (Figure 4.10C). Remarkably, 5 μ M and 20 μ M (242Q64) (red and green lines respectively) showed similar ThT intensity, which was also 3-fold less ThT fluorescence intensity than ataxin-3 (Q64). It is also worth mentioning that while the full-length ataxin-3 proteins,

(Q15) and (Q64) reached their reaction plateau around 30 - 35 h and 20 - 25 h respectively, fusions (SpA242Q15), (SpA242Q64) and fragments (242Q15), (242Q64) reached their plateau much earlier in under 5 h.

The aggregation kinetics of the ataxin-3 proteins and fusion variants were therefore further analysed. The curves for 5 μ M and 20 μ M (SpA242Q15) and (SpA242Q64) were corrected with TEV protease alone (20 μ M) to obtain a baseline for the reaction. The graphs were normalised and fitted to single exponential functions. Midpoints were derived and Table 4.3 shows a summary of the values obtained. A graph was annotated to compare the midpoints obtained for all proteins at 20 μ M (Figure 4.11E). At 5 μ M and 20 μ M concentrations, (242Q64) aggregated much faster (Figure 4.11D) than (242Q15) at the same concentrations (Figure 4.11B). At 20 μ M, (242Q64) exhibited the fastest aggregation reaction on its own, having a midpoint value of 0.5 h. The ThT midpoint value of 10.6 h for ataxin-3 (Q64) obtained in this study is comparable to a previously reported value of 10.4 h (58). It is interesting to observe that 5 μ M (SpA242Q15) exhibited similar kinetics to the ataxin-3 (Q15), having midpoints that were approximately 20 h. However, this trend is not observed for (SpA242Q64) to its respective full-length counterpart.

Overall, the ThT fluorescence data suggest that Poly-Q fragment aggregation appears to be both concentration dependent, as well as polyQ-tract length dependent. It has been previously proposed that ataxin-3 has an inherent property to form ThT positive aggregates, possibly driven by the Josephin domain and independent of the poly-Q tract (58, 69). The diminished intensity of ThT fluorescence recorded for both fusion and fragment (Q15) and (Q64) proteins strongly suggest the presence of the Josephin domain in providing that inherent propensity of ataxin-3 to form ThT positive aggregates. Low ThT fluorescence intensities are not commonly known for poly-Q proteins (58, 164) but it was reported in another study that simple poly-Q peptides bind ThT with very low intensities (200). Hence, with poor ThT fluorescence intensities, using this technique as a measurement of aggregation proved challenging. As such, we proceeded to analyse aggregation of both the fusion and fragment proteins using a characteristic of Poly-Q aggregates, detergent insolubility.

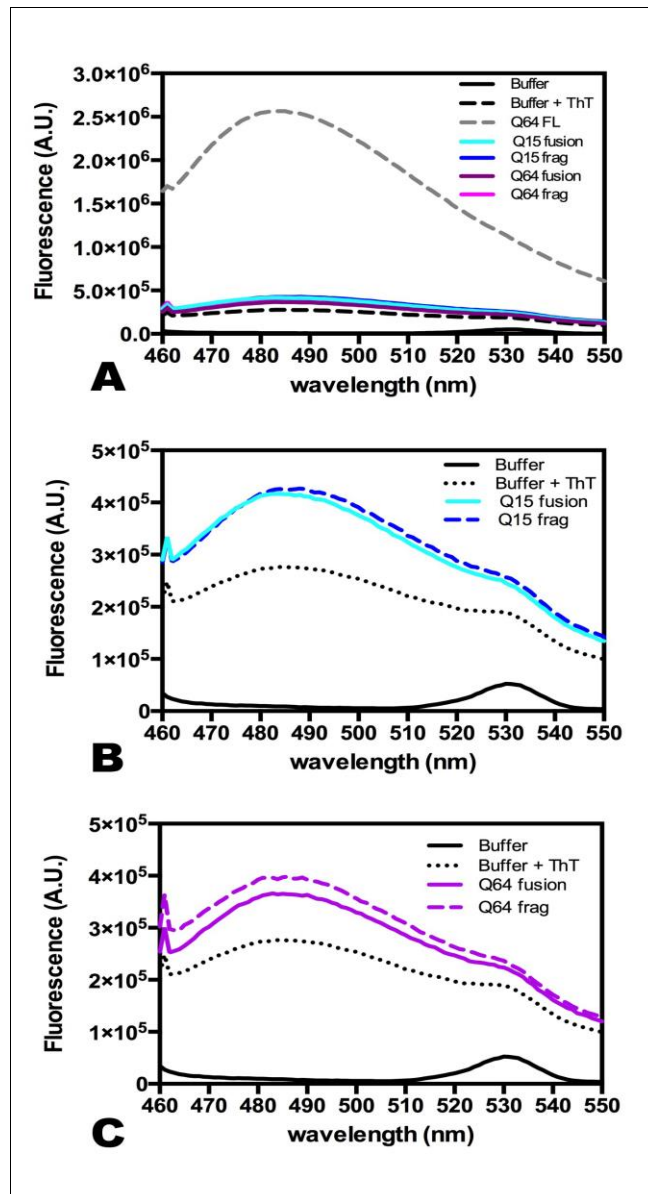


Figure 4.10 Discontinuous measurement of ThT fluorescence of fusion and fragment ataxin-3 proteins after aggregation assay. (A) Overview of ThT fluorescence of all the fusion and fragment ataxin-3 proteins in comparison to full length ataxin-3 Q64 (grey, dash) after their respective incubation period and buffer alone is black. (B) Fluorescence of end point aggregates (SpA242Q15) (light blue), (242Q15) (blue, dash) after 81 h and (C) SpA242Q64 (purple) and (242Q64) (purple, dash) after 86 h.

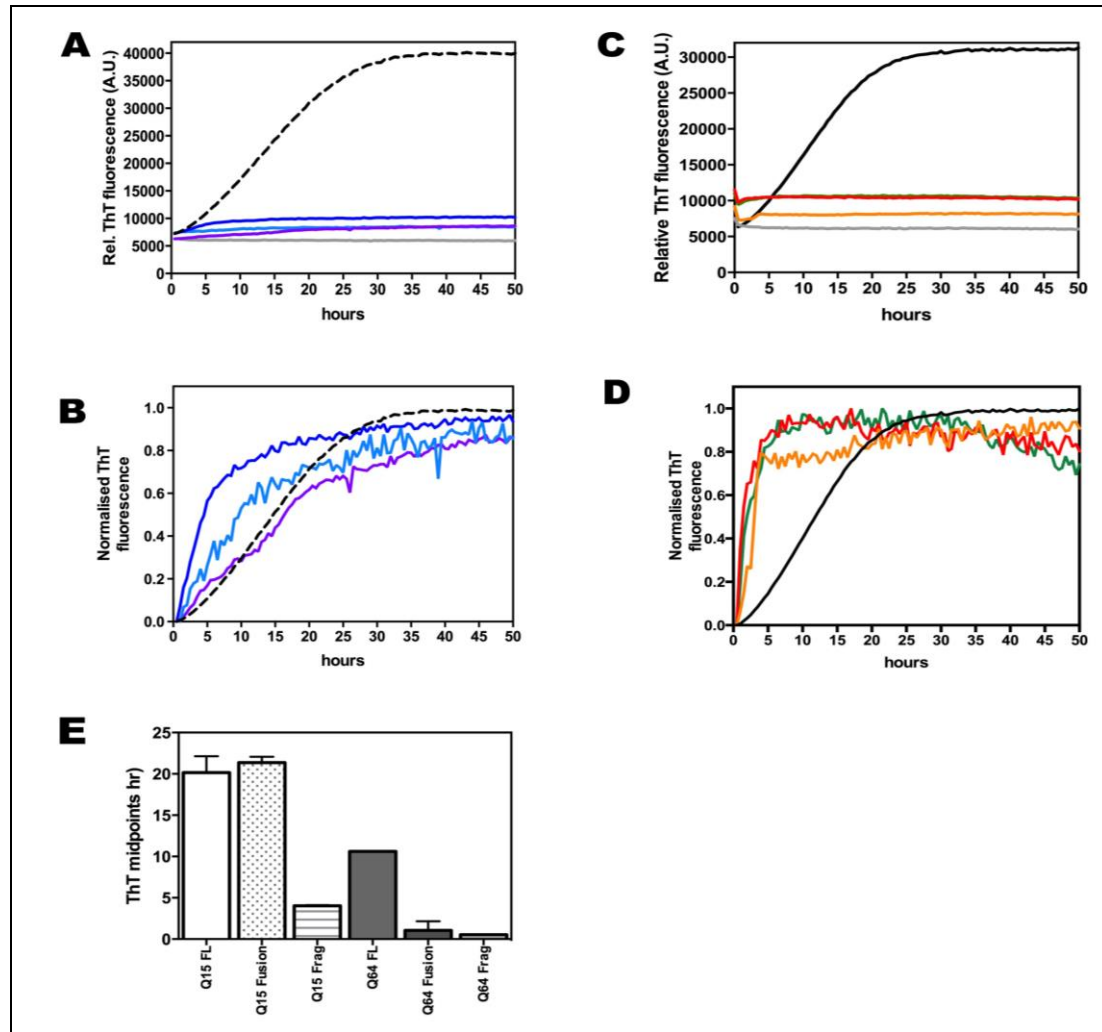


Figure 4.11 Continuous Thioflavin-T fluorescence measurement of (SpA242Q15) and (SpA242Q64) aggregation (A) Relative ThT fluorescence emitted over time by 5 μM (242Q15) (light blue), 20 μM (242Q15) (dark blue), 20 μM (SpA242Q64) (purple), 20 μM TEV protease alone (grey) and 20 μM full-length ataxin-3 (Q15) full (black, dash). Curves are means of two independent sets of experiments and fit to single exponential curve (B) (SpA242Q15) and (242Q15) curves are normalized after subtracting the fluorescence emitted by TEV protease alone. (C) ThT fluorescence emitted over by 5 μM (242Q64) (orange), 20 μM (242Q64) (red), 20 μM (SpA242Q64) (green), 20 μM TEV protease alone (grey) and 20 μM full-length ataxin-3 (Q64) (black, full). Curves presented here are also means from two independent sets of experiments. (D) (SpA242Q64) and (242Q64) curves are normalized after subtracting the fluorescence emitted by TEV protease alone. R^2 values for exponential fits of fusion and fragment (Q15) proteins is ≥ 0.97 while for fusion and fragment (Q64) proteins is ≥ 0.86 (E) Midpoints of ThT fluorescence aggregation reaction of (SpA242Q15), (242Q15), (SpA242Q64), (242Q64); compared to their full length ataxin-3 counterparts at the same concentration of 20 μM .

Table 4.3 ThT midpoints of the aggregation of fusion, fragment and full length proteins.

Midpoints are derived from single exponential functions. The values are means \pm S.E. and derived from two independent sets of data.

Sample	Conc. (μ M)	ThT Midpoint \pm S.E. (hours)
(242Q15)	5	9.36 ± 0.35
	20	4.04 ± 0.07
(SpA242Q15)	20	21.36 ± 0.70
Ataxin-3 (Q15) full length	20	20.15 ± 1.99
(242Q64)	5	2.02 ± 0.19
	20	0.54 ± 0.06
(SpA242Q64)	20	1.06 ± 1.09
Ataxin-3 (Q64) full length	20	10.61 ± 0.06

4.2.8 Fusion and fragment Q64 forms SDS-insoluble aggregates through their polyQ tract

Sodium dodecyl sulphate (SDS) insolubility has been used as a benchmark to characterize the biochemical properties of oligomeric or aggregated proteins associated with ND. Toxic protein aggregates, such as $A\beta_{1-42}$ peptide, α -synuclein and polyQ proteins are known to retain their oligomeric structure upon incubation with strong detergents such as SDS (197, 201-204). The SDS-insoluble aggregates may provide a more useful technique to monitor ataxin-3 fusion and fragment protein aggregation. Ataxin-3 is also reported to form SDS-insoluble aggregates in a poly-Q length dependent manner (58, 105, 180) which can be readily detected using a filter trap membrane.

Firstly, it was necessary to ascertain whether fusion and fragment (Q15) and (Q64) proteins would form SDS-insoluble aggregates. Increasing concentrations of fusion (SpA242Q15) at 0 μ M, 5 μ M, 10 μ M, 15 μ M and 20 μ M were incubated with 1:1 molar ratio of TEV protease. 20 μ M (SpA242Q15) without TEV protease was also incubated. The proteins were incubated at 37 °C and aliquots were obtained at three time points, 0, 21 and 86 h. These samples were boiled with 1% (w/v) SDS which denatures and solubilises all proteins. The sample was passed over a 0.2 μ m filter membrane that retain SDS-insoluble aggregates on the filter, while filtering SDS-soluble proteins. The

membrane was further washed with 0.1% (w/v) SDS to ensure complete retention of only SDS-insoluble aggregates. The membrane was probed with a S-tag antibody and detected by Western blotting to detect SDS-insoluble (SpA242Q15) and (242Q15). In Figure 4.12A, (SpA242Q15) and (242Q15) aggregates were not SDS-insoluble, as the aggregates were not retained on the membrane. As indicated, aggregated (SpA242Q64) at 5 μ M was used as a blotting control for the immunoblot. (SpA242Q64) and (242Q64) proteins were treated and processed in a similar fashion to (SpA242Q15) for the immunoblot. It was observed that 5 μ M and 20 μ M (242Q64) protein resulted in the formation of SDS-insoluble aggregates after 86 h (Figure 4.12B, lanes *b* and *c*). 20 μ M (SpA242Q64) also clearly formed SDS-insoluble after 86 h of incubation (Figure 4.12B, lane *d*). 20 μ M full-length ataxin-3 protein (Q64) and SpA were used as negative immunoblotting controls. The result correlates with previous studies that indicate only pathological length poly-Q fusion and fragment proteins display SDS-insolubility (58, 115, 205).

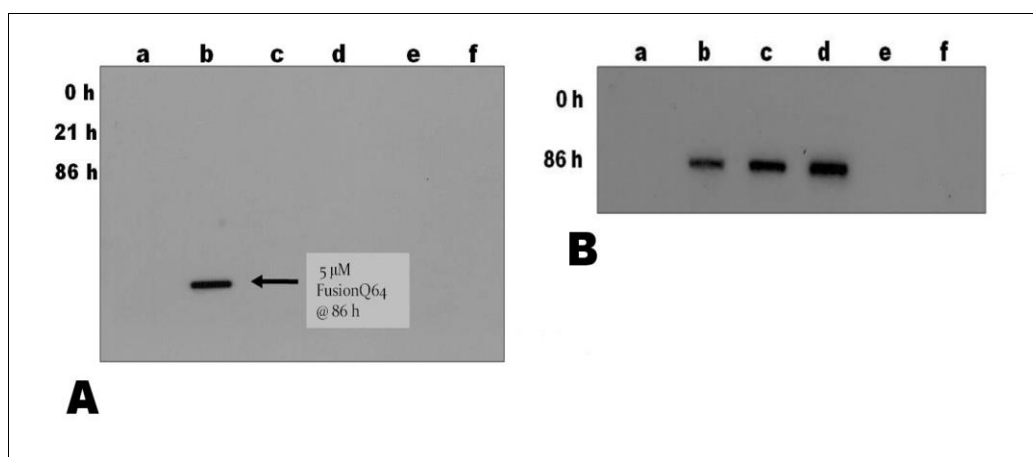


Figure 4.12 Formation of SDS-insoluble aggregates of ataxin-3 fusion proteins, (SpA242Q15) and (SpA242Q64), following S-tag antibody in Western blotting (A) Filter trap membrane result for different concentrations of (SpA242Q15) at 0 h, 21 h and 86 h. Lane (a) is 20 μ M TEV protease alone, lane (b) 1:1 5 μ M (SpA242Q15): TEV, (c) 1:1 10 μ M (SpA242Q15): TEV, (d) 1:1 15 μ M (SpA242Q15): TEV, (e) 1:1 20 μ M (SpA242Q15): TEV and (f) 20 μ M (SpA242Q15) alone. Under lane (b) shows 5 μ M (SpA242Q64) SDS-insoluble aggregates after 86 h, positive for S-tag immunoblotting. **(B)** Results of different concentration (SpA242Q64) SDS-insoluble aggregates at 0 h and 86 h. Lane (a) 20 μ M TEV protease alone, (b) 1:1 5 μ M (SpA242Q64): TEV, (c) 1:1 20 μ M (SpA242Q64): TEV (d) 20 μ M (SpA242Q64) alone, (e) 20 μ M Protein A (pA) alone and (f) 20 μ M ataxin-3 (Q64) alone.

To verify that the formation of SDS-insoluble aggregates is mediated by the presence of the poly-Q tract, the peptide QBP1 was used. QBP1 is a tryptophan rich (six

in total) peptide that binds only to pathological length poly-Q domain proteins, and efficiently inhibits subsequent poly-Q protein aggregation (58, 206). The peptide, QBP1 was mixed with 20 μ M (SpA242Q64) and 20 μ M (242Q64) at a 6:1 peptide:protein molar ratio. Samples were incubated at 37 °C and aliquots were obtained at time 0 h and 48 h. Figure 4.13 indicates that (SpA242Q64) (lane *e*, top and bottom panels) had its SDS-insolubility inhibited by QBP1. Similarly, fragment (242Q64) (lane *d*, top and bottom panels) had their aggregation inhibited by QBP1, resulting in no SDS-insoluble aggregates being formed. Using both anti-His₆ and anti-S-tag antibodies, it simultaneously indicates that neither TEV protease nor SpA affects the resulting aggregation reaction (Figure 4.13, lane *b* and *c* respectively). In the presence of QBP1, full-length ataxin-3 (Q64) did not form SDS-insoluble aggregates (Figure 4.13, lane *a*). Control lane (*f*) on both immunoblots is of 20 μ M (SpA242Q64) without the presence of QBP1. These data support that the SDS-insolubility of the ataxin-3 fusion and fragment protein aggregates is due to the expanded poly-Q tract during aggregation (207).

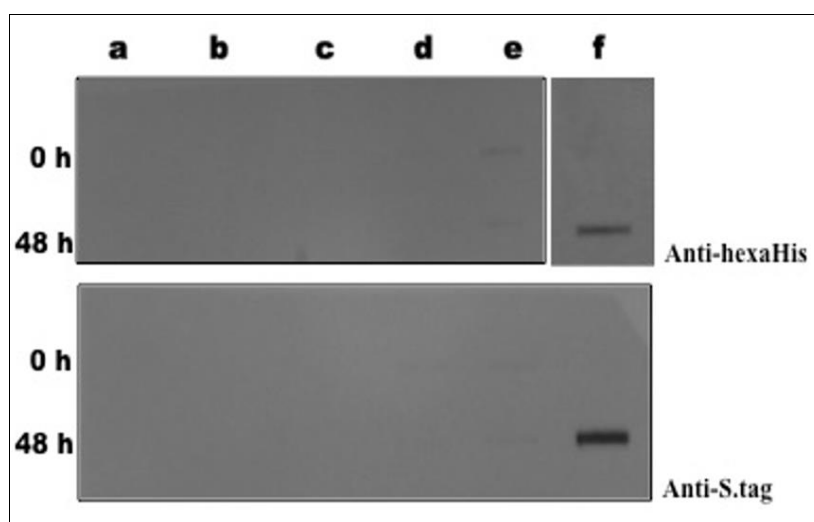


Figure 4.13 Effect of QBP1 peptide on fusion and fragment ataxin-3 (Q64) proteins monitored via filter trap membrane assay. Proteins were incubated with molar ratio of 6:1 QBP1: protein from 0 h and 48 h time points. Filter trap membranes were probed with either anti-His₆ or anti-S-tag antibody for western blotting. Lanes show (*a*) 20 μ M full-length ataxin-3 (Q64), (*b*) 20 μ M pA, (*c*) 20 μ M TEV protease, (*d*) 1:1 20 μ M (SpA242Q64): TEV, (*e*) 20 μ M (SpA242Q64) alone and (*f*) 20 μ M (SpA242Q64) alone without QBP1.

4.2.9 Monitoring aggregation kinetics of (SpA242Q64) and (242Q64) via SDS-insolubility

After ascertaining the SDS-insolubility of fusion and fragment Q64 aggregates, this method was used to monitor the aggregation kinetics of the proteins. Fusion (SpA242Q64) was incubated at different concentrations at 0, 5, 10 and 20 μM at 37 °C. Aliquots were collected at specific time points and samples were boiled with 1 % (w/v) SDS, passed over a 0.2 μm filter membrane and then washed with 0.1 % (w/v) SDS. The filter trap membrane was followed by anti-S-tag immunoblotting and densitometry was used to follow the change in band density. Figure 4.14A shows that at 5 μM (SpA242Q64), faint bands were only detected after 48 h, being slightly more distinctive around 72 h. At both 10 μM and 20 μM , (SpA242Q64) exhibited an accelerated aggregation, forming intense bands until 48 h. The reduced band intensity at 72 h suggests a possibility that the SDS-insoluble aggregates were dropping out of solution before it was analysed.

In Figure 4.14B, the kinetic profiles of (SpA242Q64) aggregation were derived from three independent sets of experiments, measuring the density of each band and plotting them against time. The values were normalized and curves were fitted to exponential functions. 5 μM (SpA242Q64) shows a sigmoidal curve with a pronounced lag phase. Increasing concentrations of (SpA242Q64) reduced the length of the lag phase, with the highest concentration of 20 μM almost abolishing the phase itself. Figure 4.14C and D both indicate the result of fragment (242Q64) aggregation kinetic profile. Increasing concentrations of 0 μM , 5 μM , 10 μM , 15 μM and 20 μM fragments were released by TEV proteolysis from fusion (SpA242Q64) and formed SDS-insoluble aggregates (Figure 4.14C). The kinetic profile of (242Q64) follows a similar trend to (SpA242Q64), where 5 μM and 10 μM exhibited a sigmoidal profile with an initial lag phase (Figure 4.14D). However, at higher fragment (242Q64) concentrations, the lag phases were no longer pronounced. Figure 4.14E and Figure 4.14F are representative of a typical filter trap assay of full-length ataxin-3 and the kinetic curve obtained from densitometry respectively. Midpoint values were also derived and a summary of the values is collated in Table 4.4.

In summary, the results show firstly that kinetics of (SpA242Q64) and (242Q64) aggregation are concentration-dependent (Figure 4.13G). Both fusion and fragment (Q64),

at the lowest concentration of 5 μM , had midpoints at 32 h and 24 h respectively. With increasing concentrations up to 20 μM , the midpoints decreased to 2.5 h for fusion (SpA242Q64) and 1.7 h for fragment (242Q64). Secondly, the classical nucleation-dependent time course, with a pronounced lag phase with a growth phase, is only observed for concentrations 5 and 10 μM . As the concentration of fusion and fragment increases, the kinetics no longer followed the sigmoidal trend. This result could suggest that as concentration of the expanded poly-Q length tract increases, the short time taken for nucleation is no longer readily detectable.

Table 4.4 SDS-insolubility midpoints of (SpA242Q64) and (242Q64) aggregation. Midpoints are derived from single exponential functions. The values are means \pm S.E. and derived from three independent sets of data. 20 μM of all proteins were compared and analysed via one-way ANOVA, where **** represents significant values at $p > 0.0001$

Sample	Conc. (μM)	Midpoint \pm S.E. (hours)
Ataxin-3 Q64 full length	20	30.1 \pm 0.39 ****
(SpA242Q64)	5	32.0 \pm 0.37
	10	6.1 \pm 0.23
	20	2.5 \pm 0.18 ****
(242Q64)	5	24.0 \pm 0.15
	10	5.3 \pm 0.35
	15	2.0 \pm 0.15
	20	1.7 \pm 0.12 ****

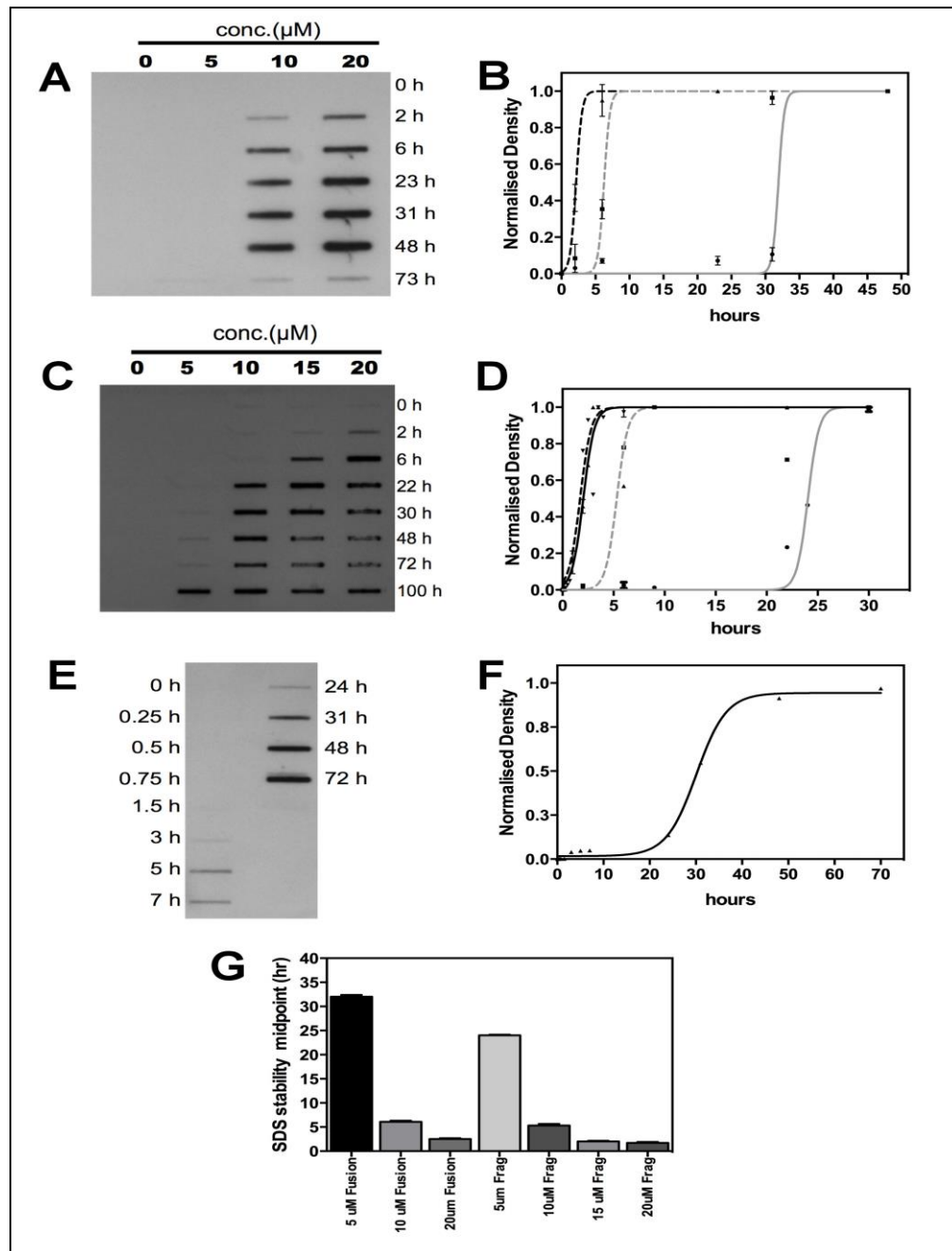


Figure 4.14 Fusion and fragment ataxin-3 proteins (SpA242Q64) and (242Q64) aggregation monitored by SDS-insolubility. Representative filter trap membrane is shown of (A) (SpA242Q64) (C) (242Q64) and (E) full length ataxin-3 (Q64). Analysis of the filter trap membranes by densitometry is shown for (B) (SpA242Q64) for 5 μM (grey), 10 μM (grey, dashed) and 20 μM (black, dashed). (D) Analysis of density against concentration of (242Q64) at 5 μM (grey), 10 μM (grey, dashed), 15 μM (black) and 20 μM (black, dashed) and (F) shows for ataxin-3 (Q64) alone (black). (G) SDS-insolubility midpoint trends observed for both (SpA242Q64) and (242Q64) protein in a concentration-dependent manner.

4.2.10 Acceleration of SDS-insoluble full-length ataxin-3 (Q64) aggregation initiated by poly-Q length fragments

After validating the stability the filter trap membrane assay to follow aggregation kinetics, the next step was to study if the fragments (242Q15) and (242Q64) modulate the aggregation kinetics of full-length ataxin-3 protein. In this experiment, 20 μ M full-length ataxin-3 (Q64) was incubated separately with 20 μ M of both fusion proteins at a 1:1 TEV protease:protein ratio respectively. The proteins were incubated together at 37 °C and aliquots were obtained over various time points. SDS-stable aggregates retained on the membrane were probed with an anti-His₆ antibody via Western blotting.

Figure 4.15A shows a representative filter trap membrane of fragment (242Q15) on full-length ataxin-3 (Q64), while the result of fragment (242Q64) on full length (Q64) is shown in Figure 4.15B. Bands for both reactions were observed as early as 30 min into the reaction. The density of the bands was plotted against time and final readings were normalised to obtain kinetic curves. Figure 4.15D clearly shows an acceleration of aggregation of full-length ataxin-3 (Q64), modulated by fragment (242Q15) (orange) and fragment (242Q64) (purple). Interestingly, both fragment proteins eliminated the presence of the lag phase, which was characteristic of full-length ataxin-3 (Q64) SDS-insoluble aggregation. In order to ascertain the midpoints of the accelerated full-length ataxin-3 (Q64), the Michaelis-Menten function was used to fit the curves. In a recent study, fibril elongation was found to fit to an enzyme-like model using Michaelis-Menton kinetics, when preformed seeds are added to a solution of protein (208). A summary of the midpoints derived is tabulated in Table 4.5 while Figure 4.15F shows an overall trend of the ataxin-3 fragments accelerating ataxin-3 (Q64) aggregation. The midpoint value for full-length ataxin-3 (Q64) was obtained at 30.1 ± 0.39 h and had shifted significantly to 2.5 ± 0.18 h and 1.7 ± 0.12 h by 20 μ M (SpA242Q64) and (242Q64) respectively (Table 4.5) (one-way ANOVA, $p < 0.0001$). The fragment (242Q15) on ataxin-3 (Q64) shifted the midpoint value to 6.6 h while fragment (242Q64) on ataxin-3 (Q64) resulted in midpoint value of 7.0 h. The results strongly suggest both fragment proteins accelerated the aggregation of ataxin-3 (Q64) at similar kinetics.

As a comparison, 20 μM monomeric ataxin-3 was ‘seeded’ with approximately 2 μM pre-formed full-length ataxin-3 (Q64) aggregates. Figure 4.14E shows the kinetic curve based on densitometry results of ataxin-3 (Q64) (grey) and when it is seeded with pre-formed ataxin-3 (Q64) seeds (black). The curve also showed a diminished but not abolished lag phase. The midpoint value also showed a shift from 30 h to 10.4 h (Table 4.5). The result suggests the accelerated SDS-insoluble ataxin-3 (Q64) aggregation by (Q64) seeds is not as rapid compared to the fragments themselves. There is a possibility that the ataxin-3 fragment proteins might be initiating expanded ataxin-3 SDS-insolubility by bypassing Stage 1 of the pathway.

It has been previously noted in the literature that expanded ataxin-3 fragments, when co-expressed with various poly-Q tract lengths of full-length ataxin-3 proteins in cell culture, were detected as co-aggregates through immunofluorescence microscopy (16, 29). Next, we wanted to explore whether we could observe aggregation of non-expanded ataxin-3 (Q15) in the presence of fragment (242Q64), and if ataxin-3 (Q15) is able to form SDS-stable aggregates in the presence of fragment (242Q64). 20 μM of fragment (242Q64) was released in the reaction with ataxin-3 (Q15) and (Q64) respectively. Aliquots were taken at time points and were processed in the filter trap assay. The membrane was probed with anti-His₆ antibody, in order to monitor the aggregation of His₆-tagged full-length ataxin-3 proteins. In Figure 4.14C, fragment (242Q64) accelerated aggregation of ataxin-3 (Q64), forming SDS-stable aggregates. However, fragment (242Q64) was unable to initiate aggregation of ataxin-3 (Q15) to form SDS-stable aggregates. These results demonstrate that the formation of SDS-insoluble aggregates is dependent on the presence of an expanded polyQ tract within the free ataxin-3 protein.

Table 4.5: SDS-insolubility midpoints of the aggregation reaction of ataxin-3 fragments on full-length ataxin-3. Midpoints are derived from single exponential functions. The values are means \pm S.E. and derived from two independent sets of data

Sample	Conc. (μM)	$K_M \pm \text{S.E.}$ (hours)	Midpoint \pm S.E. (hours)
-242Q15 frag + Q64 FL	20	6.6 ± 0.89	
-242Q64 frag + Q64 FL	20	7.0 ± 0.79	
Ataxin-3 Q64 FL seed	20		10.4 ± 0.65

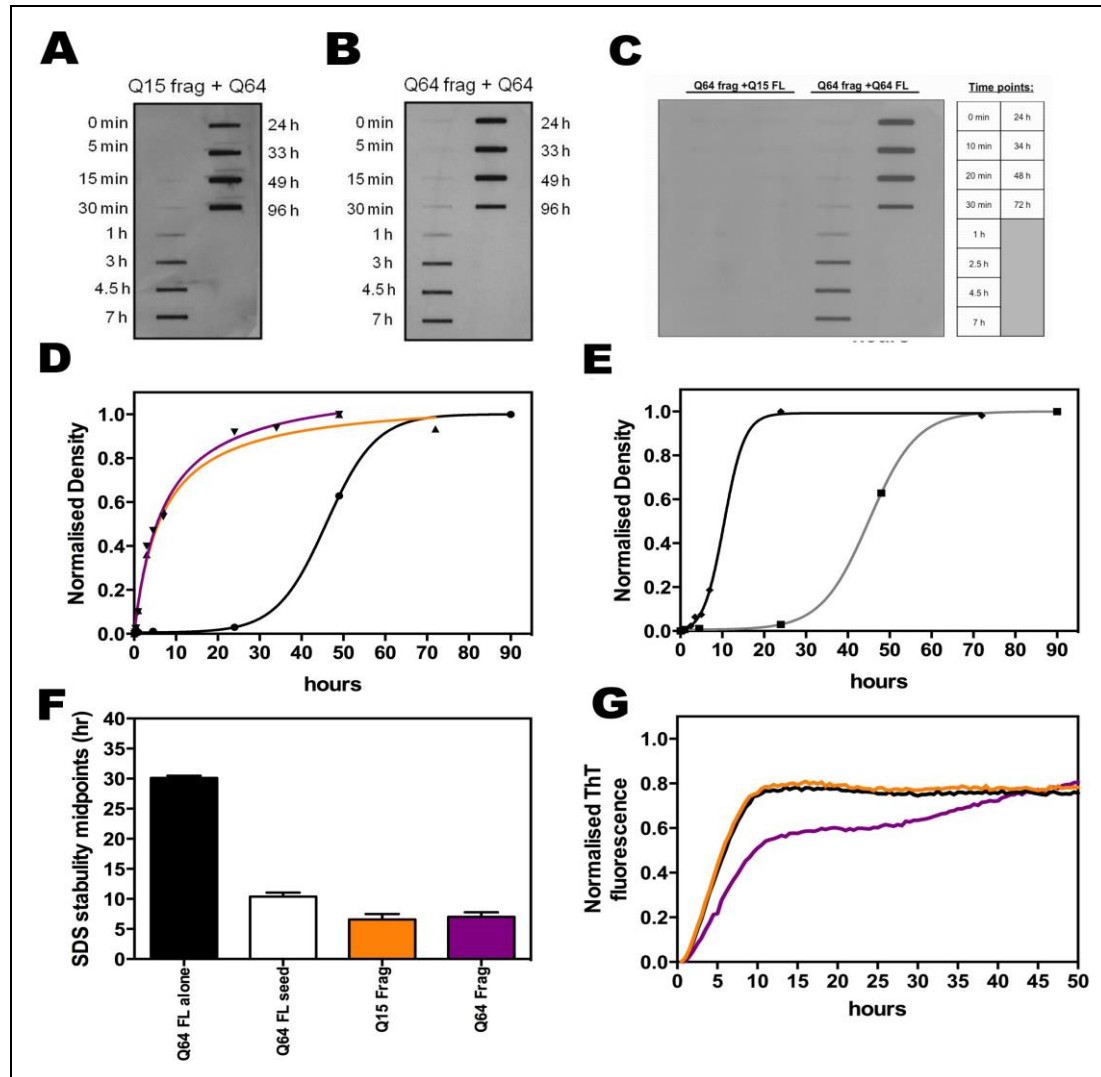


Figure 4.15: Acceleration of full-length ataxin-3 (Q64) SDS-insoluble aggregation initiated by fragment ataxin-3 proteins, (242Q15) and (242Q64). Representative filter trap membrane assay results of (A) (242Q15) and (B) (242Q64) released from their respective fusion partners by TEV protease at time 0 min onwards. (D) Densitometry analysis of the filter trap membrane assay of (242Q15) (orange) and (242Q64) (purple) initiating and accelerating aggregation reaction of full-length ataxin (Q64). Full-length ataxin-3 Q64 alone is shown here in black. The R² value for all exponential fits is ≥ 0.99 . (E) Densitometry analysis of full length ataxin (Q64) 'preformed' aggregates on full-length ataxin Q64 (black) while full-length ataxin-3 Q64 is shown in grey. R² values for all exponential fits ≥ 0.98 (C) Filter trap membrane assay results on (242Q64) on full-length ataxin-3 Q15 (left most) and ataxin-3 Q64 (right most). (F) Results of (D, E) and the observed SDS-insolubility midpoints of full-length ataxin-3 (Q64) (black), full-length ataxin-3 Q64 preformed seeds (white), fragments (242Q15) (orange) and (242Q64) (purple). (G) Cross-seeding of (242Q15) (orange) and (242Q64) (purple) on full-length ataxin-3 (Q64) (black) monitored by ThT fluorescence. All the above data is represented as means of two independent sets of experiments.

4.2.11 Fragments (242Q15) and (242Q64) do not bypass first stage of ataxin-3 aggregation pathway

Ataxin-3 C-terminus fragments (242Q15) and (242Q64) has demonstrated rapid initiation of ataxin-3 (Q64) to enter the second stage of its aggregation pathway, forming SDS-insoluble aggregates. The presence of these rapidly forming aggregates poses the interesting question of whether (242Q15) and (242Q64) were accelerating ataxin-3 (Q64) aggregation and bypassing the first stage of the pathway. Based on previous studies, ThT fluorescence is conferred only when the Josephin domain self-associates (57, 122). If the fragments were accelerating the ataxin-3 (Q64) SDS-insoluble aggregation, and bypassing the first stage, the resultant ThT fluorescence would change the kinetic profile of ataxin-3 or create a distinct plateau. Thus, it is of interest to investigate whether the fragments could have then bypassed the first stage of ataxin-3 (Q64) aggregation in this study. ThT fluorescence was used to monitor the first stage of ataxin-3 (Q64) aggregation upon seeding with (242Q15) or (242Q64) fragments. 20 μ M of each fragment was released in the reaction with 20 μ M full-length ataxin-3 (Q64) and ThT fluorescence intensities were recorded every 30 min for 50 h.

The results are shown in Figure 4.15G. In the presence of fragment (242Q64), full-length ataxin-3 (Q64) did not display any difference in ThT sensitivity or acceleration in aggregation. As there is no change observed, the results suggest that fragment (242Q15) did not instigate ataxin-3 (Q64) from bypassing the first stage of its aggregation pathway. Interestingly, when fragment (242Q64) seeded ataxin-3 (Q64), the full-length protein underwent a biphasic time course. The first phase of the time course was observed to be slightly slower. A short plateau followed before the second phase occurred. From these results, neither fragment (242Q15) nor (242Q64) altered the ThT fluorescence sensitivity of full-length ataxin-3 (Q64). The result indicates that both fragments (242Q15) and (242Q64) do not facilitate full-length ataxin-3 (Q64) into bypassing the first stage of its aggregation process.

4.3 Discussion

The role of ‘toxic proteolytic fragments’ in SCA3 and other proteins related to neurodegeneration has always been of high relevance in research aimed at a better understanding of the aberrant pathways that lead to disease (129, 181, 182). During our research, a study found that expanded poly-Q ataxin-3 proteolytic fragments are essential in initiating the ataxin-3 aggregation process and the sequestration of full-length ataxin-3 proteins in cell culture (129). In this project, we were able to characterize both non-expanded and expanded poly-Q ataxin-3 fragment proteins. We were also able to clearly demonstrate that expanded poly-Q ataxin-3 fragments are able to initiate and accelerate the aggregation reaction of full-length expanded ataxin-3 but not non-expanded poly-Q ataxin-3 protein *in vitro*.

4.3.1 Fusion ataxin-3 proteins can be successfully purified from inclusion bodies and be refolded into structured monomers

Ataxin-3 variants are routinely expressed as soluble in *E. coli* in our laboratory and purified using a robust purification protocol. Solubility only starts to decrease with the expanded poly-Q stretch in ataxin-3 (e.g. >50 glutamines) but still yield a sufficient quantity for downstream assays. In this study, the use of soluble fusion tags was necessary to assist in the expression of soluble ataxin-3 fusion proteins. It was unfortunate that even though some soluble fusion proteins were identified, such as MBP or the engineered Z-domain of Protein A, as suitable fusion partners, recurring proteolytic degradation still hindered the project. To circumvent this situation, a considerable amount of time was spent in the attempt to re-position fusion partners as ‘protective’ domains around the fragment, through genetic manipulation of the expression vector. Various *E.coli* strains were tested and every possible protease inhibitor available was used in an attempt to limit proteolysis. At the same time, a high degree of fragmentation of purified recombinant ataxin-3 fragments, 257cQ71, was also observed *in vitro* by Haacke *et. al.* (129). It is uncertain what the cause of the fragmentation might be. However, a possible explanation is that the partially folded fragments of ataxin-3 are likely to be more prone to protein degradation by contaminating *E. coli* proteases than the full-length ataxin-3 proteins (209). Despite the published results by Haacke *et. al.* showing non-specific

fragmentation of their C-terminal ataxin-3 fragments, it was paramount to obtain uncleaved proteins for *in vitro* assays in this study. The presence of contaminating fragments might bias the results obtained from downstream assays, raising questions on the validity of (242Q15) or (242Q64) fragments in modulating aggregation of ataxin-3 protein.

In order to obtain pure and un-cleaved fusion proteins, we sought to use the fusion proteins found in IB found after *E.coli* cell lysis. A protocol that was established for refolding serpins from our group was adapted for the refolding of ataxin-3 fusion proteins (191). We report here, for the first time, a successful study on the refolding and purification of an ataxin-3 fusion protein. Protein refolding using SEC was chosen over simple dilution, as there was a more controlled flow rate of diluting out the denaturant. At the same time, the porous structure of the gel resin is thought to physically separate aggregates and the refolding protein as it gravitates down the column (210). Importantly, monomers that were refolded successfully retained α -helical secondary structure and were not proteolysed. Our results supports the view held by various studies that recombinant proteins found in IB are protected from degradation (188, 211, 212). If ataxin-3 fragment proteins could be refolded from IB, was a ‘solubility’ tag necessary for use? Evidently yes, as it appears that having a fusion tag may have helped to provide stability and solubility to an otherwise hydrophobic C-terminal end stretch of the ataxin-3 fragment, which mainly consist of poly-Q residues. A study recently described denatured Z-domain tagged proteins in 8M urea being successfully refolded using cation exchange chromatography (212), suggesting that Protein A might be both a good soluble fusion tag as well as refolding protein partner.

The SEC, CD spectroscopy and MALDI results indicated fusion proteins (SpA242Q15) and (SpA242Q64) had refolded correctly, being soluble, monomeric and had retained native-like secondary structure. The monomeric nature of the refolded fusion ataxin-3 proteins was confirmed through SEC. The CD spectral results showed that the fusion ataxin-3 proteins displayed clear α -helical conformation. Also, the mass spectroscopy results indicated both fusion proteins reflected their predicted masses based on their protein sequences. These results also support the predicted composition of secondary structure elements (Figure 4.6).

4.3.2 Fusion and fragment proteins emit weak ThioT fluorescence but form aggregates with distinct morphology

From the current literature, non-expanded ataxin-3 proteins have been shown to form curvilinear structures that resemble protofibrils, which is attributed to the self-aggregating property of the Josephin domain (44, 58). The Josephin domain is thought to essentially confer ThT-reactivity to ataxin-3 proteins (58, 62, 122). Notably, the absence of Josephin domain within the fusion ataxin-3 proteins could have resulted in lowering the ThT-sensitivity of the fusion aggregates formed. Poly-Q fibrils have been reported to bind ThT but not as strongly as Josephin domain oligomers (118, 200). This is further supported by the minimal change in ThT fluorescence that is observed in the second stage (poly-Q dependent) of full-length ataxin-3 aggregation (Figure 4.11C).

The morphology of the end-point aggregates observed in this study was interesting as it was heterogeneous. Firstly, both (SpA242Q15) and fragment (242Q15) formed small oligomers while (242Q15) structures were more curvilinear. This result correlates to that observed for non-expanded ataxin-3 (Q15) (58). Likewise, another poly-Q fusion protein, GST-(Q20) Huntingtin protein (Htt) was found to form fusion aggregates that were oligomeric but did not reach the fibrillar state (213). Poirier and colleagues used the fusion protein, MBP-(Q44) Htt and observed under EM that after cleaving MBP, soluble globular oligomeric assemblies were formed within half an hour (214). This could suggest why sparsely distributed oligomeric structures were also formed at 0 h for fragment (242Q64). Fragment (242Q64) formed classical fibrils as predicted of poly-Q peptides (13, 107, 109). Interestingly, the result of fusion (SpA242Q64) aggregates showed a different morphology compared to a study described by Robertson *et. al.* (105). The fusion (SpA242Q64) formed large, banded curvilinear aggregates. In contrast, the fusion protein studied by Robertson *et. al.* which had a single B-domain of Protein A and a stretch of all 52 glutamine residues (SpA-c52) formed fibrillar structures. A possible reason to account for the differences in observed morphology was most likely due to the different pH in which the aggregates were formed. SpA-c52 was incubated at pH 5.0 while fusion Q64 was incubated at pH 7.4. These data corroborate a previous study that observed enhanced amyloid formation at a slightly acidic pH (215).

4.3.3 Aggregation of fusion (SpA242Q64) and fragment (242Q64) can be monitored through SDS-stability

It has been reported that only pathological, expanded poly-Q tract ataxin-3 forms SDS-insoluble aggregates in the second stage of the aggregation pathway (58). SDS-insolubility is thought to result from the direct interaction of expanded poly-Q tracts (58, 203) and the irreversible hydrogen bonding of glutamine side chains that results (216). The role of the expanded poly-Q tract in conferring SDS-insolubility was shown when expanded fusion (SpA242Q64) and fragment (242Q64) SDS-insoluble aggregate formation was inhibited in the presence of a poly-Q tract inhibitor peptide QBP1 (58, 105, 180, 206). To verify these results, both fusion (SpA242Q15) and fragment (242Q15) did not show SDS-stability like expanded poly-Q tract length proteins.

It was further demonstrated that fusion (SpA242Q64) and fragment (242Q64) aggregated in a concentration-dependent manner. In this study, ataxin-3 (Q64) displayed a sigmoidal kinetic profile with a pronounced lag phase. Both (SpA242Q64) and (242Q64) displayed such a sigmoidal kinetic profile with starting concentrations $\leq 10 \mu\text{M}$ but lost the lag phase with higher concentrations of protein. These data correlates well with a previous study on full-length ataxin-3 (Q64) protein (122), indicating the fusion and fragment proteins in this study, aggregate with similar characteristics to disease-causing proteins.

4.3.4 Ataxin-3 Poly-Q fragments accelerated the formation of second stage SDS-stable aggregates of ataxin-3 (Q64)

To this point, kinetics of both fusion and fragment (Q64) through SDS-stability were characterised. The overall aim of the study is to investigate kinetically if fragments (242Q15) and (242Q64) were both able to initiate the aggregation of full-length ataxin-3 (Q64) through SDS-stability as well. We first performed assays using pre-formed aggregates of full-length ataxin-3 Q64 to seed monomeric ataxin-3 protein. We were able to show that the ‘seeds’ had reduced but not abolished the lag phase of the SDS- stability sigmoidal profile considerably. Importantly, in the presence of fragment (242Q15) and

(242Q64), both fragment lengths were found to increase the rate of second stage ataxin-3 (Q64) SDS-insoluble aggregate formation. Remarkably, the aggregation of ataxin-3 (Q64) increased exponentially, eradicating the lag phase. Ataxin-3 (Q64) had its midpoint value shifted to approximately 7 h when it was 'cross-seeded', or rather in the presence of the ataxin-3 fragments. The change is significant when compared to a midpoint value of 10 h when ataxin-3 (Q64) was seeded by its own full-length aggregates. The shift in midpoint is even more dramatic when it is compared to ataxin-3 (Q64) aggregating alone (30 h). We report here, for the first time, a kinetic analysis of ataxin-3 fragments (242Q15) and (242Q64), specifically derived from calpain-2 proteolysis, initiating aggregation of expanded ataxin-3 (Q64). These C-terminal ataxin-3- end fragments show clearly the role of accelerating aggregation of full-length ataxin-3.

It was interesting that the poly-Q tract length within the fragment proteins did not distinguish much of a difference in ataxin-3 (Q64) aggregation kinetics. Fragment (242Q15) was able to accelerate ataxin-3 (Q64) aggregation at a very similar rate to (242Q64). However, it was described previously that full-length ataxin-3 (Q15) aggregates does not accelerate the formation of SDS-stable ataxin-3 aggregates (58). The difference between full-length ataxin-3 and the fragment proteins is the absence of the Josephin domain. A number of studies have proposed that a key modulator in ataxin-3 aggregation is the Josephin domain (119-122). Without the Josephin domain, fragment (242Q15) is able to initiate the second stage of ataxin-3 aggregation pathway. On the basis of the results in this study, it is proposed that the fragment proteins could be initiating ataxin-3 (Q64) through the poly-Q domain or even through the flanking domains within the fragment protein context, such as the UIM (refer to Figure 4.16). The 2UIM is found upstream of the poly-Q domain, in both fragment proteins. 2UIM has been associated with the role of co-localising ataxin-3 fragments to free ataxin-3 proteins, leading to aggregation (217). Further work needs to be done to explore the other protein motifs found within the C-terminal end of ataxin-3 fragment and its potential role in initiating ataxin-3 aggregation. For example, a titration of molar concentration of ataxin-3 (Q64), (SpA242Q15) and (SpA242Q64) would enable a better understanding of whether protein concentration affects the kinetics of ataxin-3 aggregation.

Ataxin-3 Poly-Q fragments do not assist ataxin-3 to bypass its first stage of its aggregation pathway

The ataxin-3 poly-Q fragments in this study have shown to accelerate the formation of second stage SDS-insoluble ataxin-3 aggregates. The question was asked if the fragment proteins (242Q15) and (242Q64) might have bypassed the first stage of ataxin-3 aggregation pathway in order to do so. The first stage of ataxin-3 (Q64) aggregation was monitored with ThT fluorescence, when it was in the presence of both (242Q15) and (242Q64) fragments. This result suggests that ataxin-3 (Q64) did not bypass its first stage of the aggregation pathway.

Ataxin-3 (Q64) did not display any changes in its ThT fluorescence intensity when seeded with (242Q15). The results suggest that in spite of being able to increase the rate of ataxin-3 (Q64) SDS-insoluble aggregate formation, the fragment does not circumvent past the first stage of the pathway. A biphasic ThT fluorescence profile did result for ataxin-3 (Q64) when it was seeded with (242Q64). The biphasic profile was previously observed for ataxin-3 (Q64) alone (218). The authors suggested that the first phase denoted the first stage (ThT-reactive aggregates) of ataxin-3 aggregation while the second phase corresponded to the second stage of ataxin-3 aggregation, where formation of SDS-insoluble aggregates occurs.

One could rationalise that the biphasic time course may indicate a mixed population of ataxin-3 (Q64) aggregates instead. A schematic diagram is illustrated to help explain the rationale (Figure 4.16). Upon seeding with (242Q64), the first phase of the time course could be indicating free ataxin-3 (Q64) forming a mixture of ThT-reactive and SDS-insoluble aggregates simultaneously, with ThT-reactive aggregates

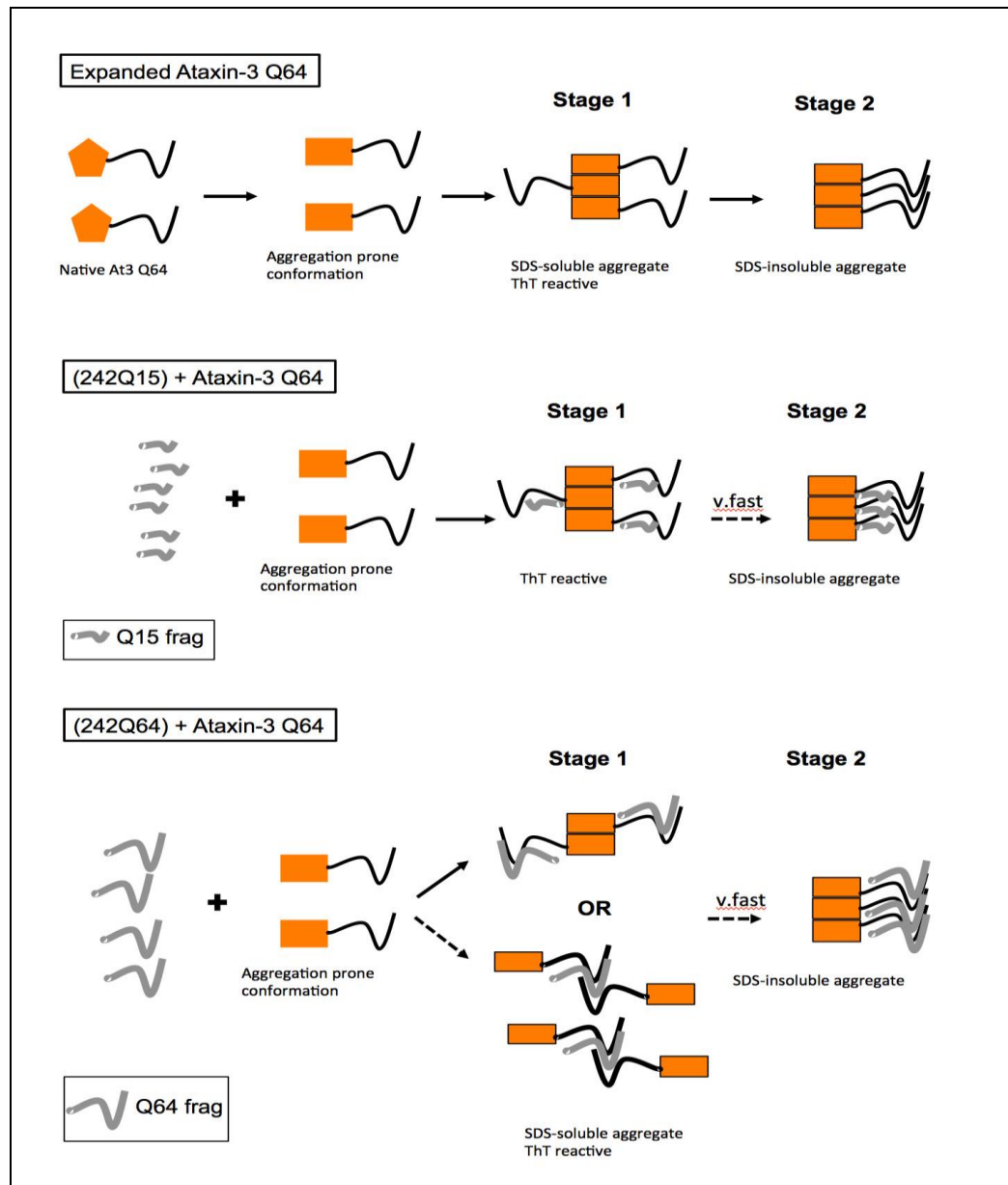


Figure 4.16 Illustration of a proposed model of ataxin-3 fragments initiating SDS-insoluble aggregation of expanded ataxin-3 (Q64) The Josephin domain is represented by the orange hexagon and rectangle. The black tail represents the C-terminal ataxin-3 tail that consists of the 2UIM and the poly-Q domain. Ataxin-3 (Q64) undergoes a two-stage aggregation pathway (top). The presence of both fragments (indicated in figure as short and long grey tail) initiates the acceleration in forming ataxin-3 (Q64) SDS-aggregates (Stage 2), without bypassing Stage 1. It is also proposed that fragment (242Q64) (long grey tail) can cross-seed ataxin-3 (Q64) to form a mixed population of aggregates.

formed at lesser extent. As the time course continues, more ThT-reactive ataxin-3 aggregates are either formed or the mixed populations of aggregates interact to result in more ThT-reactive aggregates being formed. More experiments would have to be carried out to further substantiate this model. Isolating the structures of ataxin-3 (Q64) along the biphasic time course and viewing them under EM could provide further insight on how different populations of aggregates are being formed.

4.4 Summary and conclusions

For this project, it was unfortunate that the majority of time was spent troubleshooting the challenging issue of spontaneous fragmentation of the target protein. Despite the time constraints, fusion ataxin-3 fragment proteins, (SpA242Q15) and (SpA242Q64) were, for the first time, successfully refolded from inclusion bodies. The proteins were characterised and shown to be both soluble, monomeric, have α -helical structure and importantly, uncleaved. The fragments (242Q15) and (242Q64) are released from their fusion partners with TEV protease and their aggregation kinetics were initially characterised with ThT fluorescence. Due to the fusion and fragment proteins' low sensitivity to ThT fluorescence, aggregation kinetics were then monitored and validated by SDS-insolubility membrane trap assays instead. Only fusion and fragment (Q64) were monitored for aggregation through SDS-stability and showed a concentration-dependence in forming SDS-stable aggregates. Most significantly, we were able to demonstrate kinetically that the fragments derived from calpain-2 proteolysis, (242Q15) and (242Q64) both initiated the acceleration of ataxin-3 (Q64) SDS-stable aggregate formation that does not bypass its first stage of the aggregation pathway. Together, these data highlight the potential of ataxin-3 proteolytic fragments to cross-seed the aggregation of full-length ataxin-3 within the intracellular environment.

CHAPTER 5

EFFECTS OF TRIMETHYLAMINE-N-OXIDE, TMAO, ON ATAXIN-3 AGGREGATION AND ACTIVITY

5.1 Introduction

Osmolytes are naturally occurring organic compounds and are often termed as ‘chemical chaperones’. Under stress conditions, these osmolytes assist in the stabilizing of correctly folded proteins (162, 219). Chemical chaperones have been shown to stabilize proteins against thermal denaturation and even able to inhibit the formation of a misfolded structure and subsequent amyloid formation (9, 220, 221). This study focuses on TMAO, a protective osmolyte that is thought to stabilise the protein structure by ‘preferential exclusion’, allowing the secondary structures of the protein to fold more compactly (151, 158). As a result, the denatured state of the protein is destabilized and shifts the equilibrium toward its native state (162, 220). TMAO has been used in a number of protein folding studies with mixed results. PrP has been shown to convert from an α -helical to a more β -sheet conformation with TMAO (166). TMAO has also been shown to exert a greater effect on intrinsically disordered proteins, such as α -synuclein and tau protein, helping thermodynamically unstable proteins to fold (158, 168, 222).

Interestingly, as poly-Q tracts are considered intrinsically unstructured, it would be reasonable to consider whether TMAO would be able to stabilise poly-Q proteins, such as ataxin-3 and prevent aggregation. Indeed, a previous study used TMAO in cells expressing a truncated, expanded ataxin-3 (Q77) fragment. They observed by immunofluorescence that TMAO reduced inclusion bodies within the cells, suggesting a reduction in aggregation of an expanded ataxin-3 fragment. This chapter describes a study that explores the effects of TMAO on ataxin-3, to increase our understanding of the factors that influence ataxin-3 folding and stability.

5.2 Results

5.2.1 Ataxin-3 aggregation is enhanced by TMAO.

5.2.1.1 TMAO accelerates ataxin-3 first stage (Stage 1) aggregation

Ataxin-3 variants were expressed and purified from *E. coli* as previously described in Chapter 2. These variants are stored in 1x TBS pH 7.4 without glycerol. Pathogenic length ataxin-3 (Q64) and a non-pathogenic length protein, ataxin-3 (Q15) were utilized for comparison. 20 μ M of each protein variant were incubated at 37 °C, in the presence of a range of TMAO concentrations (0, 100, 500, 750 mM and 1 M).

The influence of TMAO on the rate of ataxin-3 aggregation was investigated using ThT fluorescence (Figure 5.1A and B). In Figure 5.1C, the data shows that TMAO has an effect on the aggregation of ataxin-3. TMAO accelerated the aggregation of both ataxin-3 (Q15) and ataxin-3 (Q64) in a TMAO concentration dependent manner. At high concentrations of TMAO (750 mM and 1 M), a lag phase of the aggregation profiles for both ataxin-3 variants was diminished. The aggregation kinetics for ataxin-3 (Q15) and (Q64) were also analysed. Intriguingly, both proteins aggregated with very similar kinetics (Table 5.1). TMAO had markedly accelerated ataxin-3 (Q15) aggregation from 19.5 to 4 h, while ataxin-3 (Q64) accelerated from 14.3 to 3.5 h.

The effect of TMAO on the rate of monomer and soluble fraction loss was also monitored via SEC (Figure 5.2). Ataxin-3 (Q15) and (Q64) were incubated at 37 °C with increasing concentrations of TMAO. Samples were obtained at various time points. These samples were centrifuged and the soluble fraction of the sample was analysed, measuring for loss of area under the monomer peak. The areas were calculated and plotted against time. The results show that ataxin-3 (Q15) (Figure 5.2C) and ataxin-3 (Q64) (Figure 5.2A) showed increasing loss of monomer over time with the increase in TMAO concentration. As the monomer peak of the proteins reduced in area in the presence of TMAO, an aggregate peak was detected at the void volume.

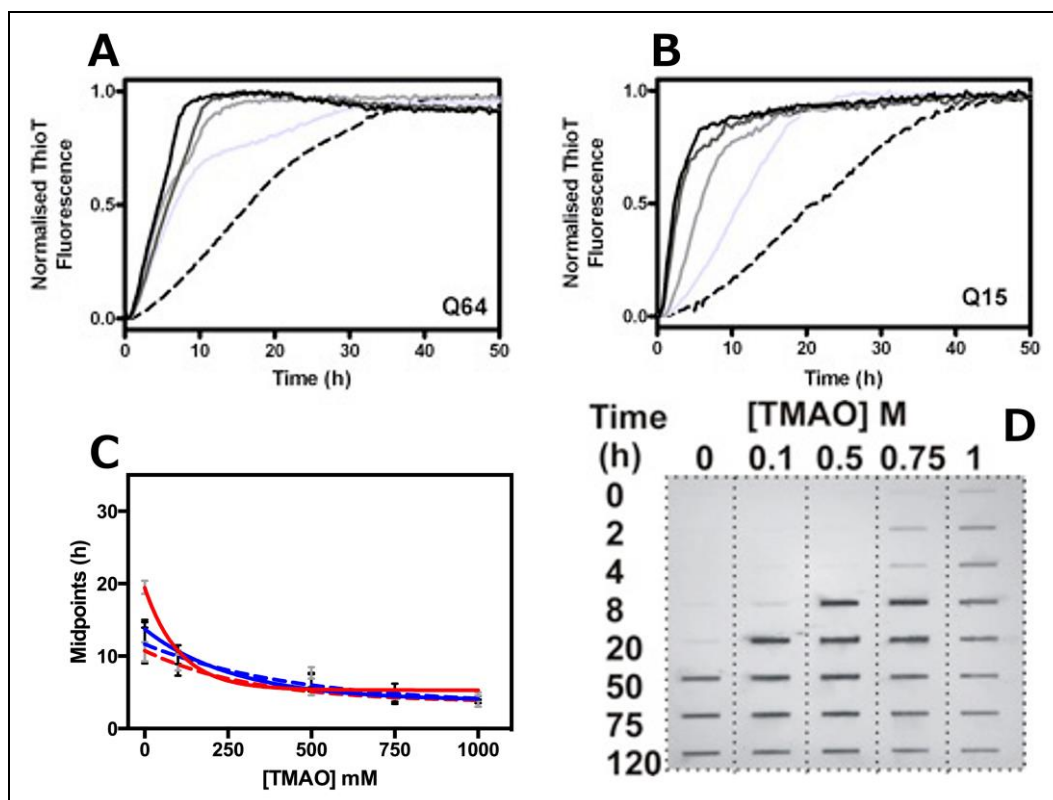


Figure 5.1 Aggregation of ataxin-3 in the presence of increasing amounts of TMAO. (A) Ataxin-3 (Q64) and (B) ataxin-3 (Q15) aggregation was monitored via ThT fluorescence at pH 7.4, at 37 °C. The protein concentration was 20 μ M and the TMAO concentrations were 0 M (dashed black), 100 mM (light grey), 500 mM (medium grey), 750 mM (dark grey) and 1 M (solid black). Readings were taken every 20 min at $\lambda_{\text{ex}} = 445$ and $\lambda_{\text{em}} = 490$. Graphs are representative graphs of five replicates. (C) Comparison of the midpoints of ThT fluorescence and monomer loss of ataxin-3 variants in TMAO (mM) where ataxin-3 (Q15) (red), (Q64) (blue) for ThT while (Q15) (red dash), (Q64) (blue dash) is for monomer loss. (D) A representative filter trap membrane assay measuring SDS-insolubility of ataxin-3 (Q64) in increasing concentrations of TMAO (M).

Table 5.1 Summary of aggregation kinetics of ataxin-3. The rates are displayed in hours in terms of aggregation mid points. These were derived from single sigmoidal functions and values are expressed as means \pm S.E and are derived from at least five experiments.

[TMAO] mM	Monomer loss (h)		ThT fluorescence (h)	
	Q64	Q15	Q64	Q15
0	12.0 \pm 3.0	10.6 \pm 1.3	14.3 \pm 0.4	19.5 \pm 0.9
100	9.4 \pm 2.1	9.1 \pm 1.1	9.6 \pm 0.7	10.5 \pm 0.3
500	6.4 \pm 1.3	5.0 \pm 0.4	6.6 \pm 0.9	7.7 \pm 0.8
750	4.8 \pm 1.4	4.0 \pm 0.3	4.4 \pm 0.7	4.5 \pm 0.4
1000	4.0 \pm 0.5	4.2 \pm 0.4	3.5 \pm 0.5	4.0 \pm 0.5
	Insoluble (h)		SDS-stable (h)	
0	29.0 \pm 1.3	26.6 \pm 1.4	29.0 \pm 0.8	
100	17.0 \pm 0.5	16.6 \pm 6.5	13.7 \pm 1.9	
500	8.8 \pm 1.1	6.5 \pm 0.4	7.7 \pm 2.3	
750	4.5 \pm 0.6	6.3 \pm 0.9	5.1 \pm 1.5	
1000	2.7 \pm 1.0	5.4 \pm 0.2	3.9 \pm 0.4	

Table 5.2: Summary of aggregation kinetics of Josephin. The rates are displayed in hours in terms of aggregation mid points. These were derived from single sigmoidal functions and values are expressed as means \pm S.E and are derived from at least five experiments.

[TMAO] mM	ThT fluorescence (h)	Monomer loss (h)
0	91.4 \pm 9.1	11.4 \pm 0.4
100	67.6 \pm 2.2	9.5 \pm 1.2
500	47.6 \pm 1.1	14.1 \pm 0.5
750	46.7 \pm 5.4	13.4 \pm 0.1
1000	39.5 \pm 13.0	16.0 \pm 0.1

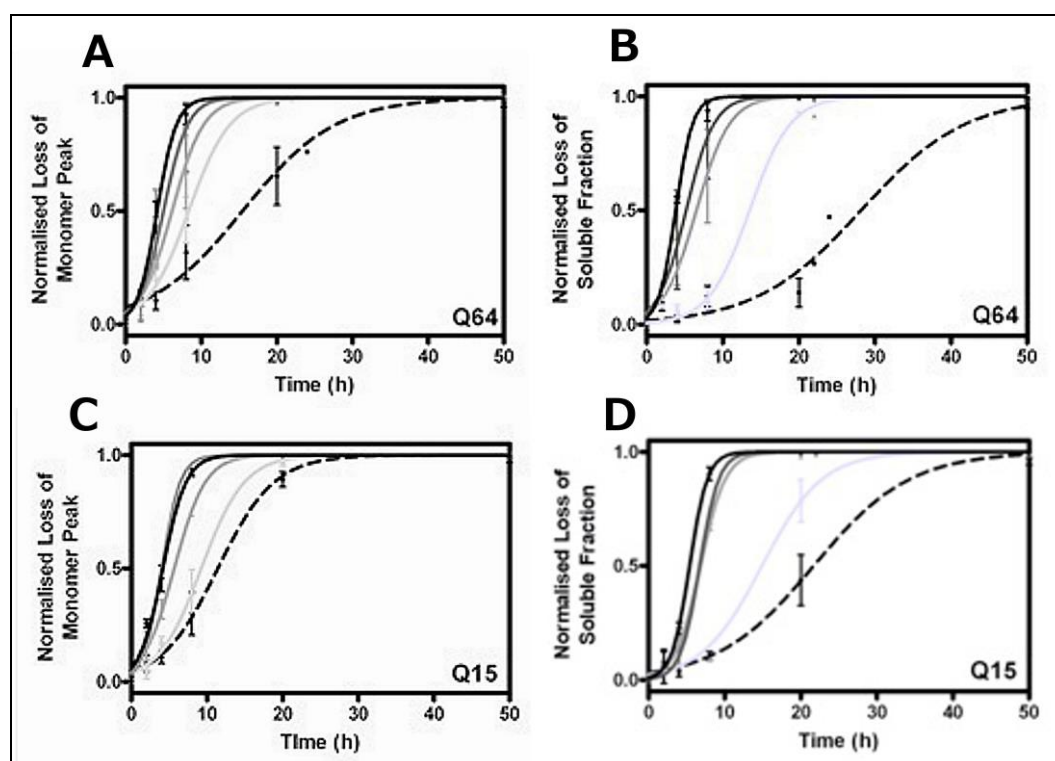


Figure 5.2 Aggregation monitored by size exclusion chromatography. Aliquots of ataxin-3 (Q64) (A-B) and ataxin-3 (Q15) (C-D) were removed from the aggregation assay and injected onto a Superose 12 column (Amersham biosciences). The TMAO concentrations analyzed were 0 M (dashed black), 100 mM (light grey), 500 mM (medium grey), 750 mM (dark grey) and 1 M (solid black). The loss of monomer (A, C) and soluble fraction (B, D) were calculated using the peak fitting and integration tools in Origin[®] 7.

This indicates that soluble aggregates are formed and is termed the 'soluble fraction'. The loss of soluble fraction peak area was also monitored and plotted against time. The results are shown in Figure 5.2B and D for ataxin-3 (Q64) and (Q15) respectively. For both ataxin-3 (Q15) and (Q64), monomer loss correlated well with aggregation monitored by ThT fluorescence (Table 5.1). A comparison of ataxin-3 aggregation kinetics monitored by ThT fluorescence and monomer loss is illustrated in Figure 5.1C. Increasing TMAO concentrations also accelerated the conversion of soluble to insoluble aggregates of ataxin (Q15) and (Q64) (Table 5.1), with ataxin-3 (Q15) converting at a slightly slower rate. These data suggest that increased TMAO accelerates the aggregation of monomeric ataxin-3, resulting in faster formation of insoluble aggregates.

5.2.1.2 TMAO also accelerates ataxin-3 Stage 2 aggregation

Based on the results that expanded poly-Q ataxin-3 (Q64) Stage 1 aggregates had rapidly formed with TMAO, the rate of Stage 2 ataxin-3 (Q64) aggregation was also monitored using the membrane filter trap assay. 20 μ M ataxin-3 (Q64) was incubated at 37 °C with increasing concentrations of TMAO (0, 100, 500, 750 mM and 1M) and samples were obtained over time. In agreement with the previous results obtained in Chapter 4, ataxin3 (Q64) was able to form SDS-stable aggregates (Figure 5.1D). Ataxin-3 (Q64) formed SDS-insoluble aggregates rapidly with increasing TMAO concentrations. Its aggregation kinetics also correlated with loss of soluble fraction (Table 5.1).

5.2.2 TMAO does not alter the morphology of ataxin-3 aggregates.

The morphologies of the ataxin-3 aggregates formed in the presence of TMAO were analysed via TEM (Figure 5.3). 20 μ M ataxin-3 (Q15) and (Q64) was incubated 37 °C with 1 M TMAO over a duration of 74 h. Ataxin-3 (Q64) and (Q15) aggregates formed small oligomers within 2 h (Figure 5.3A and E respectively). From 2 - 4 h, the structures observed for both ataxin-3 proteins were spheroid-like aggregates and small curvilinear oligomers, varying from 5 - 20 nm in width (Figure 5.3A,B; E, F). Both varieties of aggregates have been previously described for ataxin-

3, poly-Q peptides, β -amyloid and α -synuclein (42, 44, 58, 223-225). Within 8 h, both variants had formed the elongated, curvilinear structures typical of Stage 1 ataxin-3 aggregates (Figure 5.3C and G) (58, 117). The structures were more clustered in the presence of TMAO and while the individual strands of fibrils could be distinguished, they were always entwined with other fibres. Notably, the morphology of ataxin-3 (Q15) remained unchanged over time, comprising the curvilinear structures at the end time point (Figure 5.3H). After the formation of the curvilinear aggregates, ataxin-3 (Q64) formed thick, filamentous fibrils between 50 - 100 nm in width (Figure 5.3D). These aggregate structures are typical of ataxin-3 aggregation as observed previously in other studies (58, 118). The data suggests that while TMAO accelerated ataxin-3 aggregation, it did not alter the aggregate morphologies.

5.2.3 TMAO accelerates Josephin aggregation without altering its aggregate morphology

Briefly, the aggregation pathway of ataxin-3 consists of two distinct stages, Stage 1 and Stage 2 (Chapter 1). The Josephin domain is thought to undergo an aggregation prone conformation (119, 121), instigating aggregation of the ataxin-3 protein, regardless of the poly-Q tract length (58). As such, the effect of TMAO on Josephin domain alone was investigated. The Josephin domain protein was expressed and purified from *E. coli* as previously described in Chapter 2. 20 μ M Josephin was incubated at 37 °C, with increasing concentrations of TMAO (0, 100, 500, 750 mM and 1 M). The result shown in Figure 5.4A shows TMAO had an effect on the Josephin protein. The Josephin domain has been shown to aggregate at a slower rate compared to ataxin-3 proteins (58, 118). ThT fluorescence was used to monitor aggregation and the result indicates that Josephin exhibited accelerated aggregation kinetics with increased concentrations of TMAO (Table 5.2).

Monomer loss monitored by SEC was also carried out. In Figure 5.4B, monomer loss closely correlated with aggregation monitored by ThT fluorescence (Table 5.2). Intriguingly, the loss of Josephin monomer was slightly inhibited in the presence of TMAO, especially at 1 M TMAO.

Isolation of Josephin aggregates with the TMAO concentration was carried out to determine if its morphology had altered. 20 μ M of Josephin was incubated at 37 °C with 1 M TMAO for a duration of 150 h. Samples were stained and observed under TEM. In Figure 5.4C, the structure of end-point aggregates of Josephin were observed to be small and curvilinear, similar to what was observed in a previous study (118). These curvilinear structures also resembled ataxin-3 (Q15) in 1 M TMAO as well (Figure 5.4C). These results have remarkable similarities to ataxin-3, thus suggesting that TMAO may be modulating the Josephin domain in the aggregation of the ataxin-3 protein.

5.2.4 TMAO does not significantly alter the native structure of both ataxin-3 and Josephin proteins

End-point aggregates of the ataxin-3 variants (Q15) and (Q64), as well as Josephin did not show morphological changes in TMAO. It was important to understand the extent of modulation TMAO had on the native state conformations of the proteins. In order to do so, several structural approaches were used. Far-UV CD and fluorescence spectroscopy were used to determine whether the increased rate of aggregation was due to global alteration of the native secondary structure of ataxin-3 and Josephin (Figure 5.5). 20 μ M of each protein was added to solutions of increasing TMAO concentrations before analysis on the spectrometer. The CD spectral analysis of ataxin-3 (Q64), ataxin-3 (Q15) and Josephin are shown in Figure 5.5A, C and E respectively. All variants showed similar spectra, even in the presence of TMAO, to the ones previously reported (58, 62, 115). The spectra indicated that all the proteins are predominantly α -helical, with local minima at 208 nm and 222 nm. Further analyses of the spectra were de-convoluted using the K2D algorithm on Dichroweb (226)

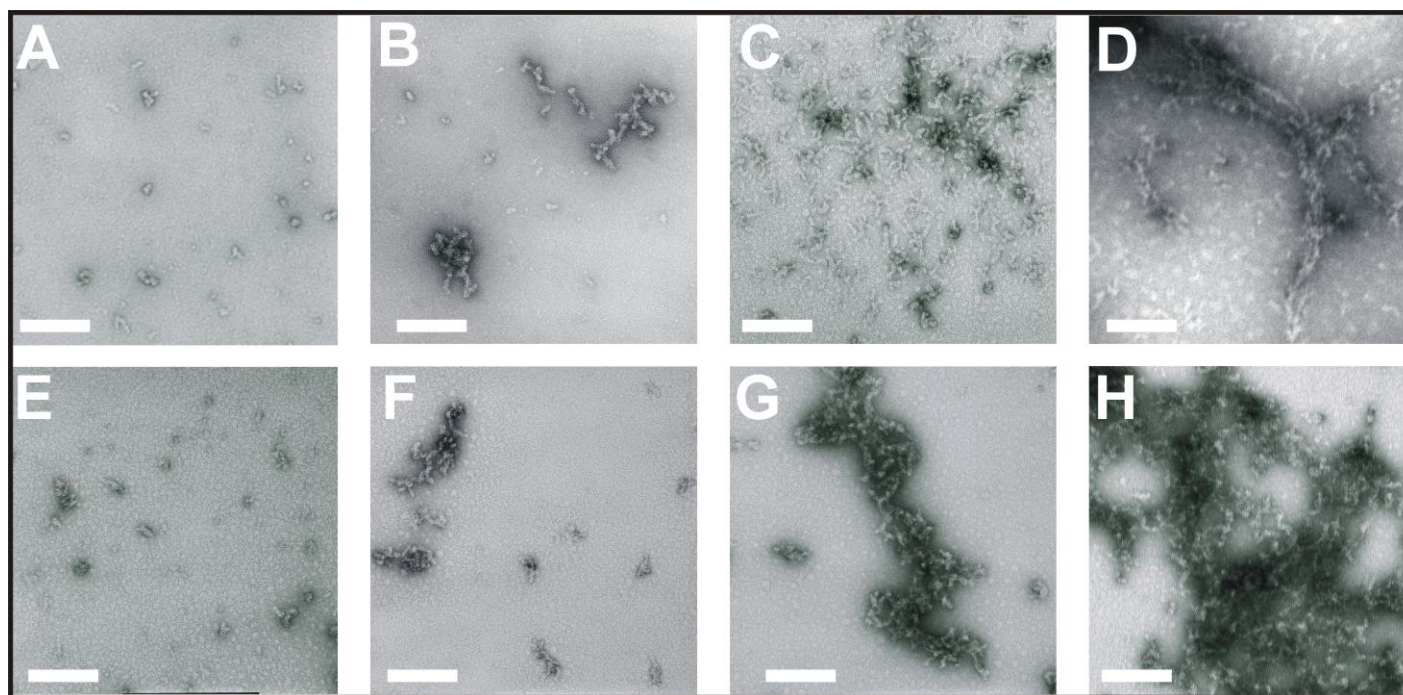


Figure 5.3: Morphology of ataxin-3 aggregates in the presence of TMAO. TEM analysis was completed on aggregates formed by ataxin-3 (Q64) (**A-D**) and ataxin-3 (Q15) (**E-H**). Time points for 2 h (**A, E**), 4 h (**B, F**), 8 h (**C, G**) and end point (**D, H**) in the presence of 1 M TMAO. The scale bars represent 100 nm.

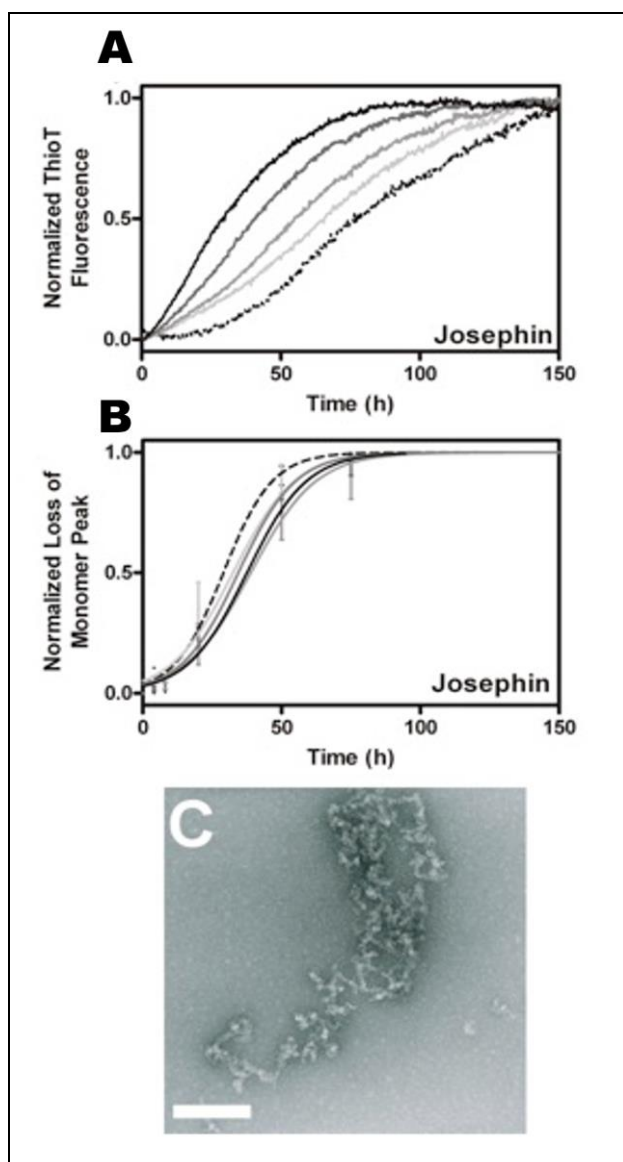


Figure 5.4: The effect of TMAO on the aggregation of Josephin. The protein concentration was 20 μ M and the TMAO concentrations were 0 M (dashed black), 100 mM (light grey), 500 mM (medium grey), 750 mM (dark grey) and 1 M (solid black). (A) The rate of aggregation was monitored by ThT fluorescence and readings were taken every 20 min at $\lambda_{\text{ex}}=445$ and $\lambda_{\text{em}}=490$. (B) The rate of monomer loss of Josephin was monitored by SEC. (C) Electron micrograph of end point Josephin aggregates in the presence of TMAO analysed by TEM. Scale bar represents 100 nm.

The results obtained are listed in Table 5.3. The comparisons of differences in secondary structure content per protein in TMAO are shown in Figure 5.5B, D and F. All proteins showed a slight increase in α -helical and random coil content, with increasing concentrations of TMAO. Interestingly, with TMAO, a decrease in β -sheet content was observed for all three proteins, being more pronounced for ataxin-3 (Q64) (Figure 5.5B). However, the increase in α -helical content observed for all three proteins are all equivalent within error (Table 5.3), suggesting that structural changes are within the Josephin domain.

The potential alterations to the tertiary structure of the ataxin-3 (Q15), (Q64) and the Josephin proteins were also analysed by monitoring intrinsic fluorescence of the proteins. Three tryptophan (Trp) residues are located at positions Trp88, Trp120 and Trp130 within the Josephin domain (Figure 1.3). 500 mM and 1 M TMAO solutions were pre-equilibrated at 37 °C before the proteins were added and analysed. These residues were followed at an excitation wavelength at 280 nm, while scanning an emission wavelength range from 300 - 450 nm. Figure 5.6C shows Josephin at all concentrations of TMAO emitting fluorescence at 333 nm. The results of Josephin in 0 M TMAO is consistent with results obtained by previous studies (227). However, there was no significant red shifting or hyper-fluorescence observed. Ataxin-3 (Q15) (Figure 5.5B) and ataxin-3 (Q64) (Figure 5.5A) also showed fluorescence spectra emitting at 333 nm at 0 M TMAO, correlating to a previously shown study (58). While there was no red shifting for ataxin-3 (Q15) and (Q64), both proteins displayed a slight increase in fluorescence with both 500 mM and 1 M TMAO. The results obtained demonstrate that in the presence of TMAO, all three proteins did not change significantly in protein conformation. Overall, TMAO induced a slight increase in α -helical content but not significant alterations in the global native structure of ataxin-3 (Q15), (Q64) and the Josephin protein.

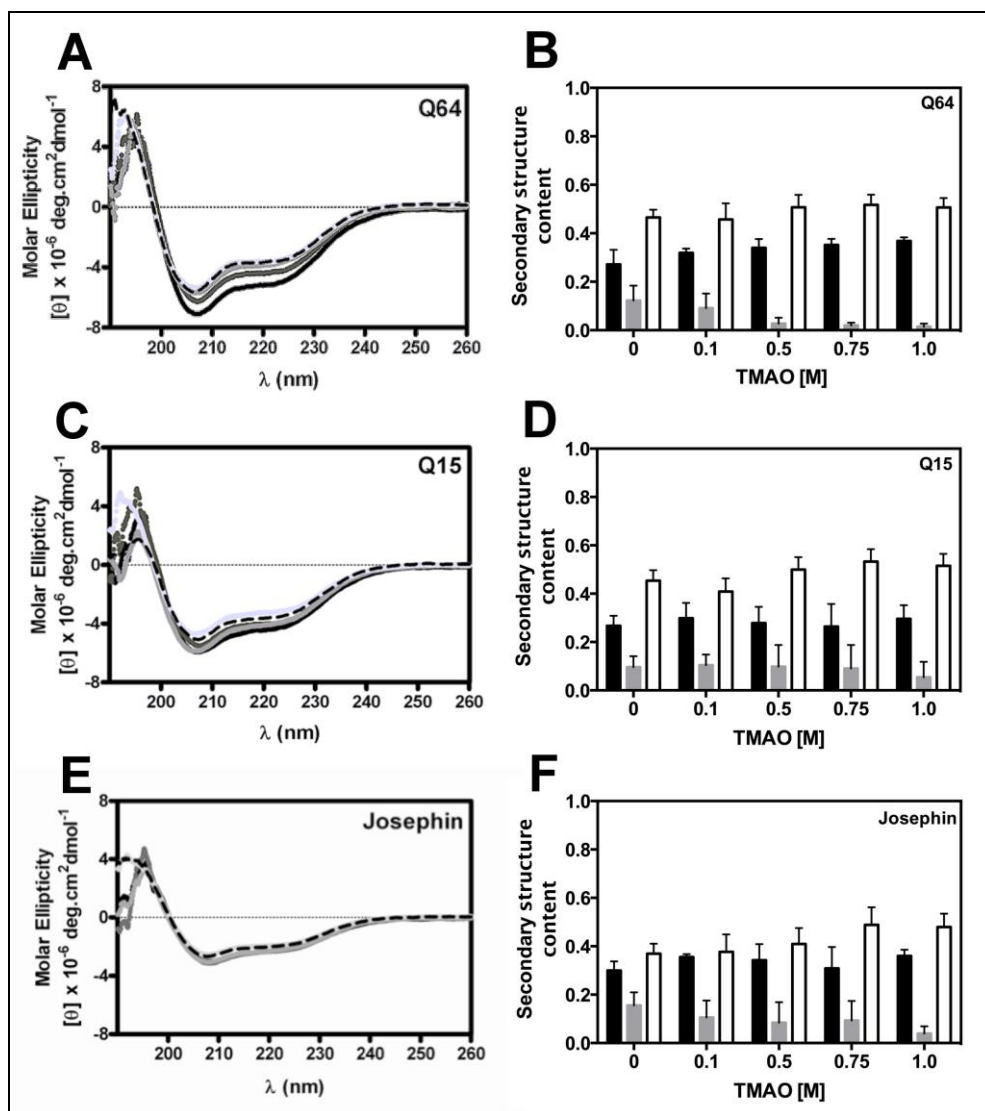


Figure 5.5: The native structure of the variants in the presence of TMAO. Far-UV CD (A, C, E) were completed at 37 °C, at a protein concentration of 20 μM . Spectra of ataxin-3 (Q64) (A), ataxin-3 (Q15) (C) and Josephin (E) were taken with 0 M TMAO (dashed black), 100 mM TMAO (light grey), 500 mM (medium grey), 750 mM TMAO (dark grey) and 1 M TMAO (solid black). The experiments were all completed a minimum of four times and representative scans are displayed. (B, D, F) Comparison of the secondary structure content of each variant after further analysis all the CD spectra. The values represented as fractions to a sum of 1. The structures of ataxin-3 (Q64) (B), ataxin-3 (Q15) (D) and Josephin (F) are α -helices (black), β -sheets (grey) and random coils (white).

Table 5.3 Deconvolution of CD spectras of ataxin-3 variants and Josephin. The data on the structural features for ataxin-3 (Q64), ataxin-3 (Q15) and Josephin in increasing concentrations of TMAO are tabulated. The values were constrained to the sum of all fractional weights equals to one.

(Q64) TMAO [mM]	α-helix	β-sheet	Turns	Random coil
0	0.271 ± 0.060	0.123 ± 0.061	0.141 ± 0.009	0.465 ± 0.032
100	0.319 ± 0.018	0.091 ± 0.060	0.133 ± 0.019	0.457 ± 0.066
500	0.340 ± 0.037	0.027 ± 0.024	0.126 ± 0.027	0.507 ± 0.052
750	0.352 ± 0.025	0.019 ± 0.012	0.099 ± 0.021	0.517 ± 0.042
1000	0.368 ± 0.014	0.015 ± 0.012	0.110 ± 0.019	0.507 ± 0.038
(Q15) TMAO [mM]	α-helix	β-sheet	Turns	Random coil
0	0.2674 ± 0.041	0.096 ± 0.045	0.152 ± 0.022	0.454 ± 0.043
100	0.2674 ± 0.063	0.104 ± 0.044	0.194 ± 0.004	0.409 ± 0.055
500	0.2786 ± 0.067	0.098 ± 0.086	0.123 ± 0.024	0.499 ± 0.056
750	0.264 ± 0.093	0.091 ± 0.097	0.112 ± 0.029	0.533 ± 0.051
1000	0.296 ± 0.057	0.054 ± 0.064	0.134 ± 0.028	0.516 ± 0.049
(Josephin) TMAO [mM]	α-helix	β-sheet	Turns	Random coil
0	0.300 ± 0.037	0.156 ± 0.054	0.163 ± 0.011	0.369 ± 0.041
100	0.356 ± 0.012	0.106 ± 0.069	0.162 ± 0.009	0.377 ± 0.072
500	0.342 ± 0.067	0.084 ± 0.085	0.165 ± 0.021	0.409 ± 0.066
750	0.309 ± 0.088	0.093 ± 0.081	0.110 ± 0.033	0.488 ± 0.073
1000	0.360 ± 0.025	0.039 ± 0.030	0.121 ± 0.019	0.479 ± 0.055

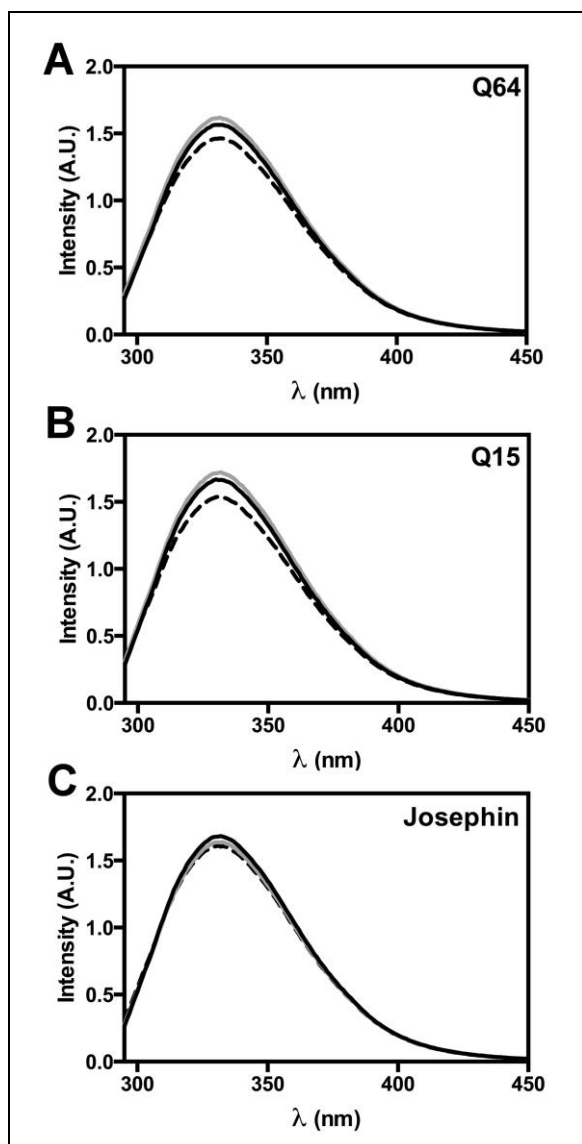


Figure 5.6: The native structure of the variants in the presence of TMAO. Fluorescence emission spectroscopy ($\lambda_{\text{ex}}=280$ nm) were completed at 37 °C, at a protein concentration of 20 μ M. Spectra of ataxin-3 (Q64) (A), ataxin-3 (Q15) (B) and Josephin (C) were taken with 0 M TMAO (dashed black), 500 mM (medium grey) and 1 M TMAO (solid black). The experiments were all completed a minimum of four times and representative scans are displayed.

5.2.5 Deubiquitinating (DUB) activity of ataxin-3 is enhanced in the presence of TMAO

Band shift assay

TMAO has been reported to promote activity in a few proteins after inducing their native folding (228-230). Josephin domain has been shown to function as a ubiquitin-specific protease (60, 62). To investigate if TMAO influences the deubiquitinating (DUB) activities of ataxin3 (Q15) and ataxin3 (Q64), a linear substrate, GST-Ub52 was used. GST-Ub52 is a fusion ubiquitin protein to human ribosomal protein and linked to a GST moiety (69, 231, 232). Ataxin-3 (Q15), (Q64) and Josephin were all incubated using a previously established protein: GST-Ub52 molar ratio of 1: 5 (62).

Each of these protein combinations was incubated in the presence of 500 mM and 1 M TMAO. The samples were incubated at 37 °C for 1 h and analysed using SDS-PAGE. GST-Ub52 substrate was cleaved into Ub52 by both ataxin-3 (Q15) and (Q64) (Figure 5.7A and B respectively). In the presence of 500 mM and 1 M TMAO, cleavage of GST-Ub2 by both proteins was increased, resulting in more intense Ub52 banding. In order to ascertain whether alterations to the DUB activity of ataxin-3 were mainly due to the Josephin domain, the band shift gel assay was repeated for Josephin protein. The Josephin protein demonstrated similar activity by cleavage of GST-Ub52 substrate, resulting in increased Ub52 banding with increasing amounts of TMAO after 1 h (Figure 5.6C). These results indicate that in the presence of 500 mM and 1 M TMAO, ataxin-3 retained and most likely enhanced its DUB activity.

Ub-AMC fluorogenic assay

The results from the band shift gel assays indicate that ataxin-3 may have enhanced DUB activity in the presence of TMAO. Using a fluorogenic ubiquitin assay, a further analysis of ataxin-3 DUB activity was carried out. A mono-ubiquitin substrate linked to an AMC reporter fluorochrome, Ub-AMC was used. This substrate has been utilised in various ataxin-3 DUB assays (53, 54, 62, 233). Ataxin-3 (Q15) and (Q64) were added to 500mM and 1 M TMAO separately. The solutions were prepared in assay buffer and were pre-equilibrated for 15 min at 37 °C, before Ub-AMC was added to the reaction.

The progress curves of the enzymatic reactions of ataxin-3 (Q15), (Q64) and Josephin were followed for 12 min and are represented in Figure 5.8. All three proteins displayed a corresponding increase in relative fluorescence and TMAO concentrations. This suggests there is increased cleavage of Ub-AMC by ataxin-3 when it is modulated by TMAO in a concentration dependent manner. The mean rate of initial velocities obtained from the slopes of the three progress curves was determined and is tabulated in Table 5.4. The increase in DUB activity across ataxin-3 (Q15), (Q64) and Josephin was consistent with the results from the band shift assay. An average of 17.6 % global increase in activity was observed by ataxin-3 (Q15) and (Q64) and Josephin in 1 M TMAO. When the changes in DUB activity were normalized to the data in 1 M TMAO (100%) for all proteins, it was observed that the activity at 0 M and 0.5 M constitutes 5 % and 27 % of the activity observed for 1 M TMAO, for all proteins (Figure 5.8A). This result suggests that modulation of ataxin-3 DUB activity by TMAO may be a global effect.

To ensure the DUB activity enhancement effect of TMAO on ataxin-3 and Josephin was not due to increased viscosity or a structural change of ubiquitin in TMAO, a number of control experiments were carried out. Glycerol was utilized at the same concentrations of TMAO for comparison (151). A 1 M TMAO solution was calculated to be a 28.8 % percentage volume (v/v). Thus, a 28.8 % (v/v) glycerol and a 1 M glycerol solution was used and incubated together with the Josephin protein. Increases in DUB activity of Josephin in the presence of glycerol was monitored by Ub-AMC assay. In Figure 5.8B, there was no increase in DUB activity of Josephin in the presence of glycerol, suggesting that increases in ataxin-3 DUB activity is unlikely due to the viscosity of TMAO solution. The secondary structure of the ubiquitin protein alone was tested in the presence TMAO. Ubiquitin was commercially purchased and dissolved in 1x TBS pH 7.4. The ubiquitin protein (81 μ M) was incubated with 1 M TMAO and monitored by far-UV CD. It was also determined that TMAO does not affect the structural conformation of ubiquitin (data not shown). Overall, the results suggest that TMAO has the capability to retain and enhance the DUB activity of ataxin-3 proteins and Josephin itself.

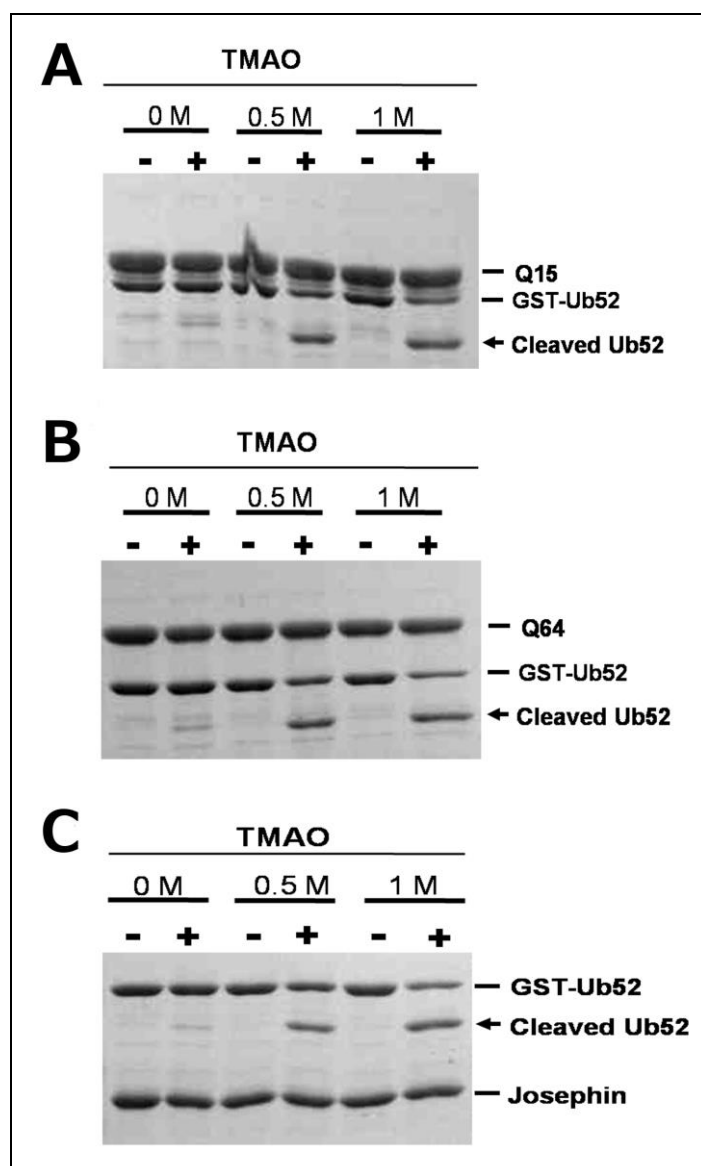


Figure 5.7 DUB activity of the variants in the presence of TMAO. The de-ubiquitinating activity of ataxin3 was determined qualitatively utilizing SDS-PAGE. 10 μ M concentrations of (A) ataxin3 (Q15), (B) ataxin3 (Q64) and (C) Josephin were incubated with the linear GST-Ub52 in the presence of increasing concentrations of TMAO at 37°C for 1h. Aliquots were analysed via SDS-PAGE.

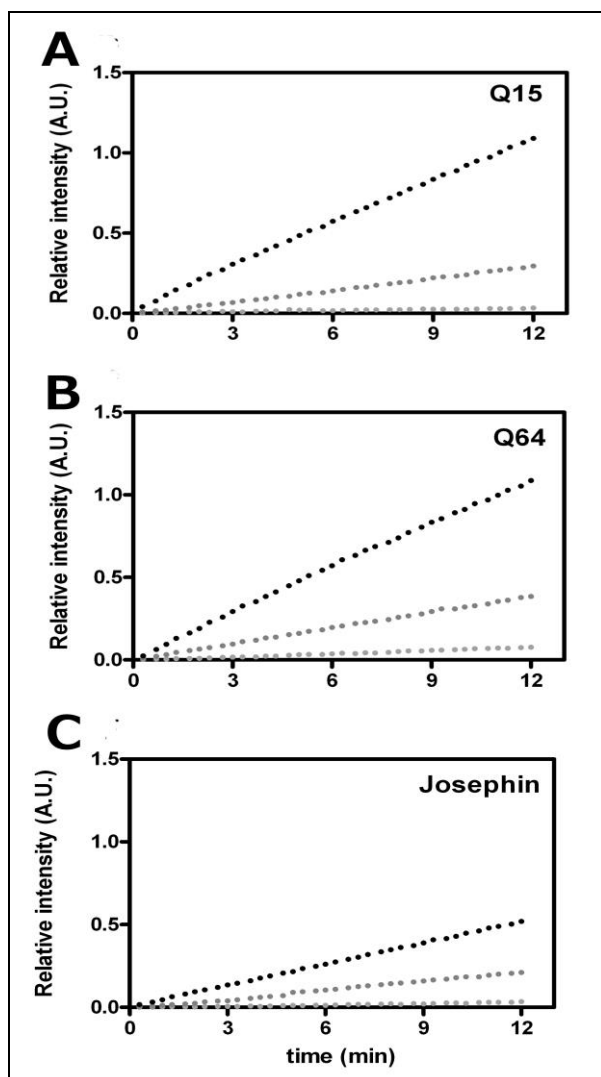


Figure 5.8 Quantitative analysis of de-ubiquitinating activity of the variants in the presence of TMAO. Progress curves showing change in fluorescence over time for cleavage reaction of substrate Ub-AMC with (A) ataxin-3 (Q15), (B) ataxin-3 (Q64) and (C) Josephin in 0 M TMAO (light grey circle); 0.5 M (grey circles) and 1 M TMAO (black circles). The variants were incubated with Ub-AMC at 37 °C and the fluorescence measured at 437 nm.

Table 5.4: Deubiquitination rates of ataxin-3 in the presence of trimethylamine N-oxide

Initial velocities of the DUB activity of Josephin, ataxin-3 (Q15) and ataxin-3 (Q64) with the mono-ubiquitin substrate, Ub-AMC in increasing concentrations of TMAO. Initial values are expressed as means \pm S.E from at least three experiments.

Protein	[TMAO] mM					
	0		500		1000	
<i>relative units min⁻¹</i>	Ave.	S.E.	Ave.	S.E.	Ave.	S.E.
Josephin	2940	386.2	12700	614.5	48210	1051.0
Q15	4826	754.6	22750	1078.0	113400	2401.0
Q64	5997	544.6	33710	975.0	96510	2189.0

5.2.6 Enhancement of DUB activity of ataxin-3 is independent of the UIMs located in the C-terminal region

The results obtained thus far indicate that ataxin-3 variants (Q15) and (Q64) exhibit greater increase in DUB activity than Josephin itself. This raises the question whether the ubiquitin interacting motifs (UIM) found in the ataxin-3 modulates this activity enhancement effect. Ataxin-3 contains two ubiquitin-interacting motifs, UIM1 and UIM2, both downstream from Josephin and N-terminal to the polyQ tract. Burnett and colleagues reported that mutations to the leucine residue at position 229 of ataxin-3 (L229A) completely inhibited poly-ubiquitin chains from binding (60). A second mutation (L249A) in UIM2 showed a lesser extent of inhibition (60). At the time of this study, double mutations of UIM1 and UIM2 of ataxin-3 variant proteins were expressed and purified in our laboratory. An aliquot of each double mutant (L229A/L249A) of ataxin-3 (Q15) and (Q64) was obtained. A 0.5 μ M of each wildtype and UIM double mutant ataxin-3 (Q15) and (Q64) was then incubated with 1 M TMAO before employing the Ub-AMC fluorogenic assay. The results in Figure 5.8C show that the double mutants of ataxin-3 (Q15) and (Q64) exhibited a similar enhancement in DUB activity compared to the wildtype variants (Table 5.4). The results suggest that the Ub-AMC substrate does not interact with the UIMs, which is consistent with current studies that the UIM binds poly-ubiquitin chains (73). This also implies that the modulation of DUB activity by TMAO is likely to be away from the C-terminus of ataxin-3.

Table 5.5: Deubiquitination rates of ataxin-3 in the presence of trimethylamine N-oxide.

Initial velocities of the DUB activity of Josephin, wild type and double UIM mutant ataxin-3(Q15) (Q64) with the mono-ubiquitin substrate, Ub-AMC in 1 M TMAO. Initial values are expressed as means \pm S.E from at least two experiments

Protein	[TMAO] mM	
	1000	
<i>relative units min⁻¹</i>	Ave.	S.E.
Josephin	45517	470.4
Q15	104272	1210.0
Q64	110047	1993.0
UIM KO Q15	111565	957.3
UIM KO Q64	124007	1809.0

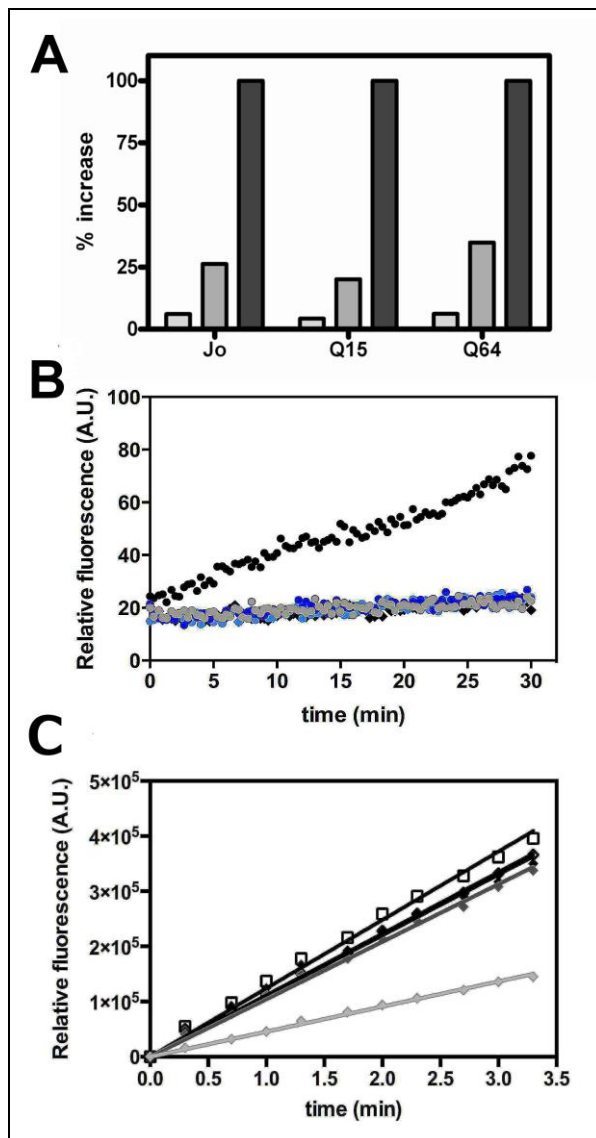


Figure 5.9 Determination of the specificity of ataxin-3 DUB activity. (A) Comparison of the % difference in activity when 1 M TMAO was based as 100%. The % activity is 5% for 0 M TMAO, 27% for 0.5 M TMAO for all proteins. (B) Glycerol does not confer the same osmolyte-induced DUB activity of Josephin as TMAO. Josephin with 0 M TMAO (grey circles), 0.5 M TMAO (blue circles), 1 M TMAO (black circles), 1 M glycerol (light blue circles) and 28.8% (v/v) glycerol (black diamonds). (C) UIM motifs is not involved in binding Ub-AMC substrate. Josephin (grey diamond), ataxin-3 (Q15) (medium grey diamond), ataxin-3 (Q64) (black diamond), UIM KO ataxin-3 (Q15) (clear diamonds) and UIM KO ataxin-3 (Q64) (clear) are incubated with 1 M TMAO and monitored via Ub-AMC fluorogenic assay.

5.3 Discussion

Osmolytes are small molecule compounds, naturally occurring within the cell system and found to have effects similar to those of molecular chaperones. They are used to stabilize and facilitate protein folding and assist in the refolding of misfolded proteins (151, 160, 234). The role of the osmolyte in SCA3 pathogenesis was first raised when TMAO was found to reduce the aggregation of over-expressed ataxin-3 fragments in cell culture (171). In the last several years, studies on TMAO have sought to elucidate its role in stabilizing aggregation or reversing misfolding for a number of proteins associated with neurodegenerative diseases, such as the Htt, tau and α -synuclein proteins (158, 164, 222). However, the influence of TMAO on full-length ataxin-3 is unknown. In this chapter, the goal was to determine the effect TMAO on ataxin-3 aggregation.

In recent studies, a new hypothesis for the protein stabiliser TMAO and its effect on protein folding was described (151, 158). TMAO was found to interact weakly with itself, and promotes water molecule re-distribution to hydrophobic residues around the peptide exterior (Figure 5.11). Importantly, this correlates with earlier studies that TMAO facilitates protein folding, where the TMAO-water and peptide backbone create an unfavourable interaction, explaining an exclusion of TMAO-water complexes. This in turn, enhances protein folding (151, 162). The re-distribution of water molecules around the peptide exterior by TMAO-water complexes encourages the formation of stable, compact protein conformations. TMAO is thought to affect subtle shifts in populations of ensembles but not necessarily induce changes in structures (158). In brief, TMAO can act to bring about an enhancement in protein folding, as well as to ‘compact’ and stabilise native conformations (151).

TMAO modulates kinetics but not the structure or pathway of ataxin-2 aggregation

The results from this study indicated that the ataxin-3 variants (Q15), (Q64) and Josephin all aggregated in the presence of TMAO. The proteins aggregated and form fibrils that closely resembled morphologies that were observed for the protein variants without TMAO (58, 117, 118), suggesting there was no distinct change in its aggregation pathway. CD spectral results indicate strong α -helical signals for ataxin-3

(Q15), (Q64) and Josephin, largely contributed by the structured Josephin domain (62). In the presence of TMAO, there were increases in structural content, especially for α -helices and random coils. However, fluorescence emission spectra of ataxin-3 (Q64), (Q15) and Josephin demonstrated no significant change with respect to its global protein conformations, suggesting the increases in structural content may be subtle.

The complex nature of the ataxin-3 aggregation pathway suggests that the effect of TMAO may not be straightforward. The aggregation process for ataxin-3 undergoes a two-stage aggregation process (58). Ataxin-3 aggregation is initiated by the aggregation of the Josephin domain (58, 62, 117), through native-like associations (119, 121). The Josephin protein aggregates and forms fibrils that resemble non-expanded poly-Q ataxin-3 aggregates (58, 117). Hence, the Josephin domain of ataxin-3 affects the stability and aggregation properties of non-expanded poly-Q ataxin-3 proteins (Stage 1). Stage 1 aggregates are characterised as ThT-reactive and are sensitive to SDS. The expanded poly-Q ataxin-3 (Q64) also undergoes Stage 1 and aggregates with faster kinetics than non-expanded ataxin-3 (58). It is able to form distinct SDS-insoluble aggregates (Stage 2) due to the expansion of poly-Q tract (58). The poly-Q tract is reported to be a flexible solvent-exposed domain that may have local destabilising effect upon expansion but does not impact the global stability of ataxin-3 (105, 115).

When TMAO was added to ataxin-3 (Q15) and (Q64), both proteins resulted in similar ThT fluorescence, monomer loss and aggregation kinetics. Those results correlated well with one another. Josephin has been recently shown to initiate the aggregation of ataxin-3 whereby a span of residues (a.a. 73-96) on helix- α 4 causes a subtle conformational change within the Josephin domain, which triggers the acceleration in ataxin-3 aggregation, especially in pathological length ataxin-3 (119). As TMAO interacts with ataxin-3 (Q64) and (Q15), especially at high TMAO concentrations, TMAO may have increased α -helical structures of ataxin-3 by folding more compactly while maintaining native conformations (151). This is supported by the absence of any significant changes in the global conformation of both ataxin-3 in TMAO from the fluorescence spectra. Based on this model, it is attractive to suggest that the increased folding kinetics may have caused more local changes to the span of

residues on helix- α 4. This may then accelerate the aggregation of ataxin-3 (Q15) and (Q64) as TMAO buries any exposed or destabilising peptide backbone. This may also support why ataxin-3 (Q15) and (Q64) both exhibit rapid aggregation kinetics as determined by ThT fluorescence and monomer loss. This could also explain why ataxin-3 (Q64) also rapidly forms SDS-insoluble aggregates, as the expanded poly-Q ataxin-3 enters Stage 2.

Additionally, the Josephin domain exhibited faster aggregation kinetics but a slightly hindered monomer loss, in the presence of TMAO. It is quite possible that Josephin follows the above-mentioned model of aggregation in the presence of TMAO. The Josephin domain has been shown to retain a high secondary structure content at its early stages of aggregation (120). Josephin domain monomer loss data could be indicating the early stage of aggregation while the ThT aggregation kinetics indicates the later stages of aggregation. In light of this, high concentrations of TMAO could be strongly stabilising Josephin at the early stages of aggregation possibly retaining more native, 'monomeric-like' states before Josephin self-association and late aggregation takes place.

The aggregation of a poly-Q protein with TMAO was also observed in a previous study (164). Htt exon-1 (Q53) was shown to rapidly aggregate in the presence of up to 1 M TMAO. Interestingly, they observed the morphology of Htt protein with 1 M TMAO formed amorphous aggregates instead of the typical fibrillar aggregates formed without TMAO. They deduced that the accelerated aggregation of Htt exon-1 (Q53) by TMAO was due to TMAO exerting a strong osmophobic effect on the Htt peptide backbone. This might have resulted in altering Htt folding equilibrium to an alternative pathway, resulting in different aggregate structures. Ataxin-3 (Q15), (Q64) were also investigated to observe if TMAO would have the same effect. In keeping with the aggregation kinetics earlier, the times at which the aggregates formed varied with TMAO concentration. Ataxin-3 (Q15) and (Q64) both formed small spheroid-like oligomers within 2 h at 1 M TMAO while within 8 h, elongated curvilinear structures had formed and are typical of Stage 1 aggregates (58). TEM demonstrated that both ataxin-3 (Q15) and (Q64) aggregates formed in the presence of 1 M TMAO had morphologies comparable to non-TMAO induced ataxin-

3 aggregates (58). Josephin protein aggregates that were observed under EM also did not display any morphological changes.

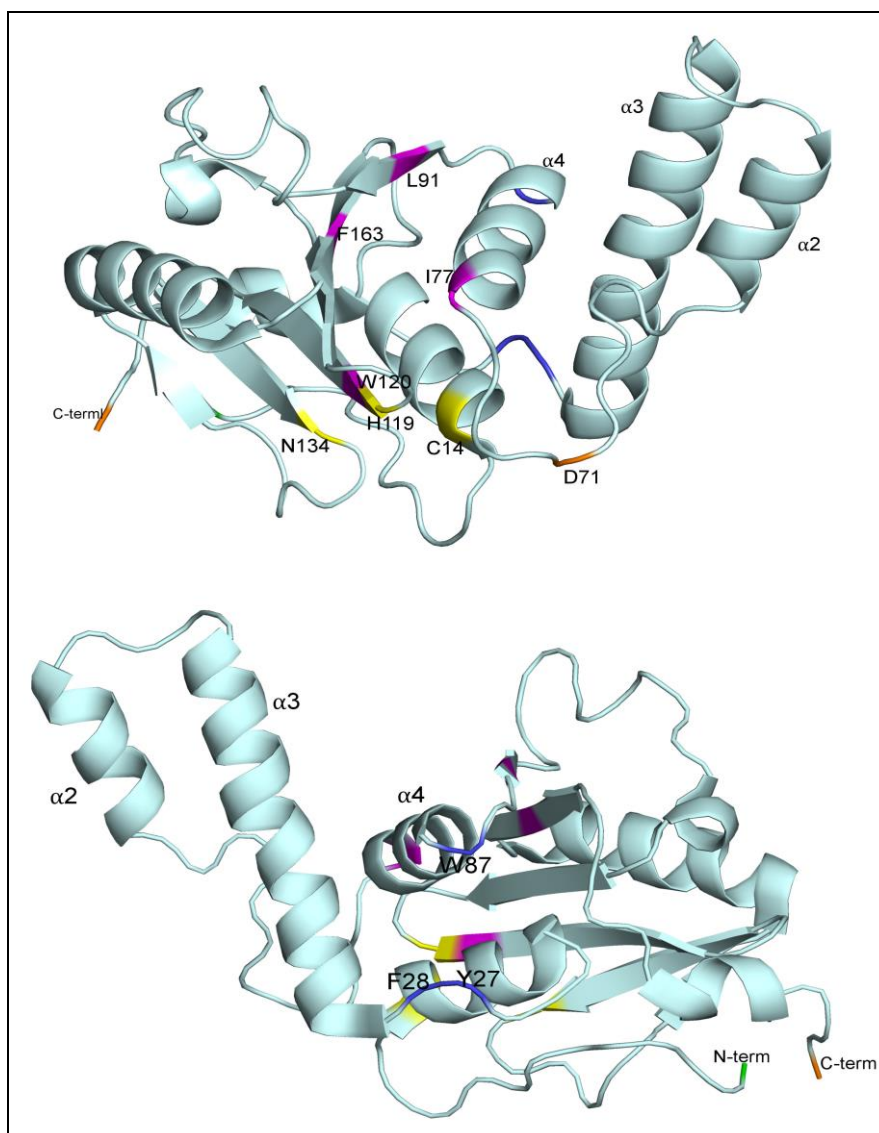


Figure 5.10 Solution structure of Josephin domain with binding sites for mono-ubiquitin. The solution structure of Josephin (PDB code: 1lyzb) is used to highlight the two weaker binding sites for single ubiquitin molecules (adapted from (69)). **(Top)** Site 1 is located at I77, L91, F163 and W120 (purple) while Site 2 is an aromatic group of Y27, F28 and W87 (blue). **(Bottom)** Site 2 is situated at the opposite interface and exposed to solvent. The catalytic site is in yellow; $\alpha2$ - $\alpha3$ makes for the flexible hairpin. D71 of Josephin is thought to be interacting with the Ub at Site 1(69).

TMAO has been shown to influence protein structure through interaction with the peptide backbone, encouraging native folds and discouraging denatured/unfolded structures (235, 236). It is likely that this interaction does not alter the overall folding/misfolding pathway of a protein. Rather, the protein folding is enhanced in a direction along the pathway that was already viable in the absence of TMAO (151, 220). These observations are also supported by the study on the intrinsically disordered structure, R2/wt tau fragment in the presence of 2 M TMAO. R2/wt tau fragment displayed accelerated aggregation and formed identical morphologies to full-length tau fibrils in the presence of TMAO (158). Overall, the data indicates that TMAO exerts no alteration in the ataxin-3 aggregation pathway. The use of TMAO with ataxin-3 has demonstrated a unique interaction between these molecules. Remarkably, TMAO accelerated ataxin-3 aggregation instead of reducing levels of misfolded protein. It would be of interest to explore other chemical chaperones, such as polyols and trehalose. These agents could be used to demonstrate discerning characteristics of ataxin-3 protein folding, compared to ataxin-3 with TMAO. For example, it has been reported that a combination of glycerol and TMAO prevented the conformational change of PrP^C into the infectious PrP^{Sc} (237). In another study, oral administration of 2% (w/v) trehalose solution to a transgenic mouse model of HD minimised the aggregation propensity of Htt (238). Apart from considering the effect of osmolytic action on ataxin-3 aggregation, other factors such as molecular crowding or salting out while using these chemical chaperones should also be considered in regards to the modulation of ataxin-3 aggregation (239, 240).

TMAO enhances the DUB activity of ataxin-3

Functionally, ataxin-3 has been associated with the binding of poly-ubiquitin chains with at least four subunits (30, 57, 60, 73). The two UIM within ataxin-3 (UIM1 and UIM2) are involved in the binding of these chains (60) while the Josephin domain confers the DUB proteolytic activity within ataxin-3 to cleave the polyubiquitin chains (57, 60). It was later shown that ataxin-3 also has two other distinct but weaker binding sites for mono-ubiquitin molecules within the Josephin domain (69) (Figure 5.10). It has also been previously reported that the enzymatic activity of Josephin was inhibited when it aggregated (120). The authors deduced that either ubiquitin sites might have been blocked for access after aggregation, thus inhibiting DUB activity.

With ataxin-3 aggregation modulated in the presence of TMAO, it was reasonable to investigate if DUB activity of ataxin-3 would also be affected. Using linear mono-ubiquitin substrates (GST-Ub52 and Ub-AMC), the results indicate an enhancement in the activity of ataxin-3 where all the variants underwent similar percentage activity changes correlating with a TMAO-concentration dependency.

Current data indicates that UIM knockout mutants of ataxin-3 did not show any decrease in activity, indicating that ubiquitin binding does not occur through the UIMs. It is most probable that the Ub-AMC substrate is binding to either or both of the reported mono-ubiquitin sites in the Josephin domain (69). Mono-ubiquitin binding site 1 (Site 1) is reportedly located at residues I77, L91, F163, W120 (Figure 5.10, top panel) while mono-ubiquitin binding site 2 (Site 2) is located at residues Y27, F28, W87 (Figure 5.10, bottom panel). Ubiquitin is thought to fit into the groove of Site 1 and the flexible hairpin helices $\alpha 2$ - $\alpha 3$ (69). The hairpin $\alpha 2$ - $\alpha 3$ is then thought to undergo subtle re-arrangements upon ubiquitin binding, forming a rigid complex. These sites were reported to be weak in binding affinity with no cooperativity (69). Based on the new hypothesis of the effect of TMAO on protein folding (158), it is proposed that as TMAO re-distributes water molecules around Josephin and creates a 'water hydration shell' around its exterior (Figure 5.11, bottom panel), TMAO is excluded due to its own water molecules and creates the polarizing 'compacting' effect on Josephin.

At the same time, a subtle increase in α -helical structures induced by TMAO in ataxin-3 may facilitate better folding and re-arrangement of hairpin $\alpha 2$ - $\alpha 3$. As such, on top of a TMAO 'compacting' effect, the hairpin could be shifted to form a more rigid complex with the ubiquitin substrates, holding the molecules in closer contact to the catalytic triad, resulting in the distinct enhancement in DUB activity. The role of the C-terminal poly-Q tract of ataxin-3 on DUB activity is currently unknown. The relative initial rates indicate that ataxin-3 (Q64) exhibits the highest activity among all three proteins in the presence of TMAO, suggesting that the poly-Q tract may play a role. However, ataxin-3 (Q64) exhibited a higher inherent DUB activity compared to Josephin (0 M TMAO). Moreover, a global change was observed for DUB activity for all proteins. More work is needed to further explore the role of the poly-Q tract on ataxin-3 aggregation in modulating DUB activity in TMAO.

At present, it is unknown which site mono-ubiquitin is binding to in the presence of TMAO. Site 1 was reported to have a specific induced fit mechanism, mediated by the hairpin $\alpha 2$ - $\alpha 3$ (69). Site 2 allows ubiquitin to sit around a hydrophobic patch that is exposed to the solvent yet it also in spatial contact with the hairpin (69). It would be interesting to determine the binding sites by mutating critical residues (I77, Q78 for Site 1; W87 for Site 2) sequentially and subjecting it to ubiquitin binding in the presence of TMAO. The complex could then be observed via NMR. Isothermal titration calorimetry can also be used to obtain finer measurements of kinetics and investigate binding affinities of ubiquitin to the sites in the presence of TMAO. Notably, residue I77 is part of the span of residues reported to initiate aggregation in Josephin as well as ataxin-3 (119). Since ubiquitin may bind to Site 1, it would provide valuable insight into whether ubiquitin binding affects ataxin-3 aggregation kinetics, in the absence and presence of TMAO. The complexities of ataxin-3 aggregation in TMAO could be further determined by analysing specific conformational changes with ESI-MS or HDX-MS.

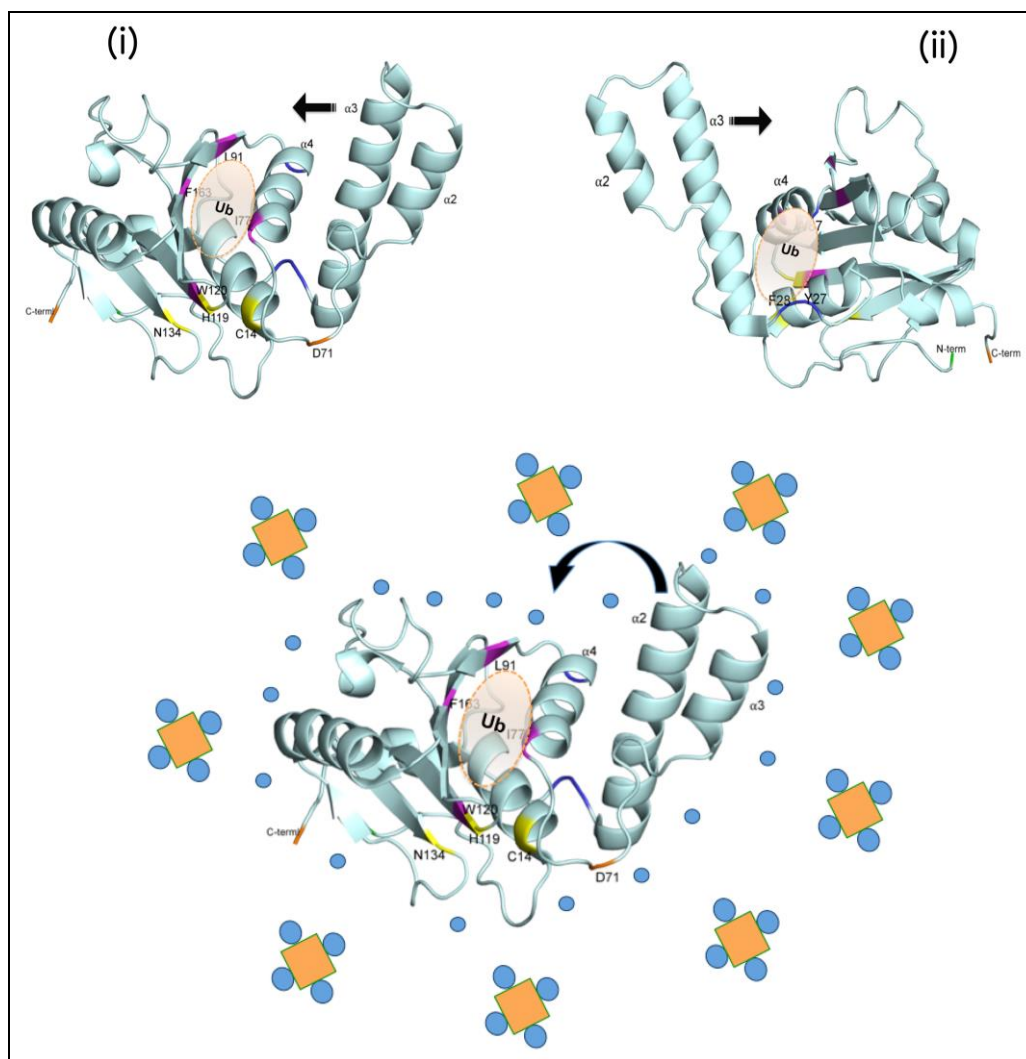


Figure 5.11 Proposed model for the compaction of Josephin molecule by TMAO resulting in the enhancement of DUB activity. The two binding sites for mono-ubiquitin was proposed by Nicastro and colleagues (69). Without TMAO, (i) shows the binding of ubiquitin into the groove of Site 1 and the hairpin while (ii) shows Ub binding to the hydrophobic patch of Site 2. The hairpin is thought to undergo a subtle rearrangement and moves to be sandwiched by the two Ub molecules, thereby becoming rigid. With TMAO molecules, (yellow box, blue spheres) it is thought to re-distribute water molecules (blue spheres) to the exterior of Josephin, forming a ‘hydration shell’ around Josephin. TMAO remains ‘excluded’ from the hydration shell presumably from its own water molecules. This results in the compaction of Josephin, with little or no structural change to the main Josephin molecule (69, 151, 158).

5.4 Summary and Conclusions

This study is the first to demonstrate that TMAO promotes both increased activity and aggregation of ataxin-3. This work showed that increasing concentrations of TMAO correlated with increased rates of aggregation as monitored by ThT-reactivity in ataxin-3 (Q15), (Q64) and Josephin proteins. This increased activity and aggregation in the presence of TMAO was correlated with only minor changes to the native structure and highlights the intricate balance of the ataxin-3 misfolding pathway. On the basis of this work and previous studies examining ataxin-3 aggregation and DUB activity, we propose that increasing TMAO concentration encourages the compaction of the native conformation of Josephin and folding of α -helical structural content. It is postulated that these subtle TMAO-induced conformational changes in the Josephin domain results in increased ataxin-3 aggregation and DUB activity. More work is needed to corroborate this further. Previous work has demonstrated the potential uses of chemical chaperones to treat a variety of disorders (9, 171, 237, 241, 242). This work highlights the importance of a greater understanding of the relationship between specific protein and specific osmolyte, as the results of these interactions reveal a complex interplay between the different structural pathways.

CHAPTER 6

PERSPECTIVES

6.1 Discussion

The Ataxin-3 protein is associated with neurodegenerative protein misfolding diseases, such as Huntington's (127). Ataxin-3 is known to be the causative agent of SCA3, which is the most common dominant autosomal ataxia among the rest of the ataxias. It is well documented that the misfolding of ataxin-3 contributes to aggregate formation, thus leading to disease pathogenesis. Nuclear inclusions found in specific neuronal cells also include ataxin-3 fragments, ubiquitin and other interacting partners (15, 129, 205, 243) suggesting that other factors may also play a role in ataxin-3 aggregation. The role of the aggregating full-length ataxin-3 as the sole causative agent for disease progression was further questioned when it was shown that mice expressing full-length ataxin-3 developed milder ataxia than mice expressing ataxin-3 with expanded poly-Q fragment lengths (134). Other studies also observed that the expression of ataxin-3 fragments exacerbated neurodegeneration in different *in vivo* models (113, 135, 244).

This thesis therefore sought to investigate the interrelationship between the length of the poly-Q tract and the effects of a range of factors and modulators on ataxin-3 aggregation, including ataxin-3 fragments generated by proteolytic cleavage (Chapters 3 and 4) and chemical chaperones (Chapter 5). The so-called toxic fragment hypothesis was proposed for ataxin-3 when proteases, such as calpain-2, were shown to cleave ataxin-3 expressed in cultured cells (56, 145) and full-length ataxin-3 aggregation was mitigated when calpain-2 specific inhibitors were used (145, 245). At present, there has been a range of calpain-2 cleavage sites proposed (56, 125, 132, 246, 247). It is important to identify these sites for the further understanding of proteolytic mechanisms on ataxin-3 and potentially identify therapeutic candidates. In addition, pathological length Htt and atrophin-1 were shown to be more sensitive to proteolysis (146, 148). Sun *et. al.* expressed non-pathological and pathological length of Htt in cultured cells and found the pathological length of Htt was more sensitive to calpain-2 proteolysis, generating an expanded poly-Q length Htt fragment (146).

As such, one of the first goals of this thesis was to ascertain if pathological ataxin-3, containing the expanded poly-Q tract, is more sensitive to proteolysis by calpain-2. Specifically, an *in vitro* kinetic assay was used to differentiate proteolytic rates between non-pathological and pathological length ataxin-3 (Chapter 3). The resulting ataxin-3 fragments derived from proteolysis, that contain the poly-Q region of the protein were then utilised to characterise their effect on ataxin-3 aggregation in Chapter 4. In order to achieve this, a new system to express and purify recombinant ataxin-3 fragments with non- and expanded poly-Q tract length was developed. The goal of this study was therefore to characterise the fragments structurally and study the aggregation kinetics of full-length ataxin-3 upon ataxin-3 fragment seeding in *in vitro* assays. Ataxin-3 has always been associated with protein misfolding induced pathogenesis, where its mutant form, with a longer expansion poly-Q tract, is known to be destabilised and aggregate. TMAO, a protein stabiliser has been known to prevent misfolding of proteins (150, 222, 248, 249) and was shown to reduce the aggregation of over-expressed ataxin-3 fragments (Q71) in cultured cells (171). The effect of TMAO on full-length ataxin-3 aggregation was therefore investigated in Chapter 5.

The poly-Q tract length of ataxin-3 does not influence calpain-2 sensitivity

In Chapter 3 of this thesis, the susceptibility to calpain-2 cleavage of ataxin-3 containing the shorter non-pathological poly-Q lengths (Q15) and (Q28), and the longer pathological poly-Q lengths (Q50) and (Q64) was studied. Upon calpain-2 cleavage, all the variants produced distinctly sized fragments by SDS-PAGE. N-terminal sequence analysis of these fragments revealed similar cleavage sites. While a majority of the fragments contained the Josephin peptide sequence, an ataxin-3 poly-Q containing fragment revealed a cleavage site at the amino acid residue 241. This site correlates with a previous study that proposed calpain-2 cleavage sites at amino acids from 241 – 248 (132). It is interesting but not surprising, that Josephin is not very sensitive to calpain-2 as it is a highly folded, globular stable structure (62, 117).

In order to establish if poly-Q expansion leads to increased proteolysis, the cleavage of ataxin-3 variants by calpain-2 were analysed in a kinetic assay to determine Michaelis-Menten (K_M and V_{max}) constants for the cleavage of a non-

chromogenic substrate (174) in the presence of a competing substrate for calpain-2. This assay was previously established by Blake *et. al.* to utilise the entire progress curve of the an enzyme-catalysed transformation and yields only steady state kinetics for the non-chromogenic substrate, without having to employ numerous equations or curve fitting routines (174). Thus, this kinetic assay allows ataxin-3 to be analysed for its sensitivity to calpain-2, without having to modify ataxin-3 with an additional chromogen and this method has been validated by various studies (177, 178, 250). Using this method, the apparent (K_M) values indicated that all the ataxin-3 variants were proteolysed by calpain-2 at rates that were not significantly different. Furthermore, apparent specificity constants (K_{cat}/K_M) suggested that calpain-2 has very similar efficiencies in proteolysing ataxin-3. Taken together, the overall values indicate that calpain-2 cleaves all the ataxin-3 variants at very similar rates, suggesting that the expansion of the poly-Q tract length in ataxin-3 does not influence the rate of calpain-2 proteolysis. These results correlate to previous studies that the poly-Q is a flexible tract that acts independently of its other domains (105, 121).

This finding suggests that a population of ataxin-3 fragments, including those with longer poly-Q tracts, may be released in a cellular environment, all at the same time (125). If these ataxin-3 fragments are not quickly removed, these fragments can further act as toxic instigators of ataxin-3 protein aggregation. The depletion of active full-length ataxin-3 proteins could in turn contribute to SCA3 pathogenesis (129). The result also suggest that if poly-Q expansion does not influence the sensitivity of calpain-2 towards ataxin-3, then in order to attenuate the severity of ataxin-3 proteolysis is to inhibit the activity of calpain-2. One such possibility is to mutate calpain-2 cleavage sites on ataxin-3, to mimic phosphorylation sites by mutating serine residues (251). It was recently shown that ataxin-3 phosphorylation decreases neurodegeneration (179, 251) and that calpain-2 is associated with reduced proteolysis against phosphorylated proteins (125, 252). Such methods have been previously employed for inhibiting Htt proteolysis (253, 254) and future studies could employ this approach to modulate ataxin-3 cleavage.

Toxicity of Ataxin-3 derived fragments confirms the toxic fragment hypothesis

In Chapter 4, the goal was to characterise the effect of ataxin-3 derived fragments on ataxin-3 aggregation via ataxin-3 fragment seeding assays and establish the toxic fragment hypothesis as an over-arching mechanism. In order to achieve this aim, recombinant fusion ataxin-3-fragment proteins (Q15) and (Q64) were constructed using the poly-Q containing ataxin-3 fragment sequence that was cleaved at amino acid 241 in Chapter 3. Following extensive optimisation, each of the ataxin-3 fragments was composed of an intact UIM2 starting from amino acid 242 and the poly-Q domain to the end of the native C-terminal region of the protein. The construct was then fused to a Protein A (SpA) molecule at its N-terminus and an S-tag at the C-terminus. Refolded (SpA242Q15) and (SpA242Q64) fusion proteins were characterised as soluble, monomeric proteins with α -helical secondary structure. The fragment proteins (242Q15) and (242Q64) were then released by TEV proteolysis. Both fusion and fragment proteins, especially the fragment (242Q64), formed aggregate structures and fibril morphologies that resembled the morphology of aggregates obtained with diseased ataxin-3 and poly-Q peptides (58, 105, 115). Due to the absence of the Josephin domain, fusion and fragment proteins emitted weak ThT fluorescence but aggregation reactions could still be monitored. These results support the current understanding that poly-Q fragments are able to aggregate and form oligomeric structures in their own right (46, 175, 204, 255). The fusion (SpA242Q64) and fragment (242Q64) were also the only two variants that formed SDS-insoluble aggregates, which further confirms that only expanded poly-Q length proteins are predisposed to do so (58, 105).

Aggregation kinetics of (SpA242Q64) and (242Q64) were then determined using SDS-insolubility filter trap membrane assay, instead of ThT fluorescence. Both (SpA242Q64) and (242Q64) showed highly aggregation-prone kinetics that was also concentration-dependent (122). The similarities in their aggregation kinetics supports the understanding that the expanded poly-Q segment has sufficient intrinsic propensity to aggregate (105, 244, 256), independent of the flanking domain, SpA (105). This is the first study to measure the aggregation kinetics of ataxin-3 derived fragments at this particular length in such detail. Most importantly, when fragment proteins (242Q15) and (242Q64) were released from their fusion partners, both fragments were able to induce and accelerate the aggregation of the full-length ataxin-

3 (Q64) to form SDS-insoluble aggregates. This result strongly supports the toxic fragment hypothesis with ataxin-3 (Q64) in this study. It also confirms that proteolysis of ataxin-3 is a pivotal step in SCA3 pathogenesis (125, 129). Following from this result, the next logical step would be to apply this system, using the expanded poly-Q fragment length 242, to study the toxic fragment hypothesis in a cellular environment and determine whether potential differences exist in the co-aggregation kinetics and aggregate morphology in the cell. A study previously co-expressed a shorter expanded ataxin-3 fragment (without 2UIM), as well as full-length expanded ataxin-3 and observed co-aggregation of fragments and full-length proteins by immunofluorescence in neuroblastoma cells (129). Intriguingly, both poly-Q length fragments (242Q15, 242Q64) induced aggregation of full-length ataxin-3 (Q64) at comparable kinetics. To explore the possibility that the fragments promote aggregation past Stage 1 of the ataxin-3 misfolding pathway, the aggregation of full-length (Q64) was monitored by ThT fluorescence. Intriguingly, ataxin-3 (Q64) displayed a ThT fluorescence aggregation profile in the presence of both fragments, suggesting Stage 1 of the ataxin-3 pathway was not circumvented. This correlates well with studies that suggest that ataxin-3 aggregation is also strongly influenced by the Josephin domain (57, 58, 117, 120, 121).

Multi-domain influence on fragment induced aggregation of ataxin-3

The complexity of ataxin-3 aggregation, as with most poly-Q protein aggregation, has made the delineation of the ‘seeding’ mechanisms of ataxin-3 very challenging. The biphasic time course profile of ataxin-3 (Q64) (Figure 4.14G) suggests a mixed population of ataxin-3 (Q64) aggregates formed simultaneously upon the seeding of (242Q64). It is possible that ataxin-3 (Q64) SDS-insoluble aggregates are formed to a greater extent than ThT-reactive species during this phase. The shorter poly-Q fragment (242Q15) did not appear to accelerate ataxin-3 (Q64) Stage 1 of its aggregation pathway, even though it was able to accelerate Stage 2. In fact, both fragments did not accelerate the aggregation of Josephin-associated Stage 1 but increased aggregation kinetics of expanded poly-Q ataxin-3 (Q64) Stage 2 to form SDS-insoluble aggregates. This implies that the fragments, regardless of poly-Q length, drive the formation of SDS-insoluble aggregates of ataxin-3 (Q64) faster than ataxin-3 (Q64) itself, possibly through motifs or domains that act as a ‘molecular templates’ for this association.

Apart from the poly-Q region within each fragment, aggregation-prone regions may also have an effect on ataxin-3 aggregation. A scan of the C-terminal region of ataxin-3 protein on TANGO (187) (Appendix C) shows a highly aggregation-prone hydrophobic tail (residues FIMFATFTLYLT-stop). Indeed, a recent study proposed that the hydrophobic tail remains buried in its native form but becomes exposed within aggregation-prone conformations (53). The exposed region then helps to increase the local poly-Q concentration and favour the formation of SDS-stable aggregates. Thus, it is rather attractive to suggest that the hydrophobic tail within the fragments may play a role in accelerating the formation of Stage 2 ataxin-3 (Q64) aggregates in this study. It is also unclear as to whether other domains, such as the 2UIM is involved in aggregation. However, it was previously observed that full-length ataxin-3 proteins had co-localised with aggregating fragments of ataxin-3 due to the presence of the UIMs (217). Clearly more work is necessary to further understand the intricacies of the role of the ataxin-3 fragments in inclusion formation, and subsequent neurotoxicity. Identification of plausible intermediate species from protein cleavage to protein aggregation will prove to be insightful in understanding ataxin-3 aggregation.

TMAO, a unique modulator of ataxin-3 misfolding and DUB activity

Osmolytes, such as TMAO have been previously used and shown to reduce the aggregation of some neurodegenerative diseases, such as PrP and in particular, ataxin-3 fragments (171, 249). In recent years, there has been an increased interest in the use of TMAO to study the complexities of protein folding, especially in intrinsically disordered proteins such as α -synuclein, tau fragment and even the relatively unstructured poly-Q tract in poly-Q proteins (150, 158, 164, 222). While it has been previously shown that TMAO reduces the aggregation of poly-Q containing fragments in cultured cells (171), there have not been any subsequent studies on the fragments nor full-length ataxin-3 proteins. In Chapter 5, the aggregation of full-length ataxin was therefore explored in the presence of TMAO, to investigate if TMAO can stabilise and prevent the aggregation of ataxin-3.

The results indicated that ataxin-3 rapidly aggregated in a TMAO-concentration dependent manner, displaying an increased ThT fluorescence reactivity and monomer loss. This result was not anticipated as TMAO is widely used to facilitate protein folding while stabilizing proteins (150). Moreover, TMAO was found to reduce the aggregation of the ataxin-3 C-terminal fragment, containing only the poly-Q domain (Q71ΔN286) expressed in cells. It is unknown which ataxin-3 isoform transcript was used in that study (171). However, TMAO has been reported to facilitate fibrillisation of some intrinsically disordered proteins such as tau and α -synuclein, although structural changes are variable in each study (158, 167, 168). Ataxin-3 (Q15) and (Q64) showed no significant changes in the morphology of its end stage aggregates. Each ataxin-3 variant displayed characteristic curvilinear or fibrillar types, closely resembling the morphologies of non-TMAO induced aggregates (58). It was suggested that while TMAO accelerated ataxin-3 aggregation, ataxin-3 maintained its aggregation pathway. This result is in contrast to a study in which TMAO altered the aggregation pathway and caused the formation of bulky, amorphous instead of fibrillar aggregates of mutant Htt exon 1 (Q53) (164). The indication that ataxin-3 did not alter its aggregation pathway was supported by the observation from fluorescence spectroscopy that TMAO did not destabilise the overall global conformation of the ataxin-3 variants in this study.

Keeping in mind that ataxin-3 undergoes a two-stage aggregation process and to further tease out the potential effects of TMAO on ataxin-3, the folding of the Josephin domain alone was investigated with TMAO. The results from Josephin also indicated rapid ThT fluorescence-reactive aggregation kinetics in increasing TMAO concentrations. Josephin also maintained aggregate morphology compared to non-TMAO conditions and its native conformation was unchanged in the presence of TMAO. However, two slight variations were observed, firstly the Josephin domain decelerated in the rate in monomer loss in increased TMAO concentrations. Secondly, there was an increase in α -helical secondary structure for all ataxin-3 variants and Josephin in increased TMAO concentrations. It has been proposed that TMAO increases the folding of α -helical secondary structures (151). Thus, it is postulated that even a small increase in folding for α -helical structures within the Josephin domain may have resulted in 'further folding' of aggregation prone helix- α 4 that is suggested to initiate ataxin-3 aggregation (119, 121). This 'folding' may lead to a

subtle conformational change that further initiates and accelerates Josephin aggregation, as well as the ataxin-3 variants. At the same time, this same increase in α -helical secondary structures may have fortuitously enabled the stabilisation of Josephin in its early stages of aggregation, resulting in the observed somewhat slower rate of monomer loss. More work on the detailed analysis of Josephin conformational changes with TMAO is required. Overall, these data support and build upon, the suggestion that ataxin-3 aggregation is greatly underpinned by the influence and stability of its N-terminal Josephin, even in the presence of TMAO. The impact of the role of N-terminal Josephin corroborates with a study showing that in the presence of the chaperone-like heat-shock protein, α -crystallin, the chaperone inhibited Josephin self-association and thus slowed ataxin-3 aggregation (218).

TMAO enhances apparent DUB activity of ataxin-3

It was previously shown that aggregated Josephin inhibited its enzymatic DUB activity (120, 257). The enzymatic DUB activity of ataxin-3 (Q15), (Q64) and Josephin were therefore investigated upon aggregation in the presence of TMAO. Linear mono-ubiquitin assays indicated an active protease with an enhancement in activity for all three proteins. The binding of ubiquitin substrates did not appear to involve either of the two UIMs in ataxin-3 protein. The enhancement of DUB activity is also not attributed to molecular crowding or viscosity as shown in results with glycerol. The enhancement of DUB activity observed in Josephin alone corroborates that ubiquitin molecules are likely to bind at the proposed mono-ubiquitin binding sites in Josephin (69). Furthermore, the distinctive $\alpha 2$ - $\alpha 3$ flexible hairpin of Josephin is thought to bring ubiquitin substrates at both Site 1 and 2, closer to the catalytic triad (Chapter 5, Figure 5.11) (69). TMAO has been previously shown to increase or enhance the activity of trypsin and chymotrypsin (228, 229). TMAO was shown to also promote both microtubule assembly activity as well as fibrillisation of the C-terminal fragment, tau¹⁸⁷ (167). A similar finding was seen with the cold-adapted protease deseasin MCP-01 which showed significant increase in activity with no significant changes to its monomeric structure in the presence of 1 M TMAO (258).

The results of this study suggest that an increase in α -helices in the presence of TMAO, along with the 'preferential exclusion effect' of TMAO leads to the enhancement in DUB activity by exerting an allosteric change in the $\alpha 2$ - $\alpha 3$ flexible

hairpin, drawing ubiquitin substrates even closer towards the catalytic site. Indeed, future work to confirm the structural basis of this effect through for example NMR can provide evidence for specific conformational changes in Josephin binding ubiquitin, in the presence of TMAO. Further work and analysis is also necessary to ascertain the impact of the poly-Q expansion upon aggregation in the presence of TMAO. It would be interesting to observe C-terminal ataxin-3 derived fragments, (Chapter 4) and its aggregation behaviour in the presence of TMAO, providing a clearer insight into how TMAO modulates the multi-domains of ataxin-3 in its aggregation.

6.2 Overview

Protein misfolding and aggregation has always been one of the central pathogenic mechanisms of many ND diseases and nuclear inclusions composed mainly of ataxin-3 proteins are hallmarks of SCA3. Ataxin-3, a small poly-Q protein associated with SCA3 has a unique two-stage aggregation pathway that requires the Josephin domain to self-associate or aggregate forming SDS-soluble aggregates (Stage 1). All variant poly-Q lengths of ataxin-3 undergo this stage. Only expanded poly-Q tract variants enter into the second stage (Stage 2) forming SDS-insoluble aggregates due to the expanded polyQ tract. Recently, the effects of ‘modulators’ have been represented as key steps or alternate pathways towards SCA3 pathogenicity. Proteolytic fragments of ataxin-3 have been shown to induce a greater toxic effect than full-length ataxin-3 proteins in various experimental models. Small molecules, such as osmolytes have been used as a tool to study aggregation or even shown to reduce aggregation.

Indeed, the results of this thesis have provided new insight into the additional factors that influence ataxin-3 aggregation and how these factors impact on the mechanism of ataxin-3 misfolding in the context of the toxic fragment hypothesis. The results are summarised in Figure 6.1 and demonstrate an increased complexity of ataxin-3 misfolding and aggregation. In summary, it has been shown that ataxin-3 is sensitive to calpain-2 proteolysis but that the rate is not dependent on the length of the poly-Q tract (Chapter 3). Ataxin-3 derived fragments from Chapter 3 were expressed and were both successfully refolded and characterised (Chapter 4). The fragments,

(242Q15) and (Q242Q64) can ‘seed’ and accelerate the aggregation of ataxin-3 (Q64) (Chapter 4), rapidly forming Stage 2 aggregates. It was also shown that the fragments do not by-pass Stage 1 of ataxin-3 aggregation. In the final part of this thesis, the osmolyte, TMAO was used to investigate the aggregation of ataxin-3 (Chapter 5). It was observed that TMAO enhanced the DUB activity of ataxin-3 and increased ataxin-3 aggregation. An overview on how TMAO and ataxin-3 fragments may modulate ataxin-3 aggregation is also illustrated in Figure 6.1

Overall, this study has explored and provided significant new insight into the roles of certain modulators of ataxin-3 aggregation and toxicity, in particular, proteolytically generated ataxin-3 fragments and the osmolyte, TMAO, which was shown to be act as a ‘protein stabiliser’. This thesis has therefore opened up new avenues to modulate ataxin-3 aggregation in which has enormous significance in terms of potential therapeutic interventions in SCA3 and NDs in general.

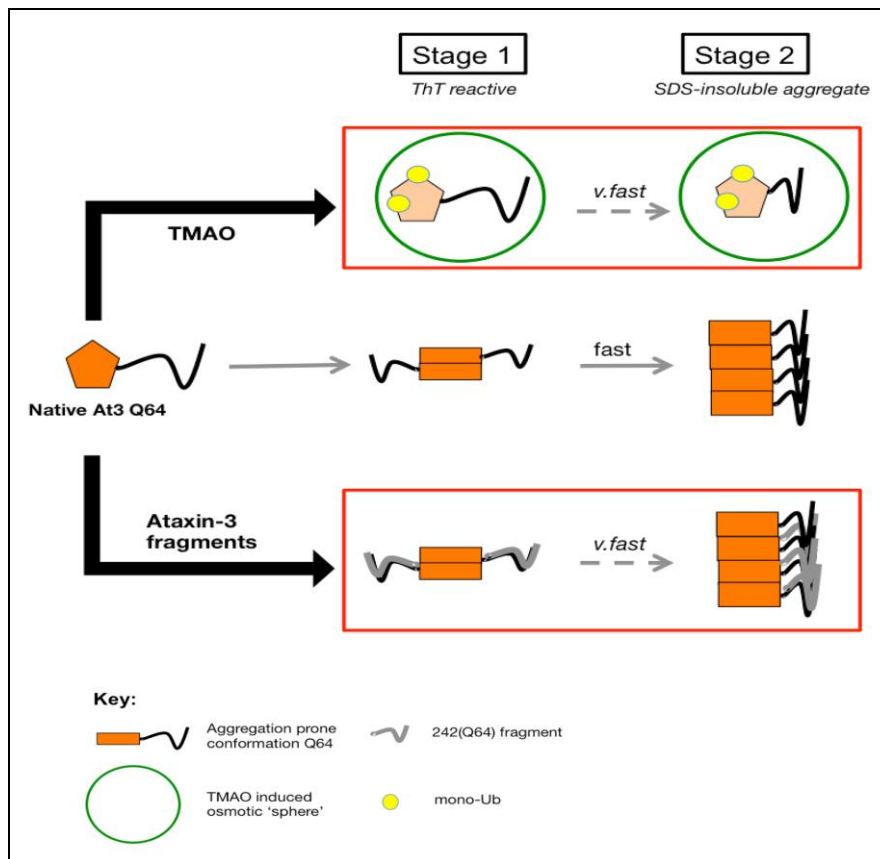


Figure 6.1 An overview on the effects of modulators that contribute further complexity to the mechanism of ataxin-3 aggregation. The illustration highlights how the expanded poly-Q ataxin-3 (Q64) aggregation is modulated by TMAO and ataxin-3 fragments (red box). Ataxin-3 fragments accelerate the aggregation of (Q64) to form SDS-insoluble aggregates, thus potentially reducing the levels of ataxin-3 available to carry out its function. The presence of TMAO enhanced DUB activity of ataxin-3 (yellow circles) but also accelerated ataxin-3 aggregation (top panel). This provided insight into how the osmolyte, TMAO can affect both structure and activity of ataxin-3. The conformation of Josephin (light orange) when ubiquitin bound and aggregating is currently undetermined and requires further studies.

References

1. Knowles TP, Vendruscolo M, Dobson CM. The amyloid state and its association with protein misfolding diseases. *Nature reviews Molecular cell biology*. 2014;15(6):384-96.
2. Martin JB. Molecular basis of the neurodegenerative disorders. *The New England Journal of Medicine*. 1999;340(25):1970-80.
3. Chiti F, Dobson CM. Protein misfolding, functional amyloid, and human disease. *Annual review of biochemistry*. 2006;75:333-66.
4. L. Vergara KA, C Soto. Protein Misfolding, a Common Mechanism in the Pathogenesis of Neurodegenerative Diseases. 2008. *Handbook of Neurochemistry and Molecular Neurobiology*. Springer US; [285-304].
5. Masters CL, Simms G, Weinman NA, Multhaup G, McDonald BL, Beyreuther K. Amyloid plaque core protein in Alzheimer disease and Down syndrome. *Proceedings of the National Academy of Sciences of the United States of America*. 1985;82(12):4245-9.
6. Giasson BI, Uryu K, Trojanowski JQ, Lee VM. Mutant and wild type human alpha-synucleins assemble into elongated filaments with distinct morphologies in vitro. *The Journal of Biological Chemistry*. 1999;274(12):7619-22.
7. Prusiner SB. Prions. *Proceedings of the National Academy of Sciences of the United States of America*. 1998;95(23):13363-83.
8. Williams AJ, Paulson HL. Polyglutamine neurodegeneration: protein misfolding revisited. *Trends in Neurosciences*. 2008;31(10):521-8.
9. Chaudhuri TK, Paul S. Protein-misfolding diseases and chaperone-based therapeutic approaches. *The FEBS journal*. 2006;273(7):1331-49.
10. Forno LS. Neuropathology of Parkinson's disease. *Journal of neuropathology and experimental neurology*. 1996;55(3):259-72.
11. Matos CA, de Macedo-Ribeiro S, Carvalho AL. Polyglutamine diseases: the special case of ataxin-3 and Machado-Joseph disease. *Progress in Neurobiology*. 2011;95(1):26-48.
12. Coutinho P, Andrade C. Autosomal dominant system degeneration in Portuguese families of the Azores Islands. A new genetic disorder involving cerebellar, pyramidal, extrapyramidal and spinal cord motor functions. *Neurology*. 1978;28(7):703-9.
13. Almeida B, Fernandes S, Abreu IA, Macedo-Ribeiro S. Trinucleotide repeats: a structural perspective. *Frontiers in Neurology*. 2013;4:76.
14. Kawaguchi Y, Okamoto T, Taniwaki M, Aizawa M, Inoue M, Katayama S, et al. CAG expansions in a novel gene for Machado-Joseph disease at chromosome 14q32.1. *Nature Genetics*. 1994;8:221-8.
15. Paulson H. Machado-Joseph disease/spinocerebellar ataxia type 3. *Handbook of clinical neurology*. 2012;103:437-49.
16. Perez MK, Paulson HL, Pendse SJ, Saionz SJ, Bonini NM, Pittman RN. Recruitment and the role of nuclear localization in polyglutamine-mediated aggregation. *Journal of Cell Biology*. 1998;143(6):1457-70.

17. Perez MK, Paulson HL, Pittman RN. Ataxin-3 with an altered conformation that exposes the polyglutamine domain is associated with the nuclear matrix. *Human molecular genetics*. 1999;8(13):2377-85.
18. Antony PM, Mantele S, Mollenkopf P, Boy J, Kehlenbach RH, Riess O, et al. Identification and functional dissection of localization signals within ataxin-3. *Neurobiology of Disease*. 2009;36(2):280-92.
19. Macedo-Ribeiro S, Cortes L, Maciel P, Carvalho AL. Nucleocytoplasmic shuttling activity of ataxin-3. *PLOS one*. 2009;4(6):e5834.
20. La Spada AR, Wilson EM, Lubahn DB, Harding AE, Fischbeck KH. Androgen receptor gene mutations in X-linked spinal and bulbar muscular atrophy. *Nature*. 1991;352(6330):77-9.
21. Orr HT, Chung MY, Banji S, Kwiatkowski Jr. TJ, Servadio A, Beaudet AL, et al. Expansion of an unstable trinucleotide CAG repeat in spinocerebellar ataxia type 1. *Nature Reviews: Genetics*. 1993;4:221-6.
22. Ross CA. When more is less: Pathogenesis of glutamine repeat neurodegenerative diseases. *Neuron*. 1995;15(3):493-6.
23. Ross CA, Poirier MA, Wanker EE, Amzel M. Polyglutamine fibrillogenesis: the pathway unfolds. *Proceedings of the National Academy of Sciences of the United States of America*. 2003;100(1):1-3.
24. Saunders HM, Bottomley SP. Multi-domain misfolding: understanding the aggregation pathway of polyglutamine proteins. *Protein engineering, design & selection*. 2009;22(8):447-51.
25. Schmitz-Hubsch T, Coudert M, Bauer P, Giunti P, Globas C, Baliko L, et al. Spinocerebellar ataxia type 1, 2, 3, and 6. Disease severity and nonataxia symptoms. *Neurology*. 2008;71(13):982-9.
26. Paulson HL, Das SS, Crino PB, Perez MK, Patel SC, Gotsdiner D, et al. Machado-Joseph disease gene product is a cytoplasmic protein widely expressed in brain. *Annals of Neurology*. 1997;41(4):453-62.
27. Orr HT. Cell biology of spinocerebellar ataxia. *The Journal of Cell Biology*. 2012;197(2):167-77.
28. Messaëd C, Rouleau GA. Molecular mechanisms underlying polyalanine diseases. *Neurobiology of Disease*. 2009;34(3):397-405.
29. Paulson HL, Perez MK, Trotter Y, Trojanowski JQ, Subramony SH, Das SS, et al. Intranuclear inclusions of expanded polyglutamine protein in spinocerebellar ataxia type 3. *Neuron*. 1997;19(2):333-44.
30. Chai Y, Koppenhafer SL, Shoesmith SJ, Perez MK, Paulson HL. Evidence for proteasome involvement in polyglutamine disease: localization to nuclear inclusions in SCA3/MJD and suppression of polyglutamine aggregation in vitro. *Human molecular genetics*. 1999;8(4):673-82.

31. Fujigasaki H, Uchihara T, Takahashi J, Matsushita H, Nakamura A, Koyano S, et al. Preferential recruitment of ataxin-3 independent of expanded polyglutamine: an immunohistochemical study on Marinesco bodies. *Journal of neurology, neurosurgery, and psychiatry*. 2001;71(4):518-20.
32. Bichelmeier U, Schmidt T, Hubener J, Boy J, Ruttiger L, Habig K, et al. Nuclear localization of ataxin-3 is required for the manifestation of symptoms in SCA3: in vivo evidence. *The Journal of neuroscience*. 2007;27(28):7418-28.
33. Butland SL, Devon RS, Huang Y, Mead CL, Meynert AM, Neal SJ, et al. CAG-encoded polyglutamine length polymorphism in the human genome. *BioMed Central Genomics*. 2007;8:126.
34. Mangelsdorf DJ, Thummel C, Beato M, Herrlich P, Schutz G, Umesono K, et al. The nuclear receptor superfamily: the second decade. *Cell*. 1995;83(6):835-9.
35. Nedelsky NB, Pennuto M, Smith RB, Palazzolo I, Moore J, Nie Z, et al. Native functions of the androgen receptor are essential to pathogenesis in a *Drosophila* model of spinobulbar muscular atrophy. *Neuron*. 2010;67(6):936-52.
36. Katsuno M, Adachi H, Kume A, Li M, Nakagomi Y, Niwa H, et al. Testosterone reduction prevents phenotypic expression in a transgenic mouse model of spinal and bulbar muscular atrophy. *Neuron*. 2002;35(5):843-54.
37. Takeyama K, Ito S, Yamamoto A, Tanimoto H, Furutani T, Kanuka H, et al. Androgen-dependent neurodegeneration by polyglutamine-expanded human androgen receptor in *Drosophila*. *Neuron*. 2002;35(5):855-64.
38. Kazantsev A, Preisinger E, Dranovsky A, Goldgaber D, Housman D. Insoluble detergent-resistant aggregates form between pathological and nonpathological lengths of polyglutamine in mammalian cells. *Proceedings of the National Academy of Sciences of the United States of America*. 1999;96(20):11404-9.
39. Nucifora FC, Jr., Sasaki M, Peters MF, Huang H, Cooper JK, Yamada M, et al. Interference by huntingtin and atrophin-1 with cbp-mediated transcription leading to cellular toxicity. *Science*. 2001;291(5512):2423-8.
40. Steffan JS, Bodai L, Pallos J, Poelman M, McCampbell A, Apostol BL, et al. Histone deacetylase inhibitors arrest polyglutamine-dependent neurodegeneration in *Drosophila*. *Nature*. 2001;413(6857):739-43.
41. Arrasate M, Mitra S, Schweitzer ES, Segal MR, Finkbeiner S. Inclusion body formation reduces levels of mutant huntingtin and the risk of neuronal death. *Nature*. 2004;431(7010):805-10.
42. Kaye R, Head E, Thompson JL, McIntire TM, Milton SC, Cotman CW, et al. Common Structure of Soluble Amyloid Oligomers Implies Common Mechanism of Pathogenesis. *Science*. 2003;300(5618):486-9.
43. Stefani M, Dobson CM. Protein aggregation and aggregate toxicity: new insights into protein folding, misfolding diseases and biological evolution. *Journal of Molecular Medicine*. 2003;81(11):678-99.

44. Gales L, Cortes L, Almeida C, Melo CV, do Carmo Costa M, Maciel P, et al. Towards a Structural Understanding of the Fibrillization Pathway in Machado-Joseph's Disease: Trapping Early Oligomers of Non-expanded Ataxin-3. *Journal of Molecular Biology*. 2005;353(3):642-54.
45. Nagai Y, Inui T, Popiel HA, Fujikake N, Hasegawa K, Urade Y, et al. A toxic monomeric conformer of the polyglutamine protein. *Nature Structural & Molecular biology*. 2007;14(4):332-40.
46. Takahashi T, Kikuchi S, Katada S, Nagai Y, Nishizawa M, Onodera O. Soluble polyglutamine oligomers formed prior to inclusion body formation are cytotoxic. *Human Molecular Genetics*. 2008;17(3):345-56.
47. Weissmann C, Brandt R. Mechanisms of neurodegenerative diseases: insights from live cell imaging. *Journal of neuroscience research*. 2008;86(3):504-11.
48. Almeida MR, Saraiva MJ. Clearance of extracellular misfolded proteins in systemic amyloidosis: experience with transthyretin. *Federation of European Biochemical Societies Letters*. 2012;586(18):2891-6.
49. Gusella JF, MacDonald ME. Molecular genetics: unmasking polyglutamine triggers in neurodegenerative disease. *Nature reviews Neuroscience*. 2000;1(2):109-15.
50. Evers MM, Toonen LJ, van Roon-Mom WM. Ataxin-3 protein and RNA toxicity in spinocerebellar ataxia type 3: current insights and emerging therapeutic strategies. *Molecular neurobiology*. 2014;49(3):1513-31.
51. Scheel H, Tomiuk S, Hofmann K. Elucidation of ataxin-3 and ataxin-7 function by integrative bioinformatics. *Human molecular genetics*. 2003;12(21):2845-52.
52. Albrecht M, Golatta M, Wullner U, Lengauer T. Structural and functional analysis of ataxin-2 and ataxin-3. *Federation of European Biochemical Societies*. 2004;271(15):3155-70.
53. Harris GM, Dodelzon K, Gong L, Gonzalez-Alegre P, Paulson HL. Splice isoforms of the polyglutamine disease protein ataxin-3 exhibit similar enzymatic yet different aggregation properties. *PLOS one*. 2010;5(10):e13695.
54. Burnett B, Li F, Pittman RN. The polyglutamine neurodegenerative protein ataxin-3 binds polyubiquitylated proteins and has ubiquitin protease activity. *Human Molecular Genetics*. 2003;12(23):3195-205.
55. Mao Y, Senic-Matuglia F, Di Fiore PP, Polo S, Hodsdon ME, De Camilli P. Deubiquitinating function of ataxin-3: insights from the solution structure of the Josephin domain. *Proceedings of the National Academy of Sciences, USA*. 2005;102(36):12700-5.
56. Haacke A, Hartl FU, Breuer P. Calpain inhibition is sufficient to suppress aggregation of polyglutamine-expanded ataxin-3. *Journal of Biological Chemistry*. 2007;282(26):18851-6.
57. Nicastro G, Menon RP, Masino L, Knowles PP, McDonald NQ, Pastore A. The solution structure of the Josephin domain of ataxin-3: structural determinants for molecular recognition. *Proceedings of the National Academy of Sciences, USA*. 2005;102(30):10493-8.

58. Ellisdon AM, Thomas B, Bottomley SP. The two-stage pathway of ataxin-3 fibrillogenesis involves a polyglutamine-independent step. *Journal of Biological Chemistry*. 2006;281(25):16888-96.
59. Nicastro G, Habeck M, Masino L, Svergun DI, Pastore A. Structure validation of the Josephin domain of ataxin-3: conclusive evidence for an open conformation. *Journal of Biomolecular NMR*. 2006;36(4):267-77.
60. Burnett B, Li F, Pittman RN. The polyglutamine neurodegenerative protein ataxin-3 binds polyubiquitylated proteins and has ubiquitin protease activity. *Human molecular genetics*. 2003;12(23):3195-205.
61. Chai Y, Berke SS, Cohen RE, Paulson HL. Poly-ubiquitin binding by the polyglutamine disease protein ataxin-3 links its normal function to protein surveillance pathways. *Journal of Biological Chemistry*. 2004;279(5):3605-11.
62. Chow MK, Mackay JP, Whisstock JC, Scanlon MJ, Bottomley SP. Structural and functional analysis of the Josephin domain of the polyglutamine protein ataxin-3. *Biochemical and biophysical research communications*. 2004;322(2):387-94.
63. Masino L, Kelly G, Leonard K, Trottier Y, Pastore A. Solution structure of polyglutamine tracts in GST-polyglutamine fusion proteins. *Federation of European Biochemical Societies Letters*. 2002;513(2-3):267-72.
64. Masino L, Musi V, Menon RP, Fusi P, Kelly G, Frenkiel TA, et al. Domain architecture of the polyglutamine protein ataxin-3: a globular domain followed by a flexible tail. *Federation of European Biochemical Societies Letters*. 2003;549(1-3):21-5.
65. Goto J, Watanabe M, Ichikawa Y, Yee SB, Ihara N, Endo K, et al. Machado-Joseph disease gene products carrying different carboxyl termini. *Neuroscience Research*. 1997;28(4):373-7.
66. Schmidt T, Landwehrmeyer GB, Schmitt I, Trottier Y, Auburger G, Laccone F, et al. An isoform of ataxin-3 accumulates in the nucleus of neuronal cells in affected brain regions of SCA3 patients. *Brain Pathology*. 1998;8(4):669-79.
67. Breuer P, Haacke A, Evert BO, Wullner U. Nuclear aggregation of polyglutamine-expanded ataxin-3: fragments escape the cytoplasmic quality control. *The Journal of biological chemistry*. 2010;285(9):6532-7.
68. Mueller T, Breuer P, Schmitt I, Walter J, Evert BO, Wullner U. CK2-dependent phosphorylation determines cellular localization and stability of ataxin-3. *Human molecular genetics*. 2009;18(17):3334-43.
69. Nicastro G, Masino L, Esposito V, Menon RP, De Simone A, Fraternali F, et al. Josephin domain of ataxin-3 contains two distinct ubiquitin-binding sites. *Biopolymers*. 2009;91(12):1203-14.
70. Doss-Pepe EW, Stenroos ES, Johnson WG, Madura K. Ataxin-3 interactions with Rad23 and valosin-containing protein and its associations with ubiquitin chains and the proteasome are consistent with a role in ubiquitin-mediated proteolysis. *Molecular and Cellular Biology*. 2003;23(18):6469-83.
71. Fang S, Weissman AM. A field guide to ubiquitylation. *Cellular and molecular life sciences*. 2004;61(13):1546-61.

-
72. Lim KL, Lim GG. K63-linked ubiquitination and neurodegeneration. *Neurobiology of Disease*. 2011;43(1):9-16.
73. Winborn BJ, Travis SM, Todi SV, Scaglione KM, Xu P, Williams AJ, et al. The deubiquitinating enzyme ataxin-3, a polyglutamine disease protein, edits K63-linkages in mixed linkage ubiquitin chains. *Journal of Biological Chemistry*. 2008;283(39):26436 - 43.
74. Todi SV, Winborn BJ, Scaglione KM, Blount JR, Travis SM, Paulson HL. Ubiquitination directly enhances activity of the deubiquitinating enzyme ataxin-3. *The EMBO journal*. 2009;28(4):372-82.
75. Wang G, Sawai N, Kotliarova S, Kanazawa I, Nukina N. Ataxin-3, the MJD1 gene product, interacts with the two human homologs of yeast DNA repair protein RAD23, HHR23A and HHR23B. *Human molecular genetics*. 2000;9(12):1795-803.
76. Zhong X, Pittman RN. Ataxin-3 binds VCP/p97 and regulates retrotranslocation of ERAD substrates. *Human molecular genetics*. 2006;15(16):2409-20.
77. Boeddrich A, Gaumer S, Haacke A, Tzvetkov N, Albrecht M, Evert BO, et al. An arginine/lysine-rich motif is crucial for VCP/p97-mediated modulation of ataxin-3 fibrillogenesis. *The European Molecular Biology Organization Journal*. 2006;25(7):1547-58.
78. Wang Q, Li L, Ye Y. Regulation of retrotranslocation by p97-associated deubiquitinating enzyme ataxin-3. *The Journal of cell biology*. 2006;174(7):963-71.
79. Shimohata T, Nakajima T, Yamada M, Uchida C, Onodera O, Naruse S, et al. Expanded polyglutamine stretches interact with TAFII130, interfering with CREB-dependent transcription. *Nature genetics*. 2000;26(1):29-36.
80. McCampbell A, Taylor JP, Taye AA, Robitschek J, Li M, Walcott J, et al. CREB-binding protein sequestration by expanded polyglutamine. *Human molecular genetics*. 2000;9(14):2197-202.
81. Chai Y, Shao J, Miller VM, Williams A, Paulson HL. Live-cell imaging reveals divergent intracellular dynamics of polyglutamine disease proteins and supports a sequestration model of pathogenesis. *Proceedings of the National Academy of Sciences of the United States of America*. 2002;99(14):9310-5.
82. Li F, Macfarlan T, Pittman RN, Chakravarti D. Ataxin-3 is a histone-binding protein with two independent transcriptional corepressor activities. *The Journal of biological chemistry*. 2002;277(47):45004-12.
83. Evert BO, Araujo J, Vieira-Saecker AM, de Vos RA, Harendza S, Klockgether T, et al. Ataxin-3 represses transcription via chromatin binding, interaction with histone deacetylase 3, and histone deacetylation. *The Journal of neuroscience*. 2006;26(44):11474-86.
84. Scaglione KM, Zavodszky E, Todi SV, Patury S, Xu P, Rodriguez-Lebron E, et al. Ube2w and ataxin-3 coordinately regulate the ubiquitin ligase CHIP. *Molecular Cell*. 2011;43(4):599-612.
85. Karplus M. The Levinthal paradox: yesterday and today. *Folding & Design*. 1997;2(4):S69-75.
86. Dobson CM. Protein folding and misfolding. *Nature*. 2003;426(6968):884-90.

87. Dobson CM. Principles of protein folding, misfolding and aggregation. *Seminars in cell & developmental biology*. 2004;15(1):3-16.
88. Dinner AR, Sali A, Smith LJ, Dobson CM, Karplus M. Understanding protein folding via free-energy surfaces from theory and experiment. *Trends in biochemical sciences*. 2000;25(7):331-9.
89. Capaldi AP, Kleanthous C, Radford SE. Im7 folding mechanism: misfolding on a path to the native state. *Nature structural biology*. 2002;9(3):209-16.
90. Bukau B, Horwich AL. The Hsp70 and Hsp60 chaperone machines. *Cell*. 1998;92(3):351-66.
91. Hartl FU, Hayer-Hartl M. Molecular chaperones in the cytosol: from nascent chain to folded protein. *Science*. 2002;295(5561):1852-8.
92. Schiene C, Fischer G. Enzymes that catalyse the restructuring of proteins. *Current opinion in structural biology*. 2000;10(1):40-5.
93. Hartl FU, Bracher A, Hayer-Hartl M. Molecular chaperones in protein folding and proteostasis. *Nature*. 2011;475(7356):324-32.
94. Schubert U, Anton LC, Gibbs J, Norbury CC, Yewdell JW, Bennink JR. Rapid degradation of a large fraction of newly synthesized proteins by proteasomes. *Nature*. 2000;404(6779):770-4.
95. Hammond C, Helenius A. Quality control in the secretory pathway. *Current opinion in cell biology*. 1995;7(4):523-9.
96. Kaufman RJ, Scheuner D, Schroder M, Shen X, Lee K, Liu CY, et al. The unfolded protein response in nutrient sensing and differentiation. *Nature reviews Molecular cell biology*. 2002;3(6):411-21.
97. Radford SE, Dobson CM. From computer simulations to human disease: emerging themes in protein folding. *Cell*. 1999;97(3):291-8.
98. Diaz-Villanueva JF, Diaz-Molina R, Garcia-Gonzalez V. Protein Folding and Mechanisms of Proteostasis. *International journal of molecular sciences*. 2015;16(8):17193-230.
99. Wetzel R. For protein misassembly, it's the "I" decade. *Cell*. 1996;86(5):699-702.
100. Sipe JD. Amyloidosis. *Annual review of biochemistry*. 1992;61:947-75.
101. Temussi PA, Masino L, Pastore A. From Alzheimer to Huntington: why is a structural understanding so difficult? *The European Molecular Biology Organization Journal*. 2003;22(3):355-61.
102. Murphy MP, LeVine H, 3rd. Alzheimer's disease and the amyloid-beta peptide. *Journal of Alzheimer's disease*. 2010;19(1):311-23.
103. Masino L, Pastore A. Glutamine repeats: structural hypotheses and neurodegeneration. *Biochemical Society Transactions*. 2002;30(4):548-51.

-
104. Barton S, Jacak R, Khare SD, Ding F, Dokholyan NV. The length dependence of the polyQ-mediated protein aggregation. *The Journal of biological chemistry*. 2007;282(35):25487-92.
105. Robertson AL, Horne J, Ellisdon AM, Thomas B, Scanlon MJ, Bottomley SP. The structural impact of a polyglutamine tract is location-dependent. *Biophysical journal*. 2008;95(12):5922-30.
106. Kagan BL, Thundimadathil J. Amyloid peptide pores and the beta sheet conformation. *Advances in experimental medicine and biology*. 2010;677:150-67.
107. Perutz MF, Staden R, Moens L, De Baere I. Polar zippers. *Current biology*. 1993;3(5):249-53.
108. Buchanan LE, Carr JK, Fluitt AM, Hoganson AJ, Moran SD, de Pablo JJ, et al. Structural motif of polyglutamine amyloid fibrils discerned with mixed-isotope infrared spectroscopy. *Proceedings of the National Academy of Sciences of the United States of America*. 2014;111(16):5796-801.
109. Perutz MF, Pope BJ, Owen D, Wanker EE, Scherzinger E. Aggregation of proteins with expanded glutamine and alanine repeats of the glutamine-rich and asparagine-rich domains of Sup35 and of the amyloid beta-peptide of amyloid plaques. *Proceedings of the National Academy of Sciences of the United States of America*. 2002;99(8):5596-600.
110. Chan JC, Oyler NA, Yau WM, Tycko R. Parallel beta-sheets and polar zippers in amyloid fibrils formed by residues 10-39 of the yeast prion protein Ure2p. *Biochemistry*. 2005;44(31):10669-80.
111. Bugg CW, Isas JM, Fischer T, Patterson PH, Langen R. Structural features and domain organization of huntingtin fibrils. *The Journal of biological chemistry*. 2012;287(38):31739-46.
112. Costa Mdo C, Paulson HL. Toward understanding Machado-Joseph disease. *Progress in neurobiology*. 2012;97(2):239-57.
113. Warrick JM, Paulson HL, Gray-Board GL, Bui QT, Fischbeck KH, Pittman RN, et al. Expanded polyglutamine protein forms nuclear inclusions and causes neural degeneration in *Drosophila*. *Cell*. 1998;93(6):939-49.
114. Bevivino AE, Loll PJ. An expanded glutamine repeat destabilizes native ataxin-3 structure and mediates formation of parallel beta -fibrils. *Proceedings of the National Academy of Sciences of the United States of America*. 2001;98(21):11955-60.
115. Chow MK, Ellisdon AM, Cabrita LD, Bottomley SP. Polyglutamine expansion in ataxin3 does not affect protein stability. *Journal of Biological Chemistry*. 2004;279(46):47643-51.
116. Marchal S, Shehi E, Harricane MC, Fusi P, Heitz F, Tortora P, et al. Structural instability and fibrillar aggregation of non-expanded human ataxin-3 revealed under high pressure and temperature. *The Journal of biological chemistry*. 2003;278(34):31554-63.
117. Masino L, Nicastro G, Menon RP, Piaz FD, Calder L, Pastore A. Characterization of the structure and the amyloidogenic properties of the Josephin domain of the polyglutamine-containing protein ataxin-3. *Journal of molecular biology*. 2004;344(4):1021-35.

118. Saunders HM, Gilis D, Rooman M, Dehouck Y, Robertson AL, Bottomley SP. Flanking domain stability modulates the aggregation kinetics of a polyglutamine disease protein. *Protein Science*. 2011;20(10):1675-81.
119. Scarff CA, Almeida B, Fraga J, Macedo-Ribeiro S, Radford SE, Ashcroft AE. Examination of Ataxin-3 (atx-3) Aggregation by Structural Mass Spectrometry Techniques: A Rationale for Expedited Aggregation upon Polyglutamine (polyQ) Expansion. *Molecular & Cellular Proteomics*. 2015;14(5):1241-53.
120. Masino L, Nicastro G, De Simone A, Calder L, Molloy J, Pastore A. The Josephin domain determines the morphological and mechanical properties of ataxin-3 fibrils. *Biophysical journal*. 2011;100(8):2033-42.
121. Lupton CJ, Steer DL, Wintrode PL, Bottomley SP, Hughes VA, Ellisdon AM. Enhanced molecular mobility of ordinarily structured regions drives polyglutamine disease. *The Journal of biological chemistry*. 2015;290(40):24190-200.
122. Ellisdon AM, Pearce MC, Bottomley SP. Mechanisms of Ataxin-3 Misfolding and Fibril Formation: Kinetic Analysis of a Disease-associated Polyglutamine Protein. *Journal of molecular biology*. 2007;368(2):595-605.
123. Scarff CA, Snelling JR, Knust MM, Wilkins CL, Scrivens JH. New structural insights into mechanically interlocked polymers revealed by ion mobility mass spectrometry. *Journal of the American Chemical Society*. 2012;134(22):9193-8.
124. Santambrogio C, Frana AM, Natalello A, Papaleo E, Regonesi ME, Doglia SM, et al. The role of the central flexible region on the aggregation and conformational properties of human ataxin-3. *The FEBS journal*. 2012;279(3):451-63.
125. Weber JJ, Sowa AS, Binder T, Hubener J. From pathways to targets: understanding the mechanisms behind polyglutamine disease. *BioMed research international*. 2014;2014:701758.
126. Cooper JK, Schilling G, Peters MF, Herring WJ, Sharp AH, Kaminsky Z, et al. Truncated N-terminal fragments of huntingtin with expanded glutamine repeats form nuclear and cytoplasmic aggregates in cell culture. *Human molecular genetics*. 1998;7(5):783-90.
127. Mangiarini L, Sathasivam K, Seller M, Cozens B, Harper A, Hetherington C, et al. Exon 1 of the HD gene with an expanded CAG repeat is sufficient to cause a progressive neurological phenotype in transgenic mice. *Cell*. 1996;87(3):493-506.
128. Tarlac V, Turnbull V, Stefani D, Kelly L, Walsh R, Storey E. Inclusion formation by ataxins -1, -2, -3, and -7. *The International journal of neuroscience*. 2007;117(9):1289-314.
129. Haacke A, Broadley SA, Boteva R, Tzvetkov N, Hartl FU, Breuer P. Proteolytic cleavage of polyglutamine-expanded ataxin-3 is critical for aggregation and sequestration of non-expanded ataxin-3. *Human molecular genetics*. 2006;15(4):555-68.
130. Goldberg YP, Nicholson DW, Rasper DM, Kalchman MA, Koide HB, Graham RK, et al. Cleavage of huntingtin by apopain, a proapoptotic cysteine protease, is modulated by the polyglutamine tract. *Nature genetics*. 1996;13(4):442-9.

131. Wellington CL, Ellerby LM, Gutekunst CA, Rogers D, Warby S, Graham RK, et al. Caspase cleavage of mutant huntingtin precedes neurodegeneration in Huntington's disease. *The Journal of Neuroscience*. 2002;22(18):7862-72.
132. Berke SJ, Schmied FA, Brunt ER, Ellerby LM, Paulson HL. Caspase-mediated proteolysis of the polyglutamine disease protein ataxin-3. *Journal of neurochemistry*. 2004;89(4):908-18.
133. Graham RK, Deng Y, Slow EJ, Haigh B, Bissada N, Lu G, et al. Cleavage at the caspase-6 site is required for neuronal dysfunction and degeneration due to mutant huntingtin. *Cell*. 2006;125(6):1179-91.
134. Ikeda H, Yamaguchi M, Sugai S, Aze Y, Narumiya S, Kakizuka A. Expanded polyglutamine in the Machado-Joseph disease protein induces cell death in vitro and in vivo. *Nature genetics*. 1996;13(2):196-202.
135. Goti D, Katzen SM, Mez J, Kurtis N, Kiluk J, Ben-Haiem L, et al. A mutant ataxin-3 putative-cleavage fragment in brains of Machado-Joseph disease patients and transgenic mice is cytotoxic above a critical concentration. *The Journal of neuroscience*. 2004;24(45):10266-79.
136. Wellington CL, Ellerby LM, Hackam AS, Margolis RL, Trifiro MA, Singaraja R, et al. Caspase cleavage of gene products associated with triplet expansion disorders generates truncated fragments containing the polyglutamine tract. *The Journal of biological chemistry*. 1998;273(15):9158-67.
137. Earnshaw WC, Martins LM, Kaufmann SH. Mammalian caspases: structure, activation, substrates, and functions during apoptosis. *Annual review of biochemistry*. 1999;68:383-424.
138. McIlwain DR, Berger T, Mak TW. Caspase functions in cell death and disease. *Cold Spring Harbor perspectives in biology*. 2013;5(4):a008656.
139. Pozzi C, Valtorta M, Tedeschi G, Galbusera E, Pastori V, Bigi A, et al. Study of subcellular localization and proteolysis of ataxin-3. *Neurobiology of Disease*. 2008;30(2):190-200.
140. Koch P, Breuer P, Peitz M, Jungverdorben J, Kesavan J, Poppe D, et al. Excitation-induced ataxin-3 aggregation in neurons from patients with Machado-Joseph disease. *Nature*. 2011;480(7378):543-6.
141. Huang Y, Wang KK. The calpain family and human disease. *Trends in molecular medicine*. 2001;7(8):355-62.
142. Ohno S, Emori Y, Suzuki K. Nucleotide sequence of a cDNA coding for the small subunit of human calcium-dependent protease. *Nucleic acids research*. 1986;14(13):5559.
143. Hosfield CM, Elce JS, Davies PL, Jia Z. Crystal structure of calpain reveals the structural basis for Ca(2+)-dependent protease activity and a novel mode of enzyme activation. *The European Molecular Biology Organization Journal*. 1999;18(24):6880-9.
144. Strobl S, Fernandez-Catalan C, Braun M, Huber R, Masumoto H, Nakagawa K, et al. The crystal structure of calcium-free human m-calpain suggests an electrostatic switch mechanism for activation by calcium. *Proceedings of the National Academy of Sciences of the United States of America*. 2000;97(2):588-92.

145. Hubener J, Weber JJ, Richter C, Honold L, Weiss A, Murad F, et al. Calpain-mediated ataxin-3 cleavage in the molecular pathogenesis of spinocerebellar ataxia type 3 (SCA3). *Human molecular genetics*. 2013;22(3):508-18.
146. Sun B, Fan W, Balciunas A, Cooper JK, Bitan G, Steavenson S, et al. Polyglutamine repeat length-dependent proteolysis of huntingtin. *Neurobiol Dis*. 2002;11(1):111-22.
147. Schilling G, Wood JD, Duan K, Slunt HH, Gonzales V, Yamada M, et al. Nuclear accumulation of truncated atrophin-1 fragments in a transgenic mouse model of DRPLA. *Neuron*. 1999;24(1):275-86.
148. Kobayashi Y, Miwa S, Merry DE, Kume A, Mei L, Doyu M, et al. Caspase-3 cleaves the expanded androgen receptor protein of spinal and bulbar muscular atrophy in a polyglutamine repeat length-dependent manner. *Biochemical and biophysical research communications*. 1998;252(1):145-50.
149. Yancey PH, Clark ME, Hand SC, Bowlus RD, Somero GN. Living with water stress: Evolution of osmolyte systems. *Science*. 1982;217(4566):1214-22.
150. Macchi F, Eisenkolb M, Kiefer H, Otzen DE. The effect of osmolytes on protein fibrillation. *International Journal of Molecular sciences*. 2012;13(3):3801-19.
151. Yancey PH, Siebenaller JF. Co-evolution of proteins and solutions: protein adaptation versus cytoprotective micromolecules and their roles in marine organisms. *The Journal of experimental biology*. 2015;218(Pt 12):1880-96.
152. Street TO, Krukenberg KA, Rosgen J, Bolen DW, Agard DA. Osmolyte-induced conformational changes in the Hsp90 molecular chaperone. *Protein science*. 2010;19(1):57-65.
153. Orsini G, Goldberg ME. The renaturation of reduced chymotrypsinogen A in guanidine HCl. Refolding versus aggregation. *The Journal of biological chemistry*. 1978;253(10):3453-8.
154. Maeda Y, Koga H, Yamada H, Ueda T, Imoto T. Effective renaturation of reduced lysozyme by gentle removal of urea. *Protein engineering*. 1995;8(2):201-5.
155. Lim WK, Rosgen J, Englander SW. Urea, but not guanidinium, destabilizes proteins by forming hydrogen bonds to the peptide group. *Proceedings of the National Academy of Sciences of the United States of America*. 2009;106(8):2595-600.
156. Hunger J, Ottosson N, Mazur K, Bonn M, Bakker HJ. Water-mediated interactions between trimethylamine-N-oxide and urea. *Physical chemistry chemical physics*. 2015;17(1):298-306.
157. Timasheff SN. Protein-solvent preferential interactions, protein hydration, and the modulation of biochemical reactions by solvent components. *Proceedings of the National Academy of Sciences of the United States of America*. 2002;99(15):9721-6.
158. Levine ZA, Larini L, LaPointe NE, Feinstein SC, Shea JE. Regulation and aggregation of intrinsically disordered peptides. *Proceedings of the National Academy of Sciences of the United States of America*. 2015;112(9):2758-63.

159. Rosgen J, Jackson-Atogi R. Volume exclusion and H-bonding dominate the thermodynamics and solvation of trimethylamine-N-oxide in aqueous urea. *Journal of the American Chemical Society*. 2012;134(7):3590-7.
160. Bolen D, Baskakov I. The osmophobic effect: natural selection of a thermodynamic force in protein folding. *Journal of molecular biology*. 2001;310(5):955-63.
161. Street TO, Bolen DW, Rose GD. A molecular mechanism for osmolyte-induced protein stability. *Proceedings of the National Academy of Sciences of the United States of America*. 2006;103(38):13997-4002.
162. Bolen DW. Protein Stabilization by Naturally Occurring Osmolytes. In: Murphy KP, editor. *Protein Structure, Stability, and Folding*. Totowa, NJ: Humana Press; 2001. p. 17-36.
163. England JL, Kaganovich D. Polyglutamine shows a urea-like affinity for unfolded cytosolic protein. *Federation of European Biochemical Societies Letters*. 2011;585(2):381-4.
164. Borwankar T, Rothlein C, Zhang G, Tegen A, Dosche C, Ignatova Z. Natural osmolytes remodel the aggregation pathway of mutant huntingtin exon 1. *Biochemistry*. 2011;50(12):2048-60.
165. Chaudhuri TK, Paul S. Protein-misfolding diseases and chaperone-based therapeutic approaches. *The Federation of European Biochemical Societies journal*. 2006;273(7):1331-49.
166. Nandi PK, Bera A, Sizaret PY. Osmolyte trimethylamine N-oxide converts recombinant alpha-helical prion protein to its soluble beta-structured form at high temperature. *Journal of molecular biology*. 2006;362(4):810-20.
167. Scaramozzino F, Peterson DW, Farmer P, Gerig JT, Graves DJ, Lew J. TMAO promotes fibrillization and microtubule assembly activity in the C-terminal repeat region of tau. *Biochemistry*. 2006;45(11):3684-91.
168. Uversky VN, Li J, Fink AL. Trimethylamine-N-oxide-induced folding of a-synuclein. *Federation of European Biochemical Societies Letters*. 2001;509(1):31-5.
169. Herbst M, Wanker EE. Therapeutic approaches to polyglutamine diseases: combating protein misfolding and aggregation. *Current pharmaceutical design*. 2006;12(20):2543-55.
170. Cutting GR. Cystic fibrosis genetics: from molecular understanding to clinical application. *Nature reviews Genetics*. 2015;16(1):45-56.
171. Yoshida H, Yoshizawa T, Shibasaki F, Shoji S, Kanazawa I. Chemical chaperones reduce aggregate formation and cell death caused by the truncated Machado-Joseph disease gene product with an expanded polyglutamine stretch. *Neurobiology of Disease*. 2002;10(2):88-99.
172. Hanahan D, Jessee J, Bloom FR. Plasmid transformation of *Escherichia coli* and other bacteria. *Methods in enzymology*. 1991;204:63-113.
173. Cabrita LD, Gilis D, Robertson AL, Dehouck Y, Rooman M, Bottomley SP. Enhancing the stability and solubility of TEV protease using in silico design. *Protein science*. 2007;16(11):2360-7.

174. Blake RC, 2nd, Vassall RF, Blake DA. The Michaelis constants of a nonchromogenic substrate may be determined using a chromogenic substrate. *Archives of biochemistry and biophysics*. 1989;272(1):52-68.
175. Hazeki N, Nakamura K, Goto J, Kanazawa I. Rapid aggregate formation of the huntingtin N-terminal fragment carrying an expanded polyglutamine tract. *Biochemical and biophysical research communications*. 1999;256(2):361-6.
176. Kim YJ, Yi Y, Sapp E, Wang Y, Cuiffo B, Kegel KB, et al. Caspase 3-cleaved N-terminal fragments of wild-type and mutant huntingtin are present in normal and Huntington's disease brains, associate with membranes, and undergo calpain-dependent proteolysis. *Proceedings of the National Academy of Sciences of the United States of America*. 2001;98(22):12784-9.
177. Kvassman JO, Verhamme I, Shore JD. Inhibitory mechanism of serpins: loop insertion forces acylation of plasminogen activator by plasminogen activator inhibitor-1. *Biochemistry*. 1998;37(44):15491-502.
178. Tesch LD, Raghavendra MP, Bedsted-Faarvang T, Gettins PG, Olson ST. Specificity and reactive loop length requirements for crmA inhibition of serine proteases. *Protein Science*. 2005;14(2):533-42.
179. Fei E, Jia N, Zhang T, Ma X, Wang H, Liu C, et al. Phosphorylation of ataxin-3 by glycogen synthase kinase 3 β at serine 256 regulates the aggregation of ataxin-3. *Biochemical and biophysical research communications*. 2007;357(2):487-92.
180. Saunders HM, Hughes VA, Cappai R, Bottomley SP. Conformational behavior and aggregation of ataxin-3 in SDS. *PloS one*. 2013;8(7):e69416.
181. Suhr ST, Senut MC, Whitelegge JP, Faull KF, Cuizon DB, Gage FH. Identities of sequestered proteins in aggregates from cells with induced polyglutamine expression. *The Journal of cell biology*. 2001;153(2):283-94.
182. Simoes AT, Goncalves N, Koeppen A, Deglon N, Kugler S, Duarte CB, et al. Calpastatin-mediated inhibition of calpains in the mouse brain prevents mutant ataxin 3 proteolysis, nuclear localization and aggregation, relieving Machado-Joseph disease. *Brain : a journal of neurology*. 2012;135(Pt 8):2428-39.
183. Chen S, Wetzel R. Solubilization and disaggregation of polyglutamine peptides. *Protein science*. 2001;10(4):887-91.
184. Terpe K. Overview of tag protein fusions: from molecular and biochemical fundamentals to commercial systems. *Applied microbiology and biotechnology*. 2003;60(5):523-33.
185. Nallamsetty S, Waugh DS. Solubility-enhancing proteins MBP and NusA play a passive role in the folding of their fusion partners. *Protein Expression and Purification*. 2006;45(1):175-82.
186. Jansson B, Uhlen M, Nygren PA. All individual domains of staphylococcal protein A show Fab binding. *Federation of European Microbiological Societies Immunology and medical microbiology*. 1998;20(1):69-78.

187. Fernandez-Escamilla AM, Rousseau F, Schymkowitz J, Serrano L. Prediction of sequence-dependent and mutational effects on the aggregation of peptides and proteins. *Nature biotechnology*. 2004;22(10):1302-6.
188. Murby M, Uhlen M, Stahl S. Upstream strategies to minimize proteolytic degradation upon recombinant production in *Escherichia coli*. *Protein Expression and Purification*. 1996;7(2):129-36.
189. Ventura S, Villaverde A. Protein quality in bacterial inclusion bodies. *Trends in biotechnology*. 2006;24(4):179-85.
190. de Groot NS, Espargaro A, Morell M, Ventura S. Studies on bacterial inclusion bodies. *Future microbiology*. 2008;3(4):423-35.
191. Cabrita LD, Bottomley SP. Protein expression and refolding--a practical guide to getting the most out of inclusion bodies. *Biotechnology Annual Review*. 2004;10:31-50.
192. Greenfield NJ. Using circular dichroism spectra to estimate protein secondary structure. *Nature protocols*. 2006;1(6):2876-90.
193. Rost B. Available from: <http://www.predictprotein.org/>.
194. Bioinformatics SIO. ProtParam. Available from: <http://web.expasy.org/protparam/>.
195. Kim JS, Raines RT. Ribonuclease S-peptide as a carrier in fusion proteins. *Protein Science*. 1993;2(3):348-56.
196. Ahmed M, Davis J, Aucoin D, Sato T, Ahuja S, Aimoto S, et al. Structural conversion of neurotoxic amyloid-beta(1-42) oligomers to fibrils. *Nature structural & molecular biology*. 2010;17(5):561-7.
197. Cappai R, Leck SL, Tew DJ, Williamson NA, Smith DP, Galatis D, et al. Dopamine promotes alpha-synuclein aggregation into SDS-resistant soluble oligomers via a distinct folding pathway. *Federation of American Societies for Experimental Biology Journal*. 2005;19(10):1377-9.
198. Regina M. Murphy RHW, Matthew D. Tobelmann, Joseph P. Bernacki. When more is not better: Expanded polyglutamine domains in Neurodegenerative Disease. 2012. *Non-fibrillar Amyloidogenic Protein Assemblies-Common cytotoxins Underlying Degenerative Diseases SpringerLink : Bücher*. Springer Science & Business Media, 2012. illustrated. [336-76].
199. Murphy RM. Kinetics of amyloid formation and membrane interaction with amyloidogenic proteins. *Biochimica et Biophysica Acta*. 2007;1768(8):1923-34.
200. Chen S, Berthelie V, Hamilton JB, O'Nuallain B, Wetzel R. Amyloid-like features of polyglutamine aggregates and their assembly kinetics. *Biochemistry*. 2002;41:7391-9.
201. Golabek AA, Kida E, Walus M, Perez C, Wisniewski T, Soto C. Sodium dodecyl sulfate-resistant complexes of Alzheimer's amyloid beta-peptide with the N-terminal, receptor binding domain of apolipoprotein E. *Biophysical journal*. 2000;79(2):1008-15.

202. Sandberg A, Luheshi LM, Sollvander S, Pereira de Barros T, Macao B, Knowles TP, et al. Stabilization of neurotoxic Alzheimer amyloid-beta oligomers by protein engineering. *Proceedings of the National Academy of Sciences of the United States of America*. 2010;107(35):15595-600.
203. Wong SL, Chan WM, Chan HY. Sodium dodecyl sulfate-insoluble oligomers are involved in polyglutamine degeneration. *FASEB journal : official publication of the Federation of American Societies for Experimental Biology*. 2008;22(9):3348-57.
204. Hoffner G, Djian P. Monomeric, oligomeric and polymeric proteins in huntington disease and other diseases of polyglutamine expansion. *Brain sciences*. 2014;4(1):91-122.
205. Yang H, Li JJ, Liu S, Zhao J, Jiang YJ, Song AX, et al. Aggregation of polyglutamine-expanded ataxin-3 sequesters its specific interacting partners into inclusions: implication in a loss-of-function pathology. *Scientific Reports*. 2014;4:6410.
206. Nagai Y, Tucker T, Ren H, Kenan DJ, Henderson BS, Keene JD, et al. Inhibition of polyglutamine protein aggregation and cell death by novel peptides identified by phage display screening. *The Journal of biological chemistry*. 2000;275(14):10437-42.
207. Popiel HA, Burke JR, Strittmatter WJ, Oishi S, Fujii N, Takeuchi T, et al. The Aggregation Inhibitor Peptide QBP1 as a Therapeutic Molecule for the Polyglutamine Neurodegenerative Diseases. *Journal of amino acids*. 2011;2011:265084.
208. Milto K, Botyriute A, Smirnovas V. Amyloid-like fibril elongation follows michaelis-menten kinetics. *PLOS one*. 2013;8(7):e68684.
209. Villaverde A, Carrio MM. Protein aggregation in recombinant bacteria: biological role of inclusion bodies. *Biotechnology Letters*. 2003;25(17):1385-95.
210. Vallejo LF, Rinas U. Strategies for the recovery of active proteins through refolding of bacterial inclusion body proteins. *Microbial Cell Factories*. 2004;3(1):11.
211. Grune T, Jung T, Merker K, Davies KJ. Decreased proteolysis caused by protein aggregates, inclusion bodies, plaques, lipofuscin, ceroid, and 'aggresomes' during oxidative stress, aging, and disease. *The international journal of biochemistry & cell biology*. 2004;36(12):2519-30.
212. Hwang PM, Pan JS, Sykes BD. Targeted expression, purification, and cleavage of fusion proteins from inclusion bodies in *Escherichia coli*. *Federation of European Biochemical Societies Letters*. 2014;588(2):247-52.
213. Legleiter J, Mitchell E, Lotz GP, Sapp E, Ng C, DiFiglia M, et al. Mutant huntingtin fragments form oligomers in a polyglutamine length-dependent manner in vitro and in vivo. *The Journal of biological chemistry*. 2010;285(19):14777-90.
214. Poirier MA, Li H, Macosko J, Cai S, Amzel M, Ross CA. Huntingtin spheroids and protofibrils as precursors in polyglutamine fibrilization. *Journal of Biological Chemistry*. 2002;277(43):41032-7.
215. Srinivasan R, Jones EM, Liu K, Ghiso J, Marchant RE, Zagorski MG. pH-dependent amyloid and protofibril formation by the ABri peptide of familial British dementia. *Journal of molecular biology*. 2003;333(5):1003-23.

216. Natalello A, Frana AM, Relini A, Apicella A, Invernizzi G, Casari C, et al. A major role for side-chain polyglutamine hydrogen bonding in irreversible ataxin-3 aggregation. *PloS one*. 2011;6(4):e18789.
217. Donaldson KM, Li W, Ching KA, Batalov S, Tsai CC, Joazeiro CA. Ubiquitin-mediated sequestration of normal cellular proteins into polyglutamine aggregates. *Proceedings of the National Academy of Sciences, USA*. 2003;100(15):8892-7.
218. Robertson AL, Headey SJ, Saunders HM, Ecroyd H, Scanlon MJ, Carver JA, et al. Small heat-shock proteins interact with a flanking domain to suppress polyglutamine aggregation. *Proceedings of the National Academy of Sciences of the United States of America*. 2010;107(23):10424-9.
219. Yang DS, Yip CM, Huang TH, Chakrabartty A, Fraser PE. Manipulating the amyloid-beta aggregation pathway with chemical chaperones. *The Journal of biological chemistry*. 1999;274(46):32970-4.
220. Yancey PH. Organic osmolytes as compatible, metabolic and counteracting cytoprotectants in high osmolarity and other stresses. *Journal of Experimental Biology*. 2005;208(15):2819-30.
221. Khan SH, Ahmad N, Ahmad F, Kumar R. Naturally occurring organic osmolytes: from cell physiology to disease prevention. *International Union of Biochemistry and Molecular Biology Life*. 2010;62(12):891-5.
222. Ferreon AC, Moosa MM, Gambin Y, Deniz AA. Counteracting chemical chaperone effects on the single-molecule alpha-synuclein structural landscape. *Proceedings of the National Academy of Sciences of the United States of America*. 2012;109(44):17826-31.
223. Walsh DM, Lomakin A, Benedek GB, Condron MM, Teplow DB. Amyloid beta - Protein Fibrillogenesis. Detection of a protofibrillar intermediate. *Journal of Biological Chemistry*. 1997;272(35):22364-72.
224. Conway KA, Lee S-J, Rochet J-C, Ding TT, Williamson RE, Lansbury Jnr PT. Acceleration of oligomerisation, not fibrillisation, is a shared property of both α -synuclein mutations linked to early-onset Parkinson's disease: Implications for pathogenesis and therapy. *Proceedings of the National Academy of Sciences, USA*. 2000;97(2):571-6.
225. Wacker JL, Zareie MH, Fong H, Sarikaya M, Muchowski PJ. Hsp70 and Hsp40 attenuate formation of spherical and annular polyglutamine oligomers by partitioning monomer. *Nature structural & molecular biology*. 2004;11(12):1215-22.
226. DichroWeb [Internet]. Available from: <http://dichroweb.cryst.bbk.ac.uk/html/home.shtml>.
227. Chow MK, Paulson HL, Bottomley SP. Destabilization of a non-pathological variant of ataxin-3 results in fibrillogenesis via a partially folded intermediate: a model for misfolding in polyglutamine disease. *Journal of molecular biology*. 2004;335(1):333-41.
228. Mashino T, Fridovich I. Effects of urea and trimethylamine-N-oxide on enzyme activity and stability. *Archives of biochemistry and biophysics*. 1987;258(2):356-60.
229. Kumar R, Serrette JM, Thompson EB. Osmolyte-induced folding enhances tryptic enzyme activity. *Archives of biochemistry and biophysics*. 2005;436(1):78-82.

230. Ishibashi M, Sakashita K, Tokunaga H, Arakawa T, Tokunaga M. Activation of halophilic nucleoside diphosphate kinase by a non-ionic osmolyte, trimethylamine N-oxide. *Journal of Protein Chemistry*. 2003;22(4):345-51.
231. Everett RD, Meredith M, Orr A, Cross A, Kathoria M, Parkinson J. A novel ubiquitin-specific protease is dynamically associated with the PML nuclear domain and binds to a herpesvirus regulatory protein. *European Molecular Biology Organization Journal*. 1997;16(3):566-77.
232. Layfield R, Franklin K, Landon M, Walker G, Wang P, Ramage R, et al. Chemically synthesized ubiquitin extension proteins detect distinct catalytic capacities of deubiquitinating enzymes. *Analytical Biochemistry*. 1999;274(1):40-9.
233. Dang LC, Melandri FD, Stein RL. Kinetic and mechanistic studies on the hydrolysis of ubiquitin C-terminal 7-amido-4-methylcoumarin by deubiquitinating enzymes. *Biochemistry*. 1998;37(7):1868-79.
234. Hartl FU. Molecular chaperones in cellular protein folding. *Nature*. 1996;381(6583):571-9.
235. Baskakov I, Bolen DW. Forcing thermodynamically unfolded proteins to fold. *Journal of Biological Chemistry*. 1998;273(9):4831-4.
236. Bolen DW, Rose GD. Structure and energetics of the hydrogen-bonded backbone in protein folding. *Annual review of biochemistry*. 2008;77(1):339-62.
237. Tatzelt J, Prusiner SB, Welch WJ. Chemical chaperones interfere with the formation of scrapie prion protein. *European Molecular Biology Organization Journal*. 1996;15(23):6363-73.
238. Tanaka M, Machida Y, Niu S, Ikeda T, Jana NR, Doi H, et al. Trehalose alleviates polyglutamine-mediated pathology in a mouse model of Huntington disease. *Nature medicine*. 2004;10(2):148-54.
239. Munishkina LA, Cooper EM, Uversky VN, Fink AL. The effect of macromolecular crowding on protein aggregation and amyloid fibril formation. *Journal of molecular recognition*. 2004;17(5):456-64.
240. Marshall H, Venkat M, Seng NS, Cahn J, Juers DH. The use of trimethylamine N-oxide as a primary precipitating agent and related methylamine osmolytes as cryoprotective agents for macromolecular crystallography. *Acta Crystallographica Section D, Biological crystallography*. 2012;68(Pt 1):69-81.
241. Song JL, Chuang DT. Natural osmolyte trimethylamine N-oxide corrects assembly defects of mutant branched-chain alpha-ketoacid decarboxylase in maple syrup urine disease. *Journal of Biological Chemistry*. 2001;276(43):40241-6.
242. Papp E, Csermely P. Chemical chaperones: mechanisms of action and potential use. *Handbook of Experimental Pharmacology*. 2006(172):405-16.
243. Fujigasaki H, Uchihara T, Koyano S, Iwabuchi K, Yagishita S, Makifuchi T, et al. Ataxin-3 is translocated into the nucleus for the formation of intranuclear inclusions in normal and Machado-Joseph disease brains. *Experimental Neurology*. 2000;165(2):248-56.

244. Warrick JM, Morabito LM, Bilen J, Gordesky-Gold B, Faust LZ, Paulson HL, et al. Ataxin-3 suppresses polyglutamine neurodegeneration in *Drosophila* by a ubiquitin-associated mechanism. *Molecular cell*. 2005;18(1):37-48.
245. Simoes AT, Goncalves N, Nobre RJ, Duarte CB, Pereira de Almeida L. Calpain inhibition reduces ataxin-3 cleavage alleviating neuropathology and motor impairments in mouse models of Machado-Joseph disease. *Human molecular genetics*. 2014;23(18):4932-44.
246. Colomer Gould VF, Goti D, Pearce D, Gonzalez GA, Gao H, Bermudez de Leon M, et al. A mutant ataxin-3 fragment results from processing at a site N-terminal to amino acid 190 in brain of Machado-Joseph disease-like transgenic mice. *Neurobiology of Disease*. 2007;27(3):362-9.
247. Mauri PL, Riva M, Ambu D, De Palma A, Secundo F, Benazzi L, et al. Ataxin-3 is subject to autolytic cleavage. *The Federation of European Biochemical Societies Journal*. 2006;273(18):4277-86.
248. Zou Q, Bennion BJ, Daggett V, Murphy KP. The molecular mechanism of stabilization of proteins by TMAO and its ability to counteract the effects of urea. *Journal of the American Chemical Society*. 2002;124(7):1192-202.
249. Bennion BJ, DeMarco ML, Daggett V. Preventing misfolding of the prion protein by trimethylamine N-oxide. *Biochemistry*. 2004;43(41):12955-63.
250. Ball JC, Puckett LG, Bachas LG. Covalent immobilization of beta-galactosidase onto a gold-coated magnetoelastic transducer via a self-assembled monolayer: toward a magnetoelastic biosensor. *Analytical chemistry*. 2003;75(24):6932-7.
251. Matos CA, Nobrega C, Louros SR, Almeida B, Ferreira E, Valero J, et al. Ataxin-3 phosphorylation decreases neuronal defects in spinocerebellar ataxia type 3 models. *The Journal of cell biology*. 2016;212(4):465-80.
252. Baudry M, Bi X. Calpain-1 and Calpain-2: The Yin and Yang of Synaptic Plasticity and Neurodegeneration. *Trends in neurosciences*. 2016;39(4):235-45.
253. Gafni J, Hermel E, Young JE, Wellington CL, Hayden MR, Ellerby LM. Inhibition of calpain cleavage of huntingtin reduces toxicity: accumulation of calpain/caspase fragments in the nucleus. *The Journal of biological chemistry*. 2004;279(19):20211-20.
254. Schilling B, Gafni J, Torcassi C, Cong X, Row RH, LaFevre-Bernt MA, et al. Huntingtin phosphorylation sites mapped by mass spectrometry. Modulation of cleavage and toxicity. *The Journal of biological chemistry*. 2006;281(33):23686-97.
255. Iuchi S, Hoffner G, Verbeke P, Djian P, Green H. Oligomeric and polymeric aggregates formed by proteins containing expanded polyglutamine. *Proceedings of the National Academy of Sciences of the United States of America*. 2003;100(5):2409-14.
256. Scherzinger E, Sittler A, Schweiger K, Heiser V, Lurz R, Hasenbank R, et al. Self-assembly of polyglutamine-containing huntingtin fragments into amyloid-like fibrils: implications for Huntington's disease pathology. *Proceedings of the National Academy of Sciences of the United States of America*. 1999;96(8):4604-9.
257. Masino L, Nicastro G, Calder L, Vendruscolo M, Pastore A. Functional interactions as a survival strategy against abnormal aggregation. *FASEB journal : official publication of the Federation of American Societies for Experimental Biology*. 2011;25(1):45-54.

258. He HL, Chen XL, Zhang XY, Sun CY, Zou BC, Zhang YZ. Novel Use for the Osmolyte Trimethylamine N-oxide: Retaining the Psychrophilic Characters of Cold-Adapted Protease Deseasin MCP-01 and Simultaneously Improving its Thermostability. *Marine biotechnology*. 2009;March 2009.

APPENDIX A

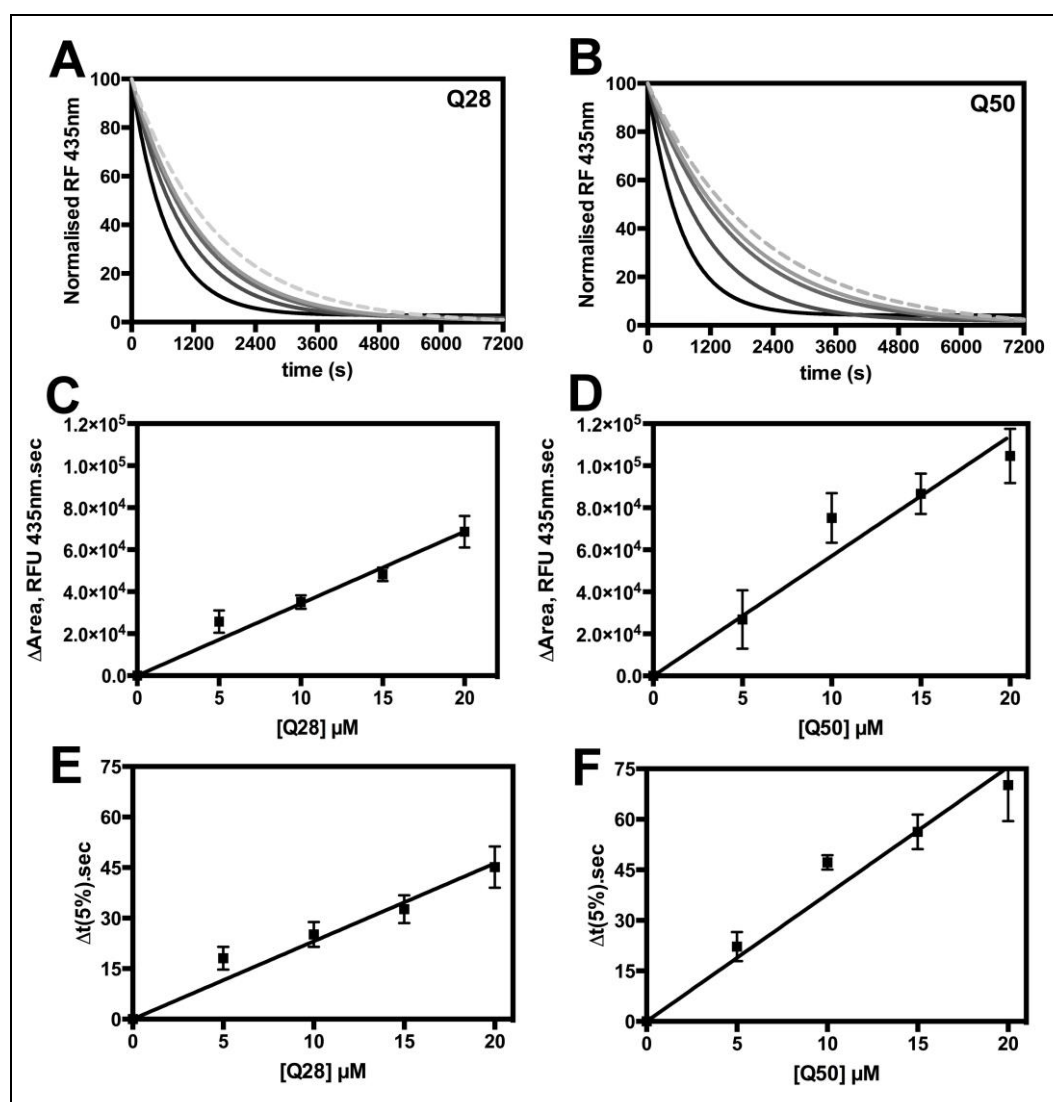


Figure A1 Ataxin-3 proteins compete for calpain-2 hydrolysis in the presence of fluorogenic substrate, Suc-LY-AMC. Progress curves were monitored at 435 nm when increasing concentrations of non-chromogenic substrate, ataxin-3 (A) (Q28) and (B) (Q50) compete with Suc-LY-AMC fluorogenic substrate at a constant concentration of calpain-2. These kinetic experiments were carried out on a 96 well plate, in a monochromatic bench top spectrometric plate reader. Dependence of ΔArea under the curves and time taken to transform 5% of substrate upon increasing concentrations of ataxin-3 (C, E) (Q28) and (D, F) ataxin-3 (Q50) are shown. Each error bar represents the standard deviation of at least four determinations and the lines drawn through the points are determined by linear regression analysis.

APPENDIX B

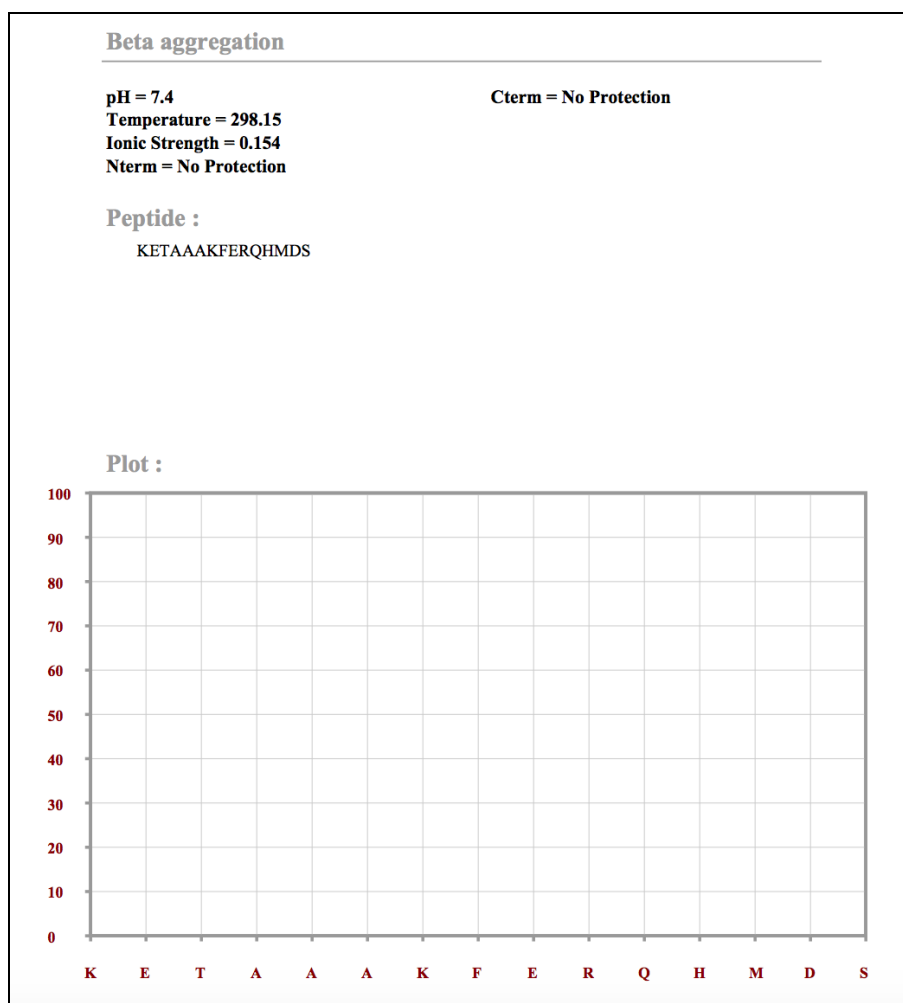


Figure B1 Predicting potential aggregation prone domain and regions of proteins using TANGO (187). Peptide sequence of the S.tag used C-terminal to ataxin-3 fragments in Chapter 4. The sequence is predicted to 0 % aggregation prone.

APPENDIX C

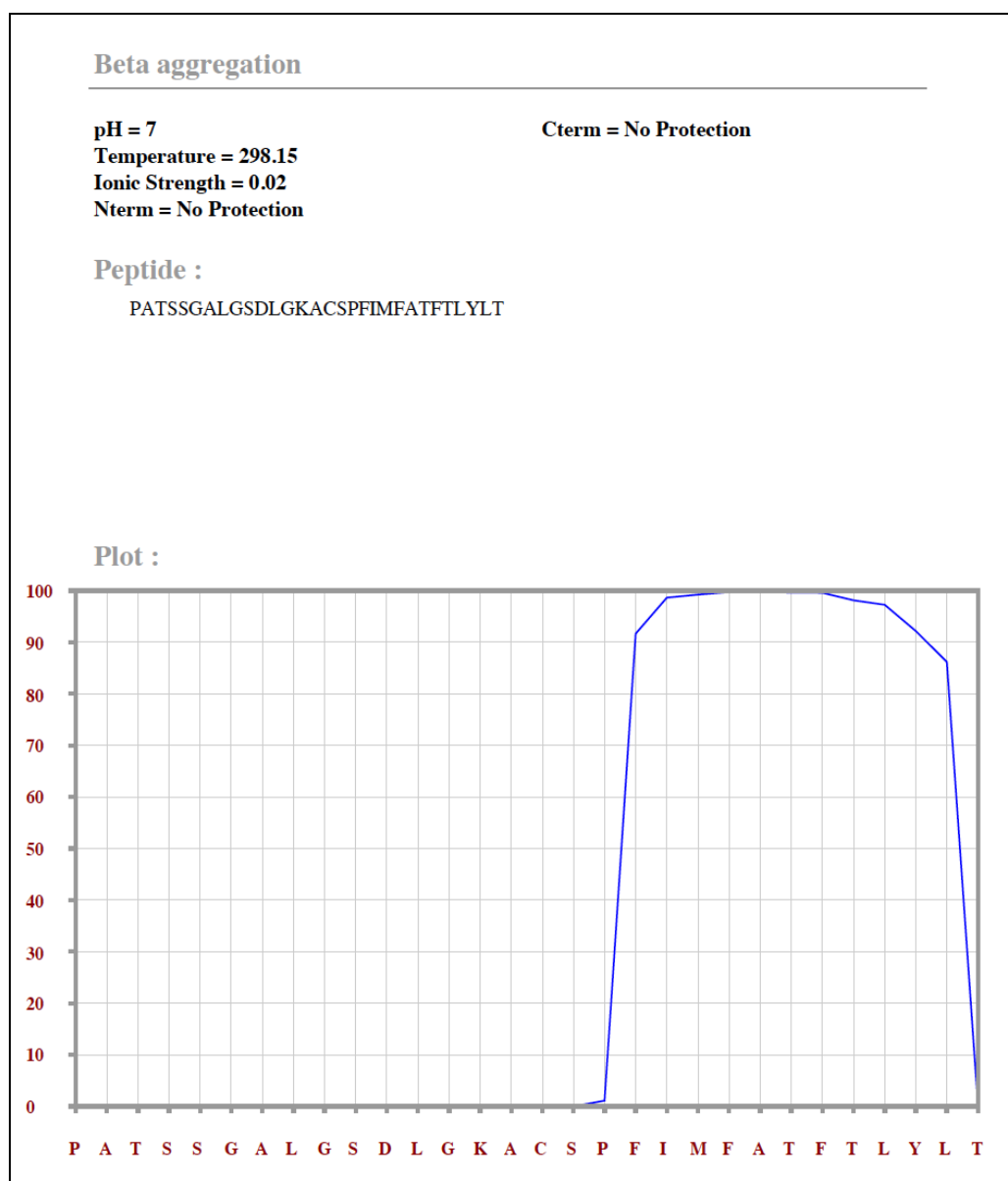


Figure C1 Predicting aggregation of hydrophobic tail in ataxin-3 using TANGO (187)
 Analysis of the last 30 amino acids of ataxin-3. Peptide sequence of FIMFATFTLYLY is predicted to be highly aggregation prone.